Improving current approaches for seismic risk assessment and design of bridges

By

Francesca Turchetti

Department of Civil and Environmental Engineering
University of Strathclyde

Declaration of authenticity and author's rights

This thesis is the result of the author's original research. It has been composed by the author and has not been previously submitted for examination which has led to the award of a degree.

The copyright of this thesis belongs to the author under the terms of the United Kingdom Copyright Acts as qualified by University of Strathclyde Regulation 3.50. Due acknowledgement must always be made of the use of any material contained in, or derived from, this thesis.

Signed:

Date: 05/06/2024

Statement of co-authorship

The following people and institutions contributed to publications which are part of this thesis:

Candidate	Francesca Turchetti, University of Strathclyde
Author 1	Enrico Tubaldi, University of Strathclyde (Primary Supervisor)
Author 2	Edoardo Patelli, University of Strathclyde (Supervisor)
Author 3	John Douglas, University of Strathclyde (Supervisor)
Author 4	Paolo Castaldo, Politecnico di Torino
Author 5	Christian Málaga-Chuquitaype, Imperial College London
Author 6	Carmine Galasso, University College London
Author 7	Ekin Ozer, University College Dublin
Author 8	Jawad Fayaz, University College London
Author 9	Pierre Gehl, BRGM
Author 10	Andrea Dall'Asta, University of Camerino
Author 11	Mariano Zanini, University of Padova

Authors and their contributions:

Paper 1: **Turchetti, F**., Tubaldi, E., Patelli, E. *et al*. Damage modelling of a bridge pier subjected to multiple earthquakes: a comparative study. *Bull Earthquake Eng* **21**, 4541–4564 (2023). https://doi.org/10.1007/s10518-023-01678-y

Francesca Turchetti: Problem formulation, research design and data collection; Formal analysis; Visualization, analysis and interpretation; Writing – original draft preparation; Writing – review & editing.

Enrico Tubaldi: Conceptualization and problem formulation; Provided theoretical material; Writing – review & editing.

Edoardo Patelli: Conceptualization; writing – review & editing.

Paolo Castaldo: Conceptualization; writing – review & editing.

Christian Málaga-Chuquitaype: Conceptualization; writing – review & editing.

All authors discussed the results and contributed to the final manuscript.

Chapter 3 is based on this article.

Paper 2: Tubaldi, E, **Turchetti, F**, Ozer, E, Fayaz, J, Gehl, P, Galasso, C. A Bayesian network-based probabilistic framework for updating aftershock risk of bridges. *Earthquake Engng Struct Dyn*. 2022; **51**: 2496-2519. https://doi.org/10.1002/eqe.3698.

Enrico Tubaldi: Took the lead in writing the manuscript; Developed the theoretical formalism, performed analytic calculations and numerical simulations; Visualization; Results interpretation; Writing – Original Draft Preparation.

Francesca Turchetti: Conceptualization; Developed the regression models for mainshock and aftershock scenarios; Performed numerical simulations; Contributed to the analysis and interpretation; Writing – Review & Editing.

Ekin Ozer: Performed analytic calculations and numerical simulations; Conceptualization; Writing – Review & Editing.

Jawad Fayaz: Performed PSHA; Data curation; Writing – Review & Editing.

Pierre Gehl: Developed the BN; Data curation; Writing – Review & Editing.

Carmine Galasso: Developed the theoretical formalism; Conceptualization; Results interpretation; Writing – Review & Editing.

All authors discussed the results and contributed to the final manuscript.

Presented as Chapter 4 in this thesis.

Paper 3: **Turchetti, F**., Tubaldi, E., Douglas, J. et al. A risk-targeted approach for the seismic design of bridge piers. Bull Earthquake Eng 21, 4923–4950 (2023). https://doi.org/10.1007/s10518-023-01717-8.

Francesca Turchetti: Conceptualization; Performed the computations; Developed the theoretical formalism; Data curation; Formal Analysis; Visualization; Writing – Original Draft Preparation; Writing – Review & Editing.

Enrico Tubaldi: Developed the theoretical formalism; Conceptualization; Data Curation; Writing – Review & Editing.

John Douglas: Developed the theoretical formalism; Conceptualization; Writing – Review & Editing.

Mariano Zanini: Performed PSHA; Writing – Review & Editing.

Andrea Dall'Asta: Developed the theoretical formalism; Writing – Review & Editing.

All authors discussed the results and contributed to the final manuscript.

Presented as Chapter 5 in this thesis.

Most of the work here presented has been included in multiple conference proceedings, including ESREL 2022, ICASP 2023 and SECED 2023:

Turchetti, F., Tubaldi, E., Douglas, J., Zanini, M. and Dall'Asta, A. (2023) A methodology for the risk-based design of bridges in Italy. In: SECED 2023 Conference, 2023-09-14 - 2023-09-15, Churchill College.

Turchetti, F., Tubaldi, E., Douglas, J., Zanini, M. A., & Dall'Asta, A. (2023) Seismic risk-based design of simply-supported bridges in Italy. In: 14th International Conference on Application of Statistics and Probability in Civil Engineering.

Turchetti, F., Tubaldi, E., Patelli, E., Castaldo, P., Di Pilato, D. and Málaga-Chuquitaype, C. (2022) Damage Assessment of Bridge Piers Subjected to Multiple Earthquakes: Markov Model vs Regression Models. In: Book of Extended Abstracts for the 32nd European Safety and Reliability Conference (ESREL), 28 August – 1 September, Dublin, Ireland

The work presented in Chapters 1, 2 and 6 is entirely attributable to the candidate.

Acknowledgements

At the end of my PhD journey, I would like to express my sincere gratitude to all those who have contributed to the successful completion of this research project.

First, I would like to thank my primary supervisor Enrico Tubaldi for offering me the opportunity to come to Glasgow and for making this work possible. His guidance and advice carried me through all the stages of my project. I am very grateful for his support.

Second, I would like to express my gratitude towards my co-supervisors, John Douglas and Edoardo Patelli, for providing invaluable guidance, support and provisions that help in the completion and success of this study.

A special thanks goes to the University of Strathclyde, particularly to all my colleagues in the Department of Civil and Environmental Engineering for welcoming me and making me feel at home. I have found true friends that made the office a very friendly place to come every day.

I thank my parents for believing in me and for always guiding me even in moments of confusion. This would not have been possible without their love and support given to me at all times.

Lastly, I would like to thank all my old friends from Ancona, with whom I have forged a connection as enduring as family, for always being there for me and to all my new friends from Glasgow for all the beautiful moments we have spent together. You have supported me to complete the research work directly or indirectly and I am very grateful to all of you.

This thesis represents the final chapter of an unforgettable journey that changed my approach to life. All the beautiful memories and the invaluable professional experience gained will remain with me, shaping the person I am becoming.

Abstract

Earthquakes are among the most dangerous natural hazards that pose significant threat to the functioning and integrity of civil infrastructures. The fact that many buildings and bridges around the world continue to fail due to earthquakes demonstrates that there is still a need of improving current tools and technologies for seismic risk evaluation and mitigation.

This Thesis aims to advance current procedures for the seismic assessment and design of bridges, with a particular focus on three areas: the performance under repeated shocks during the bridge design lifetime, the performance under aftershock events following the occurrence of a mainshock, and the optimal design of the bridge pier properties to achieve target seismic reliability levels.

With regards to the first area of research, a study to compare different methodologies for predicting damage accumulation in structures exposed to multiple earthquakes has been carried out. Global and local Engineering Demand Parameters (EDPs) have been used to describe the damage. The accuracy of these methodologies has been evaluated and improvements to the models have been proposed.

A Bayesian network-based probabilistic framework has been developed for updating the aftershock risk in bridges. The framework integrates information about mainshock earthquake intensity, structural response, and damage to critical components, reducing uncertainty in assessing the risk of bridge failure. The Bayesian network considers various random variables related to seismic damage assessment, incorporating data from seismic stations, structural health monitoring sensors, and visual inspections.

The Thesis also addresses the development of a risk-targeted design approach to assess the seismic structural safety of newly-designed bridges. This approach involves a probabilistic optimization procedure to minimize the design resisting moment at the pier base, with a surrogate model to reduce the computational effort.

The tools and analyses presented in this Thesis provide important guidance in the area of seismic analysis and design of bridges, ultimately contributing to the development of more resilient and earthquake-resistant infrastructure.

Table of Contents

List of Figures

XVIII

List of Tables

1 **Introduction**

1.1. Motivation

Ageing, degradation, and extreme events such as earthquakes can jeopardize the efficiency of civil infrastructure and have an immediate impact on the community resilience. The failure of structures like bridges, railways or dams can result in significant direct and indirect losses, and therefore it is crucial to guarantee their appropriate functioning and to take preventive actions in order to avoid irreparable damage or collapse.

In the last decades, the performance-based earthquake engineering (PBEE) has emerged as a new paradigm for the seismic safety assessment of structures (Deierlein et al., 2003; Porter, 2003). The promise of PBEE is to produce structures with predictable seismic performance.

The seismic vulnerability of bridges is usually expressed in the form of fragility curves, defined as the probability that the structure will experience damage if subjected to an earthquake ground motion of a given intensity level. Bridge fragility curves are used in the assessment of seismic performance providing valuable data for retrofit measures and they can be of great help to asset managers and public authorities in making better

informed decisions concerning the management of the risk due to future events in the short and long term. Therefore, the need for consistent and reliable fragility curves arises.

In traditional PBEE approaches, the seismic reliability assessment of a structure assumes that earthquake damage occurs in single events, and that the structure is immediately retrofitted to the as-built condition after the event. However, a large percentage of the world's infrastructure is located in earthquake-prone regions where structural systems are expected to experience more than a single shock during their design lifetime. Multiple earthquakes can, over a long period of time, result in a reduction in structural capacity and can eventually lead to structural collapse in a structure designed to resist a single event. The problem of damage accumulation under repeated events close in time has been experienced several times in the past: during the Umbria-Marche earthquake in September 1997 (Amato et al., 1998) and the Christchurch-New Zealand in September 2010 (Bradley & Cubrinovski, 2011). In both cases the weakening of structural capacities following a main shock seismic event led to collapse under the following less intense aftershocks. Recent studies have investigated the issue of damage accumulation by developing probabilistic approaches taking account of the probabilistic nature of the hazard and the inherent randomness in the response of structures under repeated earthquakes shocks (Duerr & Tesfamariam, 2012; Ghosh et al., 2015; Iervolino et al., 2016, 2020; Park & Ang, 1985). The reliability of these approaches vis-à-vis their computational cost has not been fully investigated, yet.

The development of tools able to predict potential damage after an earthquake event can prevent catastrophic collapses. In this context, structural monitoring of a bridge is an effective method used to provide, in near real time, reliable information regarding the structural health of the construction and it has been widely applied for many engineering purposes (Comisu et al., 2017). It is not possible though to monitor an entire infrastructure or even all the components within a structure, as it is economically unsustainable. A way to overcome this limitation is to install monitoring systems on a limited number of critical components and use a probabilistic approach to extend this information to the other components within a network. The state of the structure can be represented by random variables and their interdependence can be modelled using a Bayesian Network. Observations can be used to update the distribution of the random variables, thus

contributing to reduce the uncertainty in the component demand and capacity. One possible application of use of monitoring data for near real time damage assessment and risk updating is in the context of aftershock risk assessment of bridges. The risk of aftershocks has only recently been studied because, for a long time, seismic risk evaluation considered only mainshocks. A mainshock is certainly the most violent event capable of causing heavy damage to structures and a large number of victims. Nevertheless, aftershocks can be equally violent in some cases and the damage associated to aftershocks is relevant. Aftershocks can cause vast losses due to direct repair costs, business interruptions and casualties, especially if the affected structures and infrastructure are left unrepaired upon initial damage due to the first event (Abdelnaby, 2012; Amato et al., 1998).

Alongside with the problem of risk assessment and risk updating, there is also a need of improving current approaches for the design of structures. In particular, there is a need of risk-based design methodologies, able to identify the optimal properties of a structure that allow to meet prefixed performance criteria. Such approach consists in designing a structure to meet more refined performance objectives that have to be explicitly stated in terms of risk metrics associated with the exceedance of tolerable thresholds of loss (Franchin et al., 2018; Vamvatsikos & Aschheim, 2016). While several approaches have been developed for the risk-based design of buildings (Shi et al., 2012), methodologies for the risk-based design of bridges are still needed.

1.2. Aim of the research

The research project aims to improve current approaches for the risk assessment and design of structures. The specific objectives of the project are: i) evaluating alternative methods for the performance assessment of structures subjected to repeated earthquakes during their design life-time and proposing improvements to these methods, ii) developing a method for improving the knowledge of the structural state and risk of bridges following an earthquake event, by exploiting the information from available sensing data, iii) developing a methodology for the risk-targeted design of bridges and explore the variation of risk-targeted design results in areas of different seismicity.

1.3. Outline of the thesis

This manuscript is organized into six chapters. Chapter 2 contains an introduction to the seismic risk assessment problem and a review of practical methods for probabilistic risk assessment of structural systems. In particular, sub-sections 2.2 and 2.3 summarize existing work on simulation-based and conditional-based methodologies. Sub-section 2.4 presents an extension of the PEER PBEE Framework to address the cumulative effects of multiple earthquakes on structural damage. Sub-sections 2.5 and 2.6 introduce Bayesian approaches to damage assessment and seismic risk-based design approaches respectively. Chapter 3 presents a comparative study of recently developed methodologies for the prediction of damage accumulation in structures subjected to multiple earthquakes. Besides evaluating the effectiveness of each approach, possible improvements of the cumulative demand model are tested. A reinforced concrete bridge model with a single pier is examined as case study and Park-Ang damage index is considered to describe the damage accumulation. The results demonstrate the importance of considering the occurrence of multiple shocks. In Chapter 4, a probabilistic methodology based on the use of a Bayesian Network (BN) is proposed to describe the logical process of evaluating structural damage following a main earthquake event and the risk associated with possible aftershocks. This proposed approach also allows for the integration of information from data provided by sensors and visual inspections to obtain a better estimation of the structural condition and risk of failure following an earthquake event. Chapter 5 illustrates a methodology for the risk-targeted design of RC piers in multi-span bridges. Such approach aims to minimize a function related to the cost of the design, while ensuring that a prefixed target reliability level is not exceeded. The methodology is applied to a case study located in various locations across Italy to illustrate the variations in the optimal risk-based design properties of bridges across regions with varying seismic hazard. Finally, in Chapter 6, some conclusions are drawn and future developments are discussed.

2 Overarching Seismic Risk Assessment Framework

2.1 Introduction

The term *risk assessment* refers to the quantitative or qualitative determination of the risk associated with a defined situation and a known threat. It consists of a hazard analysis, which aims at identifying and evaluating probable future events that may cause harm to people and to the environment, and of a vulnerability evaluation, that allows determining the tolerance for such events. Nowadays the importance of the conservation of the surrounding environment and the safety of individuals, as well as a fair management of available natural and economical resources, has become of great concern, especially in the civil engineering field. Decision support tools based on risk and reliability analysis are extremely requested and their demand will increase in the near future.

Risk and reliability analysis are interdisciplinary engineering branches and they request the knowledge of probability, statistics and decision analysis (Faber & Stewart, 2003). The first step to a clear comprehension of risk analysis is defining the concept of risk. Usually the term risk is used as a synonym of likelihood or chance and it is described as

5

the *effect of uncertainty on objectives* (ISO 31000:2009. Risk Management—Principles and Guidelines, 2009) indicating that we are uncertain about the effects of an activity with respect to something that humans value. Technically speaking, risk is defined as the measurement of the damage expected in a given interval of time and it is a combination of three components: hazard H, vulnerability V and exposure E.

$$R = H \cdot V \cdot E \tag{2-1}$$

Hazard – a potentially destructive natural or human-induced physical phenomenon(Cardona, 1990; UNDHA, 1992; UNDRO, 1980; White, 1973). Common natural hazards include earthquakes, floods, hurricanes, tsunami, landslides, and more.

Vulnerability – the likelihood that human beings, their livelihoods and assets will suffer adverse effects when exposed to a hazard (Cardona, 1986; Thywissen, 2006; UNDRO, 1980). For example, a building with multiple floors may be more vulnerable to shaking from an earthquake and more likely to collapse than a one-story building. Another example, elderly persons may be more vulnerable to the impacts of flooding because they have a harder time evacuating or moving quickly. As discussed in Manyena (2006) Thywissen (2006), vulnerability is related to predisposition, susceptibilities, fragilities, weaknesses or deficiencies that favor adverse effects on the exposed elements.

Exposure – a measure of the extent and importance of the consequences expected in an area. It refers to the inventory of elements in an area that could be affected by a hazard (Cardona, 1990; UNISDR, 2004). Thus, it depends on population, construction, density, factories, farmland, and etc. Many times, exposure and vulnerability have been confused and exchanged but they have distinct meanings. Exposure is a necessary, but not sufficient, factor in determining risk. It is possible to be exposed without being vulnerable, e.g. residing in a flood-prone area but having adequate resources to protect the building structure and contents to minimize potential damage. However, to be vulnerable to a severe event, exposure is a prerequisite.

In many cases, the only parameter that can be controlled in order to mitigate the risk, is the vulnerability. In a way, the exposure can also be controlled if, for instance, we choose not to build in a region with expected hazard.

A crucial problem in risk analysis is the identification of the hazards associated with the system and the possible states of failure to be considered. If not all the relevant threats are identified then the analysis will be inefficient and could affect negatively in the evaluation of risk jeopardizing people's life and the environment. Engineers have developed different qualitative and quantitative tools for hazard assessment such as:

- Hazard identification: FMEA (acronym for Failure Mode and Effect Analysis) and HAZOP (acronym for Hazard and Operability Study)

- Accident Scenarios Identification: Event tree and Fault Tree

- Uncertainty Quantification and calculation of probability of failure: Reliability analysis and Monte Carlo method

Earthquake engineering stands out as one of the disciplines characterized by the highest degree of uncertainty. This uncertainty stems from the fact that earthquakes are inherently unpredictable and the features that characterize them, such as the earthquake intensity or the ground motion characteristics, cannot be determined in a deterministic way, as well as the structural response of buildings to seismic events.

Traditional seismic design philosophy is based on insuring no damage to structural and non-structural building elements in low-intensity earthquakes, limiting damage to elements that can be repaired in medium-intensity earthquakes, and preventing the complete or partial collapse of buildings in high-intensity earthquakes. In spite of the fact that the structures complied with the available seismic codes and were built in accordance with conventional design principles, the structural engineering community realized after the 1994 Northridge and 1995 Kobe earthquakes that the amount of damage, the economic loss resulting from downtime, and the repair costs of the structures were unacceptably high (Lee & Mosalam, 2005). This realization is where the idea of performance-based earthquake engineering (PBEE) first emerged.

The general procedure for seismic risk assessments has been formulated and employed by earthquake engineers for more than 40 years (Kongar et al., 2017). Companies have also embraced this procedure, developing catastrophe modeling software for the

insurance industry. The seismic risk assessment comprises four essential components: an exposure module, a hazard module, a vulnerability module, and a loss module. This is illustrated in the flowchart in **Figure 2-1**.
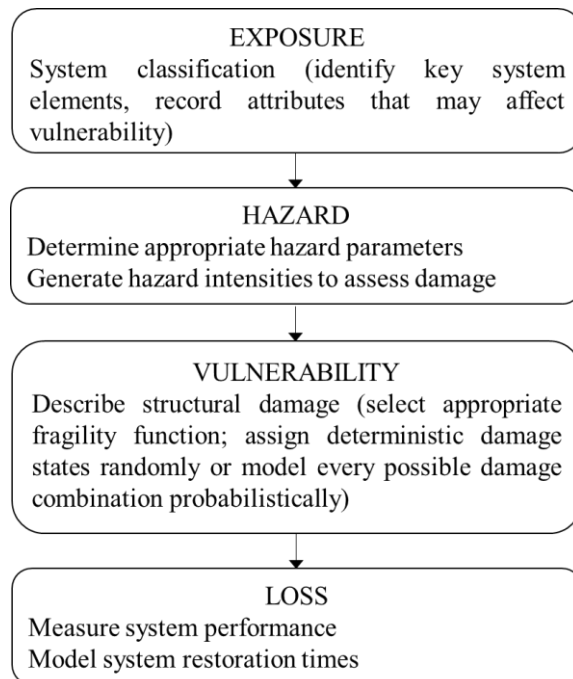
Figure 2-1 Flowchart outlining the steps in the seismic risk assessment

The exposure module identifies and categorizes the structure and its components. The hazard module simulates earthquake events, identifying appropriate earthquake hazard parameters and generating local seismic hazard intensities for each site. The vulnerability module assesses the damage level experienced by each structural component. It establishes scales for classifying damage, employing a hazard-damage relationship (a fragility function). Lastly, the loss module transforms the damage into an estimate of the loss metric, evaluating the overall system's performance based on damages assigned to the structure.

This introduction section has defined the general problem of seismic risk assessment. Sub-sections 2.2 and 2.3 describe two alternative approaches for seismic risk assessment of structures, namely the simulation-based approach (i.e. direct approach) and the conditional-based approach. Subsequently, sub-section 2.4 illustrates the extension of the risk-assessment framework to account for the accumulation of damage in the case of multiple shocks and aftershock scenarios. In sub-section 2.5, Bayesian approaches for the

damage assessment and risk updating described together with an overview of Bayesian Networks. The final sub-section introduces the concept of seismic risk-based design.

2.2 Simulation-based method

Different methods can be used to perform probabilistic risk analysis. These methods can be essentially categorized in two main classes (Cornell, 2005; Scozzese et al., 2020): (direct) simulation-based approach and conditional approach. **Table 2-1** summarizes the main features of the two approaches.

Table 2-1 Main characteristics of the conditional and simulation-based probabilistic approaches

Simulation-based	Conditional
Research-oriented	Practice-oriented
No need of conditioning to any intensity measure	Need of conditioning to an intensity measure
Robust and confident tool for estimating seismic risk	Potentially biased if ground motion records are not representative of the hazard
Large number of simulations (analyses) required	Requires a reduced number of structural analyses
A stochastic model is required to describe the seismic input	Can be applied using recorded ground motions

The simulation-based method consists in the observation of the structural system's response to the seismic input. A set of seismic inputs is generated from the joint density $f(\mathbf{x})$ of the random input parameters that describe the seismic source (e.g. random magnitude and location) and the corresponding outputs (in terms of response, or failure events, or even losses) are post-processed to infer their statistical distribution.

Mathematically, the method consists in characterising the response parameter $y \in \mathbb{R}$ (i.e. max damper displacement), knowing the parameters $x \in \Omega$ from PDF $p_X(x)$ (i.e. M, R). The performance function $g(x)$ relates the random input to the response output:

$$y = g(\boldsymbol{x}) \tag{2-2}$$

It is possible to define a failure region $F = \{\boldsymbol{x}: g(\boldsymbol{x}) > d^*\}$ as the subset of the whole sample space Ω made by samples able to provide a response which is higher than a fixed threshold d^*. The probability of failure is:

$$P(\boldsymbol{x} \in F) = P(y > d^*) = \int_{\Omega \cap F} p_X(\boldsymbol{x})dx \tag{2-3}$$

The integral $\int_{\Omega \cap F} p_X(\boldsymbol{x})dx$ is called reliability integral and it is the formal expression of the reliability problem. This integral has not a close form solution due to the inherent complexity in understanding the precise nature of the failure. By introducing the Indicator Function I_d

$$\begin{cases} I_d(\boldsymbol{x}) = 1, & if\ P(\boldsymbol{x} \in F) = 1\ (failure) \\ I_d(\boldsymbol{x}) = 0, & otherwise \end{cases} \tag{2-4}$$

it is possible to transform the integral in the following, extending it to the whole sample space Ω:

$$P(\boldsymbol{x} \in F) = P(F) = \int_{\Omega \cap F} p_X(\boldsymbol{x})dx = \int_{\Omega} I_d(\boldsymbol{x})p_X(\boldsymbol{x})dx = E[I_d] \tag{2-5}$$

The integral $\int_{\Omega} I_d(\boldsymbol{x})p_X(\boldsymbol{x})dx$ is the definition of the expected value of I_d.

The simplest but robust method for performing direct simulation is called Monte Carlo Method. The Monte Carlo method is a computational technique used for approximating numerical solutions to a variety of mathematical and statistical problems. It relies on random sampling and statistical inference to estimate values or outcomes that might be difficult or impossible to compute precisely using traditional analytical methods. In the Monte Carlo method, random samples are generated from a known or assumed distribution and are used as input values for a specific mathematical function or model relevant to the problem at hand. By calculating the average or sum of the function values from the generated samples, an estimate or approximation of the desired solution is obtained. The accuracy of the Monte Carlo method improves as the number of random samples (iterations) increases. As more samples are used, the estimated value converges toward the true value, following the law of large numbers. According to Monte Carlo Method, the probability of failure is approximated by simply counting the number of

failure samples and dividing them by the total number of samples used in the simulation. It this way, it is possible to approximate the expected value of the indicator function.

For example, we can generate N independent identically distributed samples according to a given continuous CDF $F(x)$. Given that a random variable X is represented by $F(x)$, Monte Carlo simulation aims to provide sets of samples x_i whose discrete CDF tends to $F(x)$ as the number of samples increases. The method requires calculating the inverse of the CDF to estimate x_i. **Figure 2-2** illustrates the sampling procedure, starting from generating random variables u_i from a known distribution.

$$F(x_i) = u_i \tag{2-6}$$

$$F_x^{-1}(u_i) \rightarrow x_i \tag{2-7}$$
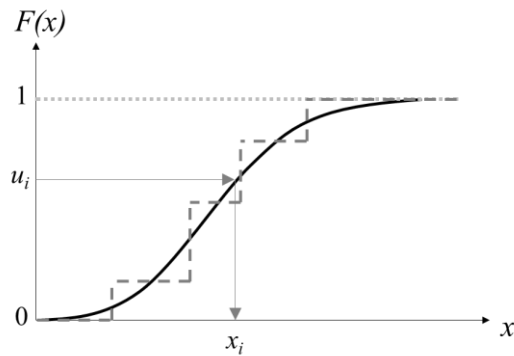
Figure 2-2 Illustration of sampling procedure

Repeating this procedure N times, it is possible to approximate a continuous CDF with a discrete CDF; to better approximate the continuous CDF, it is necessary to increase the number of simulations. It is a simple way to generate samples according to any type of CDF function.

Programming languages are able to provide samples of uniformly distributed random variables in [0,1]. Mathematically, the probability of failure computed using the Monte Carlo method is represented by:

$$E[I_d] \approx \tilde{P}(F) = \frac{1}{N}\sum_{i=1}^{N} I_d(x_i) = \frac{num\ failure\ samples}{total\ num\ samples} \qquad (2\text{-}8)$$

Equation (2-8) is the definition of "statistical averaging". The method provides the exact solution for $N \to \infty$. The advantages of using Monte Carlo simulation are the simplicity of implementation, the applicability to any integral (or system of equations), the simplifying assumptions involved in the analytical models, the attainment of a model that can be treated analytically. The limit of Monte Carlo method is the inability to efficiently generate samples with very small exceedance probabilities. This can be better appreciated by observing the complementary CDF (**Figure 2-3**).
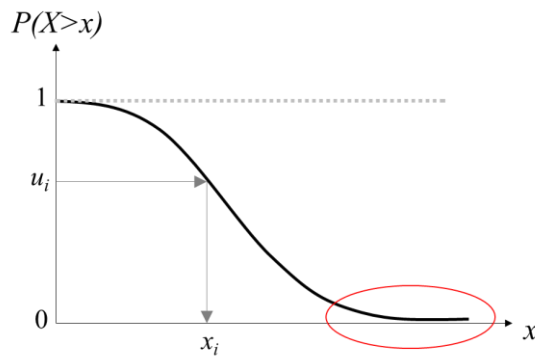
Figure 2-3 CCDF

Monte Carlo is not able to efficiently generate samples in the tail of the distribution. The coefficient of variation $\delta\left(\tilde{P}(F)\right)$, which is a measure of the accuracy of the Monte Carlo estimator $\tilde{P}(F)$, is linked to the target probability to be estimated and the number of samples (Au & Beck, 2003).

$$\delta\left(\tilde{P}(F)\right) = \frac{\sigma\left(\tilde{P}(F)\right)}{E[\tilde{P}(F)]} = \frac{\sqrt{var[I_d(X)]}}{P(F)} = \sqrt{\frac{1-P(F)}{N \cdot P(F)}} \qquad (2\text{-}9)$$

According to **Table 2-2**, to achieve an estimation of the probability of failure of 10^{-3}, denoted by a small coefficient of variation of 0.10, the number of required simulations is 10^5. This significant number of simulations is necessary to accurately characterize such a small failure probability. The challenge does not lie in the generation of random samples (i.e. magnitude values or epicentral distance values) as this can be easily accomplished using computational resources. The true challenge arises in performing a corresponding

number of numerical analyses like nonlinear time history analyses, each corresponding to a ground motion sample. If the structural model is a complex, nonlinear, multi-degree of freedom system, performing 10^5 simulation analyses implies a computational time of probably a month or more.

Table 2-2 Number of simulations required for a given *P(F)* and $\delta(\tilde{P}(F))$

$P(F)$	$\delta(\tilde{P}(F))$		
	0.30	*0.20*	*0.10*
10^{-1}	$1.11 \cdot 10^2$	$2.5 \cdot 10^2$	$1 \cdot 10^3$
10^{-3}	$1.11 \cdot 10^4$	$2.5 \cdot 10^4$	$1 \cdot 10^5$
10^{-6}	$1.11 \cdot 10^6$	$2.5 \cdot 10^7$	$1 \cdot 10^8$

There are other advanced strategies for performing direct simulations; for instance, Hypercube sampling, also known as Latin Hypercube Sampling (LHS), is a stratified sampling technique used to generate representative samples from a multidimensional probability distribution (McKay et al., 1979). This method involves defining the input space, represented by multiple dimensions or variables, and dividing it into equally probable intervals along each axis. Then, a single point is selected randomly within each interval and along each axis. This ensures that the samples are well-distributed and representative of the input space. The selected points are used to construct hypercubes within the input space. Each hypercube is characterized by one point per dimension. The points are randomly permuted within each hypercube to generate the final set of samples. Hypercube sampling provides a more uniform and efficient sampling compared to simple random sampling, as it ensures better coverage of the input space.

A more efficient and smarter tool for performing simulations is the Subset Simulation method (Au & Beck, 2003). This method enables the accurate estimation of low-probability failure events by dividing the event into more manageable subsets. The target rare event, representing a failure or undesirable outcome, is subdivided into a sequence of nested subsets with increasing probabilities. The algorithm performs sampling within these subsets, starting from the lowest probability subset and progressing to higher probability ones. For each subset, the algorithm uses Monte Carlo simulations or other

numerical techniques to estimate the probability of reaching the subset. The outcomes obtained from each subset are combined using conditional probabilities to estimate the overall probability of the rare event. Subset Simulation is particularly effective in cases where the failure event is associated with a very low probability, making it difficult to estimate using traditional Monte Carlo simulations. Breaking down the estimation process into a series of nested subsets allows for more accurate and efficient estimation of rare event probabilities while still maintaining precision.

2.3   PEER PBEE Framework

Conditional-based approaches, also called *IM*-based approaches, have been developed with the purpose to make seismic risk estimation a more practice-oriented and computationally affordable task. These approaches rely on the definition of a specific intensity measure (*IM*) that describes the ground motion intensity at the site of the structure (Cornell, 2005).

Currently, one of the most robust *IM*-based approach for the risk assessment used worldwide is the performance-based earthquake engineering (PBEE) methodology. In the last 20 years, performance-based earthquake engineering (PBEE) has evolved, from its first definitions in the SEAOC Vision 2000 (1995) and FEMA 273 (ATC/BSSC, 1997) reports, into the rigorous probabilistic framework formalized by the Pacific Earthquake Engineering Research (PEER) Center (Cornell & Krawinkler, 2000; Deierlein et al., 2003; Krawinkler & Miranda, 2004; Moehle & Deierlein, 2004), also referred to as the PEER PBEE framework. More recently, this framework was implemented in the FEMA P-58 report (FEMA, 2018) and in professional guidelines for design and assessment of tall buildings in California (e.g. Brandow, 2018; PEER, 2017).

The PEER probability-based framework is developed for seismic performance-based design and evaluation and it is designed to meet multiple performance objectives, each comprising a performance level at a seismic hazard level (Mackie & Stojadinovic´, 2001). Performance objectives are described in terms of decision variables *DV* and the evaluation of the frequency with which various levels of *DV* are exceeded during the period of interest is the main objective of the framework. However, a general probabilistic model

directly relating decision variables to seismic hazard intensity measures *IM* is too complex to be resolved in a rigorous and consistent manner. Instead, the PEER framework is based on the total probability theorem (Cornell & Krawinkler, 2000) so that the problem can be deaggregated in various sources of randomness and uncertainty. In particular, PEER PBEE methodology consists of four successive analyses: Probabilistic Seismic Hazard Analysis, Probabilistic Seismic Demand Analysis (or Structural Analysis), Probabilistic Seismic Capacity Analysis (or Damage Analysis), and Seismic Loss Analysis. Probabilistic Seismic Hazard Analysis (PSHA) involves determining the likelihood of different levels of ground shaking occurring in a specific area due to earthquakes. This is often done using historical seismic data and probabilistic models. It considers the uncertainty of the components that characterize the earthquake hazard, including factors like fault locations and recurrence rates of magnitude. Probabilistic Seismic Demand Analysis (PSDA) focuses on understanding how different types of structures (buildings, bridges, etc.) will respond to the ground shaking predicted by the hazard analysis. This involves considering factors such as building materials, construction practices, and design codes. It accounts for uncertainties arising from the structural aspects like material properties or damping, as well as uncertainties stemming from earthquake excitation characteristics, such as variations in ground motion features at the same hazard level. Probabilistic Seismic Capacity Analysis (PSCA) evaluates the potential impacts of the earthquake on people, property, and the environment and defines the level of damage corresponding to the response of the structure. Seismic Loss Analysis estimates casualties, economic losses and disruptions to critical infrastructure corresponding to damage, considering the uncertainty in damage distribution across the structure. **Figure 2-4** illustrates the stages of the PEER PBEE methodology.
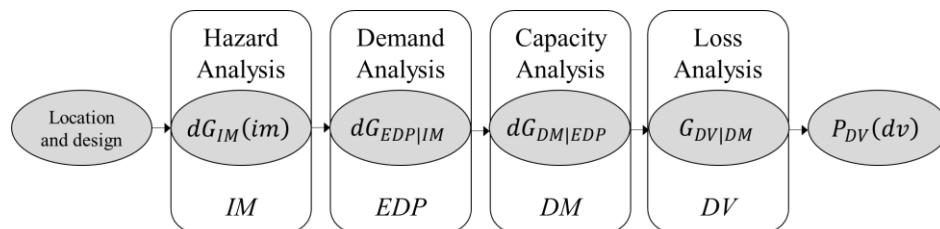
Figure 2-4 Stages of PEER PBEE methodology

This methodology reflects the probabilistic nature and the uncertainties associated with the seismic performance prediction. The outcome of each analysis is a probability of

exceedance distribution (Der Kiureghian, 2005). The framework combines ground motion hazard (*IM*, Intensity Measure), structural response (*EDP*, Engineering Demand Parameter), prediction of structural damage (*DM*, Damage Measure), and prediction of structural loss (*DV*, Decision Variable). The equation that expresses the mathematical formalization of the framework is:

$$P_{DV}(dv)$$
$$= \int_{DM} \int_{EDP} \int_{IM} G_{DV|DM}(dv|dm) \left| dG_{DM|EDP}(dm|edp) \right| \left| dG_{EDP|IM}(edp|im) \right| \left| dG_{IM}(im) \right|$$

(2-10)

The probabilistic models comprised in Equation (2-10) are:

- $G_{DV|DM}(dv|dm)$, the result of Seismic Loss Analysis. This model predicts the probability of exceeding a *DV* (e.g. repair cost or traffic capacity reduction) conditioned on a *DM*.

- $G_{DM|EDP}(dm|edp)$, the result of Probabilistic Seismic Capacity Analysis. This model provides the probability of exceeding a *DM* (e.g. crack density), conditioned on the *EDP*.

- $G_{EDP|IM}(edp|im)$, the result of Probabilistic Seismic Demand Analysis. This model provides the probability that a response parameter *EDP* (e.g. drift ratio) overcomes the value *edp*, given a value of a seismic hazard *IM*.

- $G_{IM}(im)$, the result of Probabilistic Seismic Hazard Analysis. This model predicts the probability of exceeding a seismic hazard intensity measure *IM* (e.g. spectral acceleration) in a given period of interest.

The deagreggation of the problem is possible only if the conditional probabilities involved in the framework are mutually independent (discrete Markov process). Additionally, the models should be efficient, meaning that the dispersion between the model and the data is small and constant over the entire range of variables.

Being able to outline a good deaggregated performance-based framework is not an easy task (Cornell & Krawinkler, 2000) but it is essential to simplify the problem and to decouple it into independent units that can be designed separately.

2.3.1 Probabilistic Seismic Hazard Analysis (PSHA)

PSHA is conducted to describe in a probabilistic manner the likelihood of ground shaking at a particular location over a specified period of time. PSHA takes into account the complex and uncertain nature of seismic events, adding some complexity to the procedure but making it a valuable approach for managing earthquake risks.

PSHA identifies and characterizes potential seismic sources within a given region. These sources can include known fault lines, subduction zones, and other geological features capable of generating earthquakes. The aim is to provide a probabilistic characterization of the intensity measure *IM* that includes the probabilistic definition of source-to-site distances and expected earthquake magnitudes associated with each source (Baker et al., 2021). The *IM* characterizes the intensity of the expected earthquakes and it must account for all the random variables involved in the seismic scenario. Indeed, the mathematical formulation that provides the probabilistic distribution of the *IM* is given by the following integral, found applying the Total Probability Theorem:

$$P_{IM}(im) = \int_S P_{IM|S}(im|s)f_s(s)ds \qquad (2\text{-}11)$$

where $f_s(s)$ is the joint probability density function (PDF) of all the quantities *S* involved in the seismic scenario (earthquake magnitude, source-to-site distance, etc.) and $P_{IM|S}(im|s)$ is the probability for *IM* exceeding a given treshold value *im* conditioned on the occurence of *S*. If only the magnitude *M* and the source-to-site distance *R* are considered to describe the seismic scenario and assuming they are mutually independent, i.e.

$$f_{M,R}(m,r) = f_M(m)f_R(r) \qquad (2\text{-}12)$$

equation (2-11) can be rewritten as:

$$P_{IM}(im) = \int_M \int_R P_{IM|M,R}(im|m,r) f_M(m) f_R(r) \, dm \, dr \qquad (2\text{-}13)$$

Equation (2-13) does not include any information about the frequency of occurrence of seismic events. However, it is possible to modify the equation including the mean annual rate of earthquake magnitudes M of interest ($M > m_0$) $v_M(m_0)$:

$$v_{IM}(im) = v_M(m_0) \int_M \int_R P_{IM|M,R}(im|m,r) f_M(m) f_R(r) \, dm \, dr \qquad (2\text{-}14)$$

$v_{IM}(im)$ represents the annual probability of seismic excitation expecting to exceed various levels of intensity IM and it provides the so-called seismic hazard curve.

To better understand how to characterize a seismic scenario, a detailed explanation of the source-to-site distance R and earthquake magnitude M random variables is provided in Appendix C.

To estimate the ground shaking produced by different magnitudes of earthquakes at a specific location, PSHA employs Ground Motion Prediction Equations (GMPEs), also called Ground-Motion Models (GMMs) or attenuation relations. These equations consider factors such as distance from the seismic source, site conditions, and local geological characteristics and provide estimates of ground motion parameters, such as peak ground acceleration and spectral accelerations (Baker et al., 2021). A GMPE consists of a regression on collected results which are used to model the probability of exceeding the intensity measure given the seismic scenario parameters, according to a log-normal distribution. **Figure 2-5** shows an attenuation relationship for magnitude 6.5. It can be observed how the intensity measure decreases when the distance from the source increases.
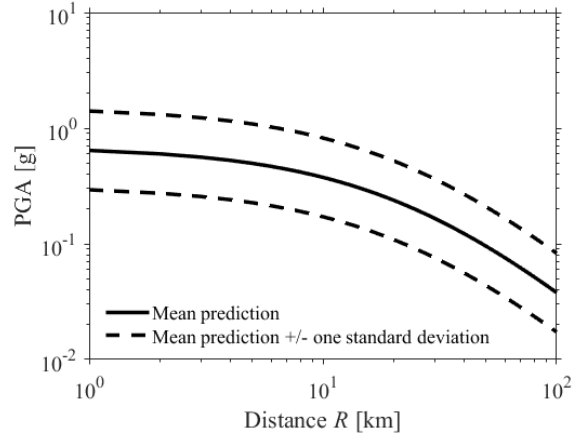
Figure 2-5 GMPM for PGA (magnitude 6.5)

Assuming a log-normal distribution, a general form of a GMPE is:

$$\ln(IM) = \mu_{\ln(IM)}(M, R, \Theta) + \sigma_{\ln(IM)}(M, R, \Theta) \cdot \varepsilon \qquad (2\text{-}15)$$

where $\mu_{\ln(IM)}(M, R, \Theta)$ is the predicted mean value of $\ln(IM)$ and $\sigma_{\ln(IM)}(M, R, \Theta)$ is the predicted standard deviation of $\ln(IM)$. These terms are functions of the magnitude (M), the distance (R) and other parameters (θ) and they are the outputs of the ground motion prediction model. ε is the standard normal random variable that accounts for the *IM* variability. The latest prediction models for $\mu_{\ln(IM)}(M, R, \Theta)$ and $\sigma_{\ln(IM)}(M, R, \Theta)$ can be very complex with numerous terms and coefficients.

It is common practice in structural analysis to use recorded ground motions, which are usually selected from a ground motion database. The primary challenge relates to the limited availability of data of strong ground motion from past seismic events. The existing dataset comprises a limited number of earthquakes and lacks records of strong ground motions. Consequently, performing a probabilistic analysis at the highest intensity measure levels requires the scaling of the recorded ground motion. Specifically, a low-intensity ground motion associated with a given seismic scenario is selected and then scaled to target a specific intensity. However, the scaling, forcing, or stretching procedures can modify the earthquake features, making the record no longer realistic and raising concerns within the scientific community. A valid alternative strategy may be using ground motion simulation models. These simulations, coupled with actual recorded ground motion data, serve to enrich the dataset.

19

Ground motion simulation models can be classified in 2 main classes: physics-based (source-based) models and site-based (stochastic) models (Douglas & Aochi, 2008). The first class comprises models that rely on a proper mathematical description which is intended to simulate the real physics of the fault rupture and the waves propagation, until the shallower ground layers (Atkinson & Silva, 2000; Brune, 1970, 1971). They are generally developed by seismologists or geophysicist who have knowledge on the physical process. In fact, the inputs required for these models are quantities not easily attainable and therefore they are not practice oriented but limited to research field.

The second class of models consists of stochastic methods that simulate the ground motions at a given site by means of ground motion models calibrated empirically on a set of past seismic events, without considering any physical aspect related to earthquake generation. There are different methods belonging to this class. Examples are spectral representation methods (Saragoni & Hart, 1973; Yamamoto & Baker, 2013), auto-regressive moving average (ARMA) models (Polhemus & Cakmak, 1981), filtered Poisson pulses (Cornell, 1964), filtered Gaussian white noise processes (Rezaeian & Der Kiureghian, 2010; Shinozuka et al., 1967).

One of the most representative and widely used stochastic ground motion model is the Atkinson and Silva (AS) ground motion (GM) model (Atkinson & Silva, 2000). This model considers the physical phenomena associated with a seismic event, including fault rupture and site-specific amplification effects. It provides the source-spectrum which represents the mean Fourier spectrum of the simulated accelerograms. The seismic input is defined through the moment magnitude M and the source-to-site distance R. The probability density function (PDF) for M for a given earthquake event is derived from the Gutenberg-Richter law, as described by (C-13). The ground motion is generated from a white noise represented by $w(t)$. The white noise is modulated in time using the function $e(t)$, resulting in the time function $z(t)=e(t)w(t)$. To obtain the amplitude and frequency content, $\bar{z}(f)$ (the Fourier transform of $z(t)$) is multiplied by the radiation spectra $\varepsilon_{mod}S(f)$. ε_{mod} is a scaling factor accounting for amplitude variability; $S(f)$ is a deterministic function of the frequency f (Jalayer & Beck, 2008). The radiation spectrum considers various physical factors affecting the propagation of seismic waves and

provides a spectral representation of the ground motion. The mathematical expression of $S(f)$ is reported in Appendix D.

The outcome of a hazard analysis is represented by a hazard curve, showing the relationship between a chosen intensity measure and the mean annual frequency (MAF) of exceedance (Algermissen et al., 1982; Bommer & Abrahamson, 2006; McGuire, 1976). In 1968, Cornell proposed (Cornell, 1968) the basic procedure to construct a hazard curve. The steps required for the evaluation of a hazard curve are (FEMA P-58-1, 2012; Kramer, 1996):

- For a given site, identify all the earthquake sources that may significantly affect the system;

- For each seismic source, characterize the probabilistic distribution of the source-to-site distances and the earthquake magnitude (and other parameters involved);

- Select an appropriate probabilistic relationship (Ground Motion Prediction Equation) between the site's intensity measure (*IM*) and a specified set of seismological parameters;

- Apply the Total Probability Theorem to estimate the probability of exceedance $P_{IM}(im)$.

The hazard curves depict the probability of experiencing ground shaking at various levels of intensity (e.g., PGA or SA) over a specific time frame (usually 50 years) at a given location. They provide a graphical representation of seismic hazard and are very useful in building codes and engineering design.

Figure 2-6 shows an example of a seismic hazard curve in terms of mean annual rate of exceedance $\nu_{IM}(im)$ of a defined value of *im*.
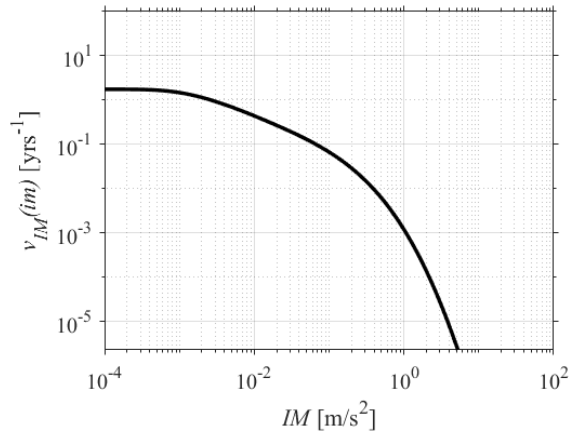
Figure 2-6 Illustrative example of a hazard curve

Sometimes, PSHA results are shown in terms of return periods of exceedance. The mean return period T_r represents the average interval between exceedances of that level of ground motion and it is defined as the reciprocal of the mean rate of occurrence:

$$T_r = \frac{1}{\nu(im)} \tag{2-16}$$

For example, a 2% probability of exceedance in 50 years corresponds to a 2,500-year return period

It can be useful to compute the exceedance probability of the intensity measure for a finite interval of time rather than the mean annual frequency of exceedance, which is a characterization of the occurrence rate per year. To do this, it is necessary to introduce a temporal distribution recurrence law for earthquake. One of the simplest model for the temporal distribution of the earthquakes occurrence is the Homogeneous Poisson model, according to which, seismic events have an equal chance of occurrence between consecutive events and these events are considered to be independent from each other. Indeed, those are strong assumptions and a certain level of interdependence exists among seismic events. For instance, seismic forces can release stress following an earthquake, leading to evolving conditions and the probability of events may fluctuate after a seismic event. However, if we exclude all aftershocks and foreshocks, this assumption yield a more realistic perspective. Nevertheless, this model is widely accepted and the most adopted.

22

According to this Poisson assumption, the probability of observing a number n of seismic events with magnitude higher than zero is given by this relation:

$$P[N = n, t] = \frac{(vt)^n e^{-vt}}{n!} \tag{2-17}$$

The parameters involved are the mean rate of occurrence of events v, the time interval of interest t and the number of samples n in the time interval. The mean value is equal to the variance of this distribution.

$$E[N] = Var[N] = vt \tag{2-18}$$

Figure 2-7 illustrates an example of Poisson distribution of earthquakes. It can be observed that the mean value is around 4.
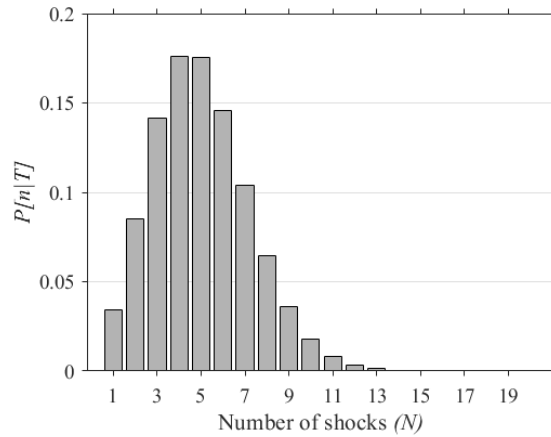
Figure 2-7 Example of a Poisson distribution

It is possible to derive the exceedance probability of events with $M > m_0$ in t from the complementary CDF (CCDF) (Probability of at least one event of $M > m_0$ in t), expressed by the following equation:

$$P[M > m_0] = 1 - P[N = 0, t] = 1 - e^{-vt} \tag{2-19}$$

This relation allows the link between the mean annual frequency and the probability of exceeding in the time interval t. Deriving Equation (2-19) with respect to time, the PDF of the distribution is obtained.

When assuming a Poisson model for the earthquake temporal distribution, it is possible to compute the probability of exceedance of a given intensity measure threshold for an interval of time of interest T_L:

$$P[IM \geq im; T_L] = 1 - e^{-\nu_{IM}(im)T_L}$$

(2-20)

2.3.1.1 Seismic Intensity Measures (IMs)

Seismic intensity measures refer to quantifiable parameters used to measure the intensity or strength of ground shaking during an earthquake. Seismic intensity measures encompass a range of parameters, including but not limited to:

- Peak Ground Acceleration (PGA): The maximum acceleration experienced by the ground during an earthquake.

- Peak Ground Velocity (PGV): The maximum velocity of ground movement during an earthquake.

- Peak Ground Displacement (PGD): The maximum displacement or movement of the ground during an earthquake.

- Spectral Acceleration (SA): Acceleration response in different periods or frequencies, typically obtained from a response spectrum.

- Average spectral acceleration (Sa,avg): Defined as the geometric mean of spectral acceleration values over a range of periods.

- RotD50Sa (Boore et al., 2006): The current state-of-the-art *IM* usually adopted by current GMPEs. Rot indicates the rotation of the two orthogonal components of the ground motion, D indicates that period-dependent rotations are used and 50 corresponds to the percentile value (the median value in this case).

The intensity measure must be chosen in such a way to fulfil two main requirements: *sufficiency* and *efficiency* of the intensity measure (Luco & Cornell, 2007). The

sufficiency is the ability to predict the structural seismic response independently from other ground motion characteristics. It allows the applicability of the total probability theorem. Magnitude, distances and other seismic scenario related parameters must be fully accounted by a sufficient intensity measure as it is the link for conditioning the structural response. The *efficiency* reflects the capability of the *IM* to predict the structural responses with low dispersion. In this case, a small set of ground motion records is required to provide a good estimate of the seismic demand.

2.3.2   Probabilistic Seismic Demand Analysis

While PSHA estimates the likelihood of ground shaking at a specific location, Probabilistic Seismic Demand Analysis (PSDA) focuses on assessing the probabilistic response of structures to these ground motions. PSDA uses the results from PSHA, which provide probabilistic estimates of ground shaking parameters like peak ground acceleration (PGA) and spectral accelerations (SA) for various levels of earthquake intensity and quantifies the probability of a structure experiencing various levels of damage or performance states under different seismic scenarios. This analysis helps engineers and decision-makers evaluate the seismic performance and potential damage of buildings and infrastructure. Engineers develop mathematical models of buildings or structures, that consider factors such as building materials, geometry, mass distribution, and damping characteristics, to simulate their behaviour during an earthquake. PSDA employs nonlinear static or dynamic analysis techniques to account for the nonlinear behaviour of structures under strong ground shaking and to capture phenomena like stiffness degradation, yielding of structural elements, and energy dissipation. The end result of a PSDA is the response spectra generated for each seismic hazard scenario defined by PSHA, that represent the variation of structural response.

For each intensity level of earthquake hazard, nonlinear time history analyses are performed to predict the structural responses using the ground motions selected for that specific intensity level. The responses are expressed in terms of chosen engineering demand parameters (*EDP*s). *EDP*s are measures that quantify the effects of an earthquake on a structure and can include displacements, accelerations, inter-story drifts, or other

quantities. The selection of appropriate *EDP*s depends on the specific project and the design criteria.

Thus, the PSDA of a system provides information about the demand of a seismic response parameter (*EDP*) including the description of uncertainties conditioned to the seismic intensity measure ($P(EDP|IM)$) (Freddi, 2012). **Figure 2-8** provides a brief description of the steps involved in PSDA.
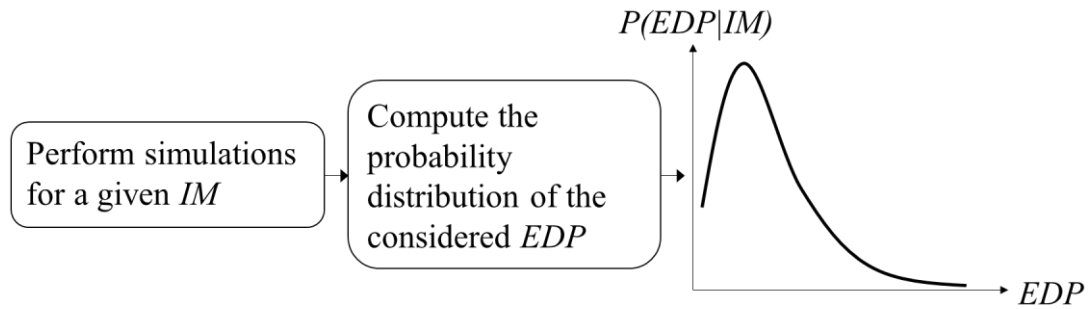
Figure 2-8 PSDA steps to derive probability distribution for *EDP*s

The probability of a global collapse event, denoted as $P(C|IM)$, can be approximated by the number of simulations resulting in global collapse divided by the total simulations conducted for the given intensity level. Conversely, the probability of no global collapse is defined as $P(NC|IM) = 1 - P(C|IM)$. These probabilities play a crucial role in the subsequent loss analysis stage.

To assign a suitable probability distribution, such as lognormal, to each considered *EDP*, the distribution parameters are calculated based on data obtained from simulations without global collapse. The total number of probability density functions resulting from PSDA is $N_{IM} \times N_{EDP}$, where N_{IM} represents the number of *IM* data points, and N_{EDP} represents the number of considered *EDP*s.

The most used conditional probabilistic methods are Incremental Dynamic Analysis (IDA), Multi-stripe analysis and Cloud Analysis.

Incremental Dynamic Analysis (IDA) is a parametric analysis method that aims at better understanding the relationship between the range of response (demands) and the levels of ground motion record, the assessment of the dynamic capacity of the entire structural

system, at having an enhanced insight into how structural response characteristics change as the intensity of ground motion increases and a better comprehension of the implications associated with more severe ground motion scenarios. IDA is useful when the assumption of homoscedasticity is not accepted, aiding in estimating the dispersion of the demand for a specific *IM* value. The method is considered as the dynamic equivalent of the static pushover analysis and involves performing multiple nonlinear dynamic analyses on a structural by scaling the same record using different values of the *IM* (Vamvatsikos & Allin Cornell, 2002). This methodology, thus, employs a single ground motion and does not account for the record-to-record variability. The results are usually presented in terms of curves of the structural response (commonly measured by an *EDP*) or a state variable (*DM*) versus seismic intensity measure *IM* (see **Figure 2-9**).
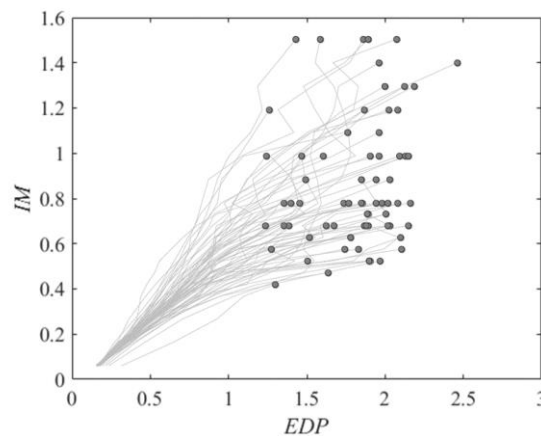
Figure 2-9 Illustrative example of IDA curves. The grey dots correspond to collapse state.

To address the limitations of IDA, Multi Stripe Analysis (MSA) method has been introduced and proven to provide accurate risk estimates with low computational cost (Scozzese et al., 2020). The method can be seen as a collection of Single-Record IDA using different ground motion records. The main difference between IDA and MSA is that IDA employs a single set of records, which are scaled to increasing amplitude levels, until the achievement of structural collapse (Jalayer & Cornell, 2009). In MSA, different sets of records are adopted for every intensity measure. **Figure 2-10** shows the steps of the Multi-Record IDA process. The first step to perform MSA is to discretize the hazard curve according to different intensity levels and for each of these levels, select a given number of recorded ground motions. All the ground motion records are scaled to a

common value of an appropriately chosen *IM* (i.e. the spectral acceleration corresponding to the first modal period T_1). Nonlinear dynamic analyses are performed and for each intensity measure, a stripe of outcomes is obtained. Each dot represents the maximum registered value of the parameter of interest for a given *IM*. The resulting plot of an MSA shows the stripes at each *IM* level.
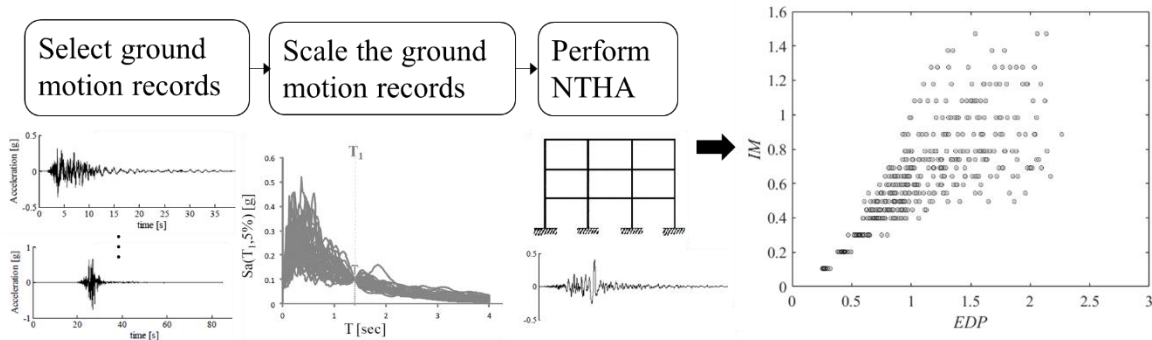
Figure 2-10 MSA process

Cloud Analysis method (Cornell et al. 2002) employs a set of unscaled recorded ground motion time-histories used to perform structural analysis (NTHA) (**Figure 2-11**). The aim is to collect a cloud of *IM-EDP* (intensity-response). The method involves the use of Probabilistic Seismic Demand Models (PSDMs) and regression analysis to compute the conditional mean and standard deviation of *EDP* given *IM* under the common assumption of lognormal distribution (Shome & Cornell, 1999). The simplest regression model is the linear model between *IM-EDP* natural logarithms (Baker & Cornell, 2006) (see Paragraph 2.3.2.1). An example of cloud analysis is shown in **Figure 2-12** below where grey points are observed values, obtained through NTHA and the black line represent the regression model.
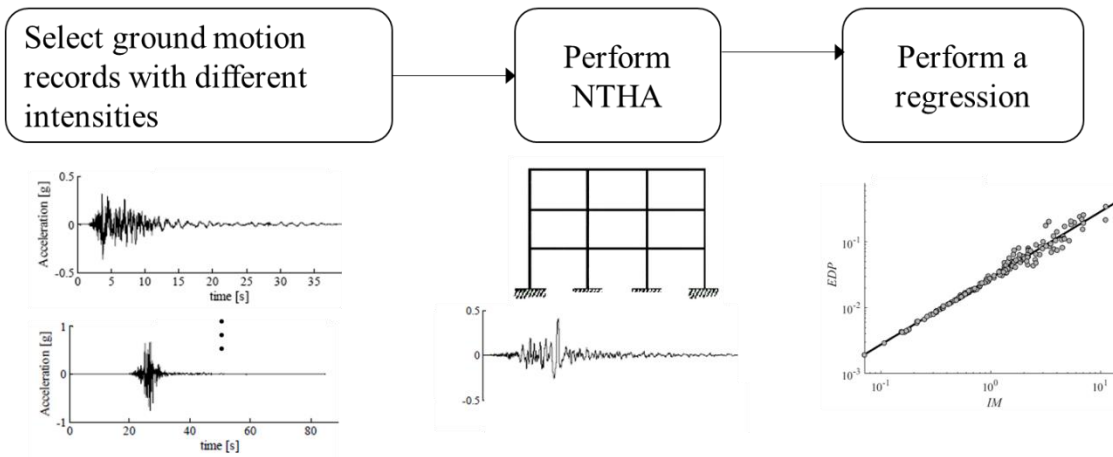
Figure 2-11 Cloud analysis process
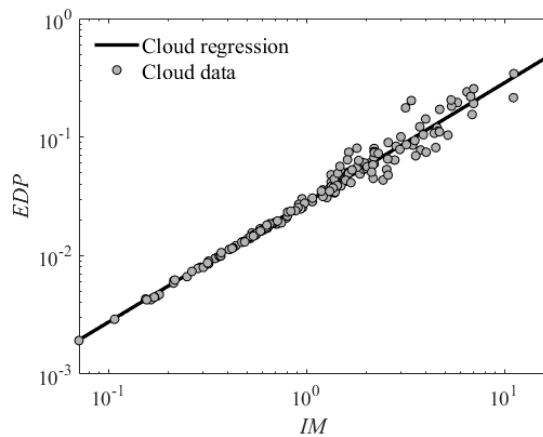
Figure 2-12 Example of a cloud analysis model

2.3.2.1 *Engineering Demand Parameters (EDPs)*

Engineering demand parameters (*EDP*s) refer to quantities used to characterize the demand on a structure or system during an extreme event. They can be divided into global and local *EDP*s. Global *EDP*s are used to provide a generic description of the structural behaviour but local parameters can more realistically and efficiently describe the mechanisms of failure for structural vulnerability evaluations (Radomir, 2015), especially if the structure has low-ductility. Several global damage indices have been proposed in scientific literature which can be classified into different categories: cumulative, non-cumulative, combined, displacement-related, energy-related, just to name a few. Concerning displacement-related damage indices, the attainment of a certain limit state is assessed from the exceedance of a maximum displacement threshold and thus of a

maximum deformation. Energy-related damage indices refer to the case in which the damage is related to energy dissipated, for example, through a hysteretic response. In addition, there are hybrid indices that essentially combines the ductility demand with the dissipated hysteretic energy to obtain a better estimate of the cyclic load effect. One of the most used hybrid index for safety assessment is the Park and Ang Index (Park & Ang, 1985). Global *EDP*s, used to study the overall structural damage, are characterized by a reduced computational effort but, in structures with low ductility, can lead to inaccurate results. Therefore, it is necessary to study local *EDP*s in order to have a more realistic estimation of the structural degradation. The correct choice of these parameters can be made analysing the possible collapse mechanisms of the structural component under examination. Among the local indices, we can list the following: bending moments, curvatures, rotations, strain for steel and concrete fibres, forces and deformations, strength of cross-section, peak absolute accelerations, residual displacements, peak transient displacements (Radomir, 2015). Different *EDP*s can be employed to evaluate the damage of different components in a structure. For instance, it is possible to use inter-story drift for the structural system of a building, while office or laboratory equipment in the same building can be assessed using floor acceleration (Günay & Mosalam, 2013).

2.3.2.2 *Probabilistic Seismic Demand Model (PSDM)*

A Probabilistic Seismic Demand Model (PSDM), known also as *regression model*, is a mathematical representation used to relate the probability distribution of ground motion *IM* to *EDP* measures. It provides a statistical description of the seismic demands that structures or systems may experience during an earthquake and it can be seen as the link between PSDA and PSHA (Shome et al., 1998). The PSDM takes into account various parameters, including the seismic source characteristics, local site conditions, and structural properties, to model the uncertainty associated with ground motion.

The selection of *IM-EDP* pairs is crucial for a successful PSDA. The properties that an optimal PSDM should have are efficiency, effectiveness, sufficiency and practicality. An *IM-EDP* pair in a demand model is practical when it aligns with engineering principles and can be readily derived from available ground motion measurements (for *IM*) and

nonlinear analysis response quantities (for *EDP*). It is crucial for both intensity and demand measures to maintain statistical independence from ground motion characteristics such as moment magnitude and epicentral distance. This condition is essential to achieve deaggregation. Demand models adhering to such conditional statistical independence are considered sufficient. The effectiveness of a demand model is evaluated by its ease of integration within a deaggregated performance-based design framework. The model gains credibility when the outcomes show strong correlations with existing experimental data.

The relationship between the structural demand *EDP* and *IM* was proposed by Cornell et al. (2002) to be approximated by a power model:

$$EDP = \alpha(IM)^\beta \tag{2-21}$$

where α and β are regression coefficients. Equation (2-21) can be transformed into a linear equation in the log-log space, as follows:

$$\ln(EDP) = \ln(\alpha) + \beta \ln(IM) \tag{2-22}$$

Employing a log-log linear demand model facilitates the closed-form evaluation of the integrals within the deaggregated performance-based design framework. Coefficients α and β are determined through linear regression analysis of the logarithms of the *IM-EDP* data, resulting in a line that represents the *IM-EDP* data when plotted on a log-log scale (as illustrated in **Figure 2-13**). The dispersion β_{EDP} of the *IM-EDP* data concerning the regression fit, defined as the standard deviation of the logarithm of regression residuals for the demand measure (Cornell et al. 2002), is a metric describing the variability of *EDP* given *IM*.

$$\beta_{EDP} = \sqrt{\frac{\sum_{i=1}^{n}[\ln(EDP_i) - (\ln(a) + b\ln(IM_i))]^2}{n-2}} \tag{2-23}$$

An efficient demand model minimizes dispersion, thereby necessitating a reduced number of distinct nonlinear time-history analyses to compute coefficients α and β with the same level of confidence.
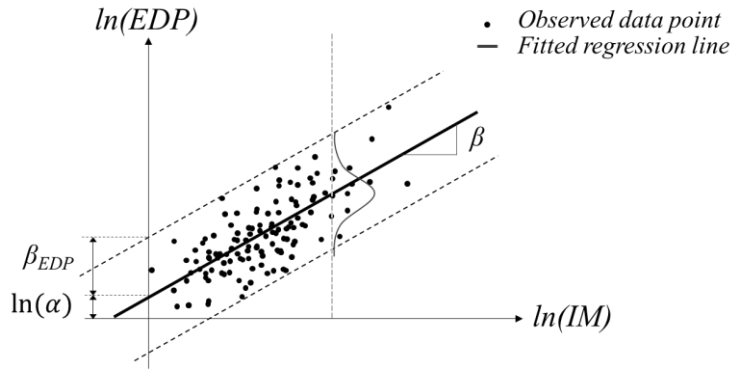
Figure 2-13 Illustrative example of a linear model

In Equations (2-22) and (2-23), *EDP* represents the value of seismic demand obtained from nonlinear dynamic analysis, and *n* is the total number of recorded responses. There is no general consensus on which *IM* to employ in PSDMs for bridges. For instance, Freddi et al. (2017) identified spectral acceleration at a 1.0-second period and peak ground velocity as the most effective structure-independent *IM*s. Conversely, Ma et al. (2019) emphasized peak ground acceleration as the optimal *IM* for the drift ratio model of bridge columns.

The traditional PSDM (Equation (2-21)) is the simplest approach for developing demand models of bridge components but it is afflicted with numerous limitations that can result in inaccurate predictions of demands and raise concerns about the reliability of associated fragility and resilience assessments. The limitations are due to the nonlinear behaviour of structures, so the linear model could be invalid for the entire *IM* range of interest. Researchers have tried to improve the traditional PSDM formulation. It has been found that a good fit can be obtained by adopting a bilinear regression. Many authors developed fragility curves based on bilinear regression models (Aljawhari et al., 2021; Bai et al., 2011; Freddi et al., 2017; Gardoni et al., 2002, 2003; Ramamoorthy et al., 2006). A bilinear model can be written as:

$$\ln(EDP)$$
$$= \begin{cases} \beta_{10} + \beta_{11} \ln(IM) + \varepsilon_1, & \ln(IM) \leq \ln(IM^*) \\ [\beta_{10} + \beta_{11} \ln(IM^*)] + \beta_{21}[\ln(IM) - \ln(IM^*)] + \varepsilon_2, & \ln(IM) > \ln(IM^*) \end{cases} \quad (2\text{-}24)$$

β_{10} controls the intercept of the first slope while β_{11} and β_{21} control the inclination (see **Figure 2-14**). $\ln(IM^*)$ identifies the point of intersection of the two segments. Two different dispersions, one for the first segment and one for the second segment, must be considered. The model parameters $\beta_{10}, \beta_{11}, \beta_{21}, \ln(IM^*)$ can be estimated by nonlinear least square regression.
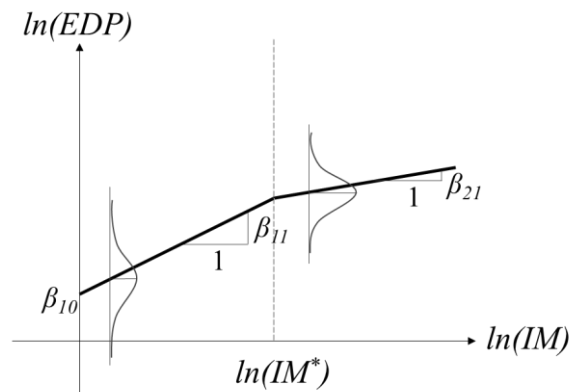
Figure 2-14 Illustrative example of a bilinear model

The PSDM formulations are typically conditioned on a single predictor, which is usually an *IM*. However, when dealing with multiple predictors, it is necessary to employ parameterized metamodels like the Polynomial Response Surface Model (PRSM), Multivariate Adaptive Regression Splines (MARS), and Artificial Neural Networks (ANN) to effectively handle these situations (Ghosh et al., 2013; Mangalathu et al., 2018; Towashiraporn, 2004).

A multiple linear (or multilinear) regression model is used to assess the relationship between multiple independent variables and one dependent variable. Unlike simple linear regression, which involves only one independent variable, multilinear regression considers several predictors to model the variability in the dependent variable. Multiple linear regression makes all of the same assumptions as simple linear regression:

- Homogeneity of variance (homoscedasticity): the error size of the in the prediction doesn't change significantly across the values of the independent variable.
- Independence of observations: the observations are collected using statistically valid sampling methods and there are no hidden relationships among variables.
- Normality: The data follows a normal distribution.

33

The generic formula for a multiple linear regression in the logarithmic space is:

$$y = \beta_0 + \beta_1 X_1 + \cdots + \beta_n X_n + \varepsilon \qquad (2\text{-}25)$$

where y is the predicted value of the dependent variable, $\beta_0, \ldots, \beta_n$ are the regression coefficients, $X_0, \ldots, X_n$ are the independent variables and ε is the model normal error.

In multiple linear regression, it is possible that some of the independent variables are actually correlated with one another, so it is important to check these before developing the regression model. If two independent variables are too highly correlated ($R^2 > {\sim}0.6$), then only one of them should be used in the regression model. The coefficient of determination, denoted as R^2, is a statistical measure that represents the proportion of the variance in the dependent variable f_i that is predictable from the independent variables y_i in a regression model. It quantifies the goodness of fit of the regression model, providing insights into the proportion of the response variable's variability that is captured by the predictor variables.

$$R^2 = 1 - \frac{\sum_i (y_i - f_i)^2}{\sum_i (y_i - \bar{y})^2} \qquad (2\text{-}26)$$

$\bar{y}$ is the mean of the observed data. The value of R^2 ranges from 0 to 1: $R^2 = 0$ indicates that the model does not explain any variability in the dependent variable. $R^2 = 1$ indicates that the model perfectly explains the variability in the dependent variable.

A model that considers several multiple linear regression models simultaneously is called multivariate regression model, where there are multiple response variables, linearly modelled in relation to several predictor variables. In other words, a multivariate regression refers to cases where Y is a vector of dependent variables:

$$Y = X\beta + \varepsilon \qquad (2\text{-}27)$$

for a predictor vector X.

The model error term ε accounts for the difference between the model and the observed data and the record-to-record variability and it is usually assumed to be normally

distributed. Different methods can be adopted to compute the error term. One of those is the sample regression residual covariance (SCOV) method which adopts a constant zero mean normal distribution to model the correlated error terms (Du & Padgett, 2020). The error covariance matrix is computed as follows:

$$\hat{\Sigma}_{SCOV} = \frac{E^T E}{n}$$

(2-28)

where E is the matrix of the sample regression residuals.

2.3.3 Probabilistic Seismic Capacity Analysis

Probabilistic Seismic Capacity Analysis (PSCA) is a crucial component of the PEER framework and consists in the assessment of the probability of exceedance of a fixed damage level or limit state, conditioned to the response of the structure *P(DM|EDP)*. PSDA and PSCA together are classified under the name of Seismic Vulnerability Assessment with the aim to provide the seismic vulnerability of the system (*P(DM|IM)*).

The outcome of PSCA is the fragility function, which is a mathematical expression that relate the probability of reaching or exceeding specified damage states (e.g., slight damage, moderate damage, collapse) to the seismic intensity. These functions provide valuable insights into the vulnerability of the structure. PSCA informs decision-making processes by helping engineers, policymakers, and building owners understand the likelihood of various performance outcomes and make informed choices regarding retrofitting, repair, or replacement strategies. Based on the results of PSCA, engineers can recommend retrofitting or mitigation measures to enhance a structure's seismic resilience. These measures are tailored to address the specific vulnerabilities identified in the analysis.

Once PSDMs have been established, it is possible to derive an analytical solution to construct the fragility curve. This solution considers various sources of uncertainty through an indirect approach. The failure of the structure is assessed by comparing the

demand against the capacity. In this probabilistic approach, the demand and the capacity do not have a unique value, but they are described by random variables that follow a probabilistic distribution. Therefore, it is necessary to define probabilistic models for the demand (x_D) and the capacity (x_C) and to include all available information about the statistical characteristics of the parameters involved. For a structural component, the probability of failure can be expressed by:

$$P_f = P(x_C \leq x_D) = P(x_C - x_D \leq 0) = \int_{-\infty}^{\infty} f_C(x) f_D(x) dx \qquad (2\text{-}29)$$

where x_D is the demand and x_C is the capacity which are represented as random variables - statistically independent of each other - with probability density function $f_D(x)$ and $f_C(x)$ respectively. The exact solution of this integral is possible, but only in the case the random variable is described by multivariate standard normal random variables and the limit state function is a linear function of the random variable. Numerical approaches that approximate the solution can be employed in most practical applications.

2.3.3.1 Fragility Curves

A fragility curve is the graphical representation of the damage exceedance probability given a level of ground shaking intensity. These curves are independent on load design and this allows a better identification of the effect of uncertainty, especially in the case of significant demand variability as for floods or earthquakes. The general equation of a fragility curve (or conditional probability) is expressed by (Billah & Alam, 2015):

$$fragility = P[DM|IM] \qquad (2\text{-}30)$$

Several equations were developed based on Equation (2-30); however, other authors, as Yamaguchi & Yamazaki (2000), Kirçil & Polat (2006) and Ibrahim & El-Shami (2011), predominantly employed the following equation:

$$P[DM|IM] = \phi\left[\frac{\ln(DM) - \mu_{\ln(DM)}(IM)}{\beta_{\ln(DM)}}\right] \qquad (2\text{-}31)$$

where $\phi(\cdot)$ is the standard normal cumulative distribution function, $\mu_{\ln(DM)}(IM)$ is the median value of the structural capacity, and $\beta_{\ln(DM)}$ is the logarithmic standard deviation,

or dispersion of the capacity. It is common to assume homoscedasticity of the demand model ($\beta_{DM|IM} = \beta_{DM}$), as observed in studies by Bai et al. (2011), Celik & Ellingwood (2010). This equation found widespread usage and was extensively tested by Yamaguchi and Yamazaki across diverse structural types.

In a fragility curve, the x-axis represents the intensity measure (*IM*), and the y-axis represents the probability of exceeding a certain damage or performance level (*DM*) (see **Figure 2-15**). The curve depicts the likelihood of experiencing damage or reaching a specified level of damage given a particular intensity measure. Different threshold values representing different damage state conditions can be chosen. For every threshold level, a different fragility curve expressing the probability of exceeding that specific threshold is obtained (**Figure 2-16**).
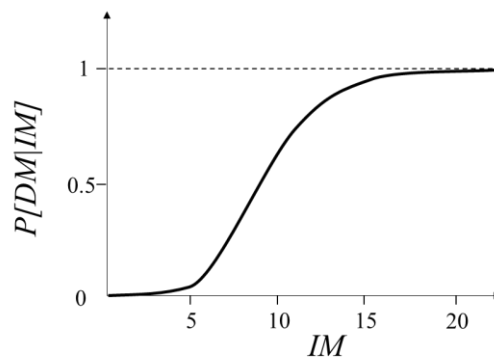
Figure 2-15 A typical fragility curve
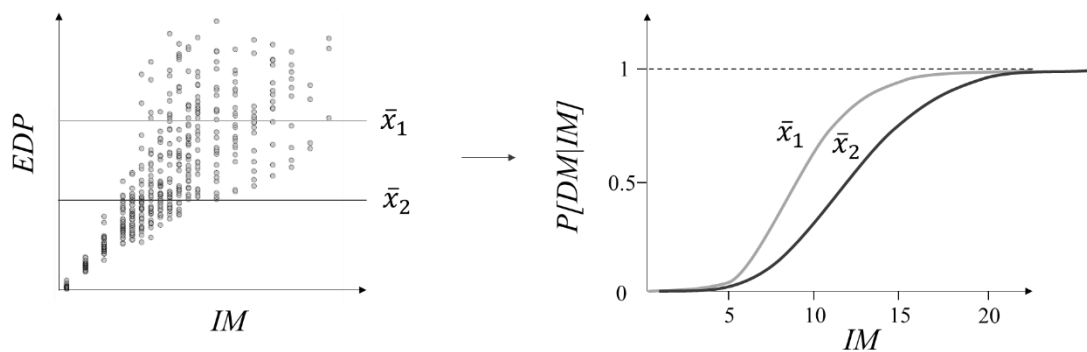
Figure 2-16 Two different fragility curves corresponding to two damage thresholds $\bar{x}_1$ and $\bar{x}_2$.

The probabilistic seismic assessment of structures therefore requires the definition of accurate fragility curves describing the vulnerability of engineering structures to seismic damage (Flenga & Favvata, 2021).

Fragility curves can be generated experimentally (Vosooghi & Saiid Saiidi, 2012), analytically (Mander & Basöz, 1999; Moschonas et al., 2009; Shinozuka et al., 2000), empirically (Basöz & Kiremidjian, 1998; Rossetto & Elnashai, 2003; Sarabandi et al., 2004) or based on the opinion of experts (Applied Technology Council (ATC), 1985; Rossetto & Elnashai, 2003).

Expert-opinion fragility curves can prove unreliable since they are based on professionals' experience and judgement. Empirical fragility curves are developed on the basis of damage observation from previous seismic events while experimental fragility curves are generated from experimental outcomes. If there are no data available from past earthquakes, it is possible to derive fragility curves employing results from analytical simulations: data can be obtained from spectral analysis, non-linear static analysis or non-linear dynamic analysis and in this is the case of analytical fragility curve. There is one last method to obtain such curves: it can be termed as hybrid method and it combines two or more of the above approaches. For example, in Kappos et al. (1995) the authors proposed a hybrid methodology that involves empirical and analytical approaches. In Kappos et al. (2006), the risk assessment of reinforced concrete and masonry buildings implicates the use of a hybrid method which combines statistical observations derived from earthquake-damaged structures with results from nonlinear static or dynamic analyses. Taking into consideration analytical fragility curves, it is necessary to determine the uncertainties concerning the demand and the capacity. In Argyroudis et al. (2018) the authors provide a comprehensive summary and review of fragility curves used for different transportation infrastructures under seismic forces, outlining key parameters and limitations associated with each. Many methodologies of developing analytical fragility curves can be found in literature: the maximum likelihood estimation method, the moment method, the probabilistic seismic demand model, Monte Carlo method, IDA, methods based on Markovian model, just to name a few. The method of maximum likelihood maximizes the likelihood of generating observed data in order to obtain the fragility curve parameters (Baker et al. 2011). Porter et al. (2007) explained the moment method where

the parameters of the fragility curves are deduced from the observed intensities of the earthquake. For a specific *IM* level, it is possible to assess the failure rate of the system by individually comparing the demand samples with the capacity samples. This evaluation allows for the determination of the proportion of cases in which the system fails and consequently, the probability of failure for that particular *IM* value. The same procedure needs to be repeated for all *IM* levels.

Fragility curves are tools used to predict potential damage during an earthquake, acting as a means for seismic risk assessment. These curves offer insights into the expected physical damage resulting from the most powerful earthquake (mainshock). Beyond this, they are instrumental in evaluating the likelihood of aftershocks, aiding decisions regarding building re-occupancy post-earthquake. Additionally, fragility functions play a direct role in minimizing damage costs and loss of life during seismic events. Consequently, fragility curves become essential decision-making tools in both pre- and post-earthquake scenarios, potentially influencing future local building code provisions.

2.3.4   Seismic Loss Analysis

Seismic loss analysis is the last stage of the PEER PBEE methodology. This process allows to assess the potential economic, social, and structural losses that may occur due to seismic events. It involves quantifying potential losses in terms of infrastructure damage, economic loss, casualties, and social disruption. In particular, the analysis aims to estimate the direct financial losses incurred due to damage to buildings, infrastructure, and other assets (including repair and reconstruction costs), to assess the economic impact caused by business interruption, loss of productivity and market disruptions, to evaluate the social and environmental consequences and to estimate potential human casualties and injuries resulting from the seismic event, considering factors like building collapse, infrastructure damage, and population density.

The data on damage derived from PSCA is converted into final decision variables (*DV*s). These *DV*s are directly applicable in the design process and decision-making. The most frequently used *DV*s are:

- Fatalities: The count of deaths directly resulting from damage to the structure.
- Economic Loss: Monetary loss incurred due to repair costs for damaged components of the structure or replacement of the facility.
- Repair Duration: The duration required for repairs, during which the structure is non-functional.
- Injuries: The count of injuries resulting directly from damage to the facility.

These first three DVs are commonly referred to as the "3 Ds" - deaths, dollars, and downtime.

The probability of exceedance of losses at various damage measures (DMs) is determined through loss functions. **Figure 2-17** shows that the loss curve $P_{DV}(dv)$ is the combination of the loss curves for individual structural and non-structural components an example of a loss curve.
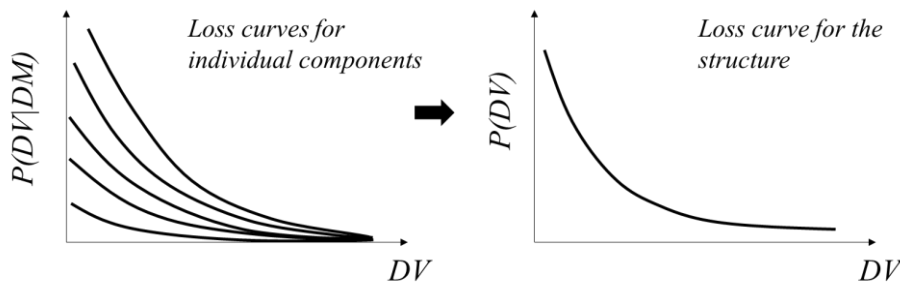
Figure 2-17 Loss function

The loss curve is derived through the total probability theorem combining hazard, demand, capacity and loss analyses. The process of calculating the loss curve involves the following (Günay & Mosalam, 2013):

- Identify the loss functions for each component j in the structure for each DM, denoted as $P(DV_j|DM_k)$.
- Combine the results of loss and capacity analyses for each component: $P(DV_j|EDP_j) = \sum_k P(DV_j|DM_k)P(DM_k|EDP_j)$.
- Determine the probability of exceedance of DV for each component under the condition of no global collapse NC, $P(DV_j|NC, IM) = \sum_k P(DV_j|EDP_j)P(EDP_j|IM)$.

- Aggregate the results for each structural component to determine the overall exceedance probability of *DV* for the entire structure for a given *IM* under the condition of no global collapse, denoted as $P(DV|NC, IM) = \sum_j P(DV_j|NC, IM)$.
- Combine the results for non-collapse and collapse cases and determine the overall exceedance probability of *DV* for the structure for a given *IM:* $P(DV|IM_j) = P(DV|NC, IM)P(NC|IM) + P(DV|C, IM)P(C|IM)$.
- Include the hazard analysis results: $P(DV) = P(DV|IM)P(IM))$. This represents the probability of exceedance of *DV* in *T* years.

Developing strategies to mitigate the identified risks and reduce potential losses is the main goal of Loss Analysis. For example, (Argyroudis et al., 2021) proposed a risk and resilience assessment framework that encloses the estimate of direct and indirect losses due to traffic disruption. A novel cost-based resilience index is presented and different restoration strategies are explored and assessed. The indices that estimate direct and indirect losses can streamline the allocation of resources, planning, and interventions for asset owners.

Seismic loss analysis is crucial for disaster risk reduction and helps in the development of effective policies, emergency response plans, and risk management strategies. It plays a significant role in enhancing resilience and minimizing the adverse effects of seismic events on communities and economies.

2.4 Extension of the framework to multiple earthquakes for damage accumulation

In the previous chapters, we discussed the fundamentals of the PBEE framework and its application to single earthquakes. However, in reality, structures are exposed to multiple earthquake events during their lifetime. Understanding the cumulative damage caused by multiple earthquakes is essential for assessing the long-term performance and resilience of structures. This chapter explores the extension of the PEER PBEE framework to account for damage accumulation over multiple earthquakes.

Most earthquakes form part of a sequence, related to each other in terms of location and time. A typical sequence consists of foreshocks, a mainshock, and then aftershocks. Potential seismic damage can accumulate due to the impact of multiple earthquakes within a cluster and/or because the structure remains unrepaired between different clusters. In the context of performance-based earthquake engineering, the traditional framework often overlooks the accumulation of seismic damage. This oversight is primarily because PSHA typically focuses on mainshocks, and classical fragility curves only depict the failure probability for a given intensity in a single event. However, for a comprehensive life cycle assessment, the accumulation of seismic damage resulting from multiple events should be considered. Previous studies have shown that a Markovian model, incorporating damage accumulation across multiple mainshocks, can be effectively calibrated by preserving PSHA from the classical PBEE framework and substituting structural fragility with a set of state-dependent fragility curves. Remarkably, this Markov chain model remains applicable even when damage accumulates from multiple aftershocks following a known mainshock magnitude and location, provided aftershock PSHA replaces the traditional PSHA.

Damage and structural failure in bridges have been extensively documented following multiple earthquakes. Seismic events like the 1989 Loma Prieta, 1994 Northridge, 2010 Chile, and more recently, the 2017 Mexico City earthquake had substantial direct and indirect economic impacts on the countries affected. These events led to the necessity of incorporating seismic loads in structural design, especially in regions prone to frequent seismic activity.

Several studies have examined the accumulation of damage from a single shock defined by repeated cyclic loadings while there is a relatively scarce literature on structural damage accumulation due to repeated earthquakes. Ballio & Castiglioni (1994) proposed a method for the estimate of cumulative damage during an earthquake calculated through dynamic linear and non-linear analyses. Jeong & Iwan (1988) investigated the aftermath of loading-unloading cycles from a single earthquake shock on the accumulation of strain. Some papers on deterministic seismic damage accumulation of structures due to repeated earthquakes can be found. For instance,Murià-Vila & Toro Jaramillo (1998) conducted a study on building founded in soft soil under repeated earthquake excitations. Elnashai &

Bommer (1998) demonstrated that the ductility demand after a multiple earthquake scenario is in most of the cases lager than the ductility demand requested for a single shock scenario. In Amadio et al. (2003) the authors studied a single degree of freedom system under repeated seismic ground motion and analysed the behaviour of the system and the effects on damage accumulation. Nevertheless, all these studies do not consider the probabilistic nature of risk and the uncertainties of the structural behaviour but they examine the problem as deterministic. Moreover, taking into consideration only a short duration between seismic occurrences, they did not capture the damage accumulation.

Recently, innovative approaches evaluated the progressive structural degradation due to the accumulation of damage from repeated main-shock events during the lifetime of structures. It is found that in earthquake-prone regions there is a high probability of observing more than one damaging earthquake in a bridge's service life. It is fundamental taking into consideration the cumulative damage in the seismic design because it can significantly influence the reliability of the structure. In Kumar et al. (2012) the authors calculated the probability of occurrence of more than one damaging event and developed a probabilistic model for computing the degraded deformation capacity of flexural RC bridge columns as a function of cumulative low-cycle fatigue damage. They concluded that the fragilities of the columns for given deformation demand increases with the increase in the value of fatigue damage and the fragilities of ductile columns increase faster than the non-ductile columns. Ghosh et al. (2015) proposed an approach based on regression models for predicting damage accumulation based on earthquake intensity and damage history. Alternatively, Iervolino et al. (2016) described the progressive structural degradation using a homogeneous discrete Markov process through which the transition probabilities between different progressive damage states are derived, given the occurrence of an earthquake. Similarly, Gusella (1998) proposed a method that estimates the safety probability of masonry structures with cumulative damage. In the work, a finite number of discrete states represents the damage and the evolution of damage is characterized by a Markov chain. The results are then compared and analysed through a numerical model that does not consider the accumulation of damage. Heredia-Zavoni et al. (2000) found an analytical close-form solution based on Bayes theorem for the probability damage accumulation after a seismic event occurred give the information of

the inelastic structural response and the distribution prior to the event. The model is applied to a reinforced concrete frame and describes the evolution of secant stiffness through cycles of inelastic response. Tolentino et al. (2020) presented an alternative approach to calculate fragility curves for bridges. The method considers sequences of seismic loading, in an instant of time, for the damage accumulation analysing the nonlinear behaviour of the structure.

The degradation process due to seismic damage accumulation can be written in terms of residual capacity $c(t)$:

$$c(t) = c_0 - c_{tot}(t) \tag{2-32}$$

where c_0 is the initial capacity at time t=0 and $c_{tot}(t)$ is the total degradation at time t (Iervolino et al., 2016). If we represent the damage increment in a single seismic event with Δd_i, $c_{tot}(t)$ can be defined as sum of the damage increments due to all earthquakes events $N(t)$ in the time t (we ignore aging):

$$c_{tot}(t) = \sum_{i=1}^{N(t)} \Delta d_i \tag{2-33}$$

The computation of the structural failure probability due to the accumulation of seismic damage.

$$P_f(t) = F_T(t) = P[c(t) \leq c_{LS}] = P[c_{tot}(t) \geq c_0 - c_{LS}] \tag{2-34}$$

Equation (2-34) represents the likelihood that the structure exceeds a specific limit state c_{LS} at any point before t. Equation (2-34) also gives the cumulative probability function $F_T(t)$ in the lifetime T of the structure. Commonly, it is assumed that $N(t)$ (i.e. seismic events) follows a Homogeneous Poisson distribution with a constant rate parameter λ. Consequently, the probability of failure can be calculated as in Equation (2-35), involving an integral of the k-th order when assessing the distribution of accumulated earthquake damage based on the number of earthquakes and their ground motion intensity measures (*IM*),

$$P_f(t) = P[c_{tot}(t) \geq c_0 - c_{LS}] \tag{2-35}$$

$$
= \sum_{k=1}^{+\infty} P[c_{tot}(t) \geq c_0 - c_{LS}|N(t) = k] \cdot P[N(t) = k]
$$

$$
= \sum_{k=1}^{+\infty} P[c_{tot}(t) \geq c_0 - c_{LS}|N(t) = k] \cdot \frac{(\lambda \cdot t)^k}{k!} e^{-\lambda t}
$$

$$
= \sum_{k=1}^{+\infty} \int_{im} P\left[\sum_{i=1}^{k} \Delta d_i \geq c_0 - c_{LS}|IM = im, N(t) = k\right]
$$

$$
\cdot f_{IM}(im)d(im)\frac{(\lambda \cdot t)^k}{k!} e^{-\lambda t}
$$

When the occurrence of seismic events $N(t)$ can be described by a Homogeneous Poisson process, the IM in different earthquakes can be considered independent and identically distributed random variable (i.i.d. RV). The function $f_{IM}(im)$ is the product of marginal distributions $f_{IM_i}(im)$. Usually, a homogeneous Poisson process is used for mainshock scenarios. In the case of aftershock scenarios, a nonhomogeneous Poisson process with time-varying hazard rate $\lambda(t)$ is employed. The time interval considered is one year (i.e., $T = 365$ days) following a main shock event, after which the risk of aftershock usually decays to a negligible level (Luco et al., 2002). In the case of aftershock scenarios (nonhomogeneous Poisson process), the probability $P[N = k, T]$ of having N shocks in time T can be computed as:

$$
P[N = k, T] = \frac{\left[\int_0^T \lambda(t)\right]^k}{k!} e^{-\int_0^T \lambda(t)} \tag{2-36}
$$

The main challenge is determining the probability of capacity exceedance, given the IM and the number of earthquakes $P[\sum_{i=1}^{k} \Delta c_i \geq c_0 - c_{LS}|IM = im, N(t) = k]$. Different approaches can be employed to evaluate this probability. Iervolino et al. (2013) found a closed-form solution using gamma or exponential distribution to model earthquake damage accumulation, suitable to be applied to simple single degree of freedom (SDOF) elastic-perfectly-plastic structures when damage accumulation is based on hysteretic energy dissipation and the structural response in one earthquake does not depend on previous shock history.

Chapter 3 presents and compares different methodologies for the prediction of damage accumulation in structures subjected to multiple earthquakes within their lifetime. In particular, a Markov-chain based approach and four different PSDMs are analysed. The study results demonstrate the importance of considering the possibility of occurrence of multiple shocks in estimating the life-cycle performance of structures and highlight strengths and drawbacks of the investigated methodologies

2.5 Damage assessment and risk updating based on inspections and sensor data– Bayesian approaches

The problem of post-earthquake functionality and the estimation of aftershock risk is nowadays becoming crucial, especially if we consider strategical structures such bridges, and the introduction of an early-warning method able to detect damage in short time and warn the competent authorities in case of imminent risk is essential. It is of great relevance to be able to recognize whether a structure, though still standing, is failing or on the other hand, if a construction is still safe and capable of carrying loads despite the presence of signs of damage. At present, this task is under the responsibility of the officials in charge and it depends on their judgements. The inspections can be slow, resource-intensive, subjective and potentially inaccurate.

In recent years, many methodologies and frameworks have been introduced to address the issue with the aim to support the decision on opening the bridge to traffic. Franchin & Pinto (2009) proposed a criterion for deciding whether or not to allow traffic on a bridge based on the survival probability of a mainshock-damaged bridge under aftershock hazard. The criterion is based on the comparison between the risk of the intact structure and the risk of the mainshock-damaged structure. The method comprises two steps: in the first step they defined increasing damage states and the fragility curve that characterizes the damage states. They used probabilistic seismic hazard analysis to evaluate the risk of collapse. In the second phase, aftershock fragility curves are calculated and used to determine the aftershock intensities that lead the bridge to collapse. Comparing the two risks, it is possible to decide whether or not to open the bridge to traffic. The problem of the uncertain knowledge of the bridge state following the mainshock was, however, not

addressed in their study. They assumed that the bridge damage is both analytically and visually detectable and that a near real-time estimation of the mainshock source and site parameters is available.

Efficient tools for rapid loss assessment are required to improve timely emergency response and rescue operations and to provide precise loss estimates and accurate information to the public immediately after the occurrence of a major earthquake. Some methods utilize shake maps derived from seismic station data to determine seismic intensity, but the use of vulnerability fragility curves is still necessary to estimate damage, introducing significant uncertainty. Structural health monitoring (SHM) systems offer valuable information for seismic damage assessment. For instance, strain gauges can be used to measure the deformation of a concrete surface or to understand whether the concrete surface is cracked or not. Accelerometers are often employed to acquire the free and forced vibration modes

Erdik et al. (2010) provides an overview of recent developments in earthquake rapid response systems aimed at estimating earthquake losses in quasi real-time. It includes a critical discussion of various methodologies for earthquake loss estimation and summarizes the features of available loss estimation software. The existing near real-time loss estimation tools are categorized into two main groups based on the coverage area: Global Systems and Local Systems. Çelebi et al. (2004) described an advanced seismic monitoring system for a 24-story building, developed by the owner of the building, in collaboration with a federal agency with expertise in seismic monitoring of buildings, private consulting engineers, and a supplier. The system enables the real-time recording of accelerations, computation of displacements, and estimation of drift ratios. The drift ratio is an indicator of the building's damage condition. This system fulfils the requirement for rapid quantitative assessments and decisions on post-earthquake occupancy. The operational system appears promising for rapid post-earthquake building assessments, for long-term assessment and damage detection.

In Soyoz & Feng (2008), advancements to promptly identify elemental stiffness values of a structure in real-time during a seismic event that causes damage are introduced. The methodology is based on the extended Kalman filtering (EKF) method and it is validated

through experiments involving a large-scale realistic bridge model exposed to realistic seismic damage.

Data from sensors like accelerometers might be easily accessible, but typically offer insights only into specific response parameters. Furthermore, processing this data can be time-consuming before useful information regarding structural damage can be obtained. A way to overcome these limitations is to exploit Bayesian inference. Bayesian inference tools are used to update the knowledge of the state of damage of an infrastructure following an event, by fusing the a priori estimates of the damage with the measurements of observed variables correlated to the damage. For this purpose, the aim is to develop Bayesian Networks to facilitate multi-disciplinary risk analysis and to allow the assessment of the status of the infrastructure given some evidence (e.g. computing the reliability of a bridge given information about earthquakes or data from sensor). They can also be adopted for diagnostic purposes to identify the most likely causes of disruption.

Alessandri et al. (2013) proposed a method for evaluating post-earthquake bridge operability based on a rational combination of information derived from numerical analyses and in-situ inspections. A Bayesian approach was developed to update the mainshock damage probability and thus the aftershock risk using the observation made by visual inspections. The study showed that in-situ inspections could drastically affect and modify the damage estimates for a structure, helping to decide whether to open traffic on bridges.

In the study described in Montes-Iturrizaga et al. (2003), the authors developed optimal strategies for maintenance or repair of structures at minimum cost. They establish a damage threshold as a decision variable for the optimization of costs given an acceptable reliability level. The underlying concept is that the structural damage accumulates over seismic events until a certain level of damage is reached: if this threshold is exceeded, the structure requires to be repaired. The expected future costs and structural reliability as a function of damage threshold are then estimated. A Markovian model is used to describe the damage accumulation process and an algorithm to evaluate the transition probabilities between damage states is proposed. Furthermore, the paper examines how information obtained from the earthquake response of instrumented structures can be included and

used for maintenance strategies. Using a Bayesian approach, this information is utilized to update the probability distribution of the damage in order to increase the reliability and accuracy of the predictions about costs.

Tubaldi, Ozer, et al. (2022) developed a Bayesian network-based approach which involves integrating high-fidelity structural models with seismic event information, such as magnitude and epicenter location, which are typically available shortly after an earthquake. Additionally, intensity recordings from nearby seismic stations and data from a wide array of sensors have been incorporated. The probabilistic BN-based framework presented in the article uses diverse sensor data to evaluate seismic damage for critical structures under earthquake loading. The framework is applied to a two-span bridge model in a high seismicity zone. The study compares the effectiveness of sensing techniques using pre-posterior variance and relative entropy reduction metrics. Two measures for quantifying the reduction in uncertainty resulting from these observations are introduced, relying on the concepts of pre-posterior variance and relative entropy reduction. The research applies this framework to evaluate the effectiveness of different sensing strategies for rapidly estimating a bridge's response and losses during moderate and strong earthquake scenarios. Two alternative parameters are defined to quantify the effectiveness of data obtained from different sensor types in reducing uncertainty concerning structural damage. The first parameter is a variance-based effectiveness measure, calculated as the ratio of the standard deviation associated with the prior probabilistic distribution of the variable of interest to the "pre-posterior" value, which represents the expected value of the posterior variance derived from averaging across all potential observations from the sensors. The second measure is derived from information theory and relies on Kullback-Leibler divergence, measuring the reduction of relative entropy. The Bayesian network framework developed by Tubaldi, Ozer, et al. (2022) focused only on mainshock scenarios. In Chapter 4, an expansion of the same framework is presented to include aftershocks in the risk evaluation of bridge structures.

Bayesian Networks are powerful tools not only for seismic risk assessment but also in the context of structures exposed multiple hazards (Lee et al., 2019; Sakovych et al., 2022; Sperotto et al., 2017). In 2016, Gehl & D'Ayala introduced a method for developing multi-hazard fragility functions using system reliability methods and Bayesian Networks

(BNs). By decomposing a bridge system into its components, the approach isolates specific failure mechanisms and damage states. At the system level, Bayesian analysis estimates the probabilities of different failure modes based on these component states, allowing for accurate predictions of downtime or traffic reduction. Applied to a bridge exposed to earthquakes, ground failures, and floods, the BN framework predicts four levels of functionality loss as functions of peak ground acceleration and flow discharge, considering cumulative damage from multiple hazards.

The paper of Liu et al., 2015 proposes a three-level framework for multi-risk assessment. The first level uses a flow chart to guide users on whether a multi-hazard approach is necessary. The second level employs a semi-quantitative method to determine if a more detailed assessment is needed. The third level involves a detailed quantitative analysis using Bayesian networks. This framework, demonstrated with examples, is essential for sustainable development, land-use planning, and risk mitigation. It includes qualitative analysis, semi-quantitative evaluation of hazard interactions and dynamic vulnerability, and accurate quantitative assessment with Bayesian networks. This structured approach allows for systematic, step-by-step multi-risk assessment.

Gehl, 2017aims to create a methodological framework for multi-risk assessment of road infrastructure systems, with a focus on deriving fragility functions for bridges facing earthquakes, floods, and ground failures. Given that network performance relies on the functional states of its physical elements, harmonizing fragility models and damage scales across various hazards is essential. The framework begins by cataloging hazard-specific damaging mechanisms for each bridge component (e.g., piers, deck, bearings). It then derives fragility curves for these failure modes and maps their functional consequences in a damage-functionality matrix based on expert surveys. These failure modes are integrated at the bridge level for specific damage configurations. A Bayesian Network approach is developed to derive system fragility functions robustly and efficiently, providing probabilities of functionality loss and accounting for multi-hazard interactions. At the network level, a fully probabilistic approach integrates multi-risk interactions at both hazard and fragility levels, incorporating a temporal dimension to account for joint independent hazard events and cascading failures. Bayesian Networks are explored as an

alternative to conventional sampling methods for quantifying extreme events, highlighting the computational challenges of large and complex systems.

The following sub-section summarises basic concepts for constructing Bayesian Networks, with a particular focus on Bayesian Inference.

2.5.1 Constructing Bayesian networks

A Bayesian Network (BN), also known as a Bayesian belief network or probabilistic graphical model, is a graphical representation of probabilistic relationships among a set of variables. It's named after Thomas Bayes, an 18th-century statistician, and is rooted in Bayesian probability theory. It employs a Directed Acyclic Graph (DAG) – a graph with no cyclic paths (no loops), allowing efficient inference and learning – where nodes represent variables, and directed arches between nodes represent probabilistic dependencies between the variables. Each node is associated with a probability distribution that quantifies the uncertainty or belief about that variable given the state of its parent nodes (nodes that have arches directed towards it). Bayesian networks are used for modelling uncertainty, reasoning under uncertainty, and making predictions or inferences based on observed or partially observed data. They find applications in various fields like artificial intelligence, machine learning, medicine, finance, natural language processing, and more. They are useful for decision-making, risk assessment, diagnosis, and many other tasks that involve uncertainty and complex relationships between variables.

The key components of a Bayesian network are:
- Nodes (Vertices): These represent random variables or attributes that are part of the model. Each node corresponds to a specific variable or event.
- Arches (Directed): These represent the probabilistic dependencies between the variables. An arch from node A to node B indicates that A is a parent or direct influence on B.
- Conditional Probability Distributions (CPDs): These specify the probability of each variable given its parent variables. They represent the conditional probabilities of a node based on its parent nodes.

51

For a given variable V in a DAG, we can define:

- Parents(V): The parent nodes of V, which constitute the set of graph variables connected to V through an oriented arc, exiting themselves and directed towards V. For instance, in **Figure 2-18**, the parents of X_2 are X_5 and X_1.

- Descendants(V): The descendants of V, referring to the variables linked to V through an oriented path directed from V to them. For example, in **Figure 2-18**, the descendants of X_5 are X_2 and X_3.

- Non-Descendants(V): Variables that are neither parents nor descendants of V. In the figure, for instance, the non-descendants of X_5 are X_1 and X_4.

Figure 2-18 depicts a simple example of Bayesian Network, illustrating five random variables $X = \{X_1, \ldots, X_5\}$ and their associated probabilistic relationships. In this example, the random variable X_2 depends probabilistically on the variables X_1 and X_5, as indicated by the arrows. Using BN terminology, X_2 is a *child* of X_1 and X_5, while X_1 and X_5 are *parents* of X_2. Similarly, X_2 is defined conditionally on X_5 and X_3 is defined conditionally on X_2. Nodes without parents, like X_5 and X_1, are often referred to as root nodes.
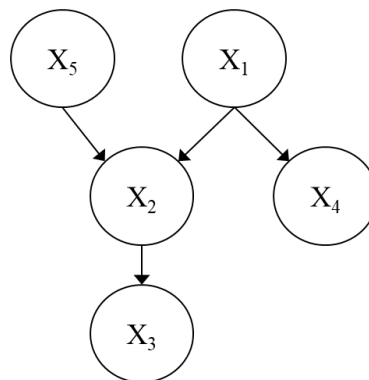
Figure 2-18 An example of a DAG

A Bayesian Network can encompass discrete, continuous, or both variables. When dealing with discrete variables, each node is associated with a set of mutually exclusive and collectively exhaustive states. There are no exact algorithms that can be used in a generic network with continuous variables. Consequently, a common approach involves discretizing the variables.

A DAG can be interpreted as a compact representation of the following relationship, defined as the independent statement:

$$I(V, Parents(V), Non\_Descendants(V)) \qquad (2\text{-}37)$$

Given the states of the parent nodes, each variable within a network is conditionally independent of the states of all non-descendant variables. This principle is referred to as the Markov assumption, and for a given generic Directed Acyclic Graph (DAG) G, it is denoted as Markov(G). When we perceive the DAG as a causal structure, Parents(V) represent the direct causes of variable V, while Descendants(V) symbolize the effects of V. The DAG depicted in **Figure 2-18** encloses the following statements:

$$I(X_3, X_2, \{X_5, X_1, X_4\})$$
$$I(X_2, \{X_5, X_1\}, X_4)$$
$$I(X_5, \emptyset, \{X_1, X_4\}) \qquad (2\text{-}38)$$
$$I(X_4, X_1, \{X_5, X_2, X_3\})$$
$$I(X_1, \emptyset, X_5)$$

The symbol $\emptyset$ indicates that the variables X_1 and X_5 have no parent nodes. Therefore, X_1 and X_5 are called root nodes.

It is necessary to define the probability distributions (*P*) of the different variables and their interrelationships when designing a BN. The relationships between variables are represented through conditional probability distributions (CPDs) of the form $P(X_j|X_i)$.

Bayesian Network with discrete variables

In a Bayesian Network with discrete variables, each node is associated with a Conditional Probability Table (CPT) that defines the probability of each possible state in relation to the values of its parent nodes. Specifically, for every variable *X* with its parent set *U*, the conditional probability *P(x/u)* is specified for each value *x* of variable *X*, corresponding to a specific state *u* of the parent node or nodes *U*. For nodes without parent nodes, a prior distribution is defined that assigns a specific probability value to each state. A Bayesian Network is fully defined when, in addition to the DAG, the conditional probability tables for each variable are provided (Darwiche, 2009).

Bayesian Network with continuous variables

In a Bayesian Network involving continuous variables, these variables are represented by continuous probability distributions. In the context of continuous variables, the probability distributions associated with each node in the Bayesian Network are typically continuous probability distributions, often characterized by probability density functions (PDFs). These PDFs describe the likelihood of the continuous variable taking on specific values. Performing inference and learning in Bayesian Networks with continuous variables involves integrating PDFs and CPDFs, often using numerical methods due to the continuous nature of the distributions

A BN is a graphical representation of a joint probability distribution (JPD) over all the variables, representing dependence and conditional independence relationships. The JPD can be expressed in terms of a product of CPDs, describing each variable in terms of its parents:

$$P(X_1, \dots X_n) = \prod_{i=1}^{n} P(X_i | X_{parents(i)}) \qquad (2\text{-}39)$$

Bayesian networks perform three principle tasks: (i) conducting probabilistic inference to estimate unobserved values based on available evidence, (ii) parameter learning and (iii) structure learning.

Probabilistic inference is the process that allows the updating of the probability distributions of a subset of variables within the BN after observing another subset of variables in the model (referred to as the evidence variables). In other terms, it allows calculating the posterior distribution of variables given the observed evidence. Indeed, a Bayesian network is a complete model that describes the random variables involved and their interrelationships and therefore it can be used to address probabilistic queries related to these variables. For example, the value of X_1 in **Figure 2-18** may be inferred from the values of the other variables, i.e. $P(X_1 | X_2, X_3, X_4)$. More generally, inferences of the values of a set of variables can be made given the evidence of another set of variables, by marginalising over unknown variables. The process of marginalization consists of considering all the values that the unknown variables might assume and averaging over them.

Theoretically, inference is calculated as a product of CPDs, exploiting Bayes' rule to compute the posterior probabilities. Given two generic variables X_A and X_B, the Bayes' formula reads:

$$P(X_A|X_B) = \frac{P(X_A, X_B)}{P(X_B)} = \frac{P(X_B|X_A) \cdot P(X_A)}{P(X_B)} \qquad (2\text{-}40)$$

where $P(X_A|X_B)$ is the posterior probability, $P(X_A)$ is the prior probability, $P(X_B|X_A)$ is the likelihood and $P(X_B)$ is the evidence.

However, computing inference in this way is hard and inefficient. Various techniques leverage the graph's structure to develop precise and efficient inference algorithms, including the sum–product and max–sum algorithms. Nevertheless, exact inference becomes impractical for many problems. Consequently, the adoption of approximation methods such as variational techniques and sampling approaches becomes necessary. The most commonly used exact inference methods include variable elimination, clique tree propagation, recursive conditioning and AND/OR search. In addition to exact inference methods, various approximate inference algorithms are employed, including importance sampling, stochastic Markov Chain Monte Carlo (MCMC) simulation, generalized belief propagation.

Probabilistic inference includes two distinct approaches: forward (predictive) analysis and backward (diagnostic) analysis. In forward analysis, the aim is to compute the probability distribution of any node within the BN based on known initial conditions or prior data. It involves propagating information from the initial state to predict future states. Backward analysis is the opposite of forward analysis and it involves working backward from a known observation to determine the possible causes or prior states that led to that result. Backward analysis in Bayesian networks is particularly powerful, as highlighted by (Bobbio et al., 2001).
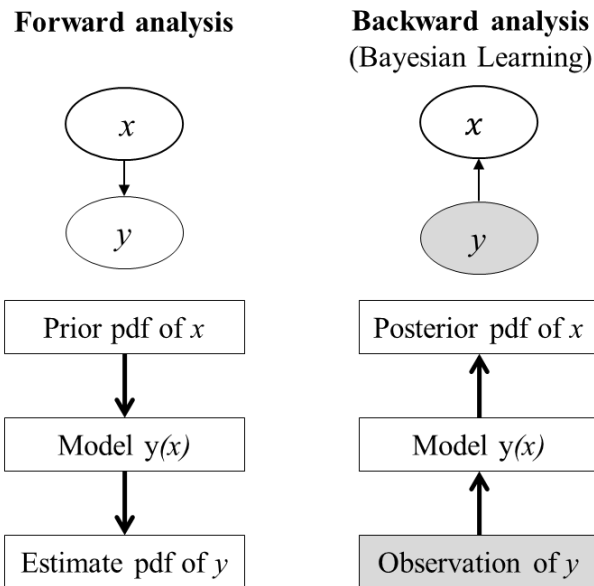
Figure 2-19 Graphical illustration of forward and backward analysis

The ability of BNs to easily compute the conditional distribution of any subset of variables in the BN given the information about the states of any other variable makes it highly suitable for applications in near-real-time seismic risk assessment and decision support. To apply precise inference algorithms effectively, discretization of all continuous random variables within the BN is usually required, excluding cases like linear functions of continuous Gaussian nodes that do not have discrete children.

Parameter learning and structure learning are data-driven techniques. Parameter learning involves estimating the unknown parameters within the conditional distributions in Bayesian networks (BNs) based on the available data to maximize their likelihood. This estimation process can be accomplished through methods like the expectation-maximization algorithm, as described in (Moon, 1996). On the other hand, Structure learning focuses on determining the graphical structure of the Bayesian network, including the arrangement of nodes and the directional relationships (edges or arrows) between them. This process is essential when the network structure is not known a priori or when you want to improve the network's performance by adjusting its topology. Structure learning methods aim to discover the most appropriate network structure based on the available data or domain knowledge. This involves identifying where and in which

direction arrows should be placed between nodes. This is outlined in studies like (Heckerman, 2008).

2.6   Seismic risk-based design

Risk-based design is an approach to designing structures that incorporates considerations of risk and performance criteria into the decision-making process. The goal is to identify and implement optimal design features that allow a structure to meet specific performance objectives while accounting for potential risks. Rather than relying only on traditional design standards, risk-based design sets explicit performance objectives. These objectives are often quantified in terms of risk metrics associated with the potential exceedance of tolerable thresholds of loss. This involves assessing and quantifying the risks associated with various design options, ensuring that the chosen design minimizes the likelihood and impact of adverse events. By identifying and addressing potential risks during the design phase, risk-based methodologies enable proactive risk management. This approach enhances the safety and performance of structures over their lifecycle. The determination of an acceptable risk, characterized by a specific probability of collapse, is subject to adopting models of acceptable risk. However, it's important to note that a universally agreed upon acceptable seismic risk is yet to be established.

The limitation of current seismic design regulations, such as Eurocode 8 (CEN, 2004b) and ACI 318-11 (ACI, 2011), is the adoption of a uniform-hazard philosophy based on deterministic and simplified practices. This approach, although established and yielding satisfactory performance, leads to varying risk levels in different regions, despite structures being designed under the same regulations (Collins et al., 1996; Silva et al., 2016a).

Modern seismic design codes typically employ a force-based approach, defining earthquake input through an acceleration response spectrum. Simplified elastic analyses are employed and the ductile behavior is considered by applying a reduction factor to convert the elastic spectrum into an inelastic design spectrum. In EC8 (CEN, 2004b), this spectrum is based on a PGA value derived from the hazard curve of the structure's site for a predetermined probability of exceedance (CEN, 2004b). The spectral shape is

assumed to be influenced only by soil conditions. However, this design framework establishes uniform hazard levels across different locations, meaning that the 'uniform-hazard' design PGA values share the same exceedance probability at every location. Notably, this approach results in non-uniform risk levels across different locations (Gkimprixis et al., 2019).

Recognizing this drawback, modern design philosophies advocate for fully probabilistic approaches to explicitly address the risk levels of structures.

The United States made the first official attempt to manage seismic risk nationally across regions with varying seismicity levels. This initiative involved regulations (ASCE, 2017;FEMA, 2009) suggesting the use of risk-targeted ground motion maps.

Observations from past earthquakes reveal that while life safety is assured by compliance with design codes, economic losses due to structural and non-structural damage can be significant. Structures designed for inelastic behavior often overlook the behavior of non-structural components, resulting in notable losses (Perrone et al., 2019).

The challenge in seismic design is balancing safety and economic considerations. Achieving both objectives can be conflicting, as enhancing safety often requires increased construction costs. Therefore, a compromise is necessary between construction expenses and targeted safety levels. This dilemma has triggered intensive research into designing techniques that can benefits from reducing future losses when the seismic design level, and consequently the initial construction cost, is elevated (Gkimprixis et al., 2020).

In the last ten years, numerous applications of 'risk-targeting' principles have been explored. Various risk-targeted design methods have been developed and applied to solve a wide range of design problems (Altieri et al., 2018; Barbato & Tubaldi, 2013; Costa et al., 2010; Dall'Asta et al., 2021; Franchin et al., 2018; O'Reilly et al., 2022; Rojas et al., 2011; Sinković et al., 2016; Vamvatsikos et al., 2020; Vamvatsikos & Aschheim, 2016)

The studies investigating this problem involve calculating seismic risk through the convolution of a seismic hazard curve, determined through probabilistic seismic hazard analysis for a specific location, with a fragility curve representing a designed structure. The ground motion intensity that the structure is designed to withstand is selected to ensure the structure attains a predetermined probability of achieving a particular performance standard, such as avoiding collapse.

Lazar & Dolšek (2012) introduces a simplified design procedure for buildings, based on the concept of acceptable risk. The authors propose an iterative process that involves a preliminary design of the structure as a first step. Subsequently, the seismic risk is assessed and compared against an acceptable threshold. If the seismic risk overpass this threshold, measures are taken to reduce it. The seismic risk is then re-evaluated for the new improved structure. To illustrate the proposed design approach, examples of an eight- and a fifteen-storey reinforced concrete building are presented.

In 2007, Luco et al. (Luco et al., 2007) introduced an approach that targets a constant risk level throughout a region. This approach offers three advantages compared to the traditional method of defining design levels: clarity, consistent risk levels across a region, and the capacity to evaluate and, ideally, manage risk for various hazard types like earthquakes and wind. However, it does introduce a downside of explicitly specifying more choices, as opposed to implicit assumptions driven by convention (e.g., opting for a 475-year design return period).

In the paper of Shi et al. (2012), the authors presented the concept and the assessment process for uniform risk-targeted seismic design. They analyzed the risks of collapse for buildings located in different Chinese regions with the same seismic fortification intensity but different seismic hazards. The results show that with China's current seismic design method, the risk of structural collapse throughout the building's service life can vary significantly across different regions.

More recently, Dang J. (2021) developed a direct risk-based seismic design approach for bridges based on incremental dynamic analysis, fragility and risk assessment, and life cycle cost analysis indicators, which are used as design input parameters to control the downtime due to the damage of key components such as rubber bearings.

Deb, Zha, et al. (2022) proposed a method for risk-targeted performance-based seismic design of bridge piers for Californian Ordinary Standard Bridges to facilitate risk-informed design and decision making. The proposed formulation has the advantage of finding a first physically realizable design point in the primary parameter space. This design point can be further refined by setting other bridge design variables to meet the requirements of capacity design, code-based minimum ductility capacity, minimum

reinforcement, and/or other external restrictions and requirements, i.e. within a risk-targeted perspective. In a companion work, the same authors expanded the previously developed formulation to account for the aleatory uncertainty associated with the choice of finite element (FE) model parameters, and the epistemic uncertainty related to the use of finite datasets to estimate the parameters of the probability distributions characterizing the FE model and LS fragilities (Deb, Conte, et al., 2022) Deb et al. (2022a). Lian et al. (2022) proposed the concept of seismic importance adjustment factor as a way to adjust the bridge seismic importance factor in seismic design codes, based on the evaluation of direct (i.e. repair costs) and indirect (i.e. increased travel time) losses. Hence, the seismic importance adjustment factor ensures the accomplishment of the target requirements in terms of seismic risk.

The risk-targeted design methodology aims to design a structure that will be exposed to an acceptable and controlled risk level. The risk level is expressed as the mean annual frequency (MAF) of collapse. The solution of the risk-targeted problem requires an iterative approach (see **Figure 2-20**) that eventually leads to assuring the target risk level to the structure.
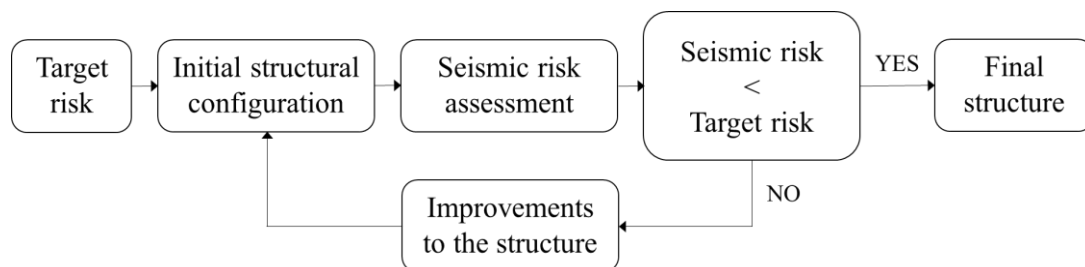
Figure 2-20 Flowchart showing the risk-based design procedure.

Overall, risk-based design methodologies provide a systematic framework for engineers and designers to create structures that are not only compliant with traditional standards but also resilient in the face of uncertainties and potential risks, contributing to enhanced safety and performance.

3 Safety assessment of bridge's piers subjected to multiple earthquakes: Markov model vs Regression model

In earthquake-prone regions, structures are exposed to repeated seismic events throughout their design life. The occurrence of multiple earthquakes, such as mainshock-aftershock sequences, can lead to a progressive reduction in structural capacity over time potentially resulting in catastrophic collapses and significant human and economic losses. As an example, the 1997 Umbria-Marche earthquake was characterized by a long sequence of earthquakes (i.e., six) of magnitude between 5 and 6 (Amato et al., 1998). In this case, although the main-shock event caused significant seismic damage in several structures, it was the subsequent events that led to structural collapse (Abdelnaby, 2012; Dolce & Larotonda, 2001).

Several studies have investigated the performance of structural systems under earthquake sequences, using models with different levels of complexity (see e.g. Aljawhari et al., 2021; Fragiacomo et al., 2004; Di Sarno, 2013; Hatzivassiliou & Hatzigeorgiou, 2015). Researches have also focused on the development of state-dependent fragility curves (Aljawhari et al., 2021; Zhang et al., 2020) which are essential tools for the life-cycle risk assessment.

Few studies have addressed the problem of damage accumulation by accounting for the probabilistic nature of the hazard, i.e. the randomness inherent to the occurrence time and intensity of the earthquakes. Specifically, Kumar et al. (2012) developed a probabilistic model for computing the degraded deformation capacity of flexural RC bridge columns under multiple damaging events as a function of cumulative low-cycle fatigue damage. They concluded that the fragilities of the piers for a given deformation demand rise with the increase in the value of fatigue damage and the fragilities of ductile piers increases faster than that of non-ductile piers. Ghosh et al. (2015) proposed an approach based on predictive regression model describing the probability of reaching a given damage level based on the intensity of the earthquake and previously accumulated damage. The model was used to predict the probability of damage exceedance conditioned on the number of earthquakes experienced by the structure. Time-dependent exceedance probabilities were computed using site-specific hazard curves for main shocks and aftershocks, characterized respectively by homogeneous and non-homogeneous Poisson process rates. Gusella (1998) proposed a method to estimate the reliability of masonry structures undergoing cumulative damage. In this methodology, the structural damage is represented by a finite number of discrete states and the evolution of damage is described as a homogeneous Markov discrete process, with a transition matrix that describes the probability of moving from a damage state to another given the occurrence of an earthquake. The occurrences of the earthquake events was modelled through a homogeneous Poisson process. Montes-Iturrizaga et al. (2003) implemented a Markovian model to describe the accumulation of damage under future multiple earthquakes and integrated it in an algorithm for optimal maintenance decisions for structures located in seismic regions. A Bayesian approach was employed for damage updating by incorporating information from sensors. Iervolino et al. (2016) evaluated alternative

approaches for defining the state transition matrix within the Markovian framework for damage accumulation, and also proposed an extension of the framework to account for non-stationary earthquake occurrence rates typical of aftershock sequences and ageing.

This Chapter present a study which aims to review, evaluate and compare the effectiveness and accuracy of the abovementioned approaches for the prediction of damage accumulation in structures subjected to multiple earthquakes within their lifetime. In particular, the method of Ghosh et al. (2015) and the Markov-chain based approach of Gusella (1998), Montes-Iturrizaga et al. (2003) and Iervolino et al. (2016) are considered. In order to evaluate these methods, a simulation-based approach similar to the one followed in Scozzese et al. (2020) for evaluating multiple stripe analysis is employed. For this purpose, a stochastic earthquake hazard model is used to generate sample sequences of ground motion records that are then used to estimate the probabilistic distribution of the damage accumulated during the time interval of interest. This simulation-based approach provides a reference solution against which the other methods are evaluated. Besides assessing the effectiveness of each approach, some possible improvements of the cumulative demand model of Ghosh et al. (2015) are proposed and evaluated.

A reinforced concrete (RC) bridge pier model (Lehman & Moehle, 2000) is considered to apply and compare the various approaches for damage assessment, and the Ang-Park damage index (Y.-J. Park & Ang, 1985) is used to describe the damage accumulation. It is noteworthy that the action of continuous progressive degradation (i.e. ageing) and the impact of retrofit interventions (e.g. Bender et al., 2018) between subsequent shocks are not considered in this study, although they may play an important role in the life-cycle assessment. Moreover, while this study focuses on a single pier and a single damage indicator, a more comprehensive assessment of the seismic risk of bridges should consider the fragility of multiple components and their contribution to the system reliability (see e.g. Gkatzogias & Kappos, 2022; Liu et al., 2022; Stefanidou et al., 2017; Stefanidou & Kappos, 2017). The study results demonstrate the importance of considering the possibility of occurrence of multiple shocks in estimating the performance of structures, highlight strengths and drawbacks of the investigated methodologies, and provide indications on the optimal procedures to follow for applying them.

Sub-section 3.1 presents the probabilistic model for the accumulation of damage and the alternative methods employed to calculate it. Sub-section 3.2 introduces the seismic hazard model and describes the details of the model of the reinforced concrete (RC) bridge pier adopted as case study. Finally, Sub-section 3.3 shows the results of the comparison of the different methodologies. This is followed by a final section that presents the conclusions drawn from this work and a discussion on future developments.

3.1 Framework for damage accumulation

3.1.1 Damage index for seismic damage accumulation

The choice of a suitable parameter for describing the damage is an essential step at the base of the development of any methodology for evaluating the structural reliability under multiple earthquake shocks. A large number of damage indicators have been proposed in the scientific literature. These can be broadly categorized in two main classes: deformation-related and energy-related indices (Cosenza & Manfredi, 2000) . The first group comprises for example the maximum ductility demand (Baig et al., 2022) or the maximum drift demand (Bouazza et al., 2022; Gentile & Galasso, 2020). The second class of damage indices comprise parameters as the amount of energy dissipated through hysteretic response (Gentile & Galasso, 2021). In addition, there are hybrid indices that capture the combined effects of deformation and energy dissipation in order to have a better assessment of the cyclic load effects. One of such parameters is the Park and Ang damage index (Park et al., 1985; Park & Ang, 1985), defined as follows for a structural component under cyclic flexural loadings:

$$D = \frac{d_{max}}{d_u} + \beta_d \frac{E_h}{F_y d_u} \qquad (3\text{-}1)$$

where d_{max} is the maximum displacement of the structural member, d_u represents the ultimate displacement under monotonic loading, E_h denotes the dissipated hysteretic energy, F_y is the yield strength and β_d is a dimensionless empirical factor describing the contribution of hysteretic energy to damage compared to the displacement demand. Experimental values of β_d are in the range of -0.3 and 1.2 (Cosenza et al., 1993).

Table 3-1 Park et al. (1985) damage index classification.

Level	Damage	Damage measure
I	$D<0.1$	No damage
II	$0.1<D<0.25$	Minor damage
III	$0.25<D<0.4$	Moderate damage
IV	$0.4<D<1.0$	Severe damage
V	$D>1.0$	Loss of the element load resistance

Park et al. (1985) proposed the relation reported in Table 1 between observed empirical damage and calculated damage index values. Values lower than 0.1 are associated with virtually no damage, while values higher than 1 are associated with a total loss of the load carrying capacity. The Park and Ang damage index has been employed in many studies on damage for RC columns under single shock scenarios (Kappos, 1997; Kunnath et al., 1997).

3.1.2 Overarching framework for seismic damage accumulation

The failure condition of a system under a seismic sequence within a time frame T is controlled by the probability of exceedance of different levels of the considered damage index. Denoting with D the damage index, the probability of D exceeding the value d during the time T can be expressed through the total probability theorem as follows:

$$P[D \geq d] = \sum_{1}^{\infty} P[D \geq d|n] * P[n, T] \qquad (3-2)$$

where $P[D \geq d|n]$ is the probability that the damage D exceeds d, conditional on having the occurrence of n shocks, and $P[n, T]$ is the probability of having n shocks during T. It is noteworthy that in this study only mainshock events are considered, and that the hazard model is assumed as time-invariant. Thus, the probabilistic distribution of the earthquake characteristics is the same at each earthquake occurrence and the occurrence of the main shock events can be described by a time-invariant Poisson process with constant hazard rate $\bar{v}$. In view of this, the term $P[n, T]$ can be evaluated as follows:

$$P[n, T] = \frac{(\bar{v}T)^n}{n!} e^{-\bar{v}T} \tag{3-3}$$

where $\bar{v}$ denotes the mean annual frequency of occurrence of events of any intensity, and it is specific for the site of interest.

In the following, two different approaches for evaluating $P[D \geq d|n]$ are illustrated: (i) the approach put forward by Ghosh et al. (2015), referred herein as "Regression-based Method (RBM)", and (ii) the approach proposed by Gusella (1998), Montes-Iturrizaga et al. (2003) and Iervolino et al. (2016) denoted as "Markovian Method (MM)". These approaches are evaluated against the classic frequentist approach, called hereafter "Simulation-based Method (SBM)". The three approaches have in common that they require a set of ground motion sequences in order to evaluate $P[D \geq d|n]$. In this study, similarly to (Scozzese et al., 2020), these sequences are generated with a Monte Carlo approach by sampling from a stochastic ground motion model. **Figure 3-1** summarizes the overarching framework for the evaluation of $P[D \geq d]$ following the three approaches. It is noteworthy that for practical purposes, the sum in Equation (3-2) is carried out up to a value of n equal to N, beyond which the probability of occurrence of the given number of events becomes negligible.
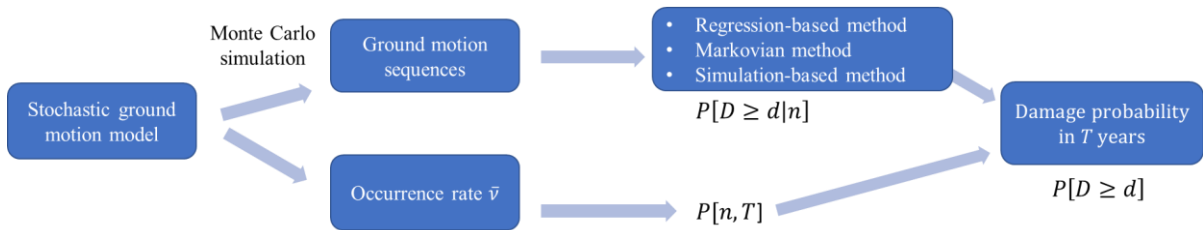
Figure 3-1 Framework for seismic damage accumulation

3.1.3   Simulation-based Method (SBM)

The Simulation-based Method (SBM) requires a stochastic representation of the earthquake hazard, as the one employed in Scozzese et al. (2020). It estimates directly $P[D \geq d|n]$ by a Monte-Carlo approach, which involves generating a series of N_s earthquake sequences from the hazard model and performing time history analyses of the finite element (FE) model of the structure to obtain samples of the damage index for different number of shocks (*N=n*). **Figure 3-2** shows an example of earthquake sequence

consisting of various shocks and the corresponding evolution of accumulated damage. Note that only the damage at the end of a shock is reported. For minor intensity earthquakes, the increase in damage is zero or not noticeable at the scale of the figure.
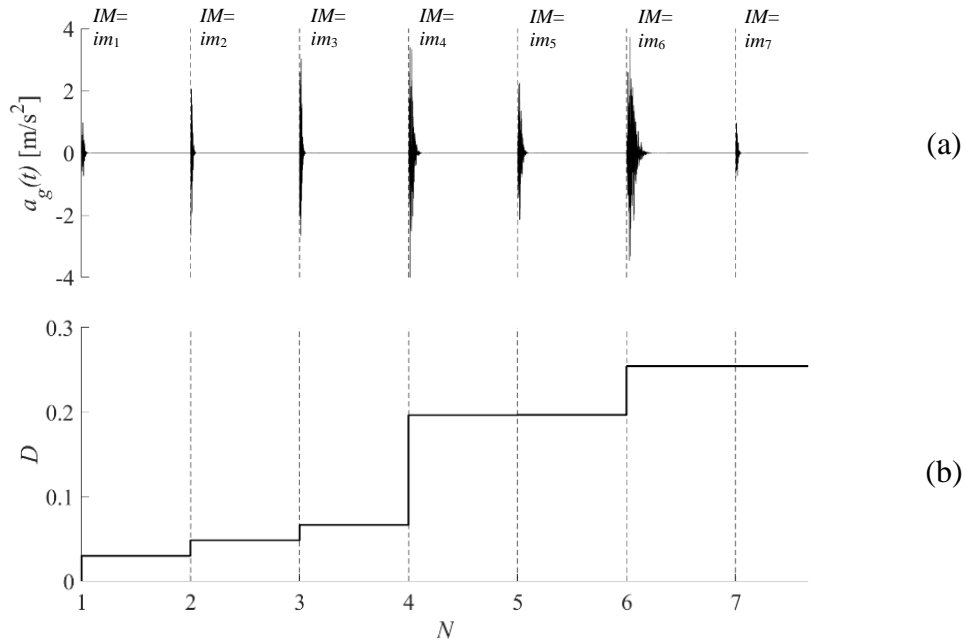
Figure 3-2 (a) Sample earthquake sequence consisting of 7 shocks with time history $a_g(t)$ and intensity *IM*, (b) damage level *D* accumulated under the various shocks

The damage exceedance probability is obtained by the following equation:

$$P[D \geq d|n] = \sum_{1}^{N_s} \frac{I[D \geq d|n]}{N_s} \qquad (3\text{-}4)$$

where *I* is the indicator function, assuming the value of 1 if $D \geq d$ conditional to the occurrence of *n* earthquakes, and zero otherwise, and N_s is the number of sequences, i.e., of samples of the damage index for a given number of shocks. Obviously, a significant number of samples is required to achieve confident estimates of $P[D \geq d|n]$, particularly for high *d* values.

3.1.4 Regression-based Method (RBM)

The approach proposed by Ghosh et al. (2015), denoted herein as RBM, is based on a probabilistic model that is a direct extension of the probabilistic seismic demand models (PSDMs) commonly used in Performance Based Earthquake Engineering (see e.g. Cornell et al., 2002 and Tubaldi et al., 2016). According to Cornell et al. (2002), for a single event, the relationship between the median value of a generic demand (in this case the damage index D) and the intensity measure of ground motions (IM) can be approximated by a power law:

$$\widehat{D_1} = a_1 (IM_1)^{b_1} \tag{3-5}$$

The linear regression model (LR) is better represented in the log-log space, with Equation (3-5) rewritten as:

$$\ln D_1 \,|IM_1 = a_1 + b_1 \ln D_1 + \varepsilon_1 \tag{3-6}$$

where a_1 and b_1 are the regression coefficients and ε_1 is the error variable relative to the regression, which has a normal distribution with zero mean and standard deviation β_1. The unknown coefficients and ε_1 can be evaluated through a least squares regression. In order to define the model for damage accumulation, Ghosh et al. (2015) introduced the Markovian assumption that the probabilistic distribution of the damage D_n at the end of the n-th earthquake (with $n>=2$), depends only on the damage accumulated up to the time when the earthquake occurs, and not on the whole earthquake sequence and damage progression history. Obviously, the probabilistic distribution of D_n must depend also on the intensity of the n-th earthquake, IM_n. This leads to the following multilinear regression model, developed by Ghosh et al. (2015) and denoted as RM1:

$$
\begin{aligned}
\ln D_n|\, IM_n, D_{n-1} \\
= a_n + b_n \ln D_{n-1} + c_n \ln IM_n + d_n \ln D_{n-1} \ln IM_n \\
+ \varepsilon_n
\end{aligned}
\tag{3-7}
$$

where a_n, b_n, c_n, d_n, are the regression coefficients and the term ε_n is the error variable relative to the regression, which is normally distributed with zero mean and lognormal standard deviation β_n. This model can be seen as an extension of the model presented in Equation (3-6) because the damage index of the structure after the n-th shock of a sequence depends on how "weak" the structure has become after being exposed to the previous n - 1 shocks (quantified herein only by D_{n-1}) (Ghosh et al. (2015).

Alternative models are proposed hereinafter to improve further the model of Equation (3-7), by introducing more terms in the regression, similar to what was done e.g. by Tubaldi et al. (2022) and Tubaldi et al. (2016).

The second regression model (RM2) considers a bilinear surface regression:

$$
\begin{aligned}
\ln D_n | & IM_n, D_{n-1} \\
& = (e_n + f_n \ln D_{n-1})H_n \\
& + (g_n \ln IM_n + h_n \ln IM_n \ln D_{n-1})(1 - H_n) + \varepsilon_n
\end{aligned}
\tag{3-8}
$$

where H_n is a step function that is $H_n = 1$ for $IM_n \leq IM^*$ and $H_n = 0$ for $IM_n > IM^*$. The IM^* parameter can also be evaluated through a nonlinear least squares regression. The third model (RM3) is an improvement of RM1, using the max function:

$$
\begin{aligned}
\ln D_n & | IM_n, D_{n-1} \\
& = \max \begin{cases} i_n + l_n \ln D_{n-1} + m_n \ln IM_n + n_n \ln D_{n-1} \ln IM_n \\ D_{n-1} \end{cases} + \varepsilon_n
\end{aligned}
\tag{3-9}
$$

The previous models may return values of D_n lower than D_{n-1} due to the nature of the regression model and ε_n. One way to overcome this physical inconsistency (i.e., damage can only increase) is to postulate that $D_n > D_{n-1}$. The fourth regression model (RM4) employs the max function to solve the issue:

$$
\begin{aligned}
\ln D_n & | IM_n, D_{n-1} \\
& = \max \begin{cases} a_n + b_n \ln D_{n-1} + c_n \ln IM_n + d_n \ln D_{n-1} \ln IM_n + \varepsilon_n \\ D_{n-1} \end{cases}
\end{aligned}
\tag{3-10}
$$

In order to fit the regression models described above, the FE model of the structure must be analysed under $N_s = 5000$ sequences of ground motions consistent with the considered

hazard model. The 5000 samples of the responses under the first shock are used to fit the model of Equation (3-6). The fitting of the model for $(D_n|IM_n, D_{n-1})$ is based on the samples of the damage indexes at the end of the *n-th* and of the (*n*-1)-th shocks, as well as of the samples of IM_n. In theory, different models should be considered for *n*=2,...,*N*. However, assuming the regression model as homogeneous, the term *n* in the regression coefficient can be dropped, or in other words the regression coefficients (and thus the probability of moving from a state of damage to another) do not depend on the number *n* of the shock considered. Thus, the samples corresponding to different values of *n* can be considered jointly to fit the regression model. Once the regression model is fitted, the unconditional probability of exceeding the specified damage levels can be assessed with a Monte Carlo-based approach. For this purpose, N_s sequences of earthquake intensities can be generated by sampling from the stochastic model of the earthquakes for the site, and the regression equations with the associated uncertainties can be repeatedly applied to estimate the damage indices conditional to the number *n* of shocks. Finally, the probability exceeding a threshold damage level is estimated following a similar approach as the one used for the SBM method (i.e. Equation (3-4)).

3.1.5 Markovian Method (MM)

The approach proposed by Gusella (1998), Iervolino et al. (2016) Montes-Iturrizaga et al. (2003), denoted herein as MM, is applied to structures accumulating seismic damage and it is based on a Markovian representation of the degradation process (Serfozo, 2009). The underlying hypothesis is the stationarity of the process meaning that the evolution of the damage after a given time depends probabilistically only on the state of the structure at that time. The vulnerability is then represented as a state-dependent phenomenon described by a homogeneous Markovian chain, modelled through the transition probability matrix (TPM) that completely characterizes the stochastic process. For this purpose, damage *d* is discretized into a finite number of states n_e where the first state corresponds to the undamaged structure (d_1=0) and the last state corresponds to failure or collapse (d_{ne}=1). Defining (*k-1*) and *k*, with *k*=2,…, *N,* as two sequential seismic events, the transition probability between two damage states can be computed as:

$$\phi_{ij}^k = P[j - th\ state\ at\ k | i - th\ state\ at\ (k - 1)],$$

$$i, j = 1, \dots, n_e \tag{3-11}$$

where ϕ_{ij}^k denotes the probability that at the end of the k-th earthquake the structure reaches damage state j, given that the initial state is i. The probabilities of transition ϕ_{ij}^k can be arranged in the TPM $\Phi(k)$ of dimensions ($n_e \times n_e$):

$$\Phi(k) = \{\phi_{ij}^k;\ i, j = 1, \dots, n_e\} \tag{3-12}$$

The rows and columns of the TPM are labelled with the damage states of the structures arranged progressively from the top one corresponding to the as-new state to the bottom one that necessarily denotes the failure of the structure. The matrix is upper triangular because of the monotonous nature of the damage process. It may be used entering the row with the pre-event condition of the structure to get the probability to find it in any of the other states. It is noteworthy that $\Phi(k)$ is estimated via simulation, as no closed form expressions are available.

The damage probability vector $P(k)$ of dimensions ($1 \times n_e$), computed at the end of the k-th event, can be express as:

$$P(k) = P(k - 1)\Phi(k) \tag{3-13}$$

where $P(k - 1)$ is the damage probability vector of dimensions ($1 \times n_e$) at the start of the k-th event. The j-th element P_j^k of the vector $P(k)$, which expresses the probability of being in damage state j at the end of the k-th seismic event, is given by:

$$P_j^k = \sum_{i=1}^{n_e} P_i^{k-1} \phi_{ij}^k \tag{3-14}$$

where P_i^{k-1} represents the probability of being in damage state i at the start of the k-th seismic event.

Under the assumption of homogeneity already introduced for the RBM, the damage accumulation process can be described as a homogeneous Markov chain defined by a

single TPM $\boldsymbol{\Phi}$, and the probability mass function after the occurrence of the N-th earthquake can be written as:

$$\boldsymbol{P}(N) = \boldsymbol{P}(0)\Phi^N \tag{3-15}$$

where $\boldsymbol{P}(0)$ is a vector $(1 \times n_e)$ that denotes the initial state of the structure. The probability that damage does not exceed a damage level d_j conditional on the number of shocks n can be expressed by:

$$P[D < d_j | n] = \sum_{i=1}^{j} \psi_{ij}^N p_i^0 = \sum_{i=1}^{j} (\sum_{l=1}^{j} q_{il}^N) p_i^0 \tag{3-16}$$

where q_{il}^N is the element at row i and column l of the N-th product of matrix $\boldsymbol{Q} = \{\phi_{il}; i, l \le j\}$. This matrix is obtained by deleting from the matrix $\boldsymbol{\Phi}$ the rows and columns whose index is higher than l. Then, the matrix $\boldsymbol{\Psi}^N = \{\psi_{ij}^N\} = \{\sum_{l=1}^{j} q_{i,l}^n\}$ can be formed. Therefore, the conditional probability of exceeding a given damage state d_j is:

$$P[D \ge d_j | n] = 1 - \sum_{i=1}^{j} \psi_{ij}^N p_i^0 \tag{3-17}$$

3.2 Case study

3.2.1 Stochastic earthquake model

Similarly, to previous studies (Altieri et al., 2018; Dall'Asta et al., 2017), the seismic scenario is described by a single source model, characterized by two main random seismological parameters, namely the moment magnitude M_m, and the epicentral distance R. Earthquakes of magnitude between $M_{min} = 5.5$ and $M_{max} = 8$ have the same likelihood of occurrence within a circular area of radius $R_{max} = 25$ km centred at the site where the structure is situated. The frequency of occurrence of the earthquakes is described by the Gutenberg-Richter recurrence law and the mean annual frequency of occurrence $\bar{v}$ of earthquakes of any intensities is 0.0997 per year. The attenuation from the source to the site of the structure is described by the Atkinson–Silva (Altieri et al., 2018) source-based ground motion model, combined with the stochastic point source simulation method of

(Boore, 2003). The Spectral acceleration $Sa(T_{fund},\xi)$ at the fundamental period T_{fund} and the damping ratio ξ of the structure is chosen as intensity measure (*IM*). **Figure 3-3a** illustrates the probability mass function of the number *n* of shock occurrences during the lifetime of the structure (*T* =50 years). It can be seen that the probability of having 15 or more shocks is negligible. **Figure 3-3b** the probability of exceedance of *IM*, conditional on the number of occurrences. The values of T_{fund} and ξ refer to the case-study pier illustrated in section 3.2.2. A pool of N_s=5000 ground motion records are generated by sampling from the probabilistic distributions of M_m and *R* and by using the Atkinson-Silva attenuation model (see Altieri et al., 2018 for further details). Since the model is homogeneous, N_s sequences of 20 consecutive ground motions are built by randomly extracting the sampled records from the pool of records. These ground motion sequences are then used as input for the time-history analyses required to estimate the evolution of damage.

(a)   (b)
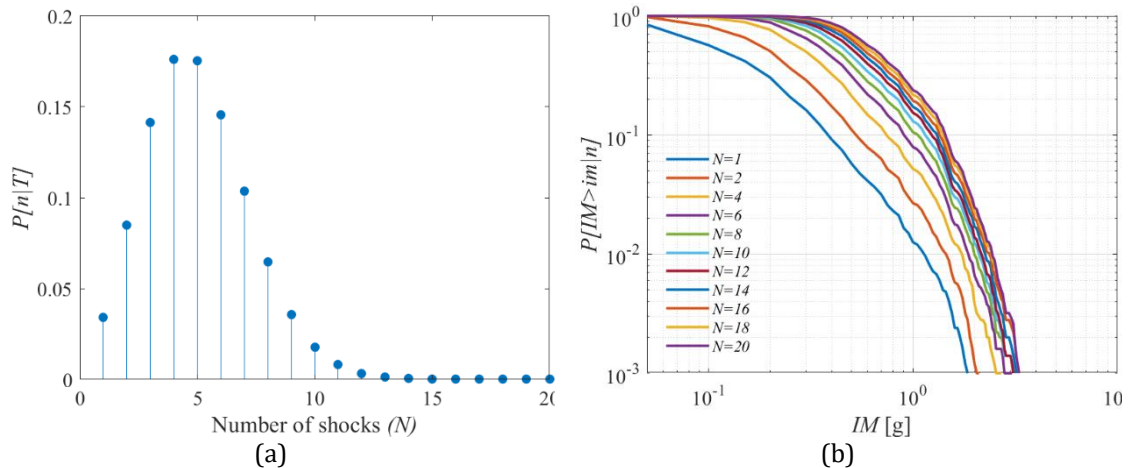
Figure 3-3 (a) Probability of *n* shocks in lifetime *T* = 50 years; (b) Probability of exceedance of *IM* in 50 years conditional to the number of shocks *n*

3.2.2 RC pier model

A RC bridge pier (**Figure 3-4**) of height *L*=4.9m is selected as case study. It corresponds to specimen denoted as 815 in Lehman & Moehle (2000). The details of the considered bridge pier are summarised in **Table 3-2**. The pier is characterized by a circular cross-section with diameter D_m=610 mm and it has a mass of 35.6 ton. The fundamental period of the pier is T_{fund} = 0.69s and the damping ratio ξ is 0.05. **Figure 3-4** represents an illustration of the chosen column.

Table 3-2 Details of the structural model Lehman & Moehle (2000)

Column ID	Height L [mm]	L/D_m	Vertical bar diameter [mm]	Number of vertical bars	Horizontal Bar diameter [mm]	Horizontal Bar spacing [mm]	ρ_l	ρ_h	T_{fund} [s]
815	4876.8	8	16	22	6.5	32	1.49	0.01	0.69
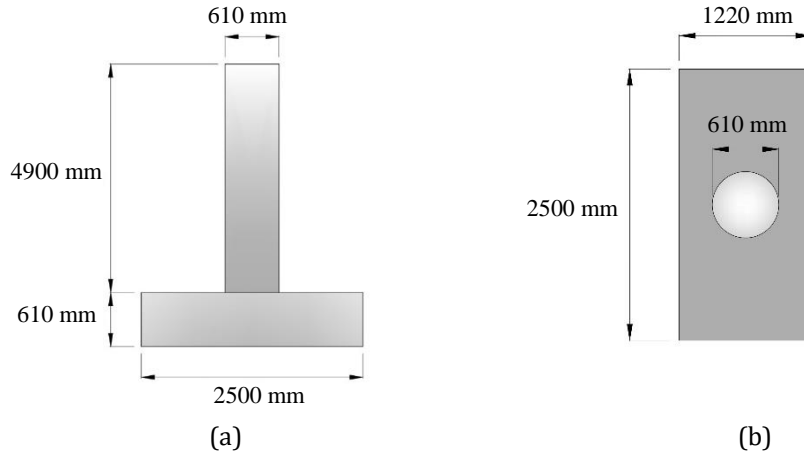
Figure 3-4 Schematic view of the bridge pier (Lehman & Moehle 2000) (a) longitudinal view (b) cross section

A detailed numerical model of the RC column was constructed in OpenSees (2011) with due account of geometric and material nonlinearities by means of the fibre-based section discretisation technique (Kashani et al., 2016, 2017; Spacone, Filippou, et al., 1996). This includes an accurate representation of the influence of inelastic steel buckling and low cycle fatigue degradation. To this end, beam-column elements were employed to model the bridge pier and the cross-section of the element was discretized into a number of steel and concrete fibres at the selected integration points. This research follows the modelling approach described in Kashani et al. (2016) in which three Gauss–Lobatto integration points (Berry & Eberhard, 2007) are specified for the first element, where most of the nonlinear response is concentrated, based on the recommendations provided by Coleman & Spacone (2001) and Pugh (2012). Similarly, a force-based element with five integration points is considered to model the top part of the column, in accordance with Berry & Eberhard (2007). A schematic view of the fibre model and fibre sections is shown in **Figure 3-5**. The following material properties were assumed: a steel yield stress of f_y=540 MPa, maximum deformations of confined and unconfined concrete under compression of

75

ε_{ccore}=0.035 (Van et al. 2003) and ε_{ccover}=0.00428 (Karthik 2009), respectively, and a maximum longitudinal concrete tensile deformation of ε_t=0.000125 (Mander et al. 1988), while a maximum deformation of the steel under compression of ε_{cs}=0.08 was adopted. The material nonlinearity was described through a uniaxial material relationship for steel (tension and compression) and concrete (confined and unconfined). In this study, the *Concrete04* model available in OpenSees (2011) was used to model the unconfined concrete in the cover and the confined concrete in the core of the pier. This model is based on the Popovics (1988) curve in compression, and a linear-exponential decay curve in tension. The Karsan–Jirsa model (Karsan and Jirsa 1969) was used to account for the stiffness degradation and determine the unloading-reloading stiffness in compression while the secant stiffness was employed to define the unloading/reloading stiffness in tension. The confinement parameters (i.e., the maximum compressive stress of the concrete and the strain at the maximum compressive stress) were taken from Mander et al. (1988). The model developed by Scott et al. (1982) was used to define the confined concrete crushing strain in the confined concrete model. Besides, the phenomenological uniaxial model developed by Kashani et al. (2015) was used to describe the behaviour of steel reinforcement. For its implementation, the *Hysteretic* material model available in OpenSees (2011) was used. Moreover, the generic uniaxial fatigue material developed by Uriz (2005) was wrapped to the steel material in order to simulate the low cycle fatigue failure of vertical reinforcing bars. Further information about the model can be found in Kashani et al. (2016) and Kashani et al. (2017).
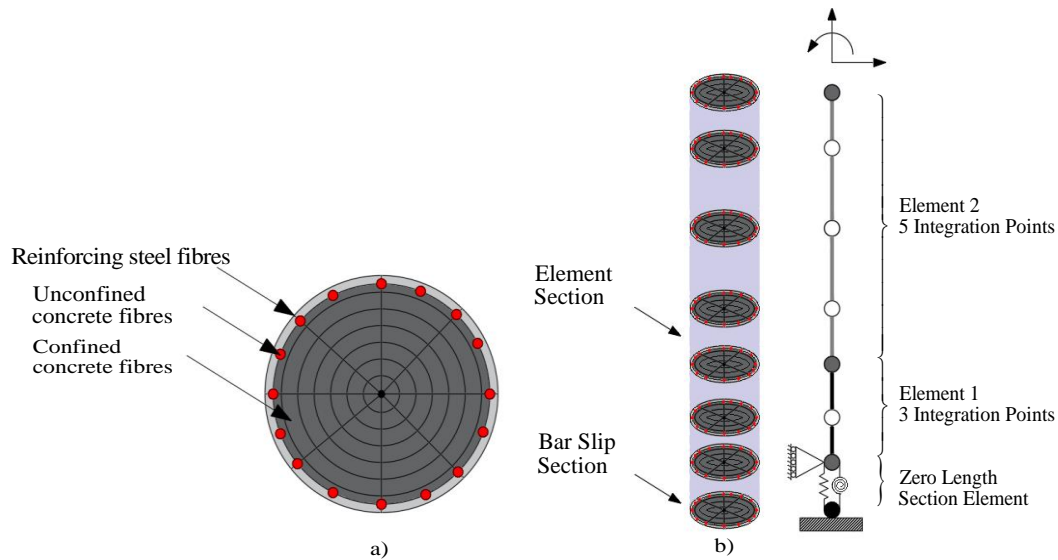
Figure 3-5 Schematization of fibre beam-column element (a) with the bar buckling and bar slip model (b)

3.3 Results

3.3.1 Reference solution via SBM

The direct simulation (SBM) approach provides the reference solution for the comparison of the RBM and MM methods. **Figure 3-6** shows the probability of damage exceedance, computed for an increasing number of earthquake sequences N_s from 200 to 5000. The total number of shocks N examined for each curve is 20, and 40 discrete damage levels between 0 and 1 were considered to calculate the probability of exceedance. The value of the coefficient β_d considered in the calculation of the damage index using Equation (3-1) is 0.05. It can be noted that by increasing N_s the exceedance curves tend toward the one calculated for N_s=5000 and the curves obtained considering $N_s \geq 1000$ are very close to each other. The maximum value of the coefficient of variation of the estimate of the exceedance probability for the highest damage level (D=1) is of the order of 6.5%. Thus, quite accurate estimate of the probability is achieved with the maximum number of sequences N_s considered. Beyond N_s=5000, there is no appreciable change in the estimated curve: the maximum relative difference in the probability of exceedance between the curves calculated with N_s =4000 and N_s =5000 is less than 2.5%. Thus, it can be assumed that the curves have reached convergence and for this reason, the solution

obtained with N_s=5000 is considered as reference solution for evaluating the accuracy of the other methods under analysis.
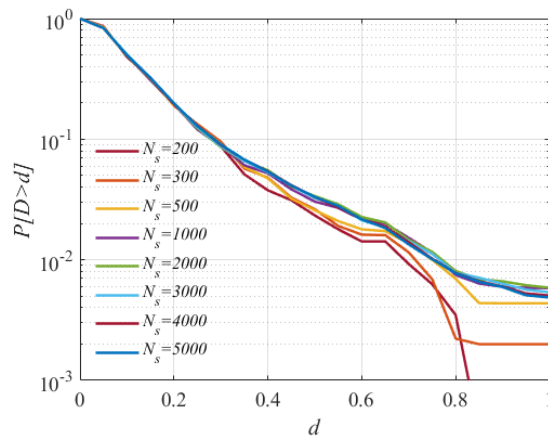
Figure 3-6 Influence of the number of samples on the probability of exceedance of the damage D computed via SBM

A further study is conducted to assess the maximum number of earthquake occurrences N to be considered during the assumed design life (T=50 years) of the structure in the summation of Equation (3-2). **Figure 3-7** shows the probability of failure for an increasing number of N and for a number of N_s equal to 5000. It can be seen that, for low values of N, by increasing the maximum number of occurrences, the probability of failure increases significantly, whereas for value of N higher than 10, there is no change in the risk estimate. The value of N in the subsequent analyses is set equal to 20.
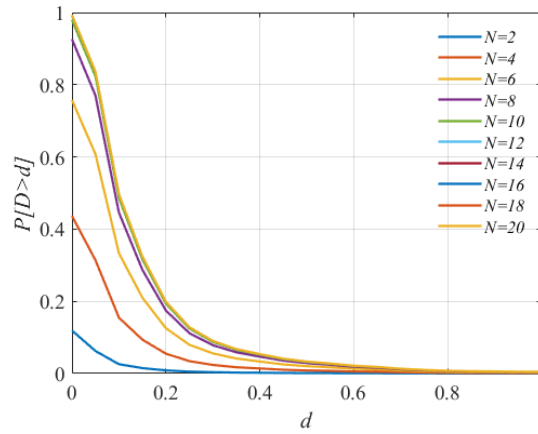
Figure 3-7 Exceedance probability of a limit threshold, evaluated via SBM for 5000 samples, for an increasing number $N=n$ of shocks in 50 years

3.3.2 RBM fitting

This subsection describes the results of the application of the linear and multi-linear regression models obtained by employing a set of $N_s=5000 \mathrm{x} N=20$ samples. **Figure 3-8** shows the sample values of the damage index D_1 versus IM_1 in the log-log plane, together with the median of the linear model of Equation (3-6). It can be observed that $\log(D_1)$ increases linearly with the $\log(IM_1)$. The high value of the coefficient of determination ($R^2=0.964$), and the low value of the mean square error or lognormal standard deviation ($\beta_1=0.187$), reported in **Table 3-3**, reveal a satisfactory fit of the model to the data. **Figure 3-9** illustrates the response samples and the fitted median demand obtained by using the various multi-linear regression models of Equations (3-7)-(3-10). Each figure shows the logarithm of the samples of the damage index D_n observed for the n-th event as a function of the logarithms of the intensity measure IM_n and of the damage index D_{n-1} observed for the (n-1)-th event. The surface plotted in the figures corresponds to the fitted median models (see **Table 3-4** for the model parameters). The values of the β_n and R^2 (**Table 3-3**) corresponding to the various models show that overall, the regression models are quite accurate, and RM3 is the one that performs best.
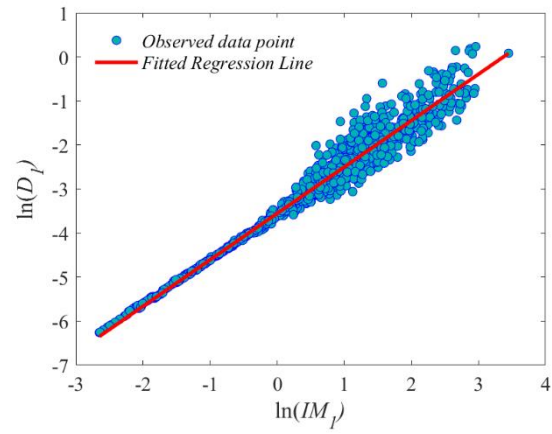
Figure 3-8 Linear regression model for predicting damage after the first occurrence
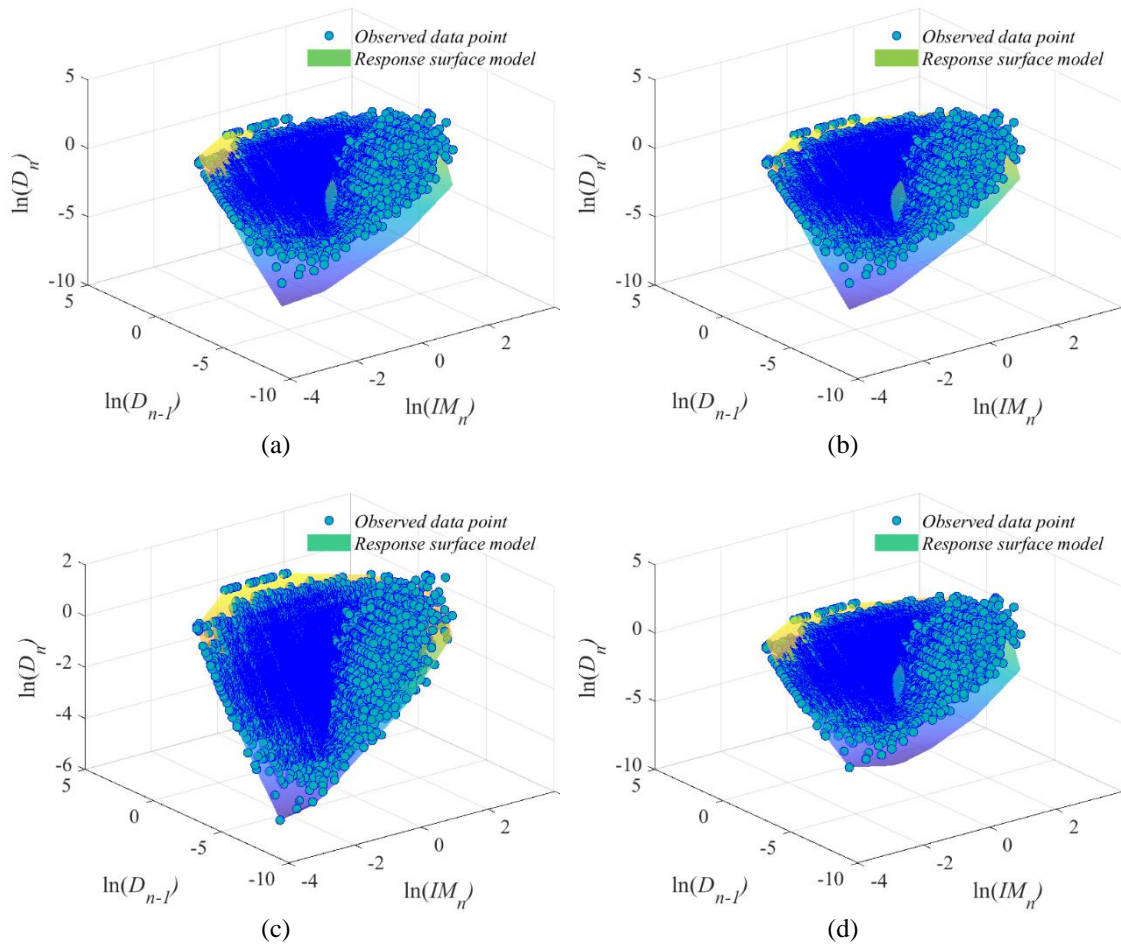
Figure 3-9 Models for damage accumulation: (a) RM1; (b) RM2; (c) RM3; (d) RM4

80

Table 3-3 β_n and R^2 values of the linear and multi-linear regression models

	β_1	β_n	R^2
LR	0.187	-	0.964
RM1	-	0.244	0.900
RM2	-	0.229	0.912
RM3	-	0.118	0.977
RM4	-	0.224	0.910

Table 3-4 Parameters of the linear and multi-linear regression models (LN, RM1, RM2, RM3, RM4)

a_1	b_1	a_n	b_n	c_n	d_n	e_n	f_n	g_n	h_n	i_n	l_n	m_n	n_n
-	1.0	-	0.8	-	-	-	0.8	-	-	-	0.0	0.9	-
3.55	5	0.20	5	0.22	0.19	0.31	1	0.32	0.24	3.24	7	7	0.02

3.3.3   Convergence analysis of the RBM

Figure 3-10 shows the estimates of the probability of damage exceedance obtained for each of the RBM models fitted in the previous sections and compares them to the reference solution. The curves are obtained considering $N_s=5000$ sequences and $N=20$ occurrences per sequence, and 40 discrete damage levels. It can be observed that the curves obtained with RM3 and RM4 are more stable and closer to the reference curve while the curves of RM1 and RM2 are more scattered for high values of D. The bias of the RM-based estimates is quantified numerically through the errors Δmax and Δmean, denoting respectively the maximum and the mean of the normalized distances between the curves obtained with each RM and the corresponding reference curve. The values of Δmax and Δmean are reported in **Table 3-5**. As already expected by observing **Figure 3-10**, the lowest values of the errors are obtained for RM3 and RM4. In particular, RM3 presents the minimum values of Δmax and Δmean, thus it can be considered in general as the most accurate model. It is noteworthy that the β_n and R^2 values of **Table 3-3** follow the same trend of the values of Δmax and Δmean in **Table 3-5**, i.e., the best performing demand models yield the most accurate risk evaluations.
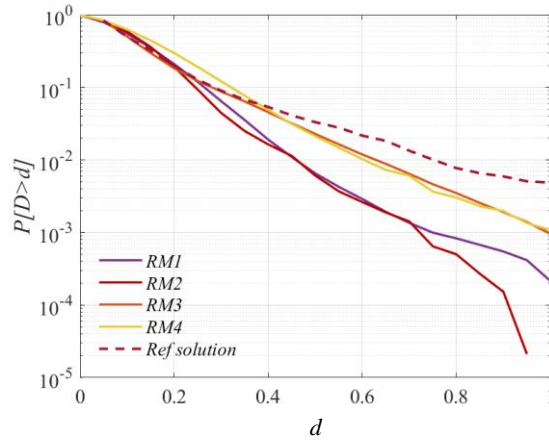
Figure 3-10 Estimate of the damage exceedance probability evaluated for the four regression models for N_s=5000 and N=20

Table 3-5 Max and mean values of the normalized distances between the probability curves computed for each RM and the reference solution (minimum values are in bold)

	Δmax	Δmean
RM1	0.9560	0.5885
RM2	0.9353	0.5451
RM3	**0.8031**	**0.3408**
RM4	0.8392	0.5243

A further study has been conducted on RM3 in order to establish the minimum number of N_s and N to be considered for estimating the probability of failure without affecting significantly the accuracy of the results. For this purpose, different regression models are built by fitting RM3 to different samples sets, obtained for an increasing number of N_s between 200 and 5000, for N =20. **Figure 3-11** shows the probability of damage exceedance obtained considering the different sample sets. **Figure 3-12** compares the corresponding values of the errors Δmax and Δmean. It can be observed that by increasing N_s, the errors tend to decrease as the exceedance curves become closer to the reference solution. The curves corresponding to values of $N_s \geq 500$ are very close to each other, and thus N_s=500 can be considered as a good number of sequences for estimating the damage exceedance curve.

82
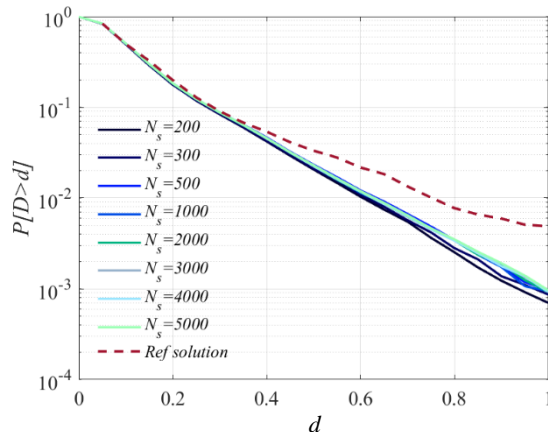
Figure 3-11 Influence of number of sequences N_s on the estimate of the damage exceedance probability for RM3 (N=20)

(a)

(b)

Figure 3-12 Plot of the normalized distances between the probability curves calculated for an increasing number of N_s and the reference solution (a) max values; (b) mean values
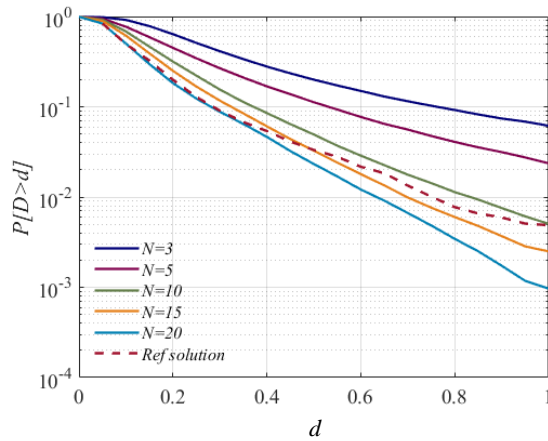
Figure 3-13 Influence of number of shocks N on the estimate of the damage exceedance probability for RM3 (N_s=500)

The influence of the number of shocks N to be considered for RM3 is also assessed. **Figure 3-13** shows the probability of damage exceedance obtained with RM3 for N_s=500

and for an increasing number of N. The deviation between each curve and the reference solution is measured by the errors reported in **Figure 3-14**: the errors are very high for low values of N, whereas they decrease and stabilise for $N \geq 10$. Thus, $N=10$ is deemed sufficient to achieve accurate estimates of the curve.

(a) (b)
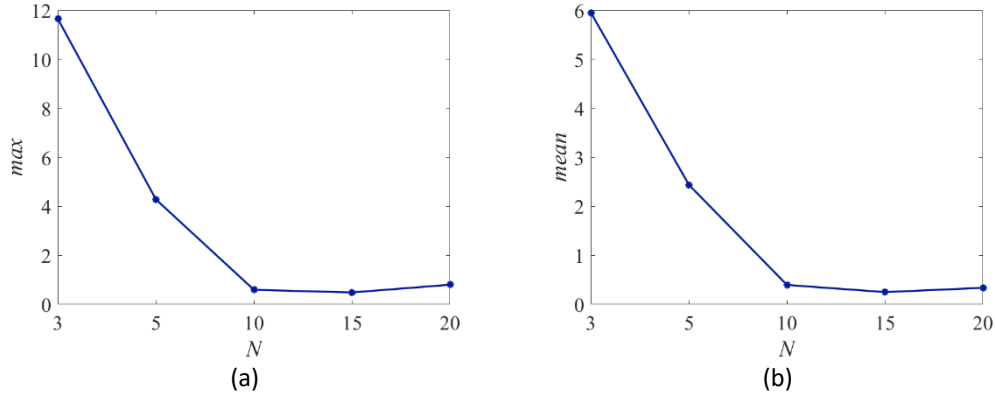
Figure 3-14 Plot of the max and mean values of the normalized distances between the probability curves calculated for an increasing number of N and the reference solution. (a) max values; (b) mean values

3.3.4 Convergence analysis of the MM

Following the same methodology of subsection 3.3.3, this subsection investigates the accuracy of the MM and examines how the number of N_s and N affects the estimation of the curve expressing the probability of damage exceedance. For these purposes, the probability curves are built initially using the MM for an increasing number of N_s between 200 and 5000, 40 damage levels and $N=20$. The obtained curves are compared against the reference solution in **Figure 3-15**. As expected, for increasing values of N_s, the probability curves approach the reference solution. **Figure 3-16** compares the error measures expressing the normalized distances between the probability curves and the reference solution. In general, the errors are low and decrease for increasing N_s values. For values of N_s increasing beyond 1000, the errors do not decrease significantly. Thus, $N_s=1000$ is a good number of sequences to be considered for fitting MM.
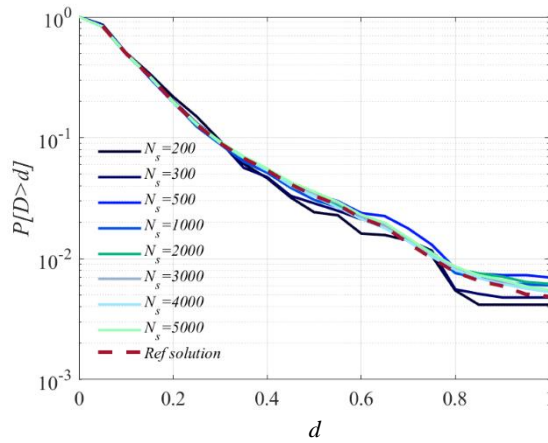
Figure 3-15 Influence of number of sequences N_s on the estimate of the damage exceedance probability evaluated with the MM (N=20)

(a)   (b)
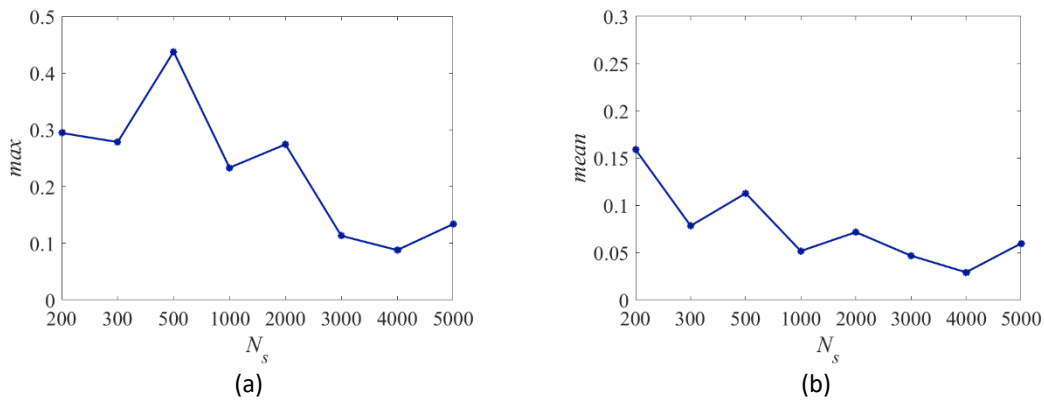
Figure 3-16 Plot of the max and mean values of the normalized distances between the probability curves calculated for an increasing number of N_s and the reference solution (a) max values; (b) mean values

In order to evaluate the effect of the number of shocks N, the probability of damage exceedance is calculated for an increasing number of N, keeping fixed the number of sequences N_s=1000. **Figure 3-17** shows the probability of damage exceedance vs D for an increasing number of N. The curves tend to overlap with the reference curve for a high number of N. **Figure 3-18** compares the error measures obtained for the different values of N. As expected, increasing the number of N improves the estimate of the exceeding probability as the values of the Δmax decrease. In this case, N=20 must be considered as the error values decrease considerably up to N=20.
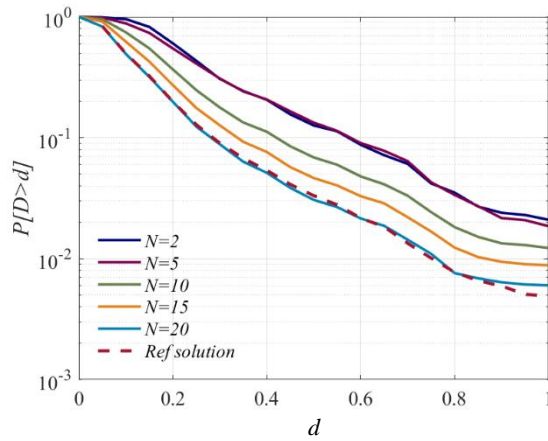
Figure 3-17 Influence of number of shocks N on the estimate of the damage exceedance probability

(a)

(b)
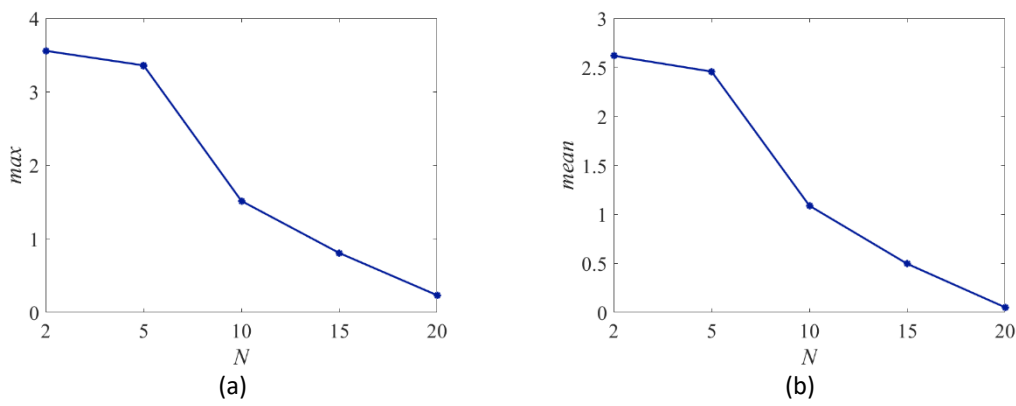
Figure 3-18 Plot of the max and mean values of the normalized distances between the probability curves calculated for an increasing number of N and the reference solution (a) max values; (b) mean values

3.3.5 Comparison of the different methods

This subsection summarizes the results obtained and shown in the previous paragraphs. The analyses whose results are reported in Sections 3.3.2 and 3.3.3 show that among the various RBMs, RM3 is the one that provides more accurate estimates of the probability of damage exceedance. It is sufficient to consider N_s=500 and N=10 to fit this model. With regards to the MM, based on the results reported in Section 3.3.4 it can be concluded that a slightly higher number of samples (N_s=1000 and N=20) is required to fit the model. **Figure 3-19** shows the curves of the probability of damage exceedance resulting from the application of the RM3 (N_s=500 and N=20) and of the MM (N_s=1000 and N=20). It is possible to observe that the MM provides results very close to the reference ones obtained with the SBM, since it introduces no simplification in the evaluation of the evolution of

damage during consecutive events. The estimates of the probability of damage exceedance obtained with the RBM, on the other hand, present some divergences due to the assumption introduced through the regression model. However, despite the differences, all methods lead to similar results. MM needs a slightly larger number of samples (and thus of analyses) with respect to RBM: this is due to the fact that in order to estimate with accuracy all the terms of the transition matrix, a greater number of samples is required, particularly to fit the bottom right part (corresponding to high levels of damage). The RBM yields some savings in terms of computational cost but at the expense of some bias.
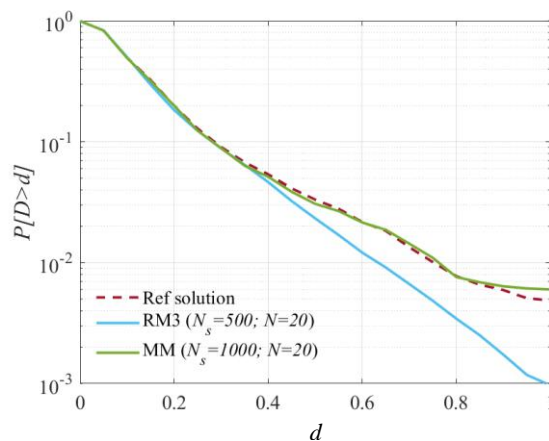
Figure 3-19 Comparison between the different approaches for evaluating the damage exceedance probability

3.3.6 Results for *T*=5 years

The methodologies investigated in this study assume that during the time T no interventions take place to return the structure to its undamaged state. This could be realistic only for small time frames. Thus, this subsection briefly illustrates some results obtained considering a shorter time interval $T = 5$ years for the evaluation of the unconditional damage exceedance probability. As shown in **Figure 3-20**, the probability of having more than 5 shocks in $T = 5$ years is negligible. Nevertheless, the value of $N=20$ has been considered in the application of the methods for computing the risk via Equation (3-2).

Figure 3-21a and **Figure 3-21b** show the probability of damage exceedances built using RM3 and the MM respectively for an increasing number of N_s between 200 and 5000.

Figure 3-22a shows the variation with N_s of the mean error measure, expressing the normalized distances between the probability curves of **Figure 3-21a** and the reference solution. It can be seen that the error values decreases only slightly for increasing N_s values, since the method provides biased estimates of the risk. For values of N_s increasing beyond 1000, the reduction of the error can be considered not significant. **Figure 3-22b** compares the error measures for the curves obtained with the MM method, which are shown in **Figure 3-21b**. For values of N_s increasing beyond 1000, the error does not decrease significantly.
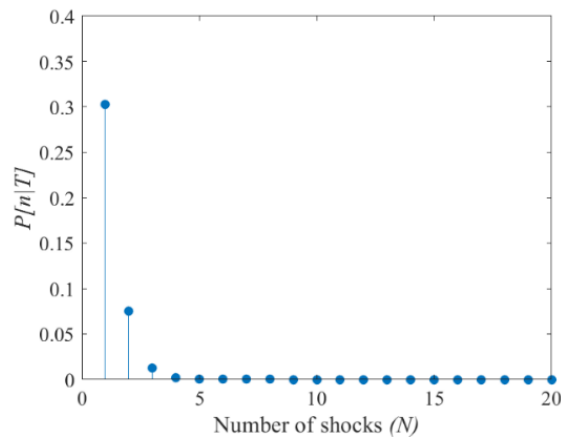
Figure 3-20 Probability of n shocks in lifetime $T = 5$ years
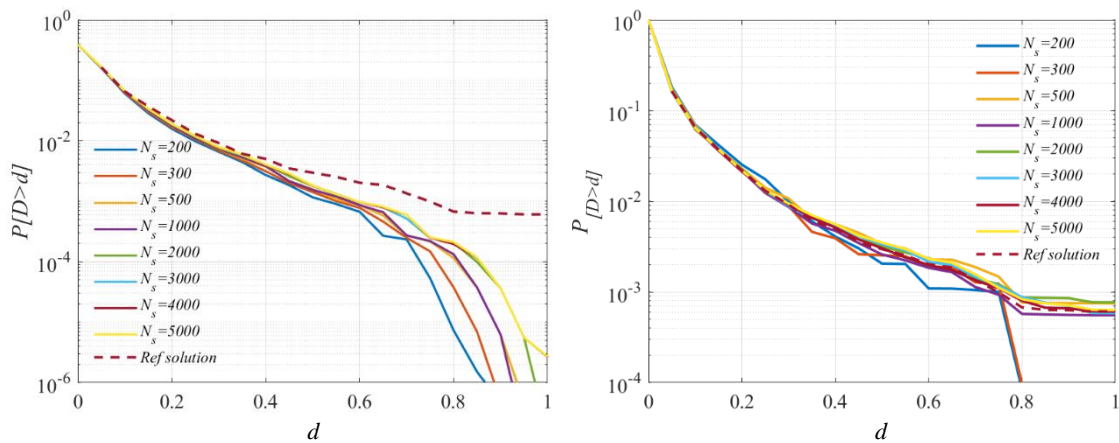
Figure 3-21 Influence of number of sequences N_s on the estimate of the damage exceedance probability computed for $N=20$ and for a period $T = 5$ years, built with (a) RM3 (b) MM
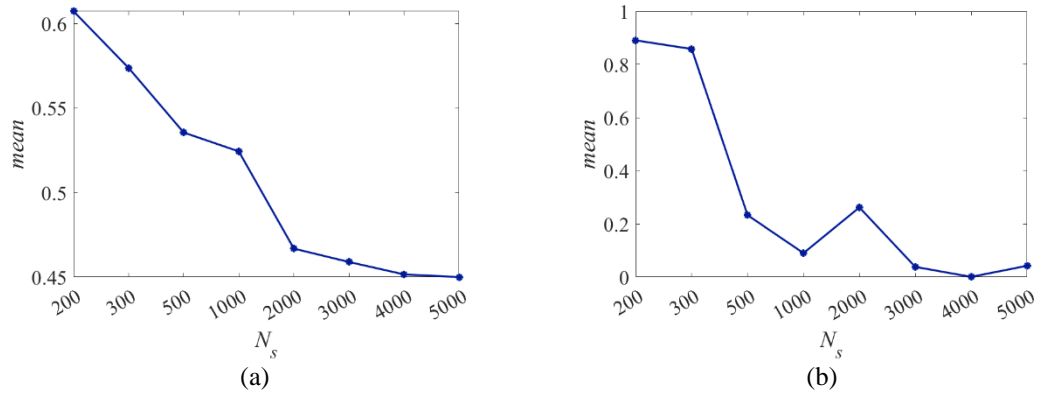
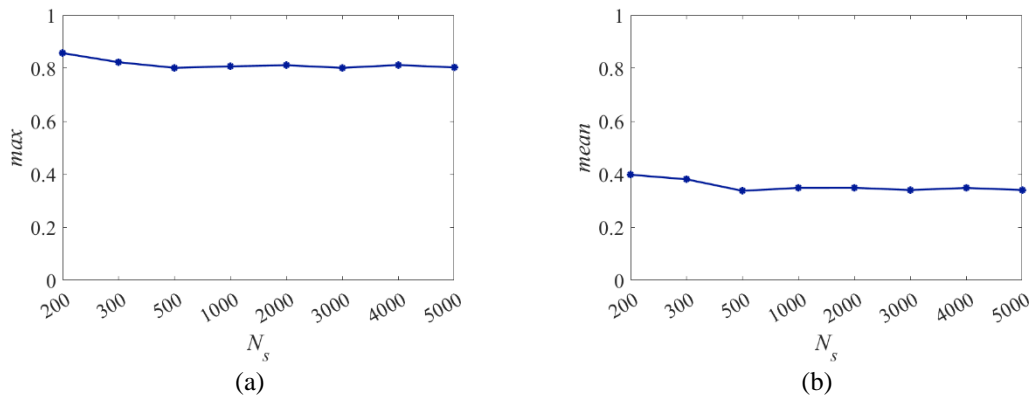**Figure 3-22** Plot of the mean values of the normalized distances between the probability curves calculated for an increasing number of N_s and the reference solution: (a) RM3, (b) MM.

### 3.3.7   Sensitivity analysis on the natural period of the pier

The natural frequency and period of a pier are indicators of its structural integrity, and these parameters can significantly change following an earthquake. When a pier is damaged by seismic activity, its stiffness typically decreases, leading to an increase in its natural period. The altered frequency may affect the selection of appropriate earthquake ground motions for analysis and design. Seismic codes and design practices often rely on the natural frequency to select ground motion records that are representative of the potential seismic demand on the structure. If the frequency changes significantly due to damage, the originally selected earthquake ground motions might no longer be appropriate, potentially underestimating or overestimating the seismic demands on the structure.

This subsection presents a sensitivity analysis that elucidates the relationship between seismic damage and the pier's period. As reported in subsection 3.2.2, the fundamental period of the initial configuration of the pier is $T_{fund} = 0.69s$. **Figure 3-23b** shows the increase of the period T after every earthquake occurrence considering five different seismic sequences (*Seq*) and **Figure 3-23a** shows the relative damage D. The trend of the curves of **Figure 3-23b** is directly proportional to the trend of the damage curves, showing the correlation. The fourth occurrence of Sequences 4 and 5 produces considerable damage to the structure and thus the period of the pier increases considerably. After the occurrence of the twentieth shock, the natural period of all the five sequences results to be greater than 1s. Considering N_s=500 sequences as a sufficient number of sequences to

obtain accurate estimates, it is possible to compute the periods of the pier after each occurrence of a shock. **Figure 3-24** shows the mean and the variance of the periods as a function of the number of occurrences N, computed considering N_s=500 sequences. It can be noticed how the period increases significantly until the occurrence of the 5th shock and then the increase diminishes. The variance of the periods decreases significantly after the 10th shock, meaning that the period of the structure almost stabilizes.

(a)   (b)
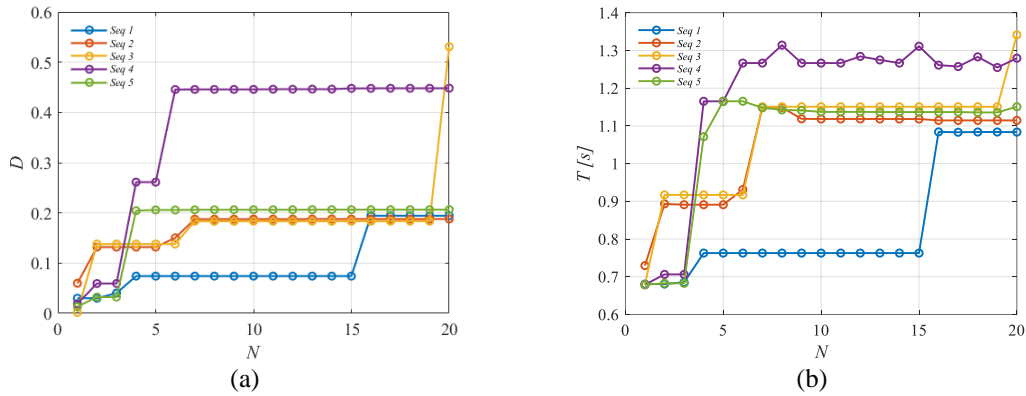
Figure 3-23 Damage D (a) and natural period (b) of the pier computed after each occurrence for five different sequences of 20 shocks.

(a)   (b)
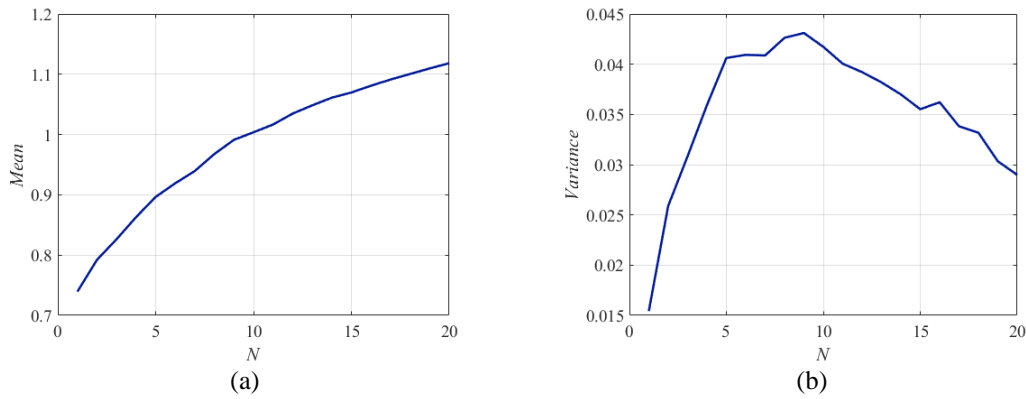
Figure 3-24 Mean (a) and variance (b) of the periods as a function of the number of occurrences N, computed considering Ns=500 sequences

More in-depth analyses can be done to identify critical thresholds of stiffness reduction that significantly alter the natural frequency and to determine when it is appropriate to select more accurate earthquake ground motions to improve the overall risk assessment. However, this is beyond the scope of this thesis.

3.3.8 Aging effect

Besides the damage directly due to earthquake shocks, the phenomenon that affects seismic structural vulnerability is the continuous deterioration of material characteristics, also known as "aging". Damage from earthquakes can be termed as shock-based damage while aging is a progressive, continuous damage. Both processes contribute to damage accumulation. Aging is often related to an aggressive environment which worsens mechanical features of structural elements. Progressive degradation is typically a slow, continuous, time-dependent phenomenon, caused by factors such as chloride ingress, corrosion, fatigue, or biodeterioration (Bastidas-Arteaga et al., 2008, 2009).

This subsection aims to show the effect of aging compared to earthquake damage in the lifespan of the structure. However a detailed understanding of this kind of wear phenomena is beyond the scope of this thesis and only a mathematical wear modelling will be given. In particular, the aim of this section is to discuss and to implement an aging mathematical model proposed by (Iervolino et al., 2013).

To define a quantitative model that accounts for factors that contributes to deteriorate the structural integrity of a concrete infrastructure, the model is referred to the specialised bibliography (Li, 2020; Lu et al., 2022; Stewart et al., 2011). As stated in Iervolino et al., 2013, it is more advantageous to model the cumulative seismic damage process separately from the progressive aging, given the lack of strong evidence for a significant correlation between progressive deterioration and shock-induced damage.

The degradation process, written in terms of residual capacity $c(t)$, is described by Equation 2-32. Considering also aging and assuming that continuous and shock-based damaging events are independent, $c_{tot}(t)$ can be written as:

$$c_{tot}(t) = d_c(t) + \sum_{i=1}^{N(t)} \Delta d_i \qquad (3\text{-}18)$$

where $d_c(t)$ is continuous damage at time t due to aging, Δd_i is the damage increment in a single seismic event and *N(t)* is the number of earthquake events in time *t*. Both

deterioration effects can be expressed in terms of the same parameter which is the ductility to collapse $\mu(t)$ (Equation (3-19)). This parameter represents the ratio between the maximum displacement u_{max} and the yield displacement u_y.

$$D(t) = \mu_c(t) + \sum_{i=1}^{N(t)} \Delta\mu_i \qquad (3\text{-}19)$$

In the case of continuous wear only, the modelling of aging can be represented by a gamma process and the probability of failure is given by (Iervolino et al., 2013):

$$P_f(t) = P[D(t) > \bar{\mu}] = P[\mu_c(t) > \bar{\mu}] = \frac{\Gamma_u(S_a \cdot t, \gamma_a \cdot \bar{\mu})}{\Gamma(S_a \cdot t)} \qquad (3\text{-}20)$$

where $\bar{\mu}$ represents the limit state and S_a and γ_a are the are the shape and scale parameters, respectively. The pdf of the damage accumulated in [0,t] is

$$f_{\mu_c(t)}(\mu) = \frac{\gamma_a(\gamma_a \cdot \mu)^{S_a t - 1} e^{-\gamma_a \mu}}{\Gamma(S_a \cdot t)} \qquad (3\text{-}21)$$

with mean and variance that vary linearly:

$$E[\mu_c(t)] = (S_a/\gamma_a) \cdot t = mt$$
$$Var[\mu_c(t)] = (S_a/\gamma_a^2) \cdot t = \sigma^2 t \qquad (3\text{-}22)$$

Fixing m and σ^2, the parameters γ_a and S_a can be obtained:

$$\gamma_a = m/\sigma^2$$
$$S_a = (m/\sigma)^2 \qquad (3\text{-}23)$$

Typical values of parameters m and σ^2 for carbonation and chloride-induced corrosion are given in (Stewart et al., 2011). Estimating the shape and scale parameters of the gamma process due to aging involves statistical methods and analysis of data that represents the aging process of the material or structure in question. To estimate these parameters, data of the degradation process must be gathered over time, collected at regular intervals. This could include measurements of material properties, structural

integrity indicators, or any other quantifiable metrics of aging. In the case only aging is considered, i.e. $D(t) = \mu_c(t)$, and assuming the degradation $D(t)$ follows a gamma distribution, the maximum likelihood estimation (MLE) can be used to estimate the shape and scale parameters. The MLE method finds the parameter values that maximize the likelihood function. Alternatively, Bayesian inference can also be used. Having no experimental data available, the specimens can be sampled from a gamma distribution.

Figure 3-25 shows the curves of the probability of failure referred to the aging process and the shock-based process for each possible damage state $\bar{\mu}$. **Figure 3-26** shows the same curves computed for $\bar{\mu} = 5$ as a function of time T. The parameters γ_a and S_a are set to 10 and 0.01 respectively, that correspond to a mild continuous deterioration (Iervolino et al., 2013, Vamvatsikos & Dolšek, 2011). As concluded in (Iervolino et al., 2013), for this specific case, the aging effect is negligible compared to the damage produced by earthquakes: the probability of experiencing a damage greater than 1 due to aging is ten times lower compared to earthquakes.
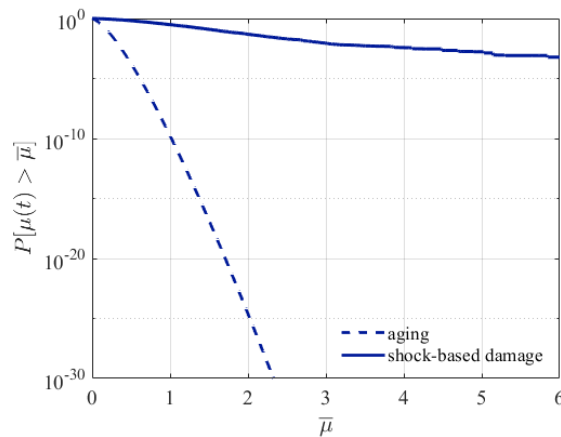
Figure 3-25 Probability of failure curves referred to the aging process (dashed line) and the shock-based process (continuous line) as a function of the damage state $\bar{\mu}$.
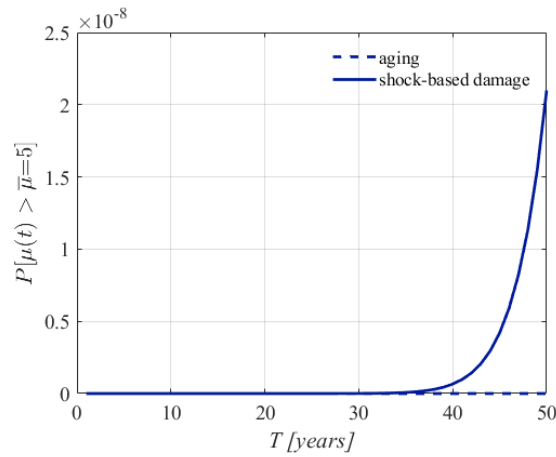
Figure 3-26 Probability of failure curves computed for $\bar{\mu} = 5$, referred to the aging process (dashed line) and the shock-based process (continuous line) as a function of time T

3.4 Conclusions

The work provides a critical evaluation of alternative approaches for evaluating the evolution of damage in structures subjected to multiple shocks during their design life. The first approach considered is based on an existing regression model (RBM) that has been improved introducing three alternative models. The second approach is based on a Markovian method (MM) that requires fitting a transition probability matrix. The estimates of the probability of damage exceedance obtained via the alternative approaches are compared against the estimates obtained using a simulation-based Monte Carlo (SBM) approach. The nonlinear numerical model of a bridge pier is considered for the comparison.

With regards to the first approach, it can be concluded that all the regression models exhibit similar performances but the RM3 model presents the lowest value of the lognormal standard deviation β and highest value of R^2. As a result of this, the estimate of the damage exceedance probability curve obtained with the proposed RM3 model for a time frame of 50 years is the closest to the reference one. Both the number of sequences N_s and the number of events within a sequence N significantly affect the estimates of the probability curves. A number of N_s equal to 500 and a number of N equal to 10 are sufficient to achieve accurate estimates of the probability of damage exceedance in 50 years.

94

With regards to the MM, a good level of accuracy in the estimates of the probability of damage exceedance in 50 years can be obtained for N_s=1000 and N=20. The mean and maximum error in the risk estimate associated with this method are lower compared to the error values associated to the RBM.

The various methods have also been applied considering a reduced time frame of 5 years for the evaluation of the probability of damage exceedance, during which it is more realistic to assume that no retrofit interventions take place following earthquake occurrences. The results obtained confirm that the RM3 model provides a biased estimate of the damage exceedance curve, and thus increasing the number of samples to consider for fitting the regression model does not result in significant improvements in terms of accuracy. On the other hand, by applying the MM method, quite accurate estimates of the probability of damage exceedance can be obtained for N_s=1000 and N=20.

An analysis is carried out to demonstrate the sensitivity of the pier's period to seismic damage, highlighting the critical points where significant changes in structural behavior occur. More refined analyses can identify critical thresholds of stiffness reduction that significantly alter the natural frequency of the structure.

The aging effect is also studied and the correlated damage is compared to the damage due to earthquakes. In the case of mild continuous deterioration, the aging effect is negligible compared to the damage produced by earthquakes.

In conclusion, the RBM is computationally more efficient than the MM, since it is able to provide quite accurate damage estimates with a lower number of samples. However, it introduces some bias in the estimates of the probability of damage exceedance. Using the MM fitted considering a slightly higher number of samples, accurate and unbiased damage estimates can be achieved.

4 A probabilistic model for risk assessment of bridges under aftershocks

Earthquakes sequences are typically characterised by a mainshock followed by several smaller-magnitude aftershocks clustered in space and time. Such seismic sequences can lead to substantial losses, including direct repair expenses, business disruptions, and casualties, particularly if damaged structures and infrastructure are not promptly repaired after the initial event, often due to the short time between successive earthquakes. The assessment of structures following major earthquakes is crucial for effective emergency management decisions and ensuring their safe use, especially under the threat of aftershocks. Additionally, accurate evaluation helps in allocating resources strategically to minimize casualties, prevent business interruptions, and expedite recovery from disruption (Erdik et al., 2011).

Many approaches and frameworks have been proposed in recent decades to address the post-earthquake functionality of bridges and their aftershock risk, with the objective of

assisting in the decision-making process regarding the reopening of bridges to traffic. Mackie & Stojadinović (2006), among others, developed an approach based on the performance-based earthquake engineering (PBEE) framework by the Pacific Earthquake Engineering Research (PEER) Center to evaluate the loss in load-carrying and traffic-carrying capacity of bridges following a mainshock. However, their approach disregarded the increased risk of damage due to aftershocks.

The accurate evaluation of the level of damage suffered by a structure following an earthquake is critical for a correct estimation of its aftershock risk (*e.g*., Aljawhari et al. (2021),Gentile & Galasso (2021)). Obviously, in the absence of direct evaluations of damage (e.g., via field inspections), knowledge of the earthquake-induced ground-motion intensity experienced by the structure is essential for inferring the level of damage sustained by it. The simplest approach for evaluating ground-motion intensity at a given target site involves using a ground motion model (GMM), estimating the amplitude of a ground-motion intensity measure (*IM*) given the information on the location and magnitude of the earthquake (and eventually other site-specific features). However, the dispersion associated with GMMs is generally large, thus leading to highly uncertain estimates of the ground-motion *IM*. This uncertainty could be reduced by using information from seismic stations near the site (Bragato, 2009; Gehl et al., 2017; Miano et al., 2016; Michelini et al., 2008; Wald et al., 2008). However, the correlation between intensities at two points reduces significantly with the distance between them; hence, the *IM* estimate is generally still quite uncertain unless a station is located very close to the site. In any case, a fragility model (i.e., probability of damage as a function of a hazard intensity measure) is needed to estimate the damage level given the uncertainty of the *IM* (and modelling uncertainties). This results in uncertainty propagation in damage and loss estimates, leading to further uncertainty in assessing structural/nonstructural risk under future earthquakes.

One way to improve the knowledge of the actual state of a structure of interest is by exploiting observations from structural health monitoring (SHM) systems (Limongelli et al., 2017). Most existing SHM methodologies rely on vibration measurements through accelerometers to detect changes in the dynamic properties of the system that can be attributed to structural damage (Soyoz & Feng, 2008). Alternative sensors have also been

proposed for the dynamic identification and damage detection (e.g. Global Positioning System (GPS) receivers, cameras, etc.) (Im et al., 2013; Ozer et al., 2017; Porter, 2004; Spencer et al., 2004). Visual inspections after earthquakes help determine the damage's severity, though they only partly capture effects of the seismic action (e.g., surface cracks in concrete, residual displacements). Moreover, conclusions on the level of damage associated with these effects can be subjective, prone to human error, and unreliable.

Further studies have proposed approaches for improving bridge damage estimates using information from sensors and visual inspections. For example, Limongelli et al. (2017) developed a framework for quantifying the value of SHM sensor information for post-earthquake emergency management of bridges, discussing alternative monitoring strategies. A similar framework was applied by Giordano & Limongelli (2022) to evaluate the value of information of SHM sensors for bridge risk management, considering aftershock hazard. The first natural frequency of the structure was considered as damage sensitive feature in the study. Tubaldi et al. (2022) developed a Bayesian network-based approach for evaluating and comparing the contribution of alternative data sources such as free-field seismic stations, GPS receivers, and structure-mounted accelerometers for bridge seismic risk assessment purposes. The comparison was conducted using two alternative measures that quantify the added value of information from the observations, based on pre-posterior variance and relative entropy reduction concepts. It was shown that the information from an accelerometer mounted on a bridge deck is superior in terms of uncertainty reduction to that provided by seismic stations located not very close to the site or by GPS receivers.

The assessment of the aftershock risk for bridges - and thus decision making on post-earthquake emergency management operations - may significantly benefit from the synergy of the various approaches outlined above and from the fusion of heterogeneous pieces of available information. The Bayesian-network (BN) framework developed by Tubaldi et al. (2022) only considers a mainshock scenario; in this Chapter, the framework is further extended to include aftershocks in the risk assessment of bridge structures. Furthermore, risk updating is carried out by combining valuable information from seismic stations, SHM sensors, and visual inspections. The framework extension requires defining an aftershock hazard model that describes the frequency and intensity of

aftershocks following a mainshock and developing a model that quantifies the damage accumulation under multiple aftershocks, given the damage experienced in the mainshock and the *IMs* of the aftershocks. The framework is applied to evaluate the aftershock risk of a case-study two-span bridge model, which is assumed to be located in Central Italy. This area was exposed to a series of aftershocks during the Central Italy earthquake of 2016-17 (e.g. Ebrahimian & Jalayer, 2017; Sebastiani et al., 2019).

Sub-section 4.1 illustrates the various models involved in the proposed BN. Sub-section 4.2 presents the BN developed to describe the relationship between the various parameters involved in seismic damage assessment and updating of these parameters based on additional available information from different sources. Finally, sub-section 4.3 illustrates the implementation of the method on the two-span bridge as an illustrative case study. This is followed by a discussion of the results and some concluding remarks in sub-section 4.4.

4.1   Models for aftershock risk assessment

This section describes the various models required to develop the BN for aftershock risk assessment, along with the parameters involved and the observations required for updating them.

4.1.1   Mainshock analysis

A GMM is required to estimate the probability distribution of a ground-motion intensity measure for the mainshock (MS) experienced by the considered bridge at the *i*-th site of interest, IM_{MSi}, given the following variables that are assumed to be known at the end of the earthquake: moment magnitude of the mainshock earthquake (M_{MS}); a measure of the source-to-site distance R_{MSi}, for instance, assuming a point-source event, for simplicity; other parameters, collected in the vector $\mathbf{s}_i$, characterising the fault (such as those describing the faulting mechanism, fault geometry, depth to the top of the rupture) and site properties. In general, a GMM is characterised by the following form (Douglas & Edwards, 2016):

$$\log(IM_{MSi}) = f(M_{MS}, R_{MSi}, \mathbf{s}_i) + \eta + \zeta_i \qquad (4\text{-}1)$$

where $f(M_{MS}, R_{MSi}, \mathbf{s}_i)$ is a function describing the lognormal mean of IM_{MSi} given M_{MS}, R_{MSi}, and $\mathbf{s}_i$; η is the inter-event (or between-event) error term, ζ_i, is the intra-event (or within-event) error term.

The inter-event and intra-event variabilities of a GMM describe the multi-level variabilities inherited in the ground motion recordings that arise from multiple station recordings for multiple earthquake events. Specifically, the inter-event error term describes the systematic variability in the ground motions throughout the region produced by different earthquakes of the same magnitude and rupture mechanism. The intra-event error describes the variability in ground-motion intensity at various sites of the same soil classification and distance from the source during a single earthquake (Bommer & Crowley, 2006). Thus, following Park et al. (2007) and Crowley et al. (2008), the same inter-event variability is applied to all sites of interest for a given earthquake scenario. In contrast, the intra-event variability is represented by a spatially-correlated Gaussian random field. This can be built based on the intra-event error terms ζ_i and the correlation coefficient ρ_{ij} between the ground-motion parameters at two sites i and j for $i,j=1,2,..N_{sites}$, where N_{sites} is the number of sites of interest. The corresponding covariance matrix of the ground motion *IM* field has the following form:

$$\mathbf{\Sigma_{IM}} = \begin{bmatrix} \sigma_\eta^2 + \sigma_{\xi i}^2 & \cdots & \sigma_\eta^2 + \rho_{ij}\sigma_{\xi i}\sigma_{\xi j} \\ \vdots & \ddots & \vdots \\ \cdots & \cdots & \sigma_\eta^2 + \sigma_{\xi j}^2 \end{bmatrix} \tag{4-2}$$

where σ_η and σ_ξ represent the standard deviations of the inter- and intra-event error terms provided by the GMM, respectively. Further details about this representation of the ground-motion field can be found in Gehl et al. (2017). The field observations of the ground-motion parameters at seismic stations can be used as evidence to update the prior estimates of the *IM* at the site of interest. The spatial correlation structure between the *IM*s at the monitored points and the target site plays a significant role in propagating the information from observed *IMs* to unobserved ones (Jayaram & Baker, 2009).

4.1.2 Aftershock hazard analysis

The magnitude and location of a mainshock event can be used to obtain realistic aftershock scenarios. Several alternate methods available in the literature can be used to

compute the seismicity/source parameters of aftershocks from the parameters of mainshocks. For example, Reasenberg & Jones (1989) proposed a stochastic Bayesian parametric model that allows the determination of probabilities for aftershocks and larger mainshocks during intervals following a mainshock. The estimate of the model parameters is obtained with Bayesian statistics using the ongoing aftershock sequence and a suite of historic California aftershock sequences. Currently, one of the most popular models to describe the seismicity of a region is the space-time Epidemic-Type Aftershock Sequence (ETAS) model (Iacoletti et al., 2021; Ogata, 1998). The model's premise is that all earthquake events tend to trigger aftershocks with a stationary magnitude-dependent relation between them. The model considers earthquake seismicity from aftershocks (caused by internal stress adjustments in the seismogenic system) and background earthquakes (caused by forces within the plate tectonics, fluid/magma intrusion, slow slip etc.). The ETAS model is a point process representing the occurrence of earthquakes for a given magnitude threshold over a given temporal and spatial range. Due to the computational complexity of the ETAS model, particularly in terms of the location of aftershocks, simpler approaches such as the branching aftershock sequence (BASS) model (Turcotte et al., 2007) are available that probabilistically compute consistent source-to-site distances between the mainshocks and aftershocks. Apart from the models that relate the earthquake sequences using the causal event parameters, some methods propose the casual relations based on the intensity measures of the ground motions. For example, Fayaz et al. (2019) proposed a novel approach that uses time-series modelling concepts to temporally correlate the Arias intensity (used as a proxy for the energy content of ground motions) of various earthquakes sequences.

Generally, for the purposes of structural analysis and risk analysis, the above-mentioned procedures are used to select consistent mainshock-aftershock ground motion records. Recently, Goda & Taylor (2012) proposed an aftershock record selection procedure that can be used to simulate time-series data for mainshock–aftershock sequences. The study used the generalised Omori's law (Shcherbakov et al., 2005) as the basis of generating artificial sequences and simulated a series of events with their time and magnitude stamps. For simplicity, they used the same source-to-site distance R for mainshock and aftershock events. Alessandri et al. (2013) combined aftershock hazard analysis using Omori's law and Latin Hypercube Sampling technique for selection of mainshock-aftershock ground

motions to conduct an aftershock risk assessment of bridge structures. Furthermore, a simplistic approach for simulating mainshock-aftershock sequences is to use Båth's law (Båth, 1965) that postulates that the largest aftershock for a given mainshock is on average 1.2 moment-magnitude units lower than the mainshock.

In this study, for simplicity, the general procedure adopted by Papadopoulos et al. (2020) is utilised to compute the number of aftershocks, their moment magnitudes (M_{AS}), time between the mainshock and aftershocks (Δt), and the distance between the epicentre of the mainshock and that of the aftershock (r_{epi}). The sequences are generated by means of the triggering component of the ETAS model. The model is based on three uncoupled probability distributions that model (a) the direct offspring productivity; (b) the spatial; and (c) the temporal distribution of the triggered earthquakes, as well as a magnitude distribution of earthquakes derived from the Gutenberg-Richter (GR) law. Specifically, the simulation of mainshock-consistent aftershock scenarios in this study uses Equations (4-3) to (4-6). First, the number of direct offspring events from a mainshock event with a magnitude M_{MS} is sampled from a Poisson distribution with mean $k(M_{AS})$ given in Equation (4-3). Then, for each of the offspring events, the distance r_{epi} between the epicentres of the two events and the inter-arrival time Δt between the parent and offspring event are simulated using Equations (4-4) and (4-5), respectively, where u_t, and u_r are uniformly distributed random variables over the range [0,1], and *A, a, p, c, D, q, γ* are constant parameters representing the general spatial and temporal distributions of aftershock events and are estimated mainly through maximum likelihood estimation (Le Cam, 1990). Similarly, for each offspring aftershock, the corresponding magnitude M_{AS} is sampled from the GR distribution using Equation (4-6), where u_m is a uniformly distributed random variable over the range [0,1], *b* is a constant parameter that represents the regional level of seismicity, and M_{min} is the minimum considered magnitude. Equation (4-6) refers to the case of untruncated GR distributions with only a lower bound. After the direct offspring aftershocks (i.e., events triggered by the mainshock) are defined, the second generation of offspring events (triggered by direct aftershocks) can be sampled by repeating the procedure using the first-generation offspring as parent events. The second-generation offspring events can be again used as seeds for a third set and so forth until the sequence eventually dies out (zero offspring are sampled) or there are no more

seed earthquakes within the time of interest. A reasonable time span can be used to dictate the time of interest within which the majority of aftershocks are expected to occur, and bridges are not likely to be repaired (e.g., 1–3 years). In this study, whose focus is on the rapid response to earthquakes, a shorter time span of a few weeks might be considered. Earthquakes simulated outside of this time interval are usually discarded (Papadopoulos et al. 2020).

$$k(M_{AS}) = A \times \exp(a(M_{MS} - M_{min})) \tag{4-3}$$

$$r_{epi} = d \times \exp(\gamma(M_{AS} - M_{min}))\sqrt{u_r^{1/(1-q)} - 1} \tag{4-4}$$

$$\Delta t = -c + c(1 - u_t)^{1/(1-p)} \tag{4-5}$$

$$M_{AS} = -\frac{\ln(1 - u_m)}{b \ln 10} + M_{min} \tag{4-6}$$

The same GMM employed for the mainshock can be used to relate the *IM* of the aftershocks, collected in the vector $\mathbf{IM}_{AS}$, to the aftershock source to site distance ($\mathbf{R}_{AS}$) as well as the magnitude of the aftershocks (M_{AS}). Though the framework can be easily updated to include aftershock specific GMPEs, based on studies like Lee et al. (2020), it was observed that the spectra of aftershocks and mainshocks do not vary significantly. Moreover, the use of average of spectral accelarations over a period range as the *IM* further reduces significant differences. Furthermore, there is a lack of usable aftershock recordings in the available databases. Due to this, the calibration process of aftershock specific GMPEs becomes unreliable (Papadopoulos et al. 2020) and hence most of the similar studies (Jalayer & Ebrahimian, 2017) have reverted to use same GMPEs for both mainshock and aftershock.

4.1.3   Mainshock response and damage assessment

Given the mainshock ground-shaking intensity, a statistical model is required to describe the joint probability distribution of the engineering demand parameters (*EDPs*) of interest for increasing intensity levels (Zhang et al., 2020). Furthermore, modelling the correlation structure between the various parameters of interest is very important as it is the basis for updating the probabilistic distribution of one *EDP* (e.g., floor acceleration in a building) given the observation of another (e.g., storey drift).

Alternative approaches can be employed to develop a joint probabilistic seismic demand model (PSDM), such as Multi-stripe analysis (Scozzese et al., 2020), Incremental Dynamic Analysis (Vamvatsikos & Cornell, 2002), or Cloud Analysis (Jalayer, 2003). Cloud analysis is adopted in this study, given its computational efficiency and resulting accuracy. For this purpose, the computational model of the considered structure is analysed under a set of ground-motion records of different *IM* levels. The response parameters (*EDP_i*, for $i = 1, 2, .., N_{EDP}$) are used as target variables for a regression model. In particular, a bilinear model is considered in this study (Freddi et al., 2017; Tubaldi et al., 2016) since it allows a better description of the trend of the structural response with the ground-motion intensity. The model for the generic *i*-th *EDP* is given in Equation (4-7) (see **Figure 4-1**):

$$ln(EDP_i|IM) = [a_{1i} + b_{1i} \, ln(IM) + \varepsilon_{1i}(\sim N(0,\beta_{1i}))]H(IM - IM^*)$$
$$+ [a_{1i} + b_{1i} \, ln(IM^*) + b_{2i}(ln(IM) - ln(IM^*))$$
$$+ \varepsilon_{2i}(\sim N(0,\beta_{2i}))][H(IM^* - IM)] \qquad (4\text{-}7)$$

where a_1 is the intercept of the first segment, b_i for $i = 1, 2$ are the slopes of the two segments, IM^* is the breakpoint *IM*, which is defined as the point of intersection of the two segments.
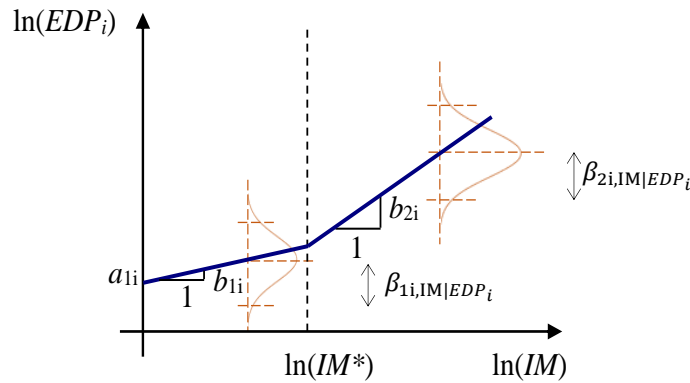
Figure 4-1: Illustration of the bilinear regression model.

The step function $H(\cdot)$ controls which of the two segments must be considered (i.e., $H = 0$ for $IM \leq IM^*$, and $H = 1$ for $IM > IM^*$). The probability distribution of each *EDP* is also described by the values of two random variables (i.e., the error terms $\varepsilon_{1i}(\sim N(0,\beta_{1i}))$ and $\varepsilon_{2i}(\sim N(0,\beta_{2i}))$), which are characterised by a normal distribution with zero mean and standard deviations β_{1i} and β_{2i}. Moreover, to define a joint probability density function

(PDF) for the various *EDPs*, a covariance matrix must be assigned, which has the same form as that of Equation (4-2). For this purpose, different correlation coefficients must be estimated for the two conditions corresponding to $IM \leq IM^*$ and $IM > IM^*$, thus, leading to two correlation matrices. The *EDPs* considered in this study are the peak transient displacement (*TD*), the residual displacement (*RD*) and the peak absolute acceleration (*PA*) at the bridge deck level. The first two parameters may be measured using GPS receivers, laser vibrometer, transducers, and cameras, whereas *PA* is measured using accelerometers.

In addition to the above response parameters, two more *EDPs* are needed to define the visual inspection outcomes, ε_{cc} and ε_{ct}, respectively denoting the maximum strain of concrete cover in compression and tension experienced during the mainshock. For simplicity, it is assumed that a visual inspection provides information only on whether concrete cracking and crushing have occurred or not at the base of bridge piers. These two events are defined by ε_{cc} and ε_{ct} exceeding their respective limits $\bar{e}_{cc}$ and $\bar{e}_{ct}$, which are in general also random variables. The state of the bridge is described in this study by a global damage index (*D*), which is an extension of the Park & Ang (1985) damage index (see Equation (3-1)) to the case of biaxial loading. Since the structure examined is subjected to biaxial loading, a biaxial damage index *D* is employed to define the bridge state. Rodrigues et al. (2013) carried out an experimental campaign on 24 reinforced concrete (RC) columns tested under bi-dimensional earthquake conditions and presented seven expressions for the evaluation of *D*. The present study considers the following one:

$$D = \sqrt{D_x^2 + D_y^2} \qquad (4\text{-}8)$$

where

$$D_x = \frac{d_{max,x}}{d_{ult,x}} + \beta_d \frac{E_x}{F_{yield,x,} \cdot d_{ult,x}} \qquad (4\text{-}9)$$

$$D_y = \frac{d_{max,y}}{d_{ult,y}} + \beta_d \frac{E_y}{F_{yield,y} \cdot d_{ult,y}} \qquad (4\text{-}10)$$

In Equations (4-9) and (4-10), D_x and D_y refer to the damage indices calculated for each independent direction, E_x and E_y are the cumulative dissipated energy for each independent direction, $d_{max,x}$ and $d_{max,y}$ denote the maximum displacements, $d_{ult,x}$ and

$d_{ult,y}$ represent the ultimate displacements, and $F_{yield,x}$ and $F_{yield,y}$ denote the yielding strength in each direction. To exploit the information from sensors and the outcomes of visual inspections for updating the knowledge of the bridge damage, the joint probabilistic model must include both the *EDPs* of interest and the damage index.

4.1.4 Aftershock damage assessment

The process describing the evolution of damage in a bridge under repeated events such as a mainshock-aftershock sequence is a state-dependent process, i.e., the increment of damage that characterises a given shock depends on the history of damage accumulated during the previous shocks. Previous studies (Iervolino et al., 2016) considered the Markovian assumption, i.e., the damage evolution under a given ground motion, conditional to the features of the ground motion, depends only on the state of the structure at the time of the shock and not on all of its damage history. Ghosh et al. (2015) demonstrated in their study that earthquake damage accumulation can be treated as a homogeneous Markov process. Introducing this assumption, the damage index at the end of the *n*-th event or ground motion can be expressed as a function of the intensity of the event and of the damage at the end of the *(n-1)*-th event or ground motion. Specifically, the multi-variate model developed by Ghosh et al. (2015) is employed in this study, which has the following form:

$$
\begin{aligned}
\ln(D_n | & IM_n, D_{n-1}) \\
&= c_n + d_n \ln(D_{n-1}) \\
&+ e_n \ln(IM_n) + f_n \ln(D_{n-1}) * \ln(IM_n) \\
&+ \varepsilon_n (\sim N(0, \beta_{AS}))
\end{aligned}
\tag{4-11}
$$

where IM_n is the ground motion intensity of the nth event, D_{n-1} is the damage index after the (*n-1*)th event; c_n, d_n, e_n, and f_n are regression coefficients, and $\varepsilon_n(\sim N(0, \beta_{AS}))$ is a random variable normally distributed with zero mean and lognormal standard deviation β_{AS}. This model can be fitted to empirical data from analyses of the structure under a series of mainshock-aftershock sequences, where $D_n = D_{MS}$ for *n*=1. It is noteworthy that Equation (4-11) may return values of D_n lower than D_{n-1} due to the nature of the regression model and ε_n. One way to overcome this physical inconsistency (i.e., damage can only increase) is to postulate that $D_n > D_{n-1}$:

$$\ln(D_n | IM_n, D_{n-1})$$
$$= \max[c_n + d_n \ln(D_{n-1}) \qquad\qquad (4\text{-}12)$$
$$+ e_n \ln(IM_n) + f_n \ln(D_{n-1}) * \ln(IM_n) + \varepsilon_n , D_{n-1}]$$

This choice is expected to provide more physics-based results than the model originally developed by Ghosh et al. (2015). It is worth mentioning that under the assumption of a homogeneous Markov process, the coefficients of the model in Equations (4-11) and (4-12) are independent of n, i.e., the probability of moving from a state of damage to another under a given ground motion does not depend on the number of ground motion in the sequence (e.g. the same model can be used for the 2nd earthquake and the 3rd earthquake in a sequence).

4.2   Bayesian framework

This section presents the Bayesian framework developed for the assessment of the aftershock risk of a bridge and for its updating using observations from seismic stations, structural monitoring sensors, and visual inspections.

4.2.1   Bayesian network

This subsection illustrates the BN developed to describe the probabilistic relationship between the parameters specified in the previous section, perform predictive analysis, and update these parameters based on additional information from different observations (see **Figure 4-2**). The magnitude of the point-source mainshock earthquake (M_{MS}) and location between the source and the site as well as the source and the seismic stations (collected in $\mathbf{R}_{MS}$) are assumed to be known. Various types of information are considered to be available for updating the probabilistic relationships of the variables in the network: on-site seismometers located close to the site of the structure, providing information on IM levels; GPS data, updating the knowledge of the RD; accelerometer data, updating the knowledge of the PA in the bridge deck; and the outcome of a visual inspection (VI), updating the knowledge of ε_{cc} and ε_{ct}. In the last case, the values of ε_{cc} and ε_{ct} are updated only if concrete cracking and/or crushing are observed, as this means that the deformations in the most critical fibre of the base section have likely exceeded the limit threshold corresponding to tensile cracking and/or crushing. Since the BN is static, i.e., it

does not account for the temporal evolution of the system between the end of the mainshock and the occurrence of the aftershocks. Thus, information from sensors and visual inspections gained at different times after the occurrence of an earthquake can potentially be merged together.

The nodes of the BN represent random variables, each characterised by a PDF. Nodes are related to their parent and child variables through edges that state conditional dependencies between variables (i.e., use of conditional probability distributions). Nodes with no parents are termed root nodes, associated with marginal probability distributions. Two forms of probabilistic inference can be carried out in BNs: predictive analysis that is based on evidence (i.e., information that the node is in a particular state) on root nodes, and diagnostic analysis, also called Bayesian learning, where observations enter into the BN through the child nodes. When evidence enters the BN, it is spread inside the network, thereby updating the probability distributions of the variables through one of the two forms of inference mentioned above.

The earthquake-induced ground shaking for the mainshock event is modelled by the deterministic root nodes M_{MS} and $\mathbf{R}_{MS}$. For demonstration purposes, two seismic stations (represented by IM_{MS2} and IM_{MS3}) are assumed to be in the vicinity of the bridge site (represented by IM_{MS1}).

Following Gehl et al. (2017), the inter-event variability is modelled by the root node W, which is parent to the three IMs of interest and follows a standard normal distribution. The intra-event variability is modelled via three root nodes, U_j, for j=1,2,3, also following a standard normal distribution. The following relation expresses the joint conditional distribution of the IMs given W and U_i:

$$ln\left(IM_{MSi}|W,U_j\right) = ln\,\overline{IM_i}\,(M_{MS},R_{MSi}) + \sigma_\xi \sum_{j=1}^{3} t_{ij}U_j + \sigma_\eta W \qquad (4\text{-}13)$$
$$i=1,2,3$$

where $\overline{IM_{MSi}}$ is the median value of the IM at the i-th site, and $ln\,\overline{IM_{MSi}}\,(M_{MS},R_{MSi})$ is the lognormal mean, which is a function of M_{MS} and R_{MSi} (see also Equation (4-1)), σ_ξ and σ_η are the lognormal standard deviations describing the intra-event and inter-event variability, respectively, t_{ij} is a term of the lower triangular matrix obtained through a Cholesky factorisation of $\mathbf{C_{IM}}$, which is the spatial correlation matrix expressing the correlation between the IMs at the various sites.

A similar approach is used for the PSDM describing the conditional distribution of the *EDP*s and damage index D_{MS} given the *IM* at the site, IM_{MS}. However, in this case, a bilinear regression model is employed, and thus two different error variables and correlation matrixes have to be considered, one for $IM_{MS} < IM^*$ and the other for $IM_{MS} > IM^*$. In addition, three additional root nodes, denoted as e_{VD}, e_{GPS} and e_{PA}, are introduced. They are used to describe the errors in the visual damage estimation and the measurement errors of the observations obtained with GPS and accelerometers. These error variables are assumed to be zero-mean normally distributed variables. They implicitly represent the accuracy and reliability of the observations from sensors and the visual inspection: for example, if the standard deviation of e_{VD} is large, the information from visual inspections is not very reliable. Thus its contribution in the BN updating will be almost negligible.

The *IMs* of the forecasted aftershock events, collected in $\boldsymbol{IM}_{AS}$, are computed by using the same GMM used for the mainshock, based on the knowledge of the distances between the aftershock source and the site, collected in the vector $\mathbf{R}_{AS}$, and the magnitude of the aftershock sequence $\boldsymbol{M}_{AS}$. Finally, the model described in Equation (4-11) is employed to describe the relationship between the damage incurred from the mainshock D_{MS} and the damage incurred from the aftershocks $\boldsymbol{D}_{AS}$, given the *IMs* of the forecasted aftershock events collected in $\boldsymbol{IM}_{AS}$.
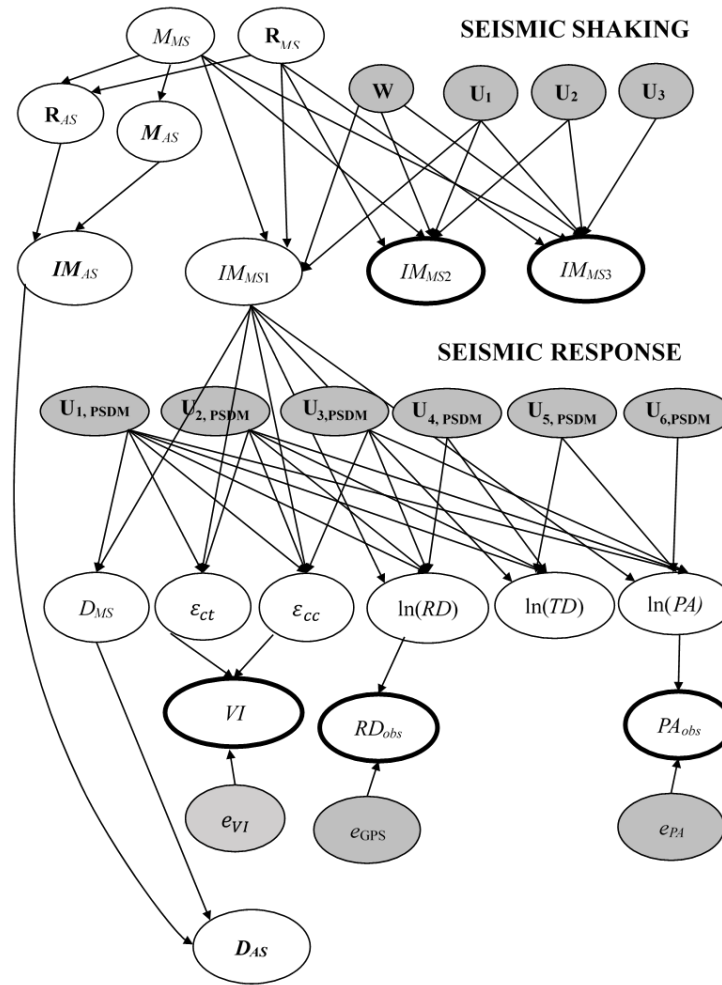
Figure 4-2: Bayesian network illustrating the relationships between the parameters involved in the damage assessment (observed quantities are indicated by thick lines, parent nodes filled with grey).

4.2.2 Bayesian updating algorithm

The BN detailed in **Figure 4-2** is used to perform a predictive analysis, starting from the prior distribution of the root nodes and a diagnostic analysis, entering an observation at the nodes IM_{MS2}, IM_{MS3}, $RD_{obs,}$ and PA_{obs} and visual observations (VI). For this purpose, the OpenBUGS software (Lunn et al., 2009) is employed, which is interfaced with the R statistical tool. OpenBUGS can treat both deterministic (e.g., M_{MS} and $\mathbf{R}_{MS}$) and probabilistic (e.g., IM_{MSi}, TD) variables. These latter are sampled through a Markov-Chain Monte-Carlo (MCMC) sampling scheme. Each chain is built with a Gibbs sampling scheme, where variables are sampled successively from the posterior distribution of previous variables: the posterior distribution of a variable is obtained from the product of the prior distribution and the likelihood function (probability of a given observation

occurring given the prior distribution). The samples are then aggregated to estimate empirical statistics of the variables of interest, representing the posterior distributions. Although Bayesian inference based on sampling provides only approximate solutions (i.e., the posterior distribution is built from the samples), it has the benefit of being much more flexible than exact inference algorithms such as junction-tree inference (Huang & Darwiche, 1996), since it allows modelling continuous variables using various probability distributions. Due to the approximate nature of the posterior distributions sampled by the MCMC scheme, there is no guarantee that exact distribution parameters may be obtained. However, in the present study, the following steps are taken to ensure reasonable accuracy of the results:

- generation of multiple MCMC chains starting with different combinations of initial conditions to ensure that all chains converge towards the same values;
- generation of a high number of samples for each chain (e.g., several tens of thousands);
- definition of a "burn-in phase", where the first part of each chain is removed from the estimation of the posterior distribution, to remove samples that have not yet converged;
- thinning of the samples (i.e., only one sample in every five is considered in each chain) to reduce autocorrelation effects inherent in MCMC sampling.

Specific statistical tools in OpenBUGS are dedicated to estimating autocorrelation and require a minimum number of samples. In any case, preliminary tests are necessary to calibrate the sampling parameters carefully. The chosen sampling results from a trade-off between the required accuracy level and the computational cost. In the present application, the relatively modest size of the BN does not imply unreasonable computational times, and the convergence towards an accurate posterior distribution is checked by estimating the "R-hat" value (Gelman & Rubin, 1992) and the effective sample size (Geyer, 2011) for all variables.

4.3 Case study

4.3.1 Case study description

For demonstration purposes, the structural system considered in this study consists of a two-span bridge with a continuous multi-span steel-concrete composite deck, hypothetically located in Aquila, Italy (latitude 42.5650N, longitude 12.6438E). The selected bridge represents a class of regular medium-span bridges commonly used in transportation networks (Dezi L, 2008; Gray, 2011; Tubaldi et al., 2013) (see **Figure 4-3**). The bridge superstructure, designed according to the specifications given in Eurocode 4 (ECS) (CEN, 2004a) consists of a reinforced concrete slab of width $B = 12$ m, which hosts two traffic lanes, and of two steel girders positioned symmetrically with respect to the deck centreline at a distance of 6 m. Class C35/45 concrete (i.e., characteristic compressive concrete strength of 35 MPa) is used for the superstructure slab. The reinforcement bars are made of grade B450C steel (characteristic yield strength of 450 MPa), and the deck girders are made of grade S355 steel (characteristic yield strength of 355 MPa). The distributed gravity load due to the deck's self-weight and nonstructural elements is 138 kN/m for a mass per unit length $m_d = 14.07$ kN/m. The reinforced concrete piers have a circular cross-section of diameter $d = 1.8$ m. They are made of class C30/37 concrete with a longitudinal reinforcement steel ratio of 1% and a transverse reinforcement volumetric ratio $r_w = 0.5\%$. Further details about the bridge can be found in Tubaldi et al. (2013).
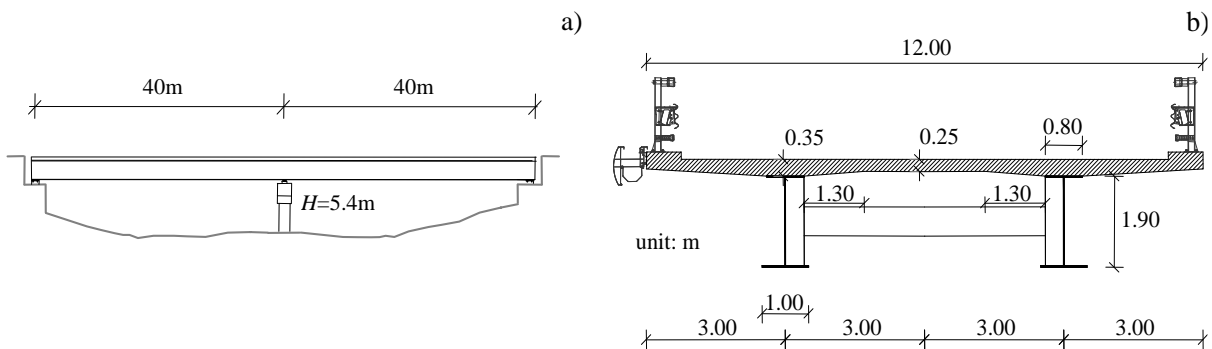
Figure 4-3: a) Two-span bridge profile, b) transverse deck section (source Tubaldi et al. (2013)).

A three-dimensional finite element (FE) model of the bridge is developed in OpenSees (McKenna et al., 2006) following the same approach as described in Tubaldi et al. (2010), i.e., using linear elastic beam elements for describing the deck, and the beam element with

inelastic hinges developed by Scott & Fenves (2006) to describe the pier. Further details of the FE model and the pier properties are given in Tubaldi et al. (2010). The elastic damping properties of the system are characterised by a Rayleigh damping model, assigning a 2% damping ratio at the first two vibration modes. The FE model described in this study is assumed to be deterministic and characterised by no epistemic uncertainties. Future extensions of the methodology will consider the introduction of modelling uncertainty (such as considering the approach outlined in Tubaldi et al. (2012) and their effects on the results.

Figure 4-4 shows the hysteretic response of the pier to a bi-directional ground-motion record, in terms of moment-curvature of the base and base shear-top displacement, along the two principal directions of the bridge. It can be observed that some degradation of stiffness and pinching characterise the model. This results from the constitutive model adopted to describe the concrete fibres in the plastic hinge region (Concrete 02 in OpenSees (McKenna et al., 2006)). However, a more sophisticated description of the hysteretic behaviour of the pier and other bridge components (see for instance Fayaz, Medalla, et al. (2020); Kashani et al. (2016)) is out of the scope of this study.
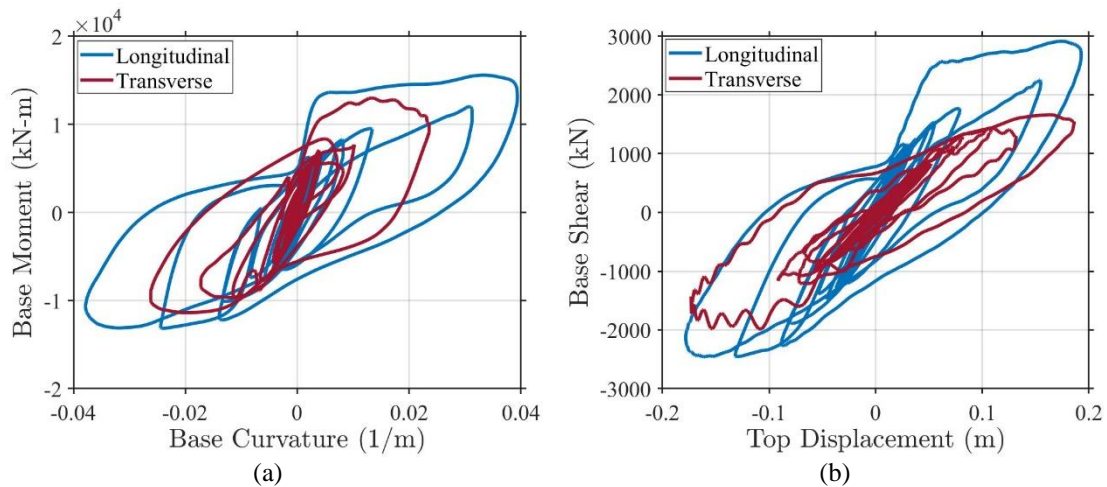
Figure 4-4: a) Base moment-curvature response and b) base shear-top displacement response, along the two principal directions of the bridge.

To develop the probabilistic seismic models that describe response and damage under the mainshock-aftershock sequences, 200 mainshock-aftershock recordings from the database developed by Goda & Taylor (2012) and Goda et al. (2015) are considered. The database contains 703 mainshock events and their corresponding strongest aftershocks (described in terms of peak ground acceleration and magnitude). The M-R_{rup} distribution

114

of the data used is provided in **Figure 4-5**, along with corresponding histograms. In addition, Appendix A provides further details on the selection process of the 200 mainshock-aftershock sequences employed in this study to build the probabilistic seismic response and damage models. The RotD50 pseudo-spectral acceleration at the fundamental period of the bridge (RotD50Sa) is the selected *IM* for both the mainshock and the aftershocks for simplicity. More advanced *IM* could be used (as done in the record selection, see Appendix A). The GMM of Lanzano et al. (2019) is used to estimate the ground motion *IM* values at the site from the considered earthquake point sources, assuming soft soil conditions (V_s=300m/s) and a normal fault mechanism.

(a)   (b)
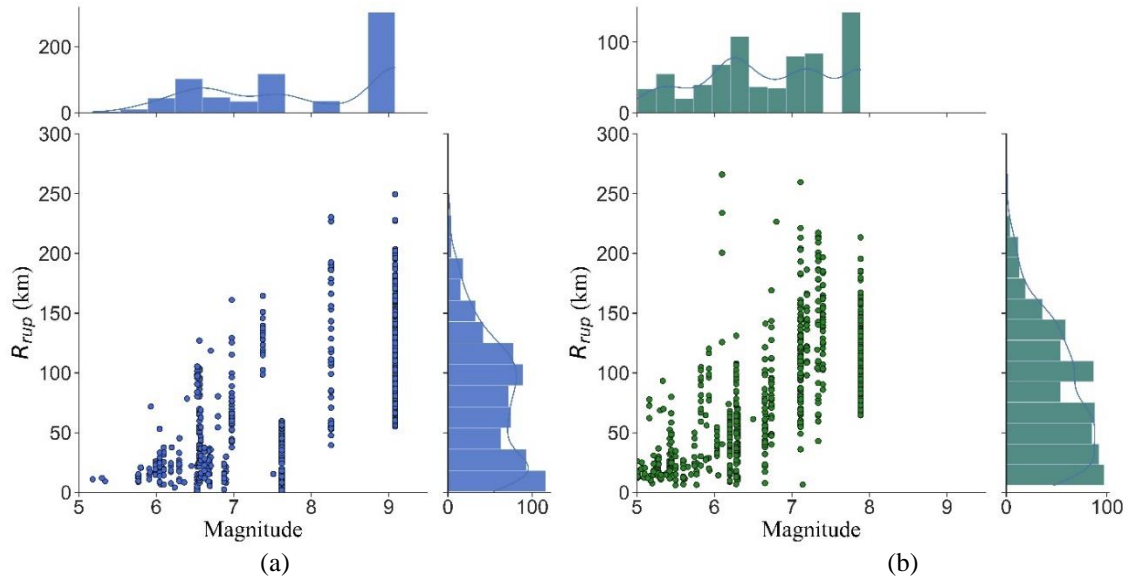
Figure 4-5: .a) M-R_{rup} distributions of: (a) mainshocks and (b) aftershocks of the selected database (703 GMs)

As described in Appendix A, the ground motion components are scaled such that their RotD50Sa matches the target spectral acceleration level. After the ground motion components are selected and scaled, the two ground motion components are randomly rotated and then applied to the two orthogonal directions of the bridge structure. This is done to avoid any assumptions regarding the incident angle of the ground motions with respect to the bridge structure (Fayaz, Dabaghi, et al., 2020). The PSDM described in sub-section 4.1.3 is built using the 200 samples of the various response parameters of interest for the performance assessment obtained under the mainshock event. These are the residual displacement (EDP_1=RD), the peak transient displacement (EDP_2=TD), the peak absolute accelerations (EDP_3=PA), the maximum strain of concrete cover under compression (EDP_4= ε_{cc}), the maximum strain of concrete cover under tension (EDP_5=

ε_{ct}) and the damage index D_{MS}. The value of the coefficient β_d considered in the calculation of the damage index is 0.8. A sensitivity analysis on the number of samples has been performed and the results have shown that the PSDM parameters and also the risk estimates shown in the later section do not change significantly by increasing the number of samples.

Figure 4-6 shows the sample values of these parameters versus IM_{MS} in the log-log plane. In the same figures, the median of the fitted PSDM is also plotted. For simplicity, the same value of IM^* is used for the various parameters of interest. The value of $IM^* = 7.39$ m/s2 corresponds to a median value of the magnitude of the top displacement vector of 0.0106 m. According to Figure 4b, the pier is expected to experience significant inelastic deformations beyond this displacement level. This corresponds to a change of slope in the demand model. It can be observed that ε_{cc} and ε_{ct} increase almost linearly with the ground-motion intensity, and their trend of variation does not change significantly when IM_{MS} exceeds IM^*. The coefficient of determination R^2, for the various fittings, ranges from a minimum value of 0.59 for the D_{MS}, to a maximum of 0.72 for PA.

(a) (b)
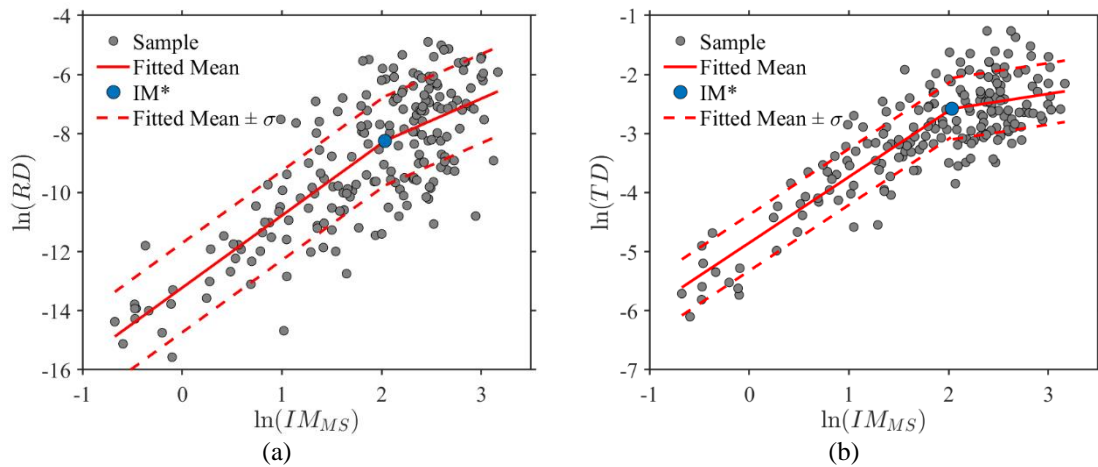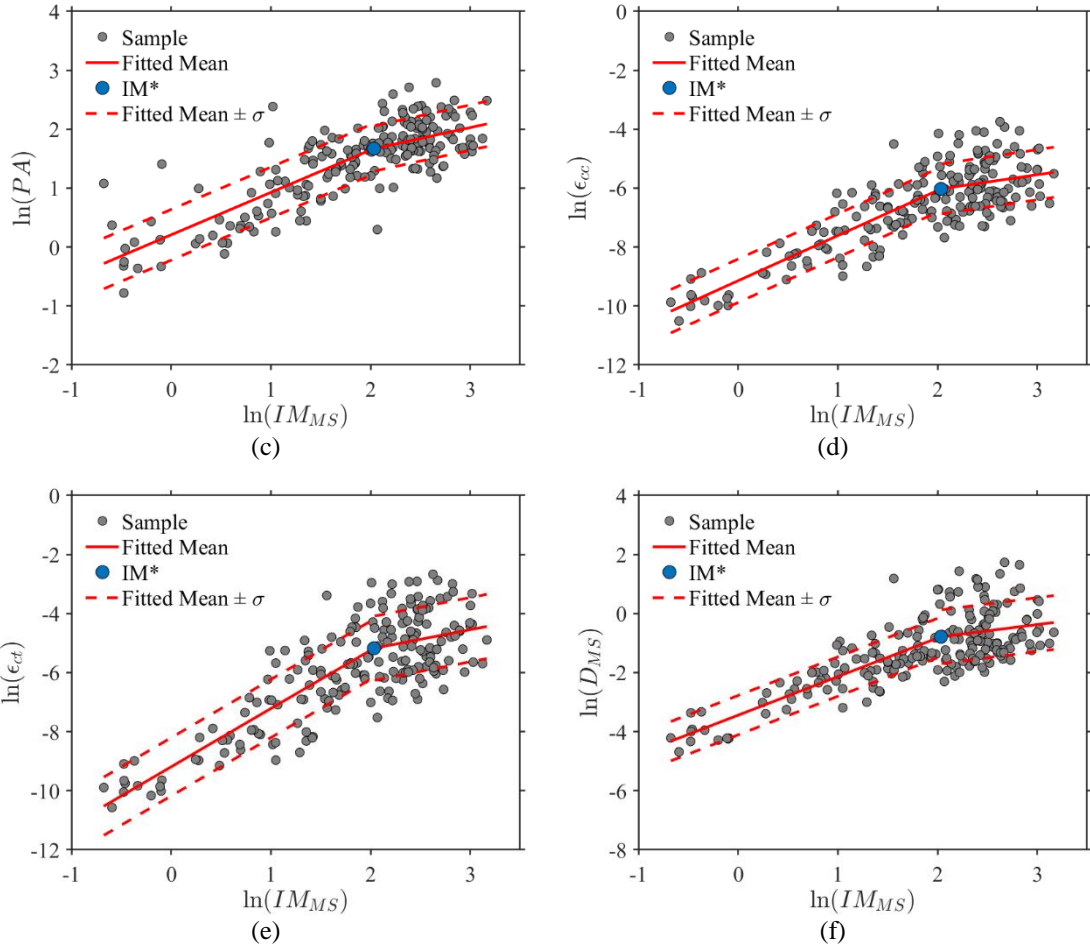
Figure 4-6: Sample values and model results in terms of (a) *RD*,(b) *TD*,(c) *PA*,(d) ε_{cc},(e) ε_{ct}, and (f) D_{MS} vs. IM_{MS} in the log-log plane

The results show that the highest correlations are observed between *TD* and D_{MS} (correlation coefficient of the order of 0.97 for both branches of the PSDM) and between ε_{cc} and ε_{ct} (correlation coefficients of the order of 0.99). On the other hand, the correlation between *TD* and *PA* is of the order of 0.7 for the first branch of the PSDM, and of 0.497 for the second branch of the PSDM. This suggests that the information on accelerations may be used to reduce uncertainty in estimating the bridge's peak transient displacements. It is noteworthy that this approach avoids the need to doubly integrate the measured acceleration signal when estimating displacements, which is characterised by several limitations (Trapani et al., 2015).

The model for damage accumulation corresponding to Equation (4-11) is fitted to the results of the time history analyses of the bridge model under the 200 mainshock-aftershock sequences. The fitted model describes the damage at the end of the first

aftershock given the mainshock earthquake. Under the homogeneous Markov process assumption for the damage accumulation process, it can also describe the damage under any aftershock event of the sequence given the previously accumulated damage.

Figure 4-7 shows the samples of the damage index after the aftershock D_{AS} as a function of the *IM* of the aftershock IM_{AS} and the damage index at the end of the mainshock D_{MS}, and the surface corresponding to the fitted median model. The coefficient of determination of the model, R^2, is 0.697. These values reveal a relatively adequate model fit to the generated damage index data. To increase the accuracy of the results, a higher-order nonlinear model would be required. The regression coefficients for the models of Equation (4-7) and Equation (4-11), the covariance matrices of the PSDM for the mainshock damage assessment and the corresponding correlation matrices can be found in Appendix B.

It is assumed that the bridge is equipped with one accelerometer mounted at the superstructure level above the pier. The measurement error of the accelerometer is characterised by a normal distribution with zero mean and a standard deviation of 0.002 m/s². This value is based on the noise root mean square (RMS) levels of exemplary low-cost sensor specifications extracted from representative datasheets (ST Microelectronics, for a typical low-cost MEMS accelerometer). Other sources of information are not considered in this specific study.
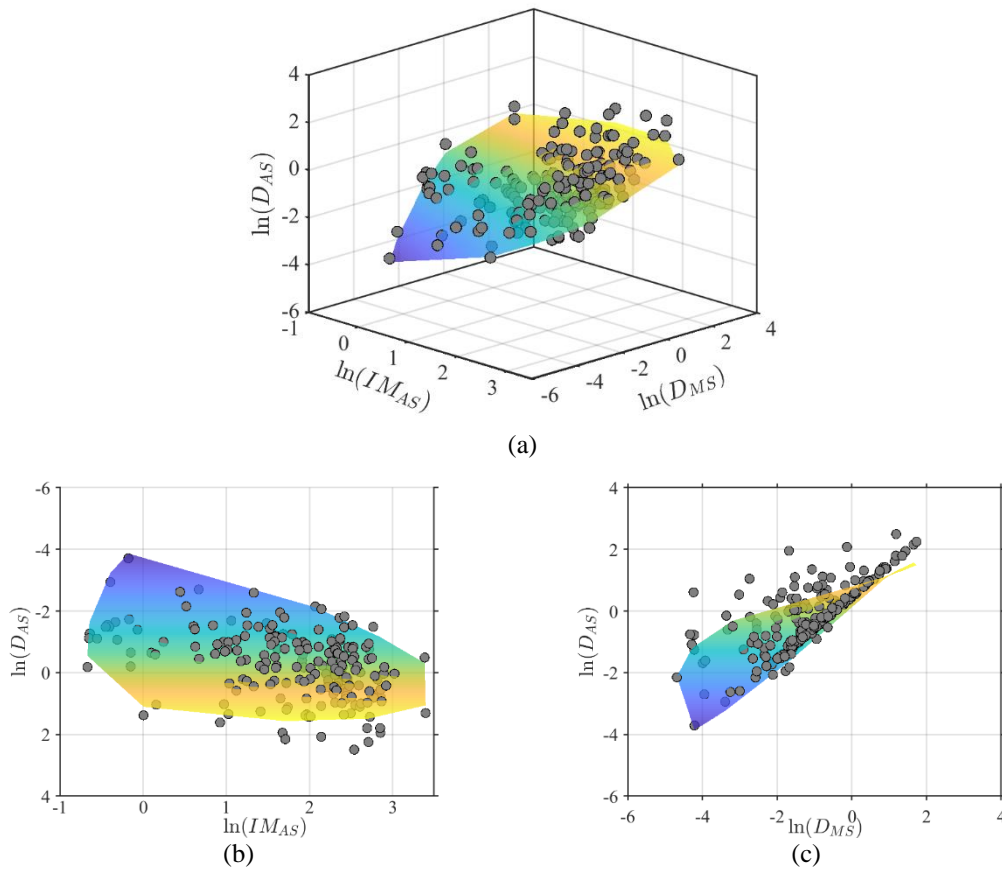
Figure 4-7: Multilinear regression model for describing the damage index after the aftershock as a function of the *IM* of the aftershock and the damage index after the mainshock. (a) 3D view (b)-(c) side views.

4.3.2 Rapid damage assessment for a single scenario

This subsection describes the results of the Bayesian updating of the aftershock risk for a single mainshock scenario, considering the information provided by an accelerometer mounted on the bridge deck above the pier and by a visual inspection carried out at the end of the mainshock. It is assumed that seismic stations are not sufficiently close to the site to provide valuable information for hazard and risk updating. The use of information from stations close to the site is explored in Tubaldi, Ozer, et al. (2022). The seismic scenario corresponds to a seismic event originating from a point source with magnitude M_{MS} 6.5, located 15 km from the site. These values are consistent with the modal values of the seismic hazard disaggregation for the region of interest.

The predictive analysis is first run based on the information at the root nodes. Subsequently, multiple independent diagnostic analyses are performed by entering a piece

119

of evidence one at a time at the nodes PA_{obs} and by entering all the information at these nodes at the same time. These analyses are performed with OpenBugs (Lunn et al., 2009) using three MCMC chains generated with different combinations of initial conditions. This is to ensure that the three different starting points converge towards similar posterior distributions. Each chain contains 10,000 samples obtained by starting from 60,000 iterations, discarding the first 10,000 (burn-in), and thinning to reduce autocorrelation. Ultimately, a total of 30,000 samples are used to estimate the posterior distributions. It is noteworthy that the computation time required to perform a single Bayesian inference analysis is low (in the order of a few seconds on a standard personal computer).

Figure 4-8 shows the empirical cumulative distribution function (ECDF) of the prior distribution of the damage at the end of the mainshock event D_{MS}, and the posterior distributions given the observations of the visual inspection (**Figure 4-8a**) and of an accelerometer on the bridge deck (**Figure 4-8b**). In the analyses, ε_{cc} and ε_{ct} have been assumed as lognormal random variables with mean values respectively equal to 0.004 and 0.001, and a coefficient of variation of 0.3. The visual inspector has been assumed to be well trained, so that concrete crushing and cracking are always correctly detected if they occurred. First of all, it is observed that the expected value of the damage index at the end of the mainshock is low according to the prior estimate of damage. However, the outcomes of the visual inspection can change this distribution significantly. Two different outcomes of the visual inspection are considered. The first one corresponds to the observation of concrete cracking and crushing, while the second one observes no cracking or crushing. In the case of the second outcome, the ECDF shifts to the left (i.e. the damage is overall less than the prior estimate), whereas in the case of cracking and crushing, it shifts significantly towards the right (damage significantly higher than expected). Two different observations of the accelerometer placed at the deck level are considered for updating the damage. In the case of a low value of recorded acceleration (PA=2.95 m/s^2), the expected value of damage reduces, whereas it increases for a very high value of the recorded acceleration (PA=7.83 m/s^2), as expected.
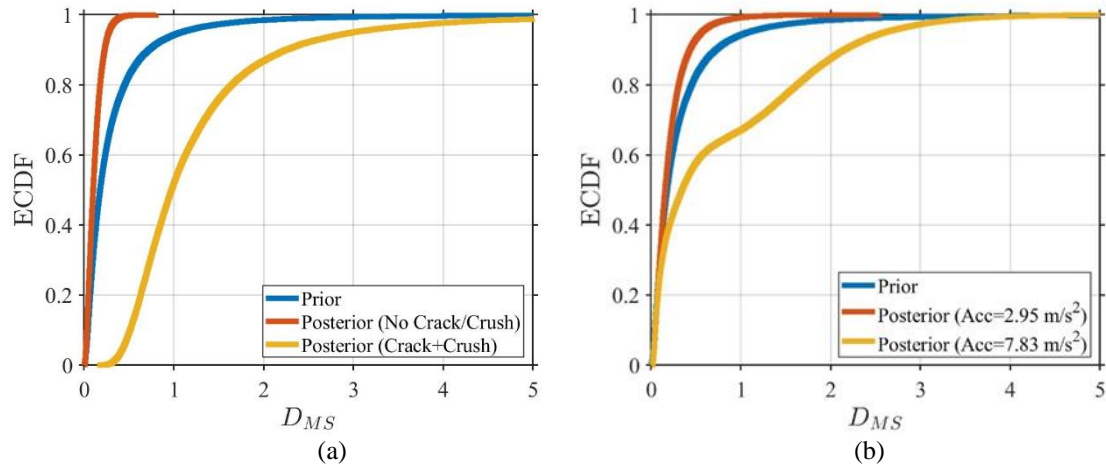
Figure 4-8: Empirical cumulative distribution function (ECDF) of the parameters of interest before and after updating with observations from visual inspection (a) and accelerometer measurements (b).

A series of 10,000 mainshock-aftershock sequences is generated following the methodology outlined in sub-section 4.1.2. Each sequence is described by the seismic intensities of the aftershocks that occur within a time window of interest following the mainshock, collected in the vector $\mathbf{IM}_{AS}$.

Figure 4-9 shows the ECDF of the number of aftershock occurrences in an interval of 10 days and 360 days following the mainshock. Obviously, the number of occurrences can assume only discrete values. It can be observed that the average number of occurrences of aftershocks of any intensity increases for increasing time. The average number of occurrences is about 1 in 10 days, and it increases to 2 in 360 days.

Figure 4-10 shows the probability of exceedance of the *IM* for the case of the mainshock event only and for the mainshock-aftershock sequence within different time windows. It can be observed that the probability of exceedance increases significantly if aftershocks are considered, despite the magnitude of the aftershock being constrained to be less of that of the mainshock. This is because the aftershock could originate from a point source closer to the site than the source of the mainshock, but also due to the uncertainty inherent in the GMM regarding the ground motion attenuation from source to site. Obviously, increasing the time window of interest, the probability of exceedance also increases, but the highest relative increase is observed when only a few days after the mainshock are considered. This is because the rate of occurrence of the aftershock decreases with time since the mainshock occurrence.

121
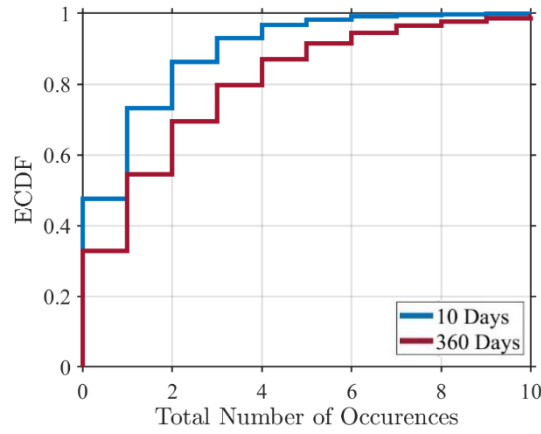
Figure 4-9: Empirical cumulative distribution of the total number of aftershock occurrences in a time frame of 10 and 360 days following the mainshock.
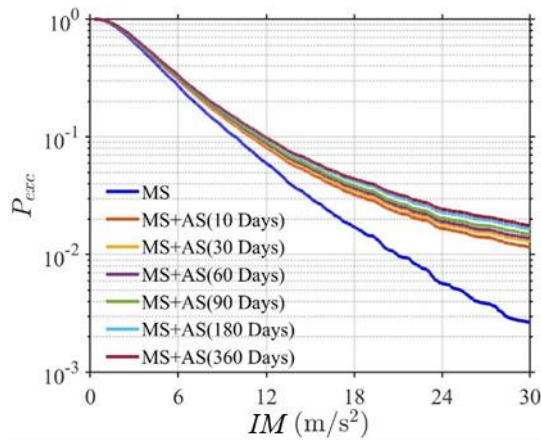
Figure 4-10: Probability of *IM* (RotD50Sa) exceedance under mainshock and mainshock-aftershock sequence for different time windows.

For each of the 10,000 sample mainshock-aftershock sequences, the evolution of the damage index is evaluated by using the model corresponding to Equation (4-12). The various samples of the mainshock damage index D_{MS} obtained by running the Bayesian network are considered as starting points for the various sequences. Obviously, different sample sets must be used, depending on whether the prior estimates or the posterior estimates of D_{MS} following an observation are considered. The $\boldsymbol{IM}_{AS}$ samples are then used together with Equation (4-12) to generate samples of the damage index vector $\boldsymbol{D}_{AS}$ collecting the damage index values at the end of each aftershock. The damage at the end of the mainshock-aftershock sequence, denoted as $D_{AS,max}$, is then used for evaluating the aftershock risk.

122

Figure 4-11 shows the result of the application of the procedure to a sample sequence, considering a time window of 360 days. In particular, **Figure 4-11a** shows the values of the *IM* of the mainshock (event 1) and of the subsequent aftershocks (events 2-8). **Figure 4-11b** shows the corresponding values of the damage index at the end of the mainshock and the subsequent aftershocks. The damage increase is observed only in correspondence to events with significant intensity, as expected. The samples of $D_{AS,max}$ obtained for the 10,000 considered sequences are used subsequently to estimate the probability of damage exceedance in the time window of interest.

Figure 4-12 shows the probability of exceeding different levels of damage at the end of the mainshock and the end of the mainshock-aftershock sequence, 10 days after the mainshock. In **Figure 4-12a**, the risk related to prior D_{MS} estimates is compared with that related to posterior estimates that result from a visual inspection in which no cracking or crushing was observed. In **Figure 4-12b,** the risk related to prior D_{MS} estimates is compared with that related to starting posterior estimates that result from a measurement of a low peak absolute acceleration (2.95 m/s^2) at deck level during the mainshock. It can be observed that the increased risk of bridge damage obtained considering the aftershocks hazard is low, though not negligible. Moreover, accounting for the observations from visual inspections or accelerometers can change the damage risk estimates significantly. The decrease in damage risk due to the observation of no cracking or crushing is more significant than the increase in damage risk due to the consideration of aftershocks. It is noteworthy that the obtained results are not significantly affected by the number of samples used to fit the demand and damage models.

(a)   (b)
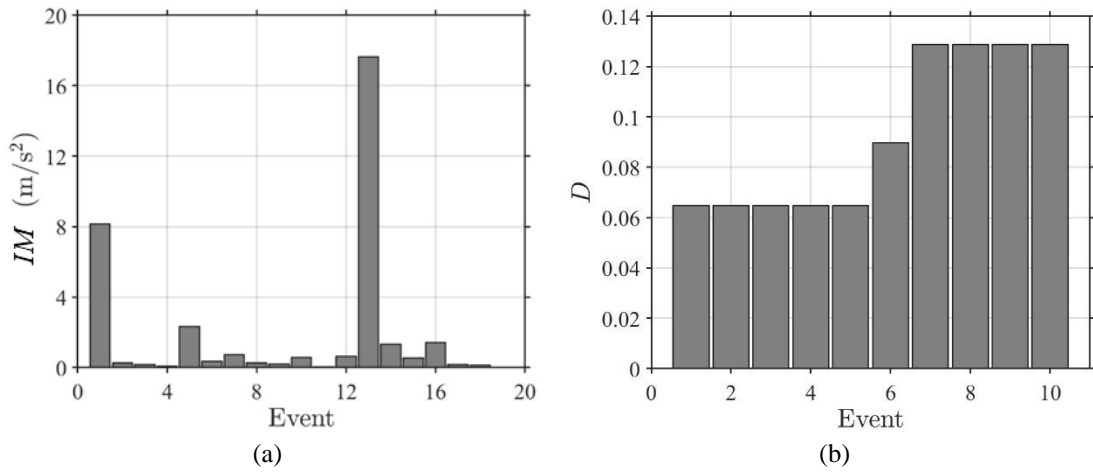
Figure 4-11: a) *IM* values for various events of a mainshock-aftershock sample sequence, b) corresponding damage index values.

(a)   (b)
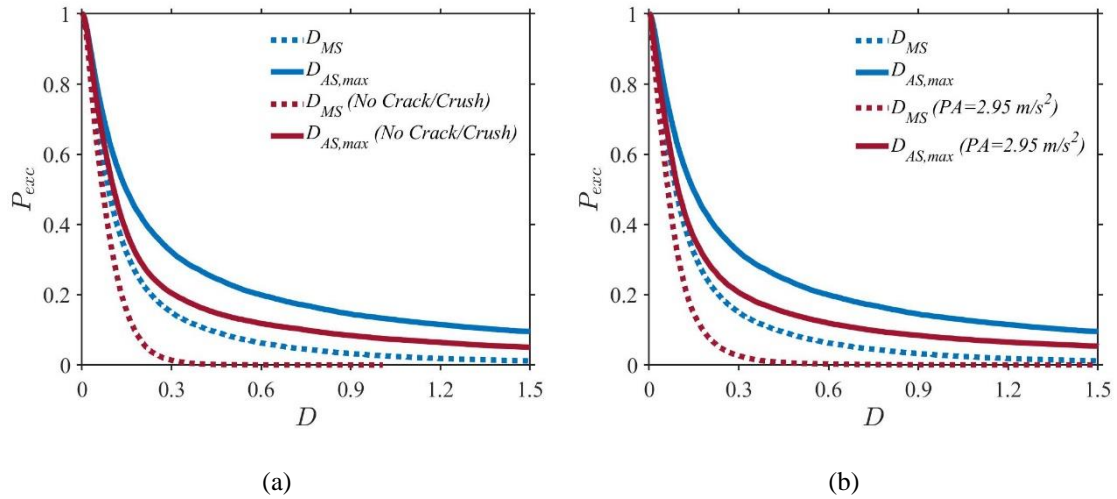
Figure 4-12: Probability of exceeding different levels of damage at the end of the mainshock and the end of the mainshock-aftershock sequence, 10 days after the mainshock, considering prior D_{MS} estimates and posterior estimates following a visual inspection (a) and an accelerometer measurement (b).

Figure 4-13 shows the time-dependent probability of exceeding various levels of the damage index under the mainshock-aftershock sequence, obtained starting from the prior estimate of D_{MS} or from the posterior estimate with no observed cracking/crushing. In general, the probability of exceedance increases for an increasing number of days elapsed after the mainshock. The rate of increase is higher a few days after the mainshock and then decreases due to two different effects: the time-decaying rate of aftershocks and the fact that the intensity of the aftershock is limited. A similar trend was observed in Jalayer et al. (2011). It is also interesting to observe that the relative increase of risk for the mainshock-aftershock sequence compared to the mainshock is more significant if the

124

posterior estimate of D_{MS} is considered as an initial condition. Starting from the prior estimate of D_{MS}, the probability of $D_{AS,max}$ exceeding the value of 1, corresponding to significant damage, is equal to about $2.67 \cdot 10^{-2}$ in the case of the mainshock event only, and it increases to $1.22 \cdot 10^{-1}$ if the whole mainshock-aftershock sequence within a time window of 360 days is considered. On the other hand, starting from the posterior estimate of D_{MS}, the probability of exceeding the damage level of 1 increases from $5.41 \cdot 10^{-6}$ at 0 days to $6.82 \cdot 10^{-2}$ after 360 days. These results could be communicated to transport agencies or bridge managers and can help make better-informed decisions concerning bridge closure in the aftermath of a mainshock.
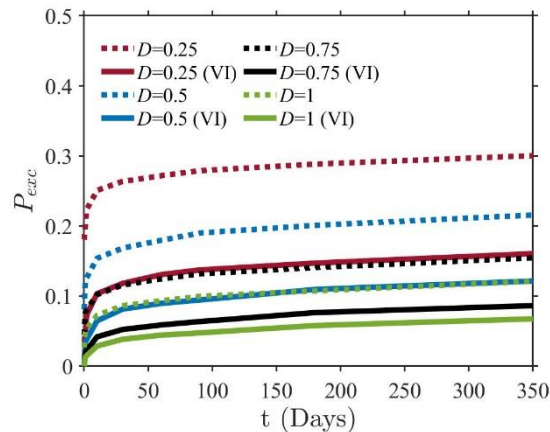
Figure 4-13: Probability of exceedance of various levels of the damage index under mainshock and mainshock-aftershock sequence vs. time elapsed since the mainshock, starting from the prior estimate of D_{MS} and posterior estimates of D_{MS} accounting for visual inspection with an observation of no cracking or crushing.

4.4 Conclusions

This study illustrated a Bayesian framework for the aftershock risk assessment of bridges. The main novelty aspect of the framework is that it allows to specifically exploit heterogeneous information from seismic stations, structural health monitoring sensors (accelerometers and GPS receivers) and visual inspections for updating knowledge of the damage state of the structure after the mainshock and thus make a more accurate assessment of the risk due to future aftershocks.

The proposed framework is applied to a hypothetical bridge in Central Italy subjected to a moderately strong mainshock scenario. A probabilistic model is fitted to describe the joint distribution of the various parameters related to the bridge state (damage index), the monitored responses (e.g. accelerations, residual displacements), and the visual

inspection outcomes (concrete cracking and crushing). The correlation between the involved variables is exploited to update the damage state given the sensor readings and the visual inspection reports.

The study results show that observations of sensors and visual inspections can significantly affect the decision-making process concerning bridge closure in the aftermath of a mainshock. For example, a bridge for which prior knowledge of the mainshock magnitude and source-to-site distance results in a high probability of large damage after a mainshock may be classified as safe following a visual inspection that reports no cracking/crushing of bridge piers. This obviously has an impact on the risk due to future aftershocks. Similar results may be obtained by exploiting the information from accelerometers, if the recorded maximum absolute accelerations are low compared to the ones based on the only knowledge of the earthquake magnitude and location. It is noteworthy that the results obtained by applying the proposed framework to the case-study bridge can be strongly affected by the modelling choices. These include the description of the earthquake aftershock hazard, the structural model and the damage accumulation under multiple events, and the outcomes of the visual inspections given a possible damage state.

5 A methodology for the risk-based design of bridges in Italy

Current design codes are mostly based on a force-based seismic design approach, which accounts for the inelastic capacity of structures by means of a reduction coefficient, i.e. behaviour factor. The earthquake action used for sizing the structural components of a system is expressed in the form of a Uniform Hazard Spectrum (UHS) (Baltzopoulos et al., 2021; Shahnazaryan & O'Reilly, 2021). The UHS provides the seismic demand for a specific location and a predefined return period (TR). The choice to design a structure in accordance with a "uniform" level of seismic demand relies on the assumption that such a procedure would lead to the same annual probability of failure (i.e. collapse) wherever the building is located (Gkimprixis et al., 2020; Silva et al., 2016b). Various limit state conditions have to be considered, corresponding to UHS for different TR values (e.g. 475 years for the ultimate limit state, which is the "benchmark" limit state in Eurocode 8 (CEN, 2004b).

Following the development of modern performance-based earthquake engineering, the research community has focused on understanding whether such a design approach is able to ensure a sufficient and uniform level of structural safety against earthquake actions for different structures located at various sites. Many studies have shown that this objective was not achievable following a uniform hazard design framework (e.g. Cornell & Krawinkler, 2000; Dall'asta et al., 2016; Ellingwood, 2008; Tubaldi, Barbato, & Ghazizadeh, 2012). A recent Italian study within the RINTC Project (Iervolino et al., 2018) aimed at computing for some representative building archetypes and a series of sites across Italy the "implicit risk" characterizing code-compliant buildings. This study showed a strong hazard-dependency of the seismic safety of code-compliant buildings (Pacifico et al., 2022).

In the last decade, risk-targeted seismic design has emerged as a highly promising approach for designing structures with controlled seismic risk and/or loss levels. Following the work of Luco et al. (2007), the principle of "risk-targeting" has been embedded in the development of design maps, which are currently used in US design codes (e.g. Proposed AASHTO Guidelines for Performance-Based Seismic Bridge Design, 2020). As discussed by Fajfar (2018), the risk-targeting paradigm and concepts of risk-targeted maps and behaviour factors (Gkimprixis et al., 2019; Žižmond & Dolšek, 2019) are expected to form the basis of future design codes for many countries (Allen et al., 2015; Douglas et al., 2013; Douglas & Gkimprixis, 2018; Talebi et al., 2021; Vanzi et al., 2015).

The majority of the mentioned studies and codes focuses on the design of buildings. The risk-targeted design for bridges is a less explored topic and only few studies have proposed risk-targeting design methods for these structures. Wang et al. (2014) proposed a method to design reinforced concrete (RC) bridge columns to achieve a uniform risk of failure. The authors proposed a multi-parameter probabilistic seismic demand model to be further used in a uniform risk framework that was specifically developed, by identifying an appropriate target ductility, for the design of RC columns. The relationship between the failure probability of typical RC columns and ductility factors was analysed to define a method to identify the target ductility factor based on an acceptable failure probability for RC bridges located in different US regions. Zakeri & Zareian (2017) also

developed a framework based on full Monte Carlo probabilistic simulation within Probabilistic-Based Seismic Assessment (PBSA) while considering the correlation between demands in different components, to estimate bridge repair-cost ratios at various levels of column drift ratio. Based on this framework, these authors implemented Monte Carlo simulations and Bayesian updating to perform an extensive parametric analysis to estimate probabilities of collapse and the probabilities of exceeding a repair-cost ratio for various design-parameter configurations. These authors also find that column ductility demand μ_d, is not a reliable factor for risk-based design of bridges due to the high level of uncertainty in deriving μ_d. This finding is in contrast to those of Wang et al. (2014).

Additionally, the implementation of a rigorous and straightforward risk-targeted seismic design procedure helps achieve resilience of bridges against multiple hazards. A growing interest in Multi-Hazard Design (MHD) that accounts for cascading effects has been also developed in recent years, with studies dealing with the interaction between different hazards (Argyroudis et al., 2020; Nikellis et al., 2019; Petrini et al., 2020; Zaghi et al., 2016) showing how the right balance between opposing design strategies can be found by adopting a "uniform-risk" strategy amongst different hazards.

The present study proposes a risk-targeted method for the seismic design of bridges. In particular, the proposed procedure addresses the design problem for RC piers in multi-span bridges. The only variables considered as free design parameters are the pier diameter and the longitudinal reinforcement ratio, which are the most important parameters that control the performance of a bridge pier designed according to capacity design principles. In order to reduce the computational effort, a metamodel is built to describe the changes in the bridge dynamic behaviour and seismic fragility with these two design parameters. The optimal values of the design parameters are found as the solution of a simplified reliability-based optimization problem aimed at minimising the pier resisting moment, without the need to resort to complex and time-consuming optimization strategies. The methodology is applied in various locations across Italy to illustrate the variations in the optimal risk-based design properties of bridges across regions with varying seismic hazard and soil conditions, and the impact of the choice of the target risk level on the design results. The proposed procedure efficiently includes the seismic hazard

at the construction site by developing a map for the design parameters for bridge piers required to obtain uniform risk over the territory. The present study is therefore the first attempt to deal with risk-targeting of bridge piers in Italy.

The Chapter is organised as follows. Sub-section 5.1 illustrates the risk-targeted design procedure for bridge piers together with some design choices in the application of the procedure, Sub-section 5.2 illustrates the case study and the results of the parametric study carried out to evaluate the fragility curves for different combinations of design parameters. Sub-section 5.3 illustrates the application of the risk-targeted design procedure to selected sites characterised by different seismicity. In Sub-section 5.4, risk-targeted design maps are developed for Italy, considering different design choices in terms of free design parameters, target risk levels, and soil type. In the final sub-section, conclusions and future studies are outlined.

5.1 Risk-targeting design procedure

The next two sub-sections present the direct and inverse reliability problems corresponding to the assessment of the bridge risk and the design of the bridge properties that satisfy a predefined performance level. Similar to Deb, Zha, et al. (2022) and Wang et al. (2014), the risk-targeted design problem for a single bridge pier (such as that in **Figure 5-1**) is considered. This simplification is introduced due to the role played by bridge piers in controlling the seismic behaviour of bridges and also to facilitate the illustration of the proposed risk-based design procedure.
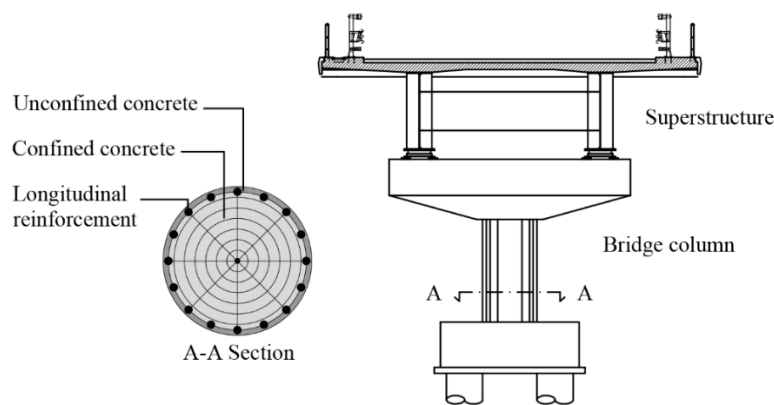
Figure 5-1 Bridge model considered.

130

5.1.1 Direct problem

The basis of the proposed design procedure is the solution of the direct reliability problem, which corresponds to evaluating the probability of exceeding one (or more) limit state(s) of interest during the time interval of interest. For this purpose, a cloud-based approach is employed (Jalayer et al., 2015), where the seismic input potentially causing the limit-state exceedance for the considered structural system and site is synthetically described by one (or more) random variable *IM*, whose realizations are positive real values *im*, and by a set of records that describe the variability of the earthquake characteristics (e.g. frequency content, duration) conditional to the *IM* value.

A capacity/demand format is used to evaluate the limit-state exceedance probability given the seismic intensity. This requires computing the probability of the demand exceeding the capacity conditional to the *IM* of the seismic input. The capacity is measured by a positive real-valued random variable *C*, whose possible realisations are denoted by *c*, with probability density function (PDF) $f_C(c)$ and cumulative density function (CDF) $F_C(c)$. The demand *D* is also expressed as a positive real valued random variable, whose possible realizations are denoted by *d*. The conditional distribution of the demand following events with a seismic intensity *im* is described by $f_{D|IM}(d|im)$. The probability of failure associated to the condition *C<D* conditional to *IM=im*, is:

$$P_{f|IM}(im) = \int F_C(z) f_{D|IM}(z|im) dz \qquad (5\text{-}1)$$

where *z* is a dummy variable.

With regards to the recursive properties of the seismic events during the time interval of interest, it is assumed that an event such that *IM>im* can be described by a Poisson process fully defined by the Mean Annual Frequency (MAF) $v_{IM}(im)$. Under the assumptions that the probability distribution of the earthquake characteristics remains the same at each earthquake occurrence as does the probability of exceedance of the limit state, the failure events also follow a Poisson process and the MAF of failure can be evaluated as follows:

$$v_f = \int_{im} P_{f|IM}(im) \cdot |dv_{IM}(im)| \qquad (5\text{-}2)$$

The probability of failure in a time interval, e.g. the design lifetime t_L, can be obtained as:

$$P_{f,t_L} = 1 - e^{-\nu_f \cdot t_L} \tag{5-3}$$

In the following, it is assumed that the capacity is a log-normal random variable and the two parameters associated to this distribution, the median $\hat{c}$ and the standard deviation of the logarithms β_C, are known and independent of the seismic intensity. It is also assumed that the demand conditional on the seismic intensity is a log-normal random variable, with the parameters $\hat{d}$ and β_D denoting the median and standard deviation of the logarithms, respectively. The relationship between *IM* and *D* can be expressed as:

$$\log[D|IM = im] = \log[\hat{d}(im)] + \varepsilon = a + b \cdot \log(im) + \varepsilon \tag{5-4}$$

where ε is a normally distributed random variable with zero mean and standard deviation β_D. This model implies that only the median value varies with the intensity, while β_D is a constant. This approximation is generally satisfactory and widely adopted in seismic reliability problems, although it may lead to some inaccuracy in the performance assessment (e.g. Gehl et al., 2015; Jalayer, 2003). The three parameters *a, b* and β_D can be determined through ordinary least squares regression, once an adequate number of *IM*-demand samples are known. The relationship expressed in Equation (5-4) is herein assumed, but other closed-form relations can be adopted, provided that they can be inverted (Romão et al., 2013). In this study, cloud analysis is carried out to develop the probabilistic seismic demand model (Jalayer, 2003).

Under the above assumptions on the form of the capacity and of the demand, the conditional probability of failure can be expressed in a closed form as:

$$P_{f|IM}(im) = \Phi\left[\frac{\log[\hat{d}(IM)/\hat{c}]}{\sqrt{\beta_D^2 + \beta_C^2}}\right] \tag{5-5}$$

and the MAF of failure can be evaluated by Equation (5-2) once the MAF of *im* is assigned.

If more than one failure mode is likely, then a system reliability analysis could be carried out to evaluate the failure probability of the bridge conditional to the *IM*, by also considering the correlation between the engineering demand parameters (EDPs) and based on the arrangement of the failure modes (e.g. series or parallel (Jalayer et al., 2007; Minnucci et al., 2022)). The same considerations can be made in the case where multiple piers bridges are analysed.

5.1.2 Inverse problem

Let $\mathbf{x} \in \mathbb{R}^n$ denote the vector of design parameters (e.g. pier longitudinal reinforcement ratio and pier diameter). The risk-targeted design of bridges is an inverse reliability problem that can be cast in the form of an optimization problem: find the set of optimal design parameters $\mathbf{x}^*$ such that an objective function (cost function) is minimised. The solution must satisfy a stochastic constraint requiring that the failure probability (or the MAF of failure) is less or equal to a pre-fixed value, as well as other constraints on the values that can be assumed by $\mathbf{x}$. In mathematical terms, the problem can be formalised as follows:

$$
\begin{aligned}
\min_{X} \quad & g(x) \\
\text{subject to} \quad & \mathbf{h}(x) \leq 0 \\
& v_f(x) - \bar{v}_f \leq 0
\end{aligned}
\tag{5-6}
$$

where $g(\mathbf{x})$ is a cost function, depending on the design parameters, and $\mathbf{h}(\mathbf{x})$ is the set of constraints on the range of variation of $\mathbf{x}$. In Equation (5-6), the dependency of the MAF of failure on the design parameters $\mathbf{x}$ has been made explicit. The choice of a suitable cost function is essential for ensuring that a single design point is obtained. In fact, various combinations of the design parameters ensure that $v_f(\mathbf{x}) - \bar{v}_f \leq 0$. Alternative formulations of the risk-based design problem for structures have been proposed (Franchin et al., 2018). It is noteworthy that under the assumption of failures following a Poisson process, targeting a level of the MAF of failure v_f is equivalent to targeting a level of failure probability in t_L years equal to $(1 - e^{-v_f * t_L})$. The optimization problem employed in this study does not require a complex algorithm. The problem is solved by first pre-mapping the values of cost function $g(\mathbf{x})$ across the domain of $\mathbf{x}$ using different techniques (simulation and interpolation, as described in the next sub-section), and then

by using these gridded values to identify the optimal solution that complies with the target MAF.

5.1.3 Design procedure

The reliability-based design procedure for this problem consists of the following steps:

1. Select various combinations of the design parameters. These could be arranged to form a design of experiments matrix $\mathbf{X}_E = [\mathbf{x}_1 \cdot \cdot \quad \mathbf{x}_j \cdot \cdot \quad \mathbf{x}_{N_E}] \in R^{n \times N_E}$, where $\mathbf{x}_j = [x_{1j} \quad x_{2j} \quad x_{nj}]^T \in R^n$ denotes the vector corresponding to the j-th combination of design parameters, and N_E denotes the total number of design points. In the following, a two-dimensional regular grid of possible design parameters (DPs) is considered as in Deb, Zha, et al. (2022). Alternatively, recourse can be made to Latin Hypercube Sampling, Sobol Sampling (Hoang et al., 2021; Shekhar & Ghosh, 2020) or alternative techniques;

2. For each combination of the DPs, the axial load value corresponding to the forces transmitted by the deck under the seismic load combination and the pier geometry is evaluated. This can be estimated using a linear FE model of the bridge. The design flexural resistance M_{Rd} of the plastic hinge section at the base of the pier is derived in accordance with Eurocode 8 provisions (CEN, 2004), i.e., by considering appropriate safety factors for the capacity of concrete and steel. Subsequently, the transverse reinforcement is designed by applying capacity design principles to ensure that the pier fails under bending rather than shear and by satisfying the minimum requirements for confinement (CEN, 2004); the confined concrete properties in the plastic hinge are evaluated using the Mander model (Mander et al., 1988) (see also Appendix E of CEN (2004)) and a nonlinear FE model of the bridge is developed;

3. Cloud analysis is performed under a set of records representative of record-to-record variability effects to develop a probabilistic demand model for the EDPs of interest. In this study, a single limit state, corresponding to the exceedance of the displacement ductility capacity of the bridge, is considered. This is likely to be the most critical failure mode in newly designed bridges, because the

application of capacity design principles ensures that the probability of occurrence of other failure modes (e.g. shear failure) is negligible;

4. Thus, the monitored EDP is the displacement demand at the pier top, which must be compared to the displacement capacity. This can be evaluated by performing a pushover analysis of the pier nonlinear model;

5. The probability $P_{f|IM}(im, \mathbf{x}_E)$ of exceedance of the limit state of interest conditional to the chosen *IM* and the combination of DPs in $\mathbf{x}_E$ is evaluated. In general, both the demand and the capacity are functions of $\mathbf{x}$. The use of a non-structure-specific *IM* is recommended to allow for comparison between fragility curves corresponding to different DP combinations. The only limit state we consider here is the exceedance of the pier displacement capacity, which is also a function of $\mathbf{x}$. This is the most critical failure mode, with other modes, such as shear failure or bearing failure, avoided due to the application of capacity design principles;

6. Based on the values of the conditional failure probability evaluated in correspondence of the support points, a surrogate model is fitted that provides the conditional failure probability for any possible value of $\mathbf{x}$ without needing to perform other seismic response analyses. The simplest approach for developing the surrogate model is to use linear interpolation. More sophisticated approaches could also be employed, such as those proposed by other authors for developing parametrized fragility functions (Dukes et al., 2018; Franchini et al., 2022; Hoang et al., 2021; Shekhar & Ghosh, 2020);

7. Given a site of interest, characterised by a hazard curve $v_{IM}(im)$, the MAF of failure given $\mathbf{x}$, $v_f(\mathbf{x})$, can be evaluated. This quantity is required for solving the problem formalised in Equation (5-6). Obviously, the solution of the problem depends on the expression of the cost function and on the failure probability target (stochastic constraint), which are discussed below.

5.1.4 Cost function

The form adopted for the optimization problem is such that the consequences of pier failure in terms of direct and indirect losses are controlled by setting a maximum value of the MAF of failure. Since the total bridge life cycle cost is the sum of the cost of bridge

construction and the cost due to failure, in order to minimise this cost one could consider the pier cost as the cost function. In order to avoid defining costs of the materials and of the construction, in the application illustrated in the next section, the cost function is assumed to coincide with the design resisting moment at the base of the pier, M_{Rd}. This quantity is expected to be correlated to the bridge construction cost, as it increases with the pier diameter, the amount of longitudinal reinforcement, the concrete class and other factors. Moreover, by minimising M_{Rd} the design shear (and thus the amount of transverse reinforcement) is also minimised and so are the forces transmitted to the foundations and to the deck.

5.1.5 Target failure probability

Fajfar (2018) discusses the difficulty in defining a target level of failure for structures because it is a reflection of personal and societal value judgements and experience in previous events. Therefore, there is no generally accepted target value. According to Eurocode 0 (CEN, 2002), the minimum recommended values of the reliability index for a reference period of 1 year should be 4.2 for consequence class CC1 structures (low consequences of failure), 4.7 for CC2 class structures (moderate consequences of failure), and 5.2 for CC3 class structures (high consequences of failure). These correspond respectively to a MAF of failure of 1.33×10^{-5} years^{-1}, 1.33×10^{-6} years^{-1}, and 9.96×10^{-8} years^{-1}. However, it is not clear whether the values recommended by Eurocode 0 should be considered for the seismic design, as the draft version of the revised Eurocode 0 explicitly exclude these (Fajfar, 2018). Appendix F of the draft version of the revised Eurocode 8 (Dolšek et al., 2017) suggests a target of 2×10^{-4} years^{-1}, which according to Fajfar (2018) is a value comparable to the probabilities of failure estimated for buildings compliant with current seismic codes, also confirmed in a discussion among European code developers.

In Wang et al. (2014), a mean annual failure probability of 2.3×10^{-4} years^{-1} was considered for the risk-based design of reinforced concrete bridge piers. This value was chosen because it is the median among the values suggested in different American codes or standards (AASHTO, 2010) for ultimate limit state (ULS) conditions. In Deb et al. (2022), different values of the target MAF of failure are associated to the various failure

modes considered: 1/225 years^{-1} for concrete cover crushing, 1/1000 years^{-1} for longitudinal bar buckling, and 1/2500 years^{-1} for longitudinal bar fracture. In Zanini et al. (2022) and Zanini & Hofer (2019) a 1-year target reliability value of 4.7 at ULS has been assumed for structural safety checks of common reinforced concrete arch bridges.

Douglas & Gkimprixis (2018) provide a summary of assessed and target MAFs of failure from the literature. Many studies have adopted the US target value of 2×10^{-4} without much discussion, although Douglas et al. (2013) conclude that a target of 1×10^{-5} or even 1×10^{-6} would be easier to justify based on risk targets from other fields such as nuclear safety. Using a database of collapsed RC buildings in Italy and Greece over the previous few decades, Douglas and Gkimprixis (2018) conclude that the observed risk of collapse for such structures is between 1×10^{-6} and 1×10^{-5}. Because of the importance of road bridges both for life safety and their economic impact during and following earthquakes, a target MAF of failure of 1×10^{-6} is adopted for the following case study. The effect of this choice is examined by also considering 1×10^{-5} and 2×10^{-4} in subsequent steps.

5.1.6 Risk-targeted methodology and Eurocodes

Designing a bridge pier following Eurocodes involves a series of steps to ensure that the pier meets the necessary structural requirements and safety standards. The primary Eurocode for seismic design is Eurocode 8 (EC8), specifically Part 2 (EN 1998-2), which addresses the seismic design of bridges. The process begins with defining the site location and the structural layout, considering the bridge's geographical and environmental context. Next, loading conditions must be established, which include both permanent loads, such as the weight of the bridge itself, and variable loads, such as traffic and environmental influences. Assessing the soil type and classification is also crucial, as it affects the pier's foundation and seismic response.

A preliminary design phase estimates the dimensions of the bridge pier based on initial loading and structural considerations. Following this, a detailed structural analysis is conducted, incorporating seismic hazard analysis to determine the seismic forces the bridge will need to withstand. The required reinforcement is calculated from this analysis, ensuring that the pier meets the ductility requirements outlined in EC8. Ductility is

essential for ensuring that the pier can undergo significant deformations without failing, which is crucial during an earthquake.

The final steps involve verifying the pier design for Serviceability Limit State (SLS) and Ultimate Limit State (ULS). SLS checks ensure that the bridge remains functional and comfortable for users under normal conditions, while ULS checks verify that the pier's design strength meets or exceeds the maximum expected loads during extreme events, such as earthquakes. Many studies have shown that following this procedure does not always ensure a predetermined risk level. To accurately determine the risk level, a detailed risk analysis is necessary, which involves computing fragility curves to predict the probability of different levels of damage under various seismic scenarios. However, this process is time-consuming and is generally not performed by industries or engineering firms due to its complexity and resource requirements.

If the risk analysis indicates that the target risk level is not met, the structure must be redesigned, following an iterative approach to refine the design until the target risk level is achieved. This iterative process can be cumbersome and inefficient. Furthermore, the Eurocode methodology, based on uniform hazard, has indirectly required that in some areas of the country, engineers design buildings more stringently, to reduce the likelihood of collapse, compared to other regions. The risk-targeted approach has mitigated this variability ensuring that the risk of collapse and the design stringency are consistent across all locations.

Conversely, designing a bridge pier using the proposed risk-targeted methodology simplifies this process. This methodology is also iterative but avoids the need for performing a detailed risk analysis each time. Instead, it directly associates a specific risk level with a corresponding resisting moment. By ensuring that the pier design meets the specified resisting moment, engineers can be confident that the structure meets the desired risk level. This approach streamlines the verification process, as it ensures compliance with specific limit states without the need for extensive fragility assessments.
While this risk-targeted methodology needs further study and refinement, it promises a more efficient and direct path to achieving and verifying structural safety and performance against seismic events.

In the future, the Eurocodes will likely be updated to incorporate risk-targeted methods. Specifically, the methodology presented herein could be included in the next generation of Eurocodes. This could be reflected in chapters focusing on seismic design provisions, where performance-based criteria are outlined to ensure that structures meet predetermined risk levels. The inclusion of risk-targeted design principles would help standardize safety and performance criteria across different regions, providing a uniform basis for seismic design that aligns with modern engineering practices and risk management strategies. By focusing on direct performance metrics linked to risk levels, this method could offer significant advantages in practical engineering applications, improving both the design process and the reliability of the resulting structures. This evolution in the Eurocodes would mark a significant advancement in the resilience and reliability of civil infrastructure.

5.2   Case study description and results of parametric analyses

A two-span bridge with a continuous multi-span deck is used to illustrate the application of the proposed risk-based design method. The bridge is representative of a class of medium-span bridges widely present in the European transport network. It was considered in previous studies by the same authors (Tubaldi et al., 2013; Tubaldi, Ozer, et al., 2022). The steel-concrete composite superstructure, designed according to Eurocode 4 (ECS) (CEN, 2004a), consists of an RC slab of width $B = 12$ m, made with class C35/45 concrete (i.e., characteristic cylindrical compressive concrete strength of 35 MPa) and with grade B450C steel reinforcement bars (characteristic yield strength of 450 MPa), and of two steel girders placed 6 m apart, made of grade S355 steel (characteristic yield strength of 355 MPa). The distributed gravity load due to the deck's self-weight and non-structural elements is 138 kN/m, corresponding to a mass per unit length $m_d = 14.07$ kg/m. The RC column is 5.4m high and has a circular cross-section with diameter D_c. It is made of class C30/37 concrete. The deck is free to move in both the longitudinal and transverse directions at the abutments.

The three-dimensional FE model of the bridge is developed in OpenSees (2011) using the beam element with inelastic hinge developed by Scott & Fenves (2006) to describe the

bottom of the pier, and linear elastic elements to describe the remaining part of the pier. The plastic hinge length is evaluated using the Eurocode 8 part 2 formula (CEN 2004). The geometric and material nonlinearities are accounted by means of the fibre-based section discretisation technique. This allows the representation of the influence of inelastic steel buckling and low cycle fatigue degradation. Degrading of stiffness in linear unloading/reloading is modelled according to Karsan & Jirsa (1969). The concrete stress-strain relationship is modelled through the Kent-Park model (Kent & Park, 1971). The reinforcement steel is modelled by the Menegotto-Pinto constitutive model (Menegotto & Pinto, 1973). The following material properties were assumed as fixed in all the models: a mean steel yield stress of f_{ym}=517.5 MPa, maximum deformations of unconfined concrete under compression ε_{ccover}=0.0035 and an ultimate steel deformation ε_{su}=0.075. The material nonlinearity was described through a uniaxial material relationship for steel (tension and compression) and concrete (confined and unconfined). In this study, the Concrete02 model and the Steel02 model available in OpenSees (2011) were used: Concrete02, which is a linear tension softening material model that considers unloading stiffness degradation, was used to model the unconfined concrete in the cover and the confined concrete in the core of the pier, whereas Steel02 was used to model the reinforcement bars. The bearings were represented by zero length elements with a module of elasticity of 210,000 MPa connected to the elastic element via a rigid link-beam (both the translational and rotational degrees of freedom are constrained). The deck was not modelled but a vertical load was added to the column to simulate the weight of the deck. The elastic damping properties of the system are characterised by a Rayleigh damping model, with a 5% damping ratio assigned to the fundamental vibration modes in the longitudinal and transverse directions.

The same bridge is assumed to be located at various sites in Italy, characterised by different seismic hazards. A soil type A (corresponding to an time-averaged shear wave velocity up to 30 meters depth of $V_{s,30}$ = 800 m/s) is considered for all the locations. Similarly to Deb, Zha, et al. (2022), the only DPs herein considered in the application of the risk-based design procedure are the pier diameter D_c and the longitudinal reinforcement ratio ρ_L,; thus $\mathbf{x}$=[D_c, ρ_L]. It is noteworthy that these parameters are, among the many others that could be considered in $\mathbf{x}$, the ones that mostly affect the bridge's

seismic performance (Deb, Zha, et al., 2022; Wang et al., 2014). These DPs are assumed to vary in a realistic range that reflects construction practice and satisfies code requirements. In particular, ρ_L can vary between 1% and 4%, whereas Dc can vary from 1.4 m to 2.2 m (source K. Mackie & Stojadinovic, 2003). In order to develop the surrogate model for the bridge fragility, a regular grid of values of D_c and ρ_L is constructed. In particular, the values of D_c of 1.4m, 1.8m, and 2.2m and the values of ρ_L of 1%, 2%, 3% and 4% are considered. For simplicity, two-dimensional linear interpolation is used to find the values of dependent variables corresponding to intermediate values of D_c and ρ_L. The various functions that are interpolated exhibit smooth and regular trends and, hence, more sophisticated interpolation methods or metamodeling techniques are not necessary.
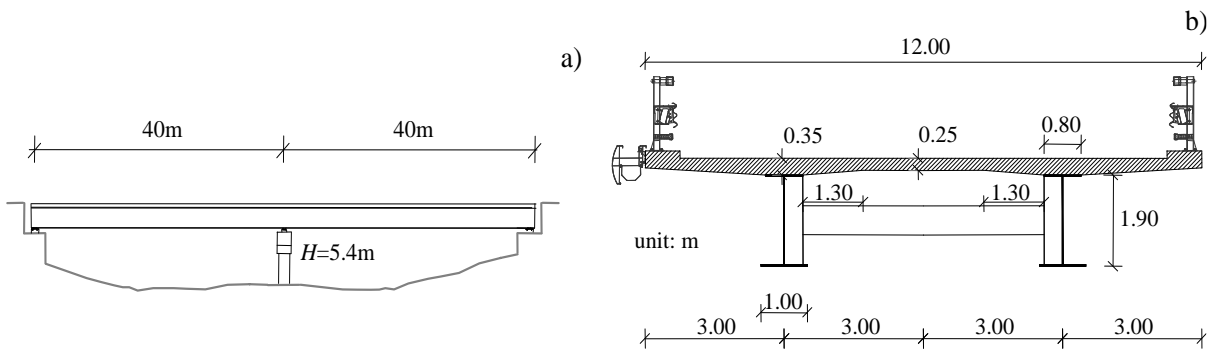
Figure 5-2 a) Two-span bridge profile, b) transverse deck section (source Tubaldi et al. (2013)).

Figure 5-3 shows the moment-curvature relationship for the section at the base of the pier for the different combinations of DPs investigated. The curves have been derived using a fiber-based discretisation of the cross section, considering different values of the axial force (to account for the effect of the pier's self-weight), as well as different levels of confinement, for the various values of D_c and ρ_L.

 In all cases, the failure of the section corresponds to the crushing of the confined concrete, whereas the ultimate strain of the longitudinal reinforcement (assumed equal to 0.075) is never exceeded.
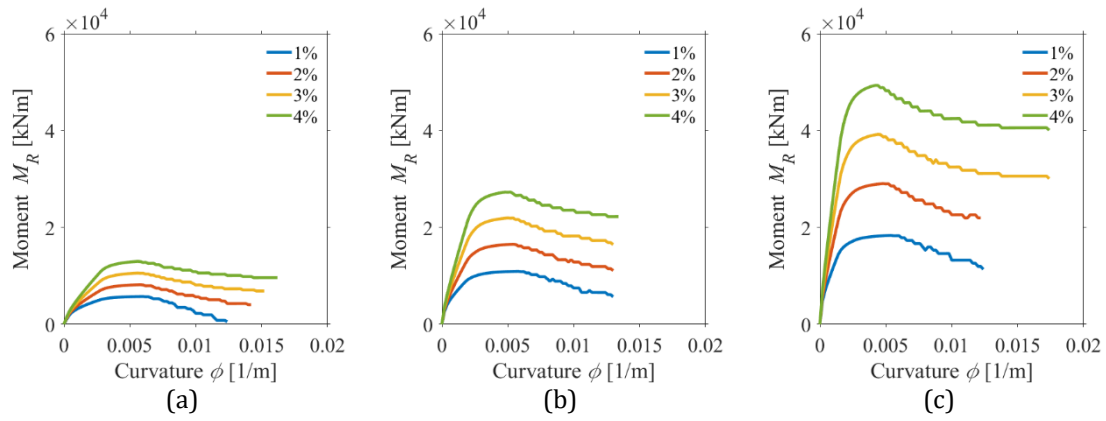
Figure 5-3 Moment-curvature relationships for different combinations of DPs along the longitudinal direction
(a) D_c =1.4m (b) D_c =1.8m (c) D_c =2.2m.

Figure 5-4 shows how the values of the design resisting moment M_{Rd} at the pier base (**Figure 5-4a**) and the transverse reinforcement ratio ρ_S (**Figure 5-4b**) increase with the diameter of the pier and the amount of longitudinal reinforcement. It can be noted that increasing D_c and ρ_L results in an increase of M_{Rd} and thus of ρ_S. The increase of ρ_S is due to the application of capacity design principles, with the design shear that increases with the base design resisting moment M_{Rd}. In general, the design resisting moment is more sensitive to D_c than to ρ_L for low D_c values. However, for high D_c values increasing ρ_L results in large increase of M_{Rd}. The transverse reinforcement ratio ρ_S varies between a minimum of 0.75% for low values of D_c and ρ_L to a maximum of 1.89% for D_c =2.2m and ρ_L=4%. The diameter of the hoop bar ranges from 16mm to 22mm with a spacing between the bars from 80mm to 35mm.

Figure 5-5 shows the variation of the fundamental vibration periods along the longitudinal and transverse direction due to the variation of D_c and ρ_L. The longitudinal period is shorter than the transverse one due to the lower effective bending length. The bending lengths are equal to the pier height in the longitudinal direction, and the pier height plus the distance between the pier top and the deck centroid in the transverse one. In fact, the bearings placed at the bottom of the two girders in the steel-concrete composite deck result in transmission of bending moments from the deck to the pier under the transverse earthquake component. Both these periods reduce by increasing D_c and ρ_L as the structure becomes stiffer. In general, it can be observed that the quantities shown in **Figure 5-4** and **Figure 5-5** exhibit smooth trends with the design parameters.

Table 5-1 reports the values of the yield displacement d_y, the yield force V_y, and the ultimate displacements d_u for twelve combinations of DPs, in the longitudinal (L) and transverse (T) directions. The ultimate displacement has been identified based on a pushover analysis as the displacement that corresponds to the attainment of the ultimate curvature at the base section. The influence of higher order mode effects has been neglected in evaluating d_u, since they are not likely to affect the displacement demand significantly. Shear failure of the pier is not likely to occur thanks to application of capacity design principles.

The yield and ultimate displacements decrease with increasing diameter D_c, as expected (see Priestley et al., 2008). On the contrary, these quantities increase for increasing values of ρ_L. The increase of stiffness (and thus reduction of period) due to the increase of longitudinal reinforcement (i.e. flexural strength) is a typical feature of reinforced concrete sections, which is at the base of the development of direct-displacement based design criteria (see Priestley et al., 2008).
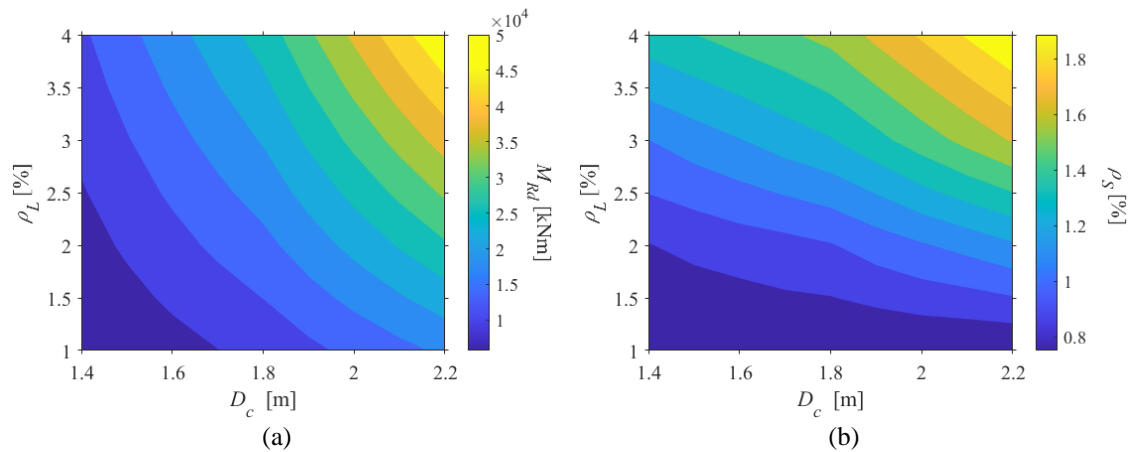
Figure 5-4 (a) Design resisting moment M_{Rd} at the pier base and (b) transverse reinforcement ratio ρ_S for different combinations of the DPs.
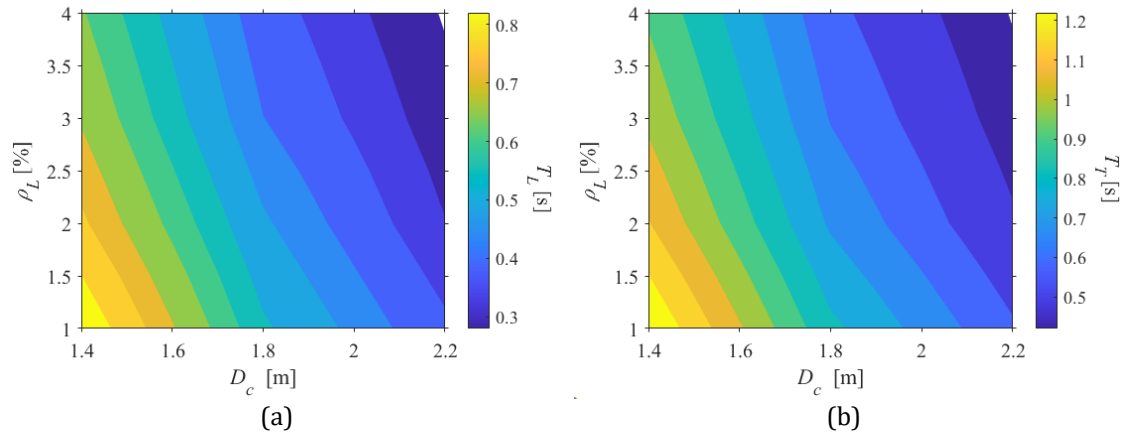
Figure 5-5 Fundamental vibration periods T (in seconds) along the (a) longitudinal and (b) transverse direction for different combinations of DPs.

Table 5-1. Values of yield displacement d_y, yield force V_y, and ultimate displacements d_u in longitudinal (L) and transverse (T) directions for different combinations of DPs.

ρ_L	D_c =1.4 m				D_c =1.8 m				D_c =2.2 m			
	1%	2%	3%	4%	1%	2%	3%	4%	1%	2%	3%	4%
$d_{y,L}$ [m]	0.036	0.039	0.041	0.043	0.027	0.030	0.032	0.033	0.022	0.024	0.026	0.027
$d_{u,L}$ [m]	0.167	0.164	0.175	0.191	0.141	0.155	0.166	0.171	0.138	0.149	0.163	0.168
$V_{y,L}$ [kN]	1520	2230	2950	3690	2780	4440	6080	7680	4710	7920	11100	14100
$d_{y,T}$ [m]	0.065	0.069	0.073	0.077	0.048	0.054	0.057	0.059	0.039	0.044	0.047	0.049
$d_{u,T}$ [m]	0.283	0.278	0.296	0.324	0.239	0.262	0.281	0.290	0.233	0.252	0.275	0.283
$V_{y,T}$ [kN]	1140	1670	2210	2760	2080	3320	4550	5750	3530	5930	8280	10600

Cloud analysis is performed to develop the probabilistic seismic demand models (PSDMs) for the various design cases. For this purpose, the same ground motion records employed in Tubaldi, Ozer, et al. (2022) is used. This consists of 221 real records (120 of which taken from Baker et al. (2011)), which are representative of a wide range of conditions in terms of source-to-site distance (R) (from 8.71 to 126.9 km), soil characteristics (the time-average shear wave velocity in the top 30 m spans from 203 to 2016 m/s) and moment magnitude (M_w) (from 5.3 to 7.9). These records are not specific to any particular local site condition. The vertical component of the input is not considered.

Figure 5-6 shows the hysteretic response of the pier to a bi-directional ground-motion record, in terms of base shear-top displacement along the two principal directions of the

bridge, for two different combinations of the design parameters. The top displacement is the displacement of the deck centroid, which coincides with the pier top displacement only in the case of longitudinal response. First of all, it can be observed that the response in the longitudinal direction is stiffer than in the transverse one. This is because the deck girders rest on two bearings, such that the effective length of flexure is larger for the transverse direction than for the longitudinal one. Moreover, the pier with higher longitudinal reinforcement is stiffer and stronger than the other one. This is also expected, given the higher bending moment capacity of the base section. Increasing the pier diameter while keeping the same amount of reinforcement ratio is also expected to increase the stiffness and strength of the system.
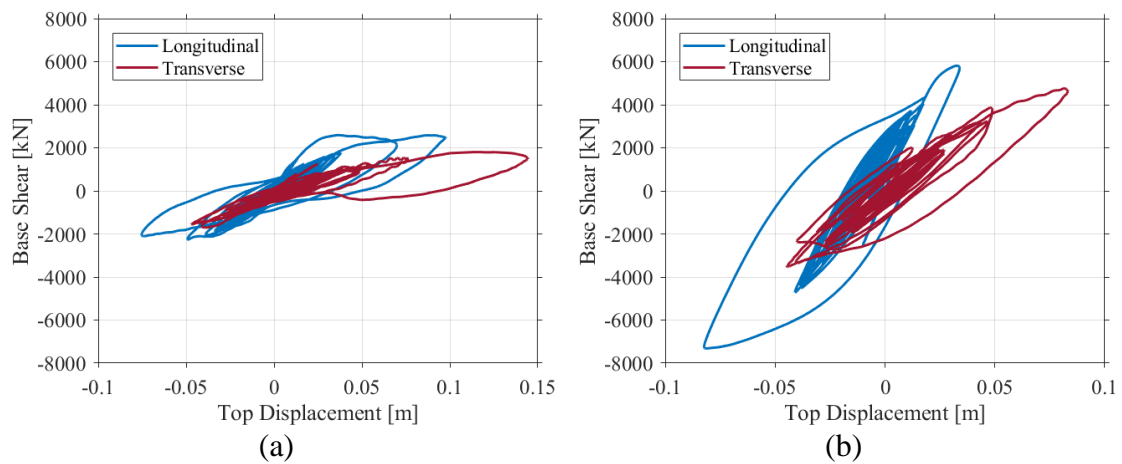
Figure 5-6 Base shear-top displacement response along the two principal directions of the bridge for D_c =1.8m, and (a) ρ_L=1% and (b) ρ_L =4%.

The maximum top displacements $u_{max,L}$ and $u_{max,T}$ along the longitudinal and transverse direction are considered to develop the PSDM and to evaluate the bridge performance. The intensity measure considered is $RotD50Sa_{avg}$, which is obtained as follows: first, the $RotD50$ (Boore, 2010) of the pseudo-acceleration response spectrum for the 221 records (two horizontal components) is computed, for a series of periods in the range between 0.1s and 2.5s, and for a 5% damping ratio. Then, the geometric mean of these is evaluated to obtain the $RotD50Sa_{avg}$. It is noteworthy that the proposed *IM* is not structure-specific.

Figure 5-7 shows the sample values of the maximum top displacement versus $RotD50Sa_{avg}$ in the log-log plane corresponding to the DP combinations of [1.4, 1%] and [2.2, 4%] along the longitudinal and transverse directions. In the same figures, the median

of the fitted PSDMs is also plotted. It can be observed that log(u_{max}) follows a linear trend with the log($RotD50Sa_{avg}$) for each combination of DPs. Nevertheless, some scatter is observed, particularly for high values of ρ_L. The displacement ductility achieved from the considered GMs ranges between 4.2 and 6.2 along the longitudinal direction and between 4.0 and 5.9 along the transverse direction. **Table 5-2** reports the PSDM parameters along with the lognormal standard deviation of the regression models, β_D. The low values of β_D reveal a satisfactory fit of the PSDM to the data. Since the logs of the maximum displacements along the two directions exhibit a negligible correlation and they are assumed to jointly follow a bivariate normal distribution, they can be treated independently.
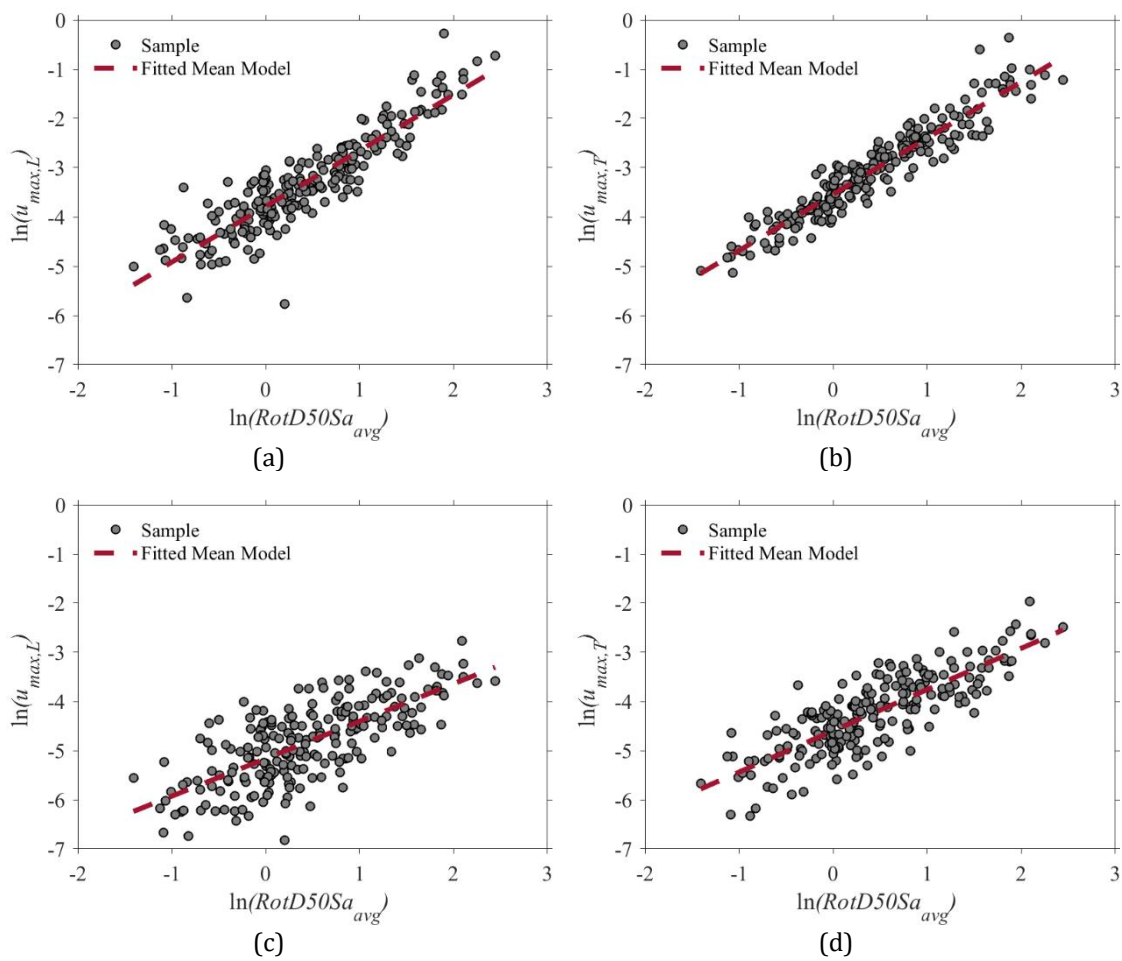
Figure 5-7 Sample values and median model in terms of maximum top displacement for (a) D_c =1.4m and ρ_L =1% in the longitudinal direction, (b) D_c =1.4m and ρ_L =1% in the transverse direction, (c) D_c =2.2m and ρ_L =4% in the longitudinal direction, (d) D_c =2.2m and ρ_L =4% in transverse direction

Table 5-2 Parameters of the regression models and values of lognormal standard deviation β_D

ρ_L	D_c =1.4 m				D_c =1.8 m				D_c =2.2 m			
	1%	2%	3%	4%	1%	2%	3%	4%	1%	2%	3%	4%
log(a)	-3.78	-3.89	-4.00	-4.07	-4.11	-4.29	-4.41	-4.52	-4.53	-4.80	-4.74	-5.16
b	1.13	1.10	1.07	1.04	1.09	0.98	0.90	0.85	1.00	0.89	0.76	0.76
β_D	0.42	0.41	0.40	0.41	0.43	0.46	0.48	0.50	0.50	0.53	0.50	0.56
log(a)	-3.54	-3.62	-3.68	-3.76	-3.91	-4.04	-4.12	-4.20	-4.21	-4.40	-4.24	-4.60
b	1.14	1.12	1.10	1.10	1.16	1.09	1.03	1.00	1.08	0.99	0.84	0.84
β_D	0.30	0.30	0.31	0.31	0.33	0.36	036	0.37	0.38	0.39	0.40	0.45
RotD50 $Sa_{avg,50\%}$	4.01	4.46	5.22	6.25	4.89	6.85	9.19	11.23	7.29	11.78	-	-

Figure 5-8 reports the fragility curves for the various combinations of DPs. These have been constructed by evaluating, for each value of $RotD50Sa_{avg}$, the probability of the pier displacement demand along each of the two directions exceeding the corresponding displacement capacity (reported in **Table 5-1**). Equation (5-5) has been used to compute this probability. It is noteworthy that the capacity limits have been evaluated based on a pushover analysis, and no account is made of damage accumulation phenomena in the performance assessment, as e.g. done in Turchetti et al. (2023) with the use of the Ang-Park damage index. It can be observed that both the diameter and the longitudinal reinforcement ratio significantly affect the bridge fragility. Overall, increasing D_c is more effective than increasing ρ_L in reducing the bridge fragility. However, increasing the reinforcement ratio has a more significant effect in terms of reduction of fragility for large pier diameters than for low ones. These trends reflect the trend of variation of the resisting moment with D_c and ρ_L (see **Figure 5-4**). **Table 5-2** reports also the values of the median fragility capacity, $RotD50Sa_{avg,50\%}$, defined as the value of $RotD50Sa_{avg}$ corresponding to a probability of failure of 50%.

(a) (b) (c)
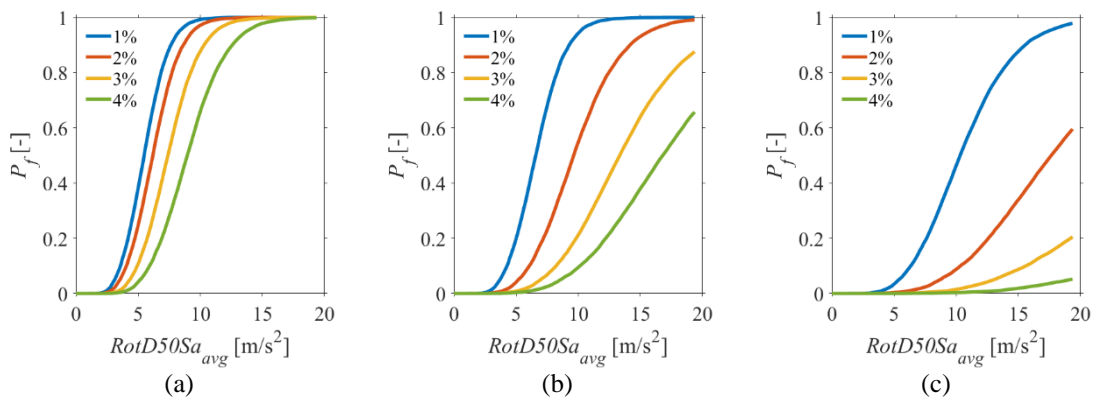
Figure 5-8 Fragility curves for different combinations of DPs (a) D_c =1.4m (b) D_c =1.8m (c) D_c =2.2m.

5.3 Results of the risk-targeting design approach for selected sites

Probabilistic seismic hazard assessment (PSHA) is carried out on a regular grid spaced by 0.05° for Italy. The same grid is used by the Italian National Institute of Geophysics and Volcanology (INGV) for developing hazard maps. The hazard curves for each site have been built using the software REASSESS V2.0 (Chioccarelli et al., 2019), using the ground motion prediction equation proposed by Lanzano et al. (2019) for *RotD50Sa*. The seismogenic source model is the one proposed by Meletti et al. (2008) with parameters taken from Barani et al. (2009). The interval of interest of the selected *IM* values ranges between $10^{-5}g$ and $+2g$, where *g* denotes acceleration due to gravity. The condition of "Soil Type A" (bedrock, i.e. vs30 ≥ 800 m/s) has been considered.

Figure 5-9a shows hazard curves in terms of MAF of exceedance of different values of *RotD50Sa$_{avg}$* for three Italian cities: Milan (latitude 45.472N; longitude 9.177E), Naples (latitude 40.852N; longitude 14.268E), and L'Aquila (latitude 42.350N; longitude 13.400E). The three sites are exposed to roughly low-, mid-, and high-seismic hazard and have been considered in RINTC project to compare the risk levels across the country of various structures designed according to the Italian seismic codes (Tubaldi, Barbato, & Ghazizadeh, 2012). **Figure 5-9b** compares the MAFs of bridge pier failure corresponding to the minimum values of DPs (ρ_L =1%, D_c =1.4m, in green), and to the maximum values of DPs (ρ_L =4%, D_c =2.2m, in grey) for the three considered sites. The MAF of failure for L'Aquila is very high for the minimum values of DPs, and it reduces by three orders of magnitude if the maximum values of DPs are considered; likewise, the MAF for Naples reduces from 6×10^{-6} to 4×10^{-9}. The MAF of failure for Milan is very low even for the

minimum DPs, and it reduces by almost four orders of magnitude by considering the maximum values of DPs.
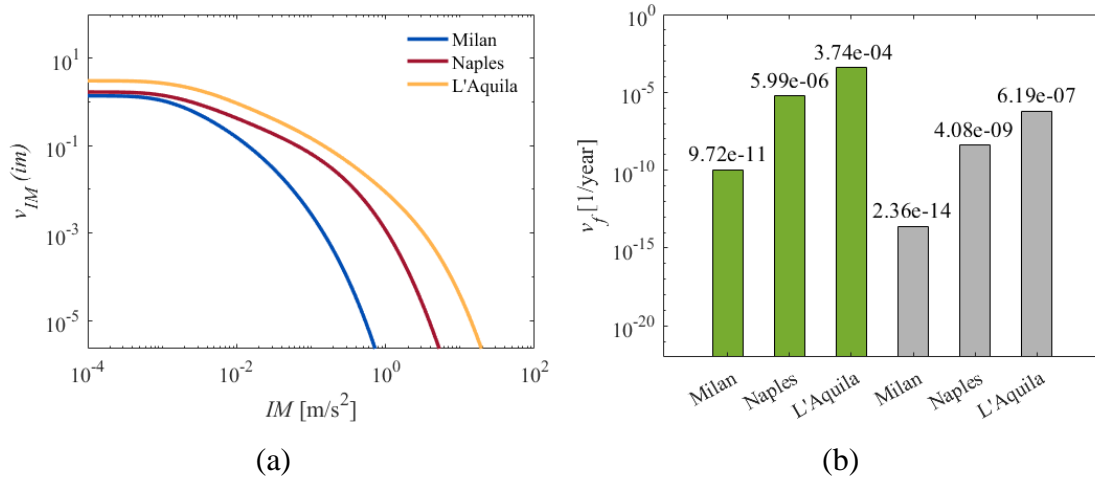
Figure 5-9 (a) Comparison of hazard curves in terms of $IM=RotD50Sa_{avg}$ for three different sites in Italy; (b) comparisons of risks for ρ_L =1%, D_c =1.4m in green and ρ_L =4%, D_c =2.2m in grey.

Figure 5-10a shows the mean annual frequency of pier failure for different combinations of DPs for the bridge located in L'Aquila. The optimal DP satisfying the stochastic constraint of a MAF of failure equal or less than 10^{-6} is also plotted in the figure and denoted by a star. Specifically, the star denotes a MAF of failure equal to 6×10^{-7}.The combinations of DPs have been evaluated by assuming discrete values for D_c and ρ_L, with an interval of 0.1m for D_c, and of 0.005 for ρ_L. These intervals can be easily refined as there is no need to perform any further analysis. It can be observed that only one DP combination satisfies the required stochastic constraint in L'Aquila, which corresponds to a value of the resisting moment M_{Rd}, plotted in **Figure 5-4a** (and replotted in **Figure 5-10b** for convenience). Thus, it is possible to identify a point that minimises M_{Rd} (cost function) while satisfying the stochastic constraint. In the case of the bridge pier located in L'Aquila, the optimum DP corresponds to D_c=2.2m and ρ_L=0.04 and a value of M_{Rd} of 49330 kNm. Regarding the choice of the target MAF of failure equal or less than 10^{-6}, this value is close to the value of 1.33×10^{-6} that corresponds to consequence class CC2. Other values of the target MAF of failure are also considered in the next section.

Figure 5-11 shows the same results already shown in **Figure 5-10**, but considering the bridge located in Naples rather than in L'Aquila. As expected, compared to L'Aquila

149

there are more combinations of design parameters that satisfy the constraint on the acceptable risk of failure. Among these, the one that minimises the resisting moment corresponds to D_c=1.4m and ρ_L=3.5%. The identification of this point is straightforward, and does not require a complex optimisation algorithm but simply finding the combination that minimises M_{Rd} among the various pairs that satisfy the stochastic constraint. It is noteworthy that at mid- and high-seismic hazard sites, like Naples and L'Aquila, it is not possible to achieve the target of 10^{-6} with the minimum reinforcement ratio ρ_L allowed by Eurocode 8.

(a) (b)
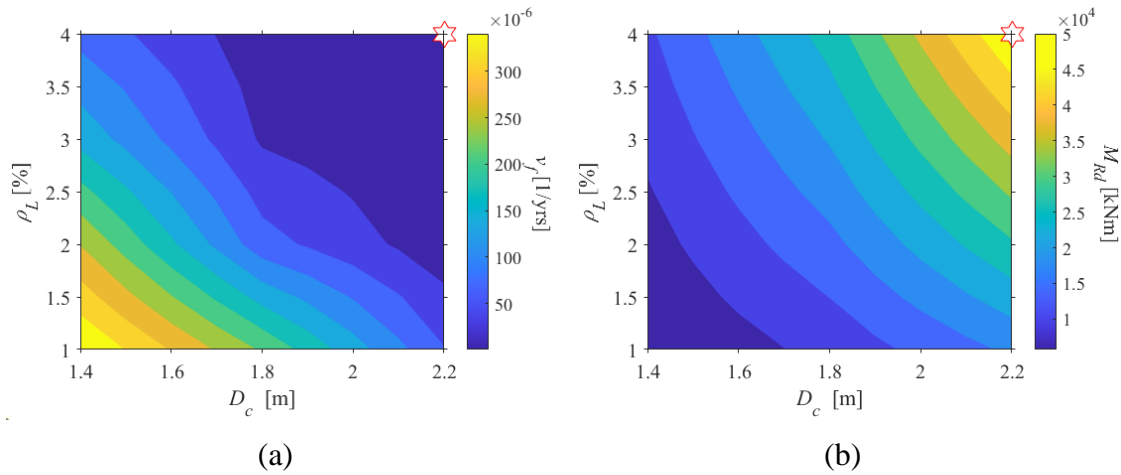
Figure 5-10 (a) MAF of pier collapse for a bridge site in L'Aquila and (b) corresponding values of the resisting moment M_{Rd} (unit kNm) for different combinations of DPs. The optimal design point is marked by a star.

(a) (b)
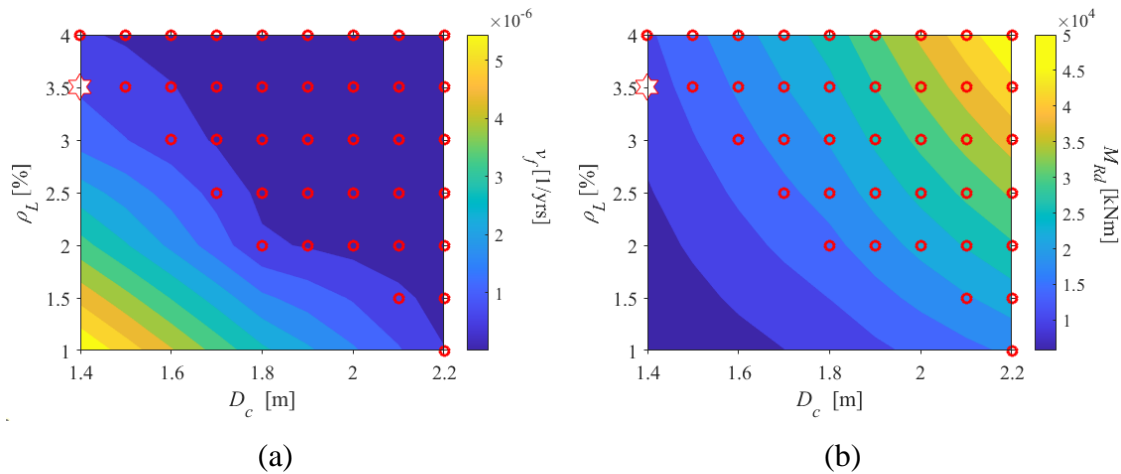
Figure 5-11 (a) MAF of pier collapse and (b) corresponding values of the resisting moment M_{Rd} (unit kNm) for different combinations of DPs for a bridge site in Naples. The design parameters satisfying the stochastic constraint are marked with a circle, the optimal design point is marked by a star.

Figure 5-12a shows the variation of the MAF of failure with the design resisting moment M_{Rd} for the site of L'Aquila. It can be observed that there is a strong and inverse

correlation between these two quantities. A similar trend is observed for other sites. The case of Naples is illustrated in **Figure 5-12b**.
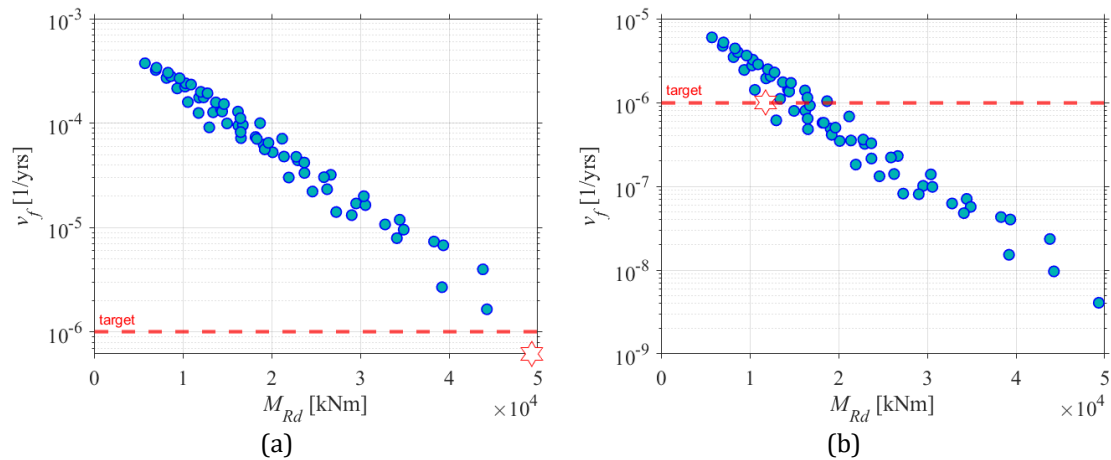
Figure 5-12 Variation of the MAF of collapse vs. design resisting moment M_{Rd} obtained for various DP combinations for a bridge site in (a) L'Aquila and (b) Naples. The dashed red line indicates the target MAF of failure of 10^{-6} and the optimal design point is marked by a star. Note that the y-scale is different in the two plots.

5.4 Risk-based design maps for Italy

The proposed risk-based design procedure is applied to design the bridge pier across the whole of Italy, considering a target MAF of failure of 10^{-6}. The purpose of this analysis it to show how the designs would change across areas of different seismic hazard, and to evaluate differences between the regional distribution of the bridge design parameters and the regional distribution of seismic hazard.

Figure 5-13 shows the variation of $RotD50Sa_{avg}$ across Italy for return periods of 100 years, 475 years, and 2 475 years, corresponding respectively to 39%, 10%, and 2% probabilities of exceedance in 50 years. The intensity distribution across Italy is quite similar for the various return periods. However, for lower return periods higher intensities are observed in central Italy compared to southern Italy, whereas for the higher return period southern Italy shows intensities closer to those in central Italy. This is the effect of the different shape of the hazard curves for different locations, as already observed in **Figure 5-9a**.

Figure 5-14 shows the variation of minimum resisting moment M_{Rd} at the base of the pier across Italy, corresponding to the optimal design point. In large parts of Italy the

minimum value of M_{Rd}, corresponding to $\rho_L =1\%$, $D_c =1.4m$, is sufficient to satisfy the constraint and achieve risk levels less than 10^{-6}. In these regions, the values of $RotD50Sa_{avg}$ for a return period of 475 years are less than about $0.1m/s^2$. In general, the contour plots of M_{Rd} follow a similar trend of $RotD50Sa_{avg}$, i.e., higher M_{Rd} values are required at sites of higher seismicity. The peak values of M_{Rd}, above 40 000 kNm, occur in parts of southern Italy, along the Apennine belt, and in the north-east, as expected.

(a)   (b)   (c)
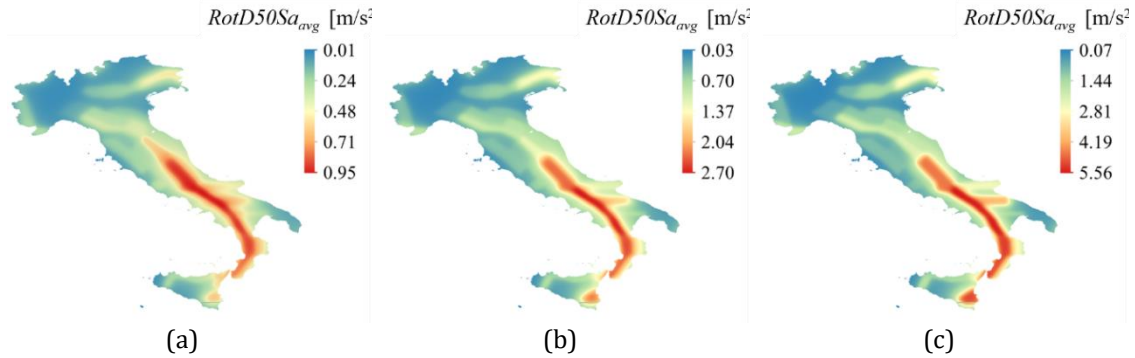
Figure 5-13 Variation of $RotD50Sa_{avg}$ across Italy (unit m/s^2) for return periods of 100 (a), 475 (b) and 2475 years (c).
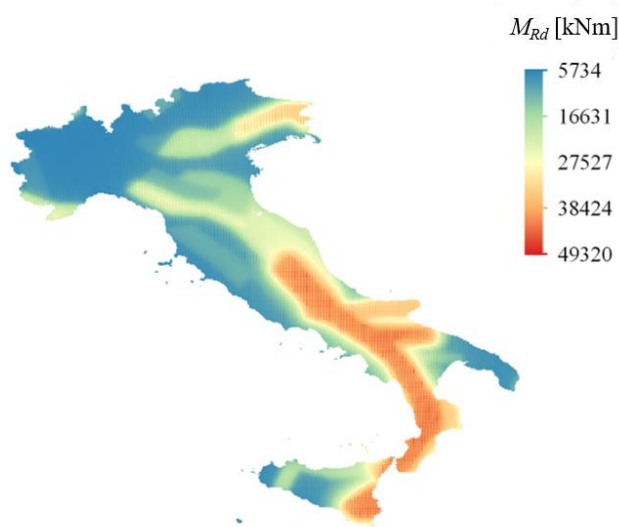
Figure 5-14 Variation across Italy of the minimum resisting moment M_{Rd} at the base of the pier.

Figure 5-15a and **Figure 5-15b** show a map of the optimal values of the pier diameter D_c and of the longitudinal reinforcement ratio ρ_L. In regions with lowest seismicity, the optimal DPs coincide with the minimum values of D_c and ρ_L, whereas in the regions with highest seismicity, they coincide with the maximum ones, as expected. Non-smooth changes of optimal DP values can be observed across adjacent regions that are

characterised by quite similar levels of hazard. This is because high values of D_c and low values of ρ_L yield similar risk levels to low values of D_c and higher values of ρ_L. For example, Nocera Umbra (latitude 43.114N; longitude 12.788E) and Pioraco (latitude 43.181N; longitude 12.974E) are two towns located closed to each other and with similar hazard levels (**Figure 5-16**). Nevertheless, the optimal values of DPs are D_c=2.2m and ρ_L=2% for the bridge in Nocera Umbra, and D_c=1.8m and ρ_L=4% for the bridge in Pioraco, as shown in **Figure 5-17**.

Obviously, a smoother variation of the optimal pier properties can be obtained if a single design parameter is considered, by keeping the other one fixed. **Figure 5-18a** shows the optimal values of ρ_L obtained considering a fixed diameter D_c of 2.2m. In this case, ρ_L exhibits a smooth variation across the country. It is found that while $\rho_L = 4\%$ is necessary only in the high-hazard regions, it is sufficient to consider the minimum percentage of ρ_L in most of Italy.
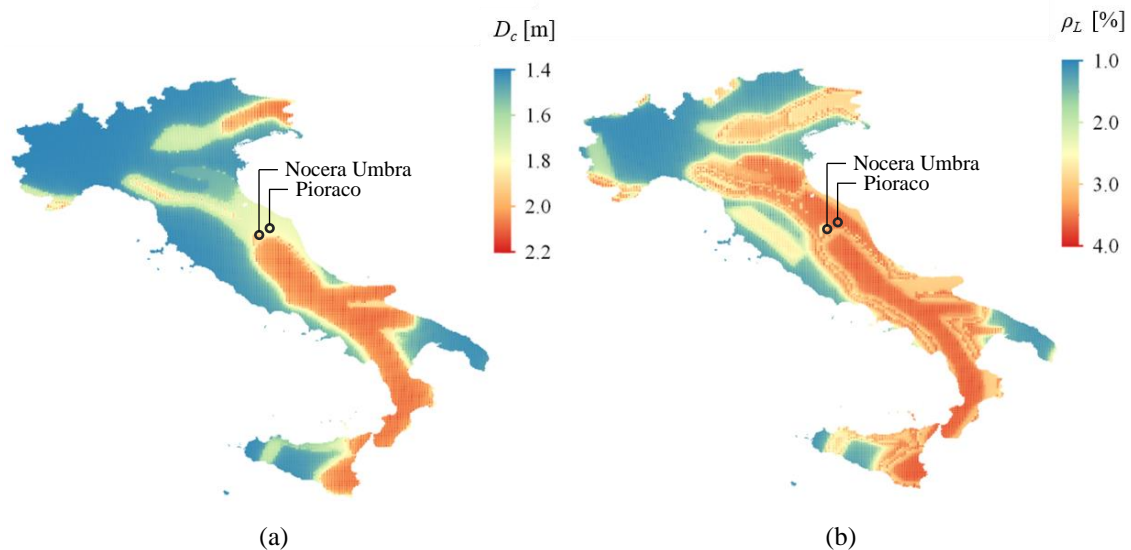
Figure 5-15 Variation across Italy of the optimal pier diameter D_c (unit m) (a) and of the optimal ρ_L (expressed in terms of percentage) (b).
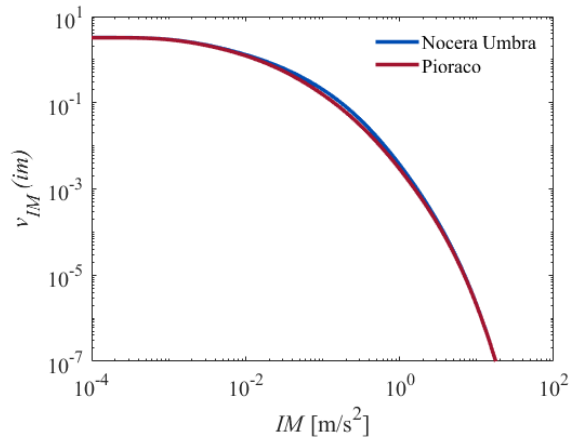
Figure 5-16 Comparison of hazard curves in terms of $IM=RotD50Sa_{avg}$ for the cities of Nocera Umbra and Pioraco.
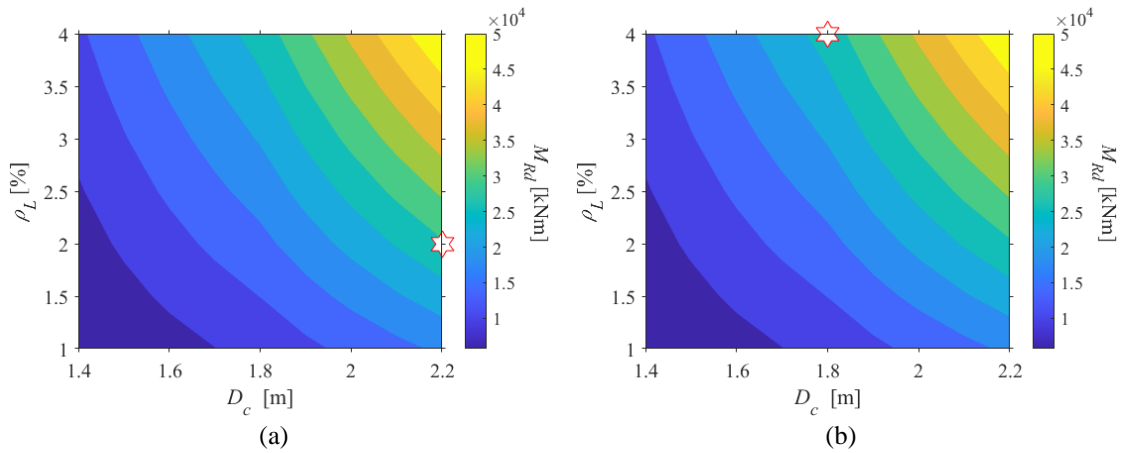
Figure 5-17 Design resisting moment M_{Rd} at the pier base (in kNm) for different combinations of DPs for a bridge site in (a) Nocera Umbra and in (b) Pioraco. The optimal design point is marked by a star.

The effect of the choice of the target risk level on the design parameters is evaluated by applying the proposed design procedure for a target MAF of failure of 10^{-5} and 2×10^{-4}. The results obtained considering a MAF of 10^{-5} for a fixed value of the pier diameter D_c = 2.2m are shown in **Figure 5-18b**. As expected, increasing the target risk level from 10^{-6} to 10^{-5} results in a significant reduction of the longitudinal reinforcement ratio across Italy. In this case, in many regions of Italy the minimum reinforcement amount according to Eurocode 8 is sufficient, and in the regions with high hazard the maximum value of ρ_L required is 3%.

154
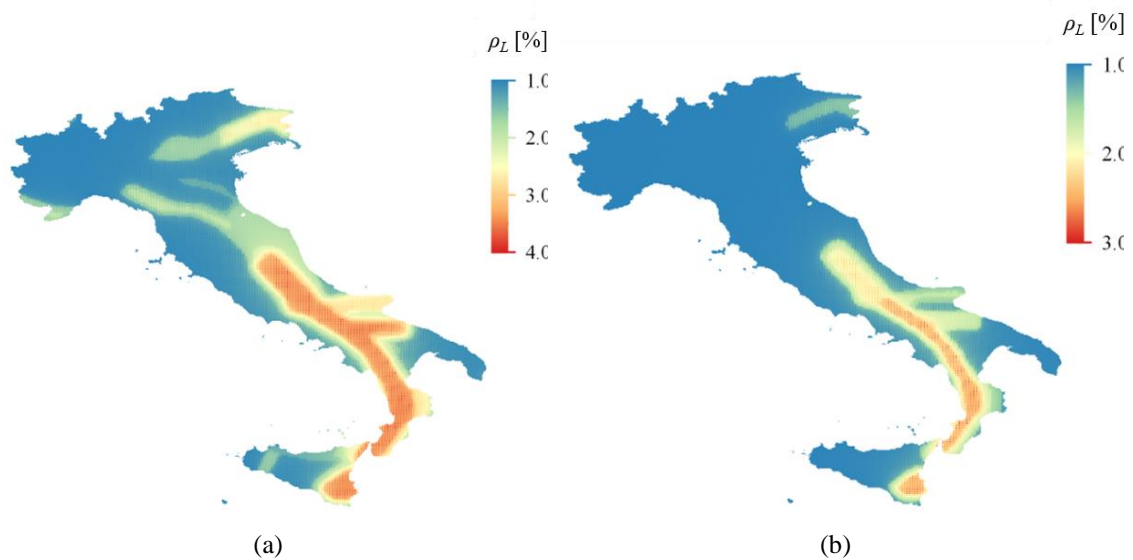
Figure 5-18 Variation of the optimal ρ_L (expressed in terms of percentage) across Italy for D_c =2.2m obtained considering a target MAF of failure of 10^{-6} (a) and 10^{-5} (b).

The application of a MAF of failure of 2×10^{-4} is presented in **Figure 5-19**. In this case, as shown in **Figure 5-19a**, the highest value of the M_{Rd} is around 12000 kNm, corresponding to a longitudinal reinforcement ratio ρ_L of 4% and D_c=1,4 m. The minimum D_c is sufficient all over Italy while it is necessary to increase the amount of ρ_L in the southern regions with highest seismic hazard (**Figure 5-19b**).
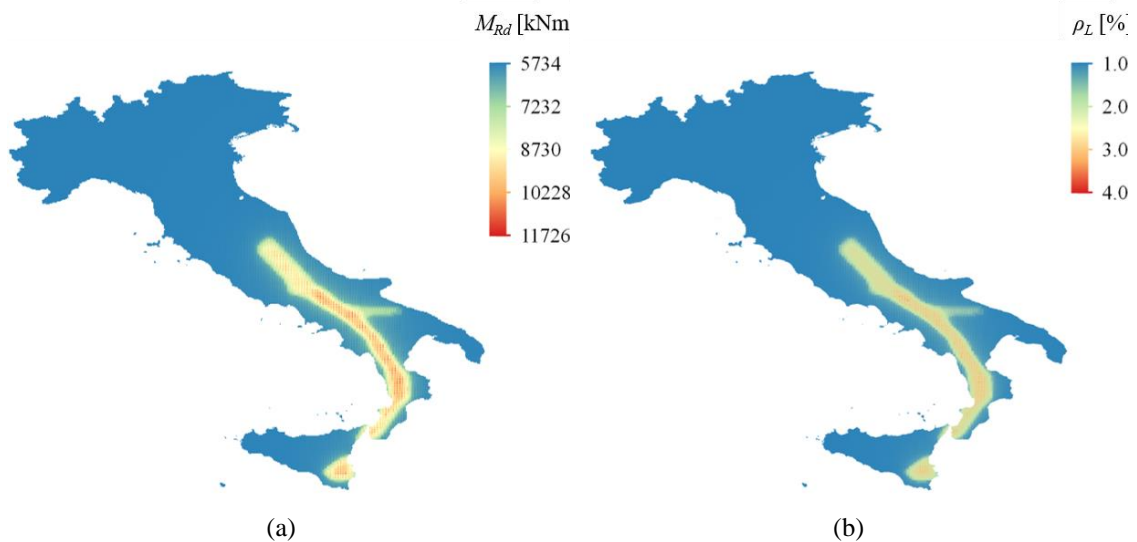
Figure 5-19 Variation across Italy of the M_{Rd} at the base of the pier (a) and of the optimal ρ_L (expressed in terms of percentage) obtained considering a target MAF of failure of 2×10^{-4}.

To provide insight into the effect of soil class on the application of the risk-targeting design procedure, the seismic hazard is assessed at the three sites previously considered

(Milan, Naples and L'Aquila) for the soil types B, C and D. The new hazard curves are obtained using the software REASSESS V2.1 (Chioccarelli et al., 2019) and using the same ground motion prediction equation adopted for soil type A. **Figure 5-20** shows the new hazard curves for the three cities computed for soil B, C and D respectively whilst **Table 5-3** reports the corresponding risk levels for two different combinations of design parameters. It can be observed that the increase of risk is highest for Milan and lowest for L'Aquila. Furthermore, the MAF of failure for the case of L'Aquila is above 10^{-6} even for the case of $\rho_L = 4\%$, $D_c = 2.2m$ and it is above 10^{-5} if soil D is considered. Thus, the soil type can have a considerable impact on the results of the risk-targeting design procedure.
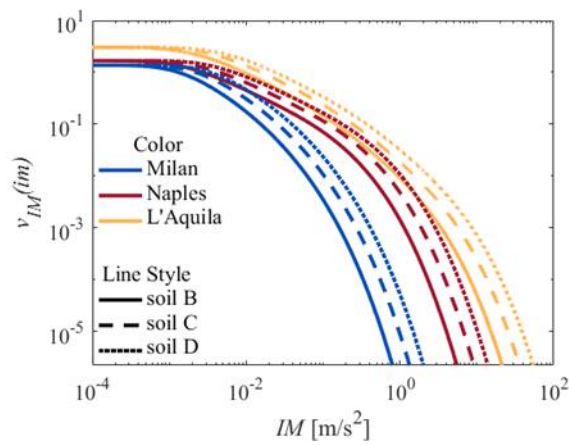
Figure 5-20 Comparison of hazard curves in terms of $IM=RotD50Sa_{avg}$ for three different sites in Italy assuming different soil classes.

Table 5-3 Risks computed for Milan, Naples and L'Aquila for two combinations of DPs ([1.4, 1%] and [2.2, 4%]) and for different soil classes

	Milan		Naples		L'Aquila	
	$D_c = 1.4m$ $\rho_L = 1\%$	$D_c = 2.2m$ $\rho_L = 4\%$	$D_c = 1.4m$ $\rho_L = 1\%$	$D_c = 2.2m$ $\rho_L = 4\%$	$D_c = 1.4m$ $\rho_L = 1\%$	$D_c = 2.2m$ $\rho_L = 4\%$
Soil B	4.75e-10	2.36e-13	1.39e-05	1.36e-08	6.26e-04	1.96e-06
Soil C	1.18e-08	7.79e-12	9.50e-05	1.19e-07	1.81e-03	8.59e-06
Soil D	1.25e-07	9.47e-11	3.67e-04	6.17e-07	3.77e-03	2.35e-05

5.5 Conclusions

This study illustrates a risk-targeting design procedure for bridge piers. The procedure identifies the optimal values of the pier diameter and longitudinal reinforcement ratio that minimise the resisting moment at the pier base while satisfying the stochastic constraint on the MAF of failure due to the exceedance of the pier displacement ductility capacity.

The proposed procedure is based on the solution of a series of direct reliability problems where the pier seismic fragility is evaluated for different combinations of the design parameters, and using linear interpolation, which is justified by smooth variation of the interpolated quantities (e.g. fragility, risk, resisting moment of the base section) with the design parameters. The application of the proposed design procedure is illustrated by considering a two-span continuous bridge representative of medium-size bridges found widely in the European transport network. The bridge is assumed to be located in various sites in Italy, characterised by very different seismicity levels. Based on the obtained results, the following main conclusions can be drawn:

- The design resisting moment at the base of the pier exhibits a significant inverse correlation with the target MAF of failure and can be used to define the objective (cost) function to be minimised, as its value also affects the design of the transverse reinforcement of the pier, the design of the foundations, as well as the forces transmitted to the superstructure;

- Targeting values of the mean annual frequency of failure lower than 10^{-6} years^{-1} in regions of high seismicity requires design parameters (e.g. pier diameter) that are out of the investigated range, which represent realistic values for bridges in Italy that comply with the Eurocode 8 requirements (e.g. on the maximum and minimum value of the longitudinal reinforcement ratio);

- A large variation of the optimal design parameters is observed across Italy, as a result of significant variations in the seismic hazard.

- In large parts of Italy, the minimum longitudinal reinforcement according to Eurocode 8 is sufficient to guarantee a target mean annual frequency of failure below 10^{-5} years^{-1}. This latter value is significantly lower than the one considered in the US for risk-targeting, i.e. 2.3×10^{-4} years^{-1}.

- If both the pier diameter and the longitudinal reinforcement ratio are assumed as design parameters, non-smooth variations of the optimal values across adjacent sites could be obtained. This issue can be avoided by considering only a single design parameter and fixing the other.

- The site classification can influence the design results, especially in regions of high seismicity. Design maps should be built for different soil types to better estimate the effect of the site classification.

6 General conclusions and future work

The present Thesis aims at enhancing current methodologies for the risk assessment and design of bridges exposed to earthquakes. Firstly, the project assessed alternative methods for evaluating the performance of bridges subjected to repeated earthquakes throughout their design life, with a proposal of improvements to these assessment methods. Secondly, a framework for the aftershock risk assessment of bridges was developed using a Bayesian Network approach and leveraging available sensing data to enhance understanding of the structural state and risk of bridges following seismic events. Lastly, the project aimed to establish a methodology for risk-targeted design of bridges, exploring variations in design outcomes across regions with differing seismicity levels. The outcomes of this research contribute insights and advancements to the field of earthquake engineering, laying the groundwork for more robust approaches to seismic risk evaluation and design.

6.1 Key findings

Summarized below are the investigations undertaken and the key findings:

- Chapter 3 introduced and compared recently developed methodologies for the prediction of damage accumulation in structures subjected to multiple earthquakes within their lifetime. A stochastic earthquake hazard model is used for generating sample sequences of ground motion records providing the reference solution and then used to estimate the probabilistic distribution of the damage accumulated during the time interval of interest. Besides evaluating the effectiveness of each approach, possible improvements of the cumulative demand model are tested. A reinforced concrete bridge model with a single pier is examined as case study and Park-Ang damage index is considered to describe the damage accumulation. The results demonstrate the importance of considering the occurrence of multiple shocks. It is proved that the RBM is computationally more efficient than the MM, providing accurate damage estimates with fewer samples. However, it introduces bias in the probability of damage exceedance estimates. On the other hand, employing the MM with a slightly higher number of samples yields accurate and unbiased damage estimates. In the study, no interventions were assumed to happen along the service life of the structure. This assumption could be realistic considering that retrofitting can often be impractical. This is the case when the level of damage following an earthquake event is visually irrelevant to motivate interventions or when economic restraints render retrofit actions infeasible after every earthquake. Despite the limitations, the analysis shows accurate results that can be used in practice.

- Chapter 4 illustrates a Bayesian network-based probabilistic framework for updating the aftershock risk of bridges. The Bayesian network is developed for describing the probabilistic relationship among various random variables (e.g., ground-motion intensity, bridge response parameters, seismic damage, etc.) involved in the seismic damage assessment. This configuration allows users to leverage data observations from seismic stations, structural health monitoring (SHM) sensors, and visual inspections. The framework is applied to a hypothetical bridge in Central Italy exposed to earthquake sequences. The uncertainty reduction in the estimate of the aftershock damage risk is evaluated by utilising various sources of information. It is shown that the information from accelerometers and

visual inspections can significantly impact bridge damage estimates, thus affecting decision-making under the threat of future aftershocks. A bridge initially assessed as having a high probability of experiencing damage based on prior knowledge of the mainshock magnitude and source-to-site distance may be classified as safe if a visual inspection reports no cracking or crushing of bridge piers. This has evident implications for the risk posed by future aftershocks. Similar outcomes can be achieved by utilizing information from accelerometers, particularly if the recorded maximum absolute accelerations are low compared to those derived solely from knowledge of the earthquake magnitude and location. It is also shown how the updating of the BN impacts the evaluation of the aftershock risk.

- In Chapter 5, a methodology for the risk-targeted design of RC piers in multi-span bridges is proposed. Such approach consists in computing the probability of failure of the structure by solving a direct reliability problem, associated with the exceedance of tolerable thresholds of loss. The methodology is applied in various locations across Italy to illustrate the variations in the optimal risk-based design properties of bridges across regions with varying seismic hazard. The study concludes that the design resisting moment at the base of the pier can be used as the objective function to be minimised. The design resisting moment is intrinsically correlated to the pier diameter and the longitudinal reinforcement ratio and it is demonstrated to be inversely correlated with the target mean annual frequency of failure. It is demonstrated that in regions of high seismicity, values of the MAF lower than 10^{-6} years^{-1} are unfeasible to target if considering design parameters that are in the range of values compliant with the Eurocode 8 requirements. On the other hand, it is possible to guarantee a target mean annual frequency of failure below 10^{-5} years^{-1} with the minimum longitudinal reinforcement ratio in most of Italy.

6.2 Future research

Some limitations and future challenges have been identified along the process, and some of them are enlisted in the following:

- Future investigations will explore the influence of aftershocks in the damage accumulation process. Furthermore, future work may involve the consideration of real earthquake ground-motion sequences instead of simulated ones. The methodologies explored could also be extended to encompass the vulnerability assessment of multiple critical components of bridges, along with the potential inclusion of retrofit interventions between successive seismic events.

- Improvements can be made in the BN framework by developing more sophisticated finite element models and more consistent mainshock-aftershock ground motion selection approaches that better represent site-specific seismic hazard with a more comprehensive ground-motion database. The inclusion of more causal parameters in the analysis and more sources of information about the seismic response (e.g., information from drone-based surveys and damage detection) can also contribute to enhancing the proposed framework.

- Future studies will include the impacts of models' uncertainty in the results of Bayesian updating and bayesian model selection approach will be used to identify the most accurate model, given the information from the sensors.

- More research is needed to develop accurate models, e.g. describing the relationship between amplitude and distribution of cracks and/or length of crushed concrete zone to the drifts and damage experienced by bridge piers. In addition, a robust definition of the levels of damage that should trigger decisions concerning the bridge serviceability should also be the object of further study. Future works will also explore the effectiveness and benefit of alternative monitoring and inspection strategies in terms of better-informed decisions concerning bridge operability, using concepts such as expected utility theory, multi-criteria decision making, and value of information.

- The impact of site classification on the risk-targeted design of new bridges, especially in regions with high seismic activity, underlines the necessity for developing different design maps for different soil types. Site-specific design maps can enhance the precision and effectiveness of structural engineering practices, ensuring that structures are appropriately designed to withstand seismic forces based on the specific characteristics of the soil.

- Further investigations are needed to evaluate the risk implicit to the design of bridge piers according to current seismic codes and to compare these results to the application of the risk-based procedure proposed in Chapter 5. The proposed procedure can be extended to consider more design parameters, as well as other possible failure modes related to different bridge components (e.g. bearings and abutments). It can also be applied to the risk-based design of other bridge types, including isolated bridges.

References

AASHTO. (2010). *AASHTO LRFD bridge design specifications*.

Abdelnaby, A. E. (2012). *Multiple earthquake effects on degrading reinforced concrete structures* [PhD dissertation]. University of Illinois.

ACI 318-11. (2011). *Building Code Requirements for Structural Concrete (ACI 318-11)*. American Concrete Institute, 38800 Country Club Drive.

Alessandri, S., Giannini, R., & Paolacci, F. (2013). Aftershock risk assessment and the decision to open traffic on bridges. *Earthquake Engineering and Structural Dynamics*, *42*(15), 2255–2275. https://doi.org/10.1002/eqe.2324

Algermissen, S. T., Perkins, D. M., Thenhaus, P. C., Hanson, S. L., & Bender, B. L. (1982). *Probabilistic estimates of maximum acceleration and velocity in rock in the contiguous*.

Aljawhari, K., Gentile, R., Freddi, F., & Galasso, C. (2021). Effects of ground-motion sequences on fragility and vulnerability of case-study reinforced concrete frames. *Bulletin of Earthquake Engineering*, *19*(15), 6329–6359. https://doi.org/10.1007/s10518-020-01006-8

Allen, T. I., Luco, N., & Halchuk, S. (2015). Exploring risk-targeted ground motions for the national building code of Canada. *11th Canadian Conference on Earthquake Engineering*.

Altieri, D., Tubaldi, E., De Angelis, M., Patelli, E., & Dall'Asta, A. (2018). Reliability-based optimal design of nonlinear viscous dampers for the seismic protection of structural systems. *Bulletin of Earthquake Engineering*, *16*(2), 963–982. https://doi.org/10.1007/s10518-017-0233-4

Amadio, C., Fragiacomo, M., & Rajgelj, S. (2003). The effects of repeated earthquake ground motions on the non-linear response of SDOF systems. *Earthquake Engineering and Structural Dynamics*, *32*(2), 291–308. https://doi.org/10.1002/eqe.225

Amato, A., Azzara, R., Chiarabba, C., Cimini, G. B., Cocco, M., Di Bona, M., Margheriti, L., Mazza, S., Mele, F., Selvaggi, G., Basili, A., Boschi, E., Courboulex, F., Deschamps, A., Gaffet, S., Bittarelli, G., Chiaraluce, L., Piccinini, D., & Ripepe, M. (1998). The 1997 Umbria-Marche, Italy, earthquake sequence: A first look at the main shocks and aftershocks. *Geophysical Research Letters*, *25*(15), 2861–2864. https://doi.org/10.1029/98GL51842

Applied Technology Council (ATC). (1985). *Earthquake Damage Evaluation Data for California; Report No. ATC-13*.

Argyroudis, S. A., Mitoulis, S. A., Hofer, L., Zanini, M. A., Tubaldi, E., & Frangopol, D. M. (2020). Resilience assessment framework for critical infrastructure in a multi-hazard environment: case study on transport assets. *Sci Total Environ*.

Argyroudis, S. A., Mitoulis, S. A., Kaynia, A. M., & Winter, M. G. (2018). Fragility assessment of transportation infrastructure systems subjected to earthquakes. *Geotechnical Earthquake Engineering and Soil Dynamics V*. https://www.researchgate.net/publication/323343143

Argyroudis, S. A., Nasiopoulos, G., Mantadakis, N., & Mitoulis, S. A. (2021). Cost-based resilience assessment of bridges subjected to earthquakes. *International Journal of Disaster Resilience in the Built Environment*, *12*(2), 209–222. https://doi.org/10.1108/IJDRBE-02-2020-0014

ASCE. (2017). Minimum design loads and associated criteria for buildings and other structures. In *ASCE/ SEI 7-16*. American Society of Civil Engineers.

ATC/BSSC. (1997). NEHRP Guidelines for the Seismic Rehabilitation of Buildings. In *FEMA 273 Report (Guidelines) and FEMA 274 Report (Commentary), prepared by the Applied Technology Council for the Building Seismic Safety Council*. Federal Emergency Management Agency.

Atkinson, G. M., & Silva, W. (2000). Stochastic Modeling of California Ground Motions. *Bulletin of the Seismological Society of America*, *90*(2), 255–274. http://pubs.geoscienceworld.org/ssa/bssa/article-pdf/90/2/255/2710102/255_ssa99064.pdf

Au, S. K., & Beck, J. L. (2003). Subset Simulation and its Application to Seismic Risk Based on Dynamic Analysis. *Journal of Engineering Mechanics*. https://doi.org/10.1061/ASCE0733-93992003129:8901

Bai, J. W., Gardoni, P., & Hueste, M. B. D. (2011). Story-specific demand models and seismic fragility estimates for multi-story buildings. *Structural Safety*, *33*(1), 96–107. https://doi.org/10.1016/j.strusafe.2010.09.002

Baig, M. A., Imteyaz Ansari, M., Islam, N., & Umair, M. (2022). Damage assessment of circular bridge pier incorporating high-strength steel reinforcement under near-fault ground motions. *Materials Today: Proceedings*, *64*, 488–498. https://doi.org/10.1016/j.matpr.2022.04.964

Baker, J., Lin, T., Shahi, S., & et al. (2011). *New ground motion selection procedures and selected motions for the PEER transportation research program*.

Baker, J. W., Bradley, B. A., & Stafford, P. J. (2021). *Seismic Hazard and Risk Analysis*. Cambridge University Press.

Baker, J. W., & Cornell, C. A. (2006). Spectral shape, epsilon and record selection. *Earthquake Engineering and Structural Dynamics*, *35*(9), 1077–1095. https://doi.org/10.1002/eqe.571

Ballio, G., & Castiglioni, C. A. (1994). An approach to the seismic design of steel structures based on cumulative damage criteria. *Earthquake Engineering & Structural Dynamics*, *23*(9), 969–986. https://doi.org/10.1002/eqe.4290230904

Baltzopoulos, G., Grella, A., & Iervolino, I. (2021). Seismic reliability implied by behavior-factor-based design. *Earthquake Engineering and Structural Dynamics*, *50*(15), 4076–4096. https://doi.org/10.1002/eqe.3546

Barani, S., Spallarossa, D., & Bazzurro, P. (2009). Disaggregation of probabilistic ground-motion Hazard in Italy. *Bulletin of the Seismological Society of America*, *99*(5), 2638–2661. https://doi.org/10.1785/0120080348

Barbato, M., & Tubaldi, E. (2013). A probabilistic performance-based approach for mitigating the seismic pounding risk between adjacent buildings. *Earthquake Engineering and Structural Dynamics*, *42*(8), 1203–1219. https://doi.org/10.1002/eqe.2267

Basöz, N., & Kiremidjian, A. S. (1998). *Evaluation of Bridge Damage Data from the Loma Prieta and Northridge, California Earthquakes*.

Bastidas-Arteaga, E., Bressolette, P., Chateauneuf, A., & Sánchez-Silva, M. (2009). Probabilistic lifetime assessment of RC structures under coupled corrosion-fatigue deterioration processes. *Structural Safety*, *31*(1), 84–96. https://doi.org/10.1016/j.strusafe.2008.04.001

Bastidas-Arteaga, E., Sánchez-Silva, M., Chateauneuf, A., & Silva, M. R. (2008). Coupled reliability model of biodeterioration, chloride ingress and cracking for reinforced concrete structures. *Structural Safety*, *30*(2), 110–129. https://doi.org/10.1016/j.strusafe.2006.09.001

Båth, M. (1965). Lateral inhomogeneities of the upper mantle. *Tectonophysics*, *2*, 483–514.

Bender, N., Tsiavos, A., Pilotto, M., & Stojadinovic, B. (2018). Engineering collapse-probability-based seismic retrofit design for existing bridges. *Integrating Science, Engineering, & Policy: 11th National Conference on Earthquake Engineering 2018 (11NCEE)*, 4650–4659.

Berry, M. P., & Eberhard, M. O. (2007). *Performance Modeling Strategies for Modern Reinforced Concrete Bridge Columns*.

Billah, A. H. M. M., & Alam, M. S. (2015). Seismic fragility assessment of highway bridges: a state-of-the-art review. *Structure and Infrastructure Engineering*, *11*(6), 804–832. https://doi.org/10.1080/15732479.2014.912243

Bobbio, A., Portinale, L., Minichino, M., & Ciancamerla, E. (2001). Improving the analysis of dependable systems by mapping fault trees into Bayesian networks. *Reliability Engineering & System Safety*, *71*(3), 249–260. www.elsevier.com/locate/ress

Bommer, J. J., & Abrahamson, N. A. (2006). Why do modern probabilistic seismic-hazard analyses often lead to increased hazard estimates? In *Bulletin of the Seismological Society of America* (Vol. 96, Issue 6, pp. 1967–1977). https://doi.org/10.1785/0120060043

Bommer, J. J., & Crowley, H. (2006). The influence of ground-motion variability in earthquake loss modelling. *Bulletin of Earthquake Engineering*, *4*(3), 231–248. https://doi.org/10.1007/s10518-006-9008-z

Boore, D. M. (2003). Simulation of Ground Motion Using the Stochastic Method. *Pure Appl Geophys*, *160*, 635–676.

Boore, D. M. (2010). Orientation-independent, nongeometric-mean measures of seismic intensity from two horizontal components of motion. In *Bulletin of the Seismological Society of America* (Vol. 100, Issue 4, pp. 1830–1835). https://doi.org/10.1785/0120090400

Boore, D. M., Watson-Lamprey, J., & Abrahamson, N. A. (2006). Orientation-independent measures of ground motion. *Bulletin of the Seismological Society of America*, *96*(4 A), 1502–1511. https://doi.org/10.1785/0120050209

Bouazza, H., Djelil, M., & Matallah, M. (2022). On the relevance of incorporating bar slip, bar buckling and low-cycle fatigue effects in seismic fragility assessment of RC bridge piers. *Engineering Structures*, *256*. https://doi.org/10.1016/j.engstruct.2022.114032

Bradley, B. A., & Cubrinovski, M. (2011). Near-source Strong Ground Motions Observed in the 22 February 2011 Christchurch Earthquake. *Seismological Research Letters*, *82*(6), 853–865.

Bragato, P. L. (2009). Assessing regional and site-dependent variability of ground motions for shakemap implementation in Italy. *Bulletin of the Seismological Society of America*, *99*(5), 2950–2960. https://doi.org/10.1785/0120090020

Brandow, G. (2018). *2017 LATBSDC Alternative Analysis and Design Procedure 1*.

Brune, J. N. (1970). Tectonic Stress and the Spectra of Seismic Shear Waves from Earthquakes. *Journal of Geophysical Research*, *76*, 4997–5009.

Brune, J. N. (1971). Tectonic Stress and the Spectra of Seismic Shear Waves from Earthquakes: Correction. *Journal of Geophysical Research*, *76*, 5002.

Cardona, O. D. (1986). Estudios de vulnerabilidad y evaluación del riesgo sísmico: Pla nificación física y urbana en áreas propensas. *Boletín Técnico de La Asociación Colombiana de Ingeniería Sísmica*, *33*(2), 32–65.

Cardona, O. D. (1990). *Terminología de Uso Común en Manejo de Riesgos. AGID Reporte No. 13*.

Çelebi, M., Sanli, A., Sinclair, M., Gallant, S., & Radulescu, D. (2004). Real-time seismic monitoring needs of a building owner - And the solution: A cooperative effort. *Earthquake Spectra*, *20*(2), 333–346. https://doi.org/10.1193/1.1735987

Celik, O. C., & Ellingwood, B. R. (2010). Seismic fragilities for non-ductile reinforced concrete frames - Role of aleatoric and epistemic uncertainties. *Structural Safety*, *32*(1), 1–12. https://doi.org/10.1016/j.strusafe.2009.04.003

CEN. (2002). EN 1990:2002 + A1 Eurocode—basis of structural design. *European Committee for Standardization, Brussels*.

CEN. (2004a). EN 1994-1-1:2004 Eurocode 4: Design of composite steel and concrete structures. Part 2: Composite bridges. *European Committee for Standardization, Brussels.*

CEN. (2004b). EN 1998-1:2004 Eurocode 8: design of structures for earthquake resistance—part 1: general rules, seismic actions and rules for buildings. *European Committee for Standardization, Brussels*.

Chioccarelli, E., Cito, P., Iervolino, I., & Giorgio, M. (2019). REASSESS V2.0: software for single- and multi-site probabilistic seismic hazard analysis. *Bulletin of Earthquake Engineering*, *17*(4), 1769–1793. https://doi.org/10.1007/s10518-018-00531-x

Coleman, J., & Spacone, E. (2001). LOCALIZATION ISSUES IN FORCE-BASED FRAME ELEMENTS. In *JOURNAL OF STRUCTURAL ENGINEERING*.

Collins, K. R., Wen, Y. K., & Foutch, D. A. (1996). Dual-level seismic design: A reliability-based methodology. *Earthquake Engineering and Structural Dynamics*, *25*(12), 1433–1467. https://doi.org/10.1002/(SICI)1096-9845(199612)25:12<1433::AID-EQE629>3.0.CO;2-M

Comisu, C. C., Taranu, N., Boaca, G., & Scutaru, M. C. (2017). Structural health monitoring system of bridges. *Procedia Engineering*, *199*, 2054–2059. https://doi.org/10.1016/j.proeng.2017.09.472

Cornell, C. A. (1964). *Stochastic Process Models in Structural Engineering*.

Cornell, C. A. (1968). Engineering seismic risk analysis. *Bulletin of the Seismological Society of America*, *58*(5), 1583–1606. http://pubs.geoscienceworld.org/ssa/bssa/article-pdf/58/5/1583/5350226/bssa0580051583.pdf

Cornell, C. A. (2005). On earthquake record selection for nonlinear dynamic analysis. *Luis Esteva Symposium*.

Cornell, C. A., Jalayer, F., Hamburger, R. O., & Foutch, D. A. (2002). Probabilistic Basis for 2000 SAC Federal Emergency Management Agency Steel Moment Frame Guidelines. *Journal of Structural Engineering*, *128*(4), 526–533. https://doi.org/10.1061/(asce)0733-9445(2002)128:4(526)

Cornell, C. A., & Krawinkler, H. (2000). Progress and challenges in seismic performance assessment. *PEER Center News*, *3*(2).

Cosenza, E., & Manfredi, G. (2000). Damage indices and damage measures. *Progress in Structural Engineering and Materials*, *2*(1), 50–59. https://doi.org/10.1002/(sici)1528-2716(200001/03)2:1<50::aid-pse7>3.0.co;2-s

Cosenza, E., Manfredi, G., & Ramasco, R. (1993). The use of damage functionals in earthquake engineering: A comparison between different methods. *Earthquake Engineering & Structural Dynamics*, *22*(10), 855–868. https://doi.org/10.1002/eqe.4290221003

Costa, A., Romão, X., & Oliveira, C. S. (2010). A methodology for the probabilistic assessment of behaviour factors. *Bulletin of Earthquake Engineering*, *8*(1), 47–64. https://doi.org/10.1007/s10518-009-9126-5

Crowley, H., Bommer, J. J., & Stafford, P. J. (2008). Recent developments in the treatment of ground-motion variability in earthquake loss models. *Journal of Earthquake Engineering*, *12*(SUPPL. 2), 71–80. https://doi.org/10.1080/13632460802013529

Dall'Asta, A., Dabiri, H., Tondi, E., & Morci, M. (2021). Influence of time-dependent seismic hazard on structural design. *Bulletin of Earthquake Engineering*, *19*(6), 2505–2529. https://doi.org/10.1007/s10518-021-01075-3

Dall'Asta, A., Scozzese, F., Ragni, L., & Tubaldi, E. (2017). Effect of the damper property variability on the seismic reliability of linear systems equipped with viscous dampers. *Bulletin of Earthquake Engineering*, *15*(11), 5025–5053. https://doi.org/10.1007/s10518-017-0169-8

Dall'asta, A., Tubaldi, E., & Ragni, L. (2016). Influence of the nonlinear behavior of viscous dampers on the seismic demand hazard of building frames. *Earthquake Engineering and Structural Dynamics*, *45*(1), 149–169. https://doi.org/10.1002/eqe.2623

Dang J. (2021). Seismic risk-based design of bridges. . In *Reliability-based analysis and design of structures and infrastructures, Book Chapter 18, Edited by Ehsan Noroozinejad Farsangi, Mohammad Noori, Paolo Gardoni, Izuru Takewaki, Humberto Varum and Aleksandra Bogdanovic*. CRC Press.

Darwiche, A. (2009). *Modeling and Reasoning with Bayesian Networks*. Cambridge: Cambridge University Press.

Deb, A., Conte, J. P., & Restrepo, J. I. (2022). Comprehensive treatment of uncertainties in risk-targeted performance-based seismic design and assessment of bridges. *Earthquake Engineering and Structural Dynamics*, *51*(14), 3272–3295. https://doi.org/10.1002/eqe.3722

Deb, A., Zha, A. L., Caamaño-Withall, Z. A., Conte, J. P., & Restrepo, J. I. (2022). Simplified Risk-Targeted Performance-Based Seismic Design Method for Ordinary Standard Bridges. *Journal of Bridge Engineering*, *27*(10).

Deierlein, G. G., Krawinkler, H., Cornell, C. A., & Blume, J. A. (2003). A framework for performance-based earthquake engineering. *Pacific Conference of Earthquake Engineering*. https://www.researchgate.net/publication/340092329

Der Kiureghian, A. (2005). Non-ergodicity and PEER's framework formula. *Earthquake Engineering and Structural Dynamics*, *34*(13), 1643–1652. https://doi.org/10.1002/eqe.504

Dezi L. (2008). Architectural and structural design of short and medium span composite bridges. *Proceedings of 7th International Conference on Steel Bridges*.

Di Sarno, L. (2013). Effects of multiple earthquakes on inelastic structural response. *Engineering Structures*, *56*, 673–681. https://doi.org/10.1016/j.engstruct.2013.05.041

Dolce, M., & Larotonda, A. (2001). Earthquake's effects on the Fabriano, Nocera Umbra and Sellano's buildings. *Italian Geotechnical Journal* , *35*, 10–19.

Dolsˇek, M., Z ˇ izˇmond, J., Kosicˇ, M., & Lazar Sinkovic´, N. (2017). *Simplified reliability-based verification format, working material for Annex F to revised EN 1998-1*.

Douglas, J., & Aochi, H. (2008). A survey of techniques for predicting earthquake ground motions for engineering purposes. *Surveys in Geophysics*, *29*(3), 187–220. https://doi.org/10.1007/s10712-008-9046-y

Douglas, J., & Edwards, B. (2016). Recent and future developments in earthquake ground motion estimation. *Earth-Science Reviews*, *160*, 203–219.

Douglas, J., & Gkimprixis, A. (2018). Risk targeting in seismic design codes: The state of the art, outstanding issues and possible paths forward. *Seismic Hazard and Risk Assessment*, 211–223. https://earthquake.usgs.gov/hazards/designmaps/rtgm.php

Douglas, J., Ulrich, T., & Negulescu, C. (2013). Risk-targeted seismic design maps for mainland France. *Natural Hazards*, *65*(3), 1999–2013. https://doi.org/10.1007/s11069-012-0460-6

Du, A., & Padgett, J. E. (2020). Investigation of multivariate seismic surrogate demand modeling for multi-response structural systems. *Engineering Structures*, *207*. https://doi.org/10.1016/j.engstruct.2020.110210

Duerr, K., & Tesfamariam, S. (2012). Damage Accumulation in Reinforced Concrete Structures due to Mainshock and Aftershock Earthquakes. *Proceedings, Annual Conference - Canadian Society for Civil Engineering*, 2199–2208. https://www.researchgate.net/publication/281656220

Dukes, J., Mangalathu, S., Padgett, J. E., & DesRoches, R. (2018). Development of a bridge-specific fragility methodology to improve the seismic resilience of bridges. *Earthquake and Structures*, *15*(3), 253–261. https://doi.org/10.12989/eas.2018.15.3.253

Ebrahimian, H., & Jalayer, F. (2017). Robust seismicity forecasting based on Bayesian parameter estimation for epidemiological spatio-temporal aftershock clustering models. *Scientific Reports*, *7*(1). https://doi.org/10.1038/s41598-017-09962-z

Ellingwood, B. R. (2008). Structural reliability and performance-based engineering. *Proc. Inst. Civ. Eng. Struct. Build*, *161*(4), 199–207.

Elnashai, A. S., & Bommer, J. J. (1998). Engineering implications of strong motion records from recent earthquakes. *Proceedings of 11th European Conference on Earthquake Engineering*.

Erdik, M., Şeşetyan, K., Demircioĝlu, M. B., Hancilar, U., & Zülfikar, C. (2011). Rapid earthquake loss assessment after damaging earthquakes. *Soil Dynamics and Earthquake Engineering*, *31*(2), 247–266. https://doi.org/10.1016/j.soildyn.2010.03.009

Erdik, M., Şeşetyan, K., Demircioğlu, M. B., Hancılar, U., & Zülfikar, C. (2010). Rapid earthquake loss assessment after damaging earthquakes. *Soil Dynamics and Earthquake Engineering*, *31*(2), 247–266.

Faber, M. H., & Stewart, M. G. (2003). Risk assessment for civil engineering facilities: Critical overview and discussion. *Reliability Engineering and System Safety*, *80*(2), 173–184. https://doi.org/10.1016/S0951-8320(03)00027-9

Fajfar, P. (2018). Analysis in seismic provisions for buildings: past, present and future: The fifth Prof. Nicholas Ambraseys lecture. In *Bulletin of Earthquake Engineering* (Vol. 16, Issue 7, pp. 2567–2608). Springer Netherlands. https://doi.org/10.1007/s10518-017-0290-8

Fayaz, J., Dabaghi, M., & Zareian, F. (2020). Utilization of Site-Based Simulated Ground Motions for Hazard-Targeted Seismic Demand Estimation: Application for Ordinary Bridges in Southern California. *Journal of Bridge Engineering*, *25*(11). https://doi.org/10.1061/(asce)be.1943-5592.0001634

Fayaz, J., Medalla, M., & Zareian, F. (2020). Sensitivity of The Response of Box-Girder Seat-Type Bridges to the Duration of Ground Motions Arising from Subduction Earthquakes. *Engineering Structures*, *219*. https://www.researchgate.net/publication/332382987

Fayaz, J., Rezaeian, S., & Zareian, F. (2021). Evaluation of simulated ground motions using probabilistic seismic demand analysis: CyberShake (ver. 15.12) simulations for Ordinary Standard Bridges. *Soil Dynamics and Earthquake Engineering*, *141*. https://doi.org/10.1016/j.soildyn.2020.106533

Fayaz, J., Xiang, Y., & Zareian, F. (2019). Performance assessment of bridges under a sequence of seismic excitations. *COMPDYN Proceedings*, *2*, 2661–2676. https://doi.org/10.7712/120119.7101.19241

FEMA. (2009). *NEHRP recommended seismic provisions for new buildings and other structures (FEMA P750)*. Federal Emergency Management Agency.

FEMA. (2018). *FEMA P-58: Seismic Performance Assessment of Buildings: Second Edition*. Federal Emergency Management Agency.

FEMA P-58-1. (2012). *Seismic Performance Assessment of Buildings, Volume 1 – Methodology, Second Edition*.

Flenga, M. G., & Favvata, M. J. (2021). Fragility curves and probabilistic seismic demand models on the seismic assessment of RC frames subjected to structural pounding. *Applied Sciences (Switzerland)*, *11*(17). https://doi.org/10.3390/app11178253

Fragiacomo, M., Amadio, C., & Macorini, L. (2004). Seismic response of steel frames under repeated earthquake ground motions. *Engineering Structures*, *26*(13), 2021–2035. https://doi.org/10.1016/j.engstruct.2004.08.005

Franchin, P., Petrini, F., & Mollaioli, F. (2018). Improved risk-targeted performance-based seismic design of reinforced concrete frame structures. *Earthq Eng Struct Dynam*, *47*, 49–67.

Franchin, P., & Pinto, P. E. (2009). Allowing traffic over mainshock-damaged bridges. *Journal of Earthquake Engineering*, *13*(5), 585–599. https://doi.org/10.1080/13632460802421326

Franchini, A., Sebastian, W., & D'Ayala, D. (2022). Surrogate-based fragility analysis and probabilistic optimisation of cable-stayed bridges subject to seismic loads. *Engineering Structures*, *256*. https://doi.org/10.1016/j.engstruct.2022.113949

Freddi, F. (2012). *Local engineering demand parameters for seismic risk evaluation of low ductility reinforced concrete buildings* [Ph.D. Dissertation]. Universita' Politecnica delle Marche.

Freddi, F., Padgett, J. E., & Dall'asta, A. (2017). Probabilistic Seismic Demand Modeling of Local Level Response Parameters of an RC Frame. *Bull. Earthq. Eng*, *15*, 1–23.

Gardoni, P., Der Kiureghian, A., & Mosalam, K. M. (2002). Probabilistic Capacity Models and Fragility Estimates for Reinforced Concrete Columns based on Experimental Observations. *J. Eng. Mech*, *128*, 1024–1038.

Gardoni, P., Mosalam, K. M., & Der Kiureghian, A. (2003). Probabilistic seismic demand models and fragility estimates for RC bridges. *Journal of Earthquake Engineering*, *7*, 79–106. https://doi.org/10.1080/13632460309350474

Gehl, P. (2017). *Bayesian Networks for the Multi-Risk Assessment of Road Infrastructure*. University College London.

Gehl, P., & D'Ayala, D. (2016). Development of Bayesian Networks for the multi-hazard fragility assessment of bridge systems. *Structural Safety*, *60*, 37–46. https://doi.org/10.1016/j.strusafe.2016.01.006

Gehl, P., Douglas, J., & D'ayala, D. (2017). Inferring earthquake ground-motion fields with Bayesian networks. *Bulletin of the Seismological Society of America*, *107*(6), 2792–2808. https://doi.org/10.1785/0120170073

Gehl, P., Douglas, J., & Seyedi, D. M. (2015). Influence of the number of dynamic analyses on the accuracy of structural response estimates. *Earthquake Spectra*, *31*(1), 97–113. https://doi.org/10.1193/102912EQS320M

Gelman, A., & Rubin, D. B. (1992). Inference from Iterative Simulation Using Multiple Sequences. In *Science* (Vol. 7, Issue 4).

Gentile, R., & Galasso, C. (2020). Gaussian process regression for seismic fragility assessment of building portfolios. *Structural Safety*, *87*. https://doi.org/10.1016/j.strusafe.2020.101980

Gentile, R., & Galasso, C. (2021). Hysteretic energy-based state-dependent fragility for ground-motion sequences. *Earthquake Engineering and Structural Dynamics*, *50*(4), 1187–1203. https://doi.org/10.1002/eqe.3387

Geyer, C. J. (2011). Introduction to Markov Chain Monte Carlo. In *Handbook of Markov Chain Monte Carlo*. Hall/CRC.

Ghosh, J., Padgett, J. E., & Dueñas-Osorio, L. (2013). Surrogate modeling and failure surface visualization for efficient seismic vulnerability assessment of highway bridges. *Probabilistic Engineering Mechanics*, *34*, 189–199. https://doi.org/10.1016/j.probengmech.2013.09.003

Ghosh, J., Padgett, J. E., & Sánchez-Silva, M. (2015a). Seismic damage accumulation in highway bridges in earthquake-prone regions. *Earthquake Spectra*, *31*(1), 115–135. https://doi.org/10.1193/120812EQS347M

Ghosh, J., Padgett, J. E., & Sánchez-Silva, M. (2015b). Seismic damage accumulation in highway bridges in earthquake-prone regions. *Earthquake Spectra*, *31*(1), 115–135. https://doi.org/10.1193/120812EQS347M

Giordano, P. F., & Limongelli, M. P. (2022). The value of structural health monitoring in seismic emergency management of bridges. *Structure and Infrastructure Engineering*, *18*(4), 537–553. https://doi.org/10.1080/15732479.2020.1862251

Gkatzogias, K. I., & Kappos, A. J. (2022). Deformation-based design of seismically isolated bridges. *Earthquake Engineering and Structural Dynamics*, *51*(14), 3243–3271. https://doi.org/10.1002/eqe.3721

Gkimprixis, A., Tubaldi, E., & Douglas, J. (2019). Comparison of methods to develop risk-targeted seismic design maps. *Bulletin of Earthquake Engineering*, *17*(7), 3727–3752. https://doi.org/10.1007/s10518-019-00629-w

Gkimprixis, A., Tubaldi, E., & Douglas, J. (2020). Evaluating alternative approaches for the seismic design of structures. *Bulletin of Earthquake Engineering*, *18*(9), 4331–4361. https://doi.org/10.1007/s10518-020-00858-4

Goda, K., & Taylor, C. A. (2012). Effects of aftershocks on peak ductility demand due to strong ground motion records from shallow crustal earthquakes. *Earthquake Engineering and Structural Dynamics*, *41*(15), 2311–2330. https://doi.org/10.1002/eqe.2188

Goda, K., Wenzel, F., & De Risi, R. (2015). Empirical assessment of non-linear seismic demand of mainshock–aftershock ground-motion sequences for Japanese earthquakes. *Frontiers in Built Environment*, *1*. https://doi.org/10.3389/fbuil.2015.00006

Gray, R. M. (2011). Entropy and Information Theory. *Springer Science & Business Media*.

Günay, M. S., & Mosalam, K. M. (2013). PEER Performance Based Earthquake Engineering Methodology, Revisited. *Journal of Earthquake Engineering*, *17*(6), 829–858.

Gusella, V. (1998). Safety estimation method for structures with cumulative damage. *Journal of Engineering Mechanics*, *124(11)*, 1200–1209.

Gutenberg, B., & Richter, C. F. (1942). Earthquake magnitude, intensity, energy and acceleration. *Bulletin of the Seismological Society of America*, *32*(3).

Hatzivassiliou, M., & Hatzigeorgiou, G. D. (2015). Seismic sequence effects on three-dimensional reinforced concrete buildings. *Soil Dynamics and Earthquake Engineering*, *72*, 77–88. https://doi.org/10.1016/j.soildyn.2015.02.005

Heckerman, D. (2008). A tutorial on learning with Bayesian networks. *Holmes, D.E., Jain, L.C. (Eds) Innovations in Bayesian Networks. Studies in Computational Intelligence*, *156*.

Heredia-Zavoni, E., Zeballos, A., & Esteva, L. (2000). Theoretical models and recorded response in the estimation of cumulative seismic damage on non-linear structures. *Earthquake Engineering and Structural Dynamics*, *29*(12), 1779–1796. https://doi.org/10.1002/1096-9845(200012)29:12<1779::AID-EQE985>3.0.CO;2-F

Hoang, P. H., Phan, H. N., Nguyen, D. T., & Paolacci, F. (2021). Kriging metamodel-based seismic fragility analysis of single-bent reinforced concrete highway bridges. *Buildings*, *11*(6). https://doi.org/10.3390/buildings11060238

Huang, C., & Darwiche, A. (1996). Inference in Belief Networks: A Procedural Guide. *International Journal of Approximate Reasoning*, *15*(3), 225–263.

Iacoletti, S., Cremen, G., & Galasso, C. (2021). *Validation of the Epidemic-Type Aftershock Sequence (ETAS) models for simulation-based seismic hazard assessments Declaration of Competing Interests*.

Ibrahim, Y. E., & El-Shami, M. M. (2011). Seismic fragility curves for mid-rise reinforced concrete frames in Kingdom of Saudi Arabia. *IES Journal Part A: Civil*

and Structural Engineering, *4*(4), 213–223. https://doi.org/10.1080/19373260.2011.609325

Iervolino, I., Chioccarelli, E., & Suzuki, A. (2020). Seismic damage accumulation in multiple mainshock–aftershock sequences. *Earthquake Engineering and Structural Dynamics*, *49*(10), 1007–1027. https://doi.org/10.1002/eqe.3275

Iervolino, I., Giorgio, M., & Chioccarelli, E. (2013). Gamma degradation models for earthquake-resistant structures. *Structural Safety*, *45*, 48–58. https://doi.org/10.1016/j.strusafe.2013.09.001

Iervolino, I., Giorgio, M., & Chioccarelli, E. (2016). Markovian modeling of seismic damage accumulation. *Earthquake Engineering and Structural Dynamics*, *45*(3), 441–461. https://doi.org/10.1002/eqe.2668

Iervolino, I., Spillatura, A., & Bazzurro, P. (2018). Seismic Reliability of Code-Conforming Italian Buildings. *Journal of Earthquake Engineering*, *22*(sup2), 5–27. https://doi.org/10.1080/13632469.2018.1540372

Im, S. B., Hurlebaus, S., & Kang, Y. J. (2013). Summary Review of GPS Technology for Structural Health Monitoring. *Journal of Structural Engineering*, *139*(10), 1653–1664. https://doi.org/10.1061/(asce)st.1943-541x.0000475

ISO 31000:2009. Risk Management—Principles and Guidelines (2009).

Jalayer, F. (2003). *Direct Probabilistic Seismic Analysis: Implementing Non-Linear Dynamic Assessments*. https://www.researchgate.net/publication/234174752

Jalayer, F., Asprone, D., Prota, A., & Manfredi, G. (2011). A decision support system for post-earthquake reliability assessment of structures subjected to aftershocks: An application to L'Aquila earthquake, 2009. *Bulletin of Earthquake Engineering*, *9*(4), 997–1014. https://doi.org/10.1007/s10518-010-9230-6

Jalayer, F., & Beck, J. L. (2008). Effects of two alternative representations of ground-motion uncertainty on probabilistic seismic demand assessment of structures. *Earthquake Engineering and Structural Dynamics*, *37*(1), 61–79. https://doi.org/10.1002/eqe.745

Jalayer, F., & Cornell, C. A. (2009). Alternative non-linear demand estimation methods for probability-based seismic assessments. *Earthquake Engineering and Structural Dynamics*, *38*(8), 951–972. https://doi.org/10.1002/eqe.876

Jalayer, F., De Risi, R., & Manfredi, G. (2015). Bayesian Cloud Analysis: Efficient structural fragility assessment using linear regression. *Bulletin of Earthquake Engineering*, *13*(4), 1183–1203. https://doi.org/10.1007/s10518-014-9692-z

Jalayer, F., & Ebrahimian, H. (2017). Seismic risk assessment considering cumulative damage due to aftershocks. *Earthquake Engineering and Structural Dynamics*, *46*(3), 369–389. https://doi.org/10.1002/eqe.2792

Jalayer, F., Franchin, P., & Pinto, P. E. (2007). A scalar damage measure for seismic reliability analysis of RC frames. *Earthquake Engineering and Structural Dynamics*, *36*(13), 2059–2079. https://doi.org/10.1002/eqe.704

Jayaram, N., & Baker, J. W. (2009). Correlation model for spatially distributed ground-motion intensities. *Earthquake Engineering and Structural Dynamics*, *38*(15), 1687–1708. https://doi.org/10.1002/eqe.922

Jeong, G. D., & Iwan, W. D. (1988). The effect of earthquake duration on the damage of structures. *Earthquake Engineering & Structural Dynamics*, *16*(8), 1201–1211. https://doi.org/10.1002/eqe.4290160808

Kappos, A. (1997). Seismic damage indices for RC buildings: evaluation of concepts and procedures. *Progress in Structural Engineering and Materials*, *1*(1), 78–87. https://doi.org/10.1002/pse.2260010113

Kappos, A., Panagopoulos, G., Panagiotopoulos, C., & Penelis, G. (2006). A hybrid method for the vulnerability assessment of R/C and URM buildings. *Bulletin of Earthquake Engineering*, *4*(4), 391–413. https://doi.org/10.1007/s10518-006-9023-0

Kappos, A., Pitilakis, K., Stylianidis, K. C., Morfidis, K., & Asimakopoulos, N. (1995). Cost-Benefit Analysis for the Seismic Rehabilitation of Buildings in Thessaloniki, Based on A Hybrid Method of Vulnerability Assessment. *Proceedings of the Fifth International Conference on Seismic Zonation*, 406–413. https://www.researchgate.net/publication/237050766

Karsan, I. D., & Jirsa, J. O. (1969). Behavior of concrete under compressive loading. *J. Struct. Div., , 95*(12), 2543–2563.

Kashani, M. M., Lowes, L. N., Crewe, A. J., & Alexander, N. A. (2016). Nonlinear fibre element modelling of RC bridge piers considering inelastic buckling of reinforcement. *Engineering Structures*, *116*, 163–177. https://doi.org/10.1016/j.engstruct.2016.02.051

Kashani, M. M., Málaga-Chuquitaype, C., Yang, S., & Alexander, N. A. (2017). Influence of non-stationary content of ground-motions on nonlinear dynamic response of RC bridge piers. *Bulletin of Earthquake Engineering*, *15*(9), 3897–3918. https://doi.org/10.1007/s10518-017-0116-8

Kent, D. C., & Park, R. (1971). Flexural Members with Confined Concrete. *Journal of the Structural Division*, *97*, 1969–1990.

Kirçil, M. S., & Polat, Z. (2006). Fragility analysis of mid-rise R/C frame buildings. *Engineering Structures*, *28*(9), 1335–1345. https://doi.org/10.1016/j.engstruct.2006.01.004

Kongar, I., Rossetto, T., Kongar, I., Giovinazzi, S., & Rossetto, T. (2017). *Seismic risk assessment of interdependent electric power and water supply systems in Christchurch, New Zealand*. https://www.researchgate.net/publication/336881482

Kramer, S. L. (1996). *Geotechnical earthquake engineering* (Prentice Hall, Ed.). Upper Saddle River.

Krawinkler, H., & Miranda, E. (2004). Performance-based earthquake engineering. In *Earthquake Engineering: From Engineering Seismology to Performance-Based Engineering*. CRC Press.

Kumar, R., Gardoni, P., & Asce, M. (2012). *Modeling Structural Degradation of RC Bridge Columns Subjected to Earthquakes and Their Fragility Estimates*. https://doi.org/10.1061/(ASCE)ST.1943

Kunnath, S. K., El-Bahy, A., Taylor, A., & Stone, W. (1997). *Cumulative Seismic Damage of Reinforced Concrete Bridge Piers*.

Lanzano, G., Luzi, L., Pacor, F., Felicetta, C., Puglia, R., Sgobba, S., & D'Amico, M. (2019). A revised ground-motion prediction model for shallow crustal earthquakes in Italy. *Bulletin of the Seismological Society of America*, *109*(2), 525–540. https://doi.org/10.1785/0120180210

Lazar, N., & Dolšek, M. (2012). Risk-based seismic design-An alternative to current standards for earthquake-resistant design of buildings. *Conference: 15th World Conference on Earthquake Engineering*.

Le Cam, L. (1990). Maximum Likelihood: An Introduction. *International Statistical Review / Revue Internationale de Statistique*, *58*(2), 153–171.

Lee, H., Park, H. J., & Kim, B. (2020). Differences between main shock and aftershock ground motions derived from the Japanese KiK-net database. *Soil Dynamics and Earthquake Engineering*, *138*. https://doi.org/10.1016/j.soildyn.2020.106325

Lee, S.-H., Student, G., Song, J., Kwag, S., & Hahm, D. (2019). Multi-Hazard Risk Assessment Using Bayesian Network and Fault Tree Analysis Considering Effects of Structural Damage ChangUk Mun. *ICASP13*.

Lee, T. H., & Mosalam, K. M. (2005). Seismic demand sensitivity of reinforced concrete shear-wall building using FOSM method. *Earthquake Engineering and Structural Dynamics*, *34*(14), 1719–1736. https://doi.org/10.1002/eqe.506

Lehman, D. E., & Moehle, J. P. (2000). *Seismic performance of well-confined concrete bridge columns*.

Li, Z. (2020). *Degradation Modeling and Reliability Analysis of Bridge Rebar Corrosion*.

Lian, Q., Yuan, W., Guo, J., & Dang, X. (2022). Bridge seismic importance adjustment factor based on seismic risk. *Soil Dynamics and Earthquake Engineering*, *160*. https://doi.org/10.1016/j.soildyn.2022.107367

Limongelli, M. P., Omenzetter, P., Yazgan, U., & Soyoz, S. (2017). Quantifying the value of monitoring for post-earthquake emergency management of bridges. *IABSE Conference, Vancouver 2017: Engineering the Future - Report*, 3245–3252. https://doi.org/10.2749/222137817822208852

Liu, Z., Nadim, F., Garcia-Aristizabal, A., Mignan, A., Fleming, K., & Luna, B. Q. (2015). A three-level framework for multi-risk assessment. *Georisk: Assessment and Management of Risk for Engineered Systems and Geohazards*, 59–74.

Liu, Z., Sextos, A., Guo, A., & Zhao, W. (2022). ANN-based rapid seismic fragility analysis for multi-span concrete bridges. *Structures*, *41*, 804–817. https://doi.org/10.1016/j.istruc.2022.05.063

Lu, M., Hydock, J., Radlińska, A., & Guler, S. I. (2022). Reliability Analysis of a Bridge Deck Utilizing Generalized Gamma Distribution. *Journal of Bridge Engineering*, *27*(4). https://doi.org/10.1061/(asce)be.1943-5592.0001842

Luco, N., & Cornell, C. A. (2007). Structure-specific scalar intensity measures for near-source and ordinary earthquake ground motions. *Earthquake Spectra*, *23*(2), 357–392. https://doi.org/10.1193/1.2723158

Luco, N., Cornell, C. A., & Yeo, G. L. (2002). Annual limit-state frequencies for partially-inspected earthquake-damaged buildings. *Structural Safety*, *24*, 281–296. www.elsevier.com/locate/strusafe

Luco, N., Hamburger, R. O., Klemencic, M., Seattle, A., Jeffrey, W., & Kimball, K. (2007). Risk-Targeted versus Current Seismic Design Maps for the Conterminous United States. *SEAOC2007 Convention, Structural Engineers Association of California*.

Lunn, D., Spiegelhalter, D., Thomas, A., & Best, N. (2009). The BUGS project: Evolution, critique and future directions. *Statistics in Medicine*, *28*(25), 3049–3067. https://doi.org/10.1002/sim.3680

Ma, H. Bin, Zhuo, W. D., Lavorato, D., Nuti, C., Fiorentino, G., Marano, G. C., Greco, R., & Briseghella, B. (2019). Probabilistic seismic response and uncertainty analysis of continuous bridges under near-fault ground motions. *Frontiers of*

Structural and Civil Engineering, *13*(6), 1510–1519.
https://doi.org/10.1007/s11709-019-0577-8

Mackie, K. R., & Stojadinović, B. (2006). Post-earthquake functionality of highway overpass bridges. *Earthquake Engineering and Structural Dynamics*, *35*(1), 77–93. https://doi.org/10.1002/eqe.534

Mackie, K., & Stojadinovic´, B. S. (2001). Probabilistic Seismic Demand Model for California Highway Bridges. *Journal of Bridge Engineering*, *6*(6), 468–481. http://peer.

Mackie, K., & Stojadinovic, B. (2003). *Seismic Demands for Performance-Based Design of Bridges*.

Mander, J. B., & Basöz, N. (1999). Seismic fragility curve theory for highway bridges. *In Proceedings of the 5th US Conference on Lifeline Earthquake Engineering: Optimazing Post-Earthquake Lifeline System Reliability*, 31–40. https://www.researchgate.net/publication/292691534

Mander, J. B., Priestley, M. J. N., & Park, R. (1988). *THEORETICAL STRESS-STRAIN MODEL FOR CONFINED CONCRETE*.

Mangalathu, S., Heo, G., & Jeon, J. S. (2018). Artificial neural network based multi-dimensional fragility development of skewed concrete bridge classes. *Engineering Structures*, *162*, 166–176. https://doi.org/10.1016/j.engstruct.2018.01.053

Manyena, S. B. (2006). The concept of resilience revisited. *Disasters*, *30*(4), 433–450.

McGuire, R. K. (1976). *FORTRAN computer program for seismic risk analysis*.

McGuire, R. K., & Arabasz, W. J. (1990). An introduction to probabilistic seismic hazard analysis. In *Geotechnical and environmental geophysics* (Ward SH, Vol. 1, pp. 333–353). Society of Exploration Geophysicist.

McKay, M. D., Beckman, R. J., & Conover, W. J. (1979). Comparison of three methods for selecting values of input variables in the analysis of output from a computer code. *Technometrics*, *21*(2), 239–245. https://doi.org/10.1080/00401706.1979.10489755

McKenna, F., Fenves, G., & Scott, M. (2006). *OpenSees: open system for earthquake engineering simulation*. Berkeley (CA): Pacific Earthquake Engineering Center.

Meletti, C., Galadini, F., Valensise, G., Stucchi, M., Basili, R., Barba, S., Vannucci, G., & Boschi, E. (2008). A seismic source zone model for the seismic hazard assessment of the Italian territory. *Tectonophysics*, *450*(1–4), 85–108. https://doi.org/10.1016/j.tecto.2008.01.003

Menegotto, M., & Pinto, P. E. (1973). Method of analysis for cyclically loaded R.C. plane frames including changes in geometry and non-elastic behaviour of elements under combined normal force and bending. *Proceeding of IABSE Symposium*. https://doi.org/10.5169/seals-13741

Miano, A., Jalayer, F., De Risi, R., Prota, A., & Manfredi, G. (2016). Model updating and seismic loss assessment for a portfolio of bridges. *Bulletin of Earthquake Engineering*, *14*(3), 699–719. https://doi.org/10.1007/s10518-015-9850-y

Michelini, A., Faenza, L., Lauciani, V., & Malagnini, L. (2008). *ShakeMap implementation in Italy*. http://www.ingv.it/progettiSV/Progetti/Sismologici/sismologici_con_frame.htm,

Minnucci, L., Scozzese, F., Carbonari, S., Gara, F., & Dall'Asta, A. (2022). Innovative Fragility-Based Method for Failure Mechanisms and Damage Extension Analysis of Bridges. *Infrastructures*, *7*(9). https://doi.org/10.3390/infrastructures7090122

Moehle, J., & Deierlein, G. G. (2004). A framework methodology for performance-based earthquake engineering. *Proceedings, 13th World Conference on Earthquake Engineering*. https://www.researchgate.net/publication/228706335

Montes-Iturrizaga, R., Heredia-Zavoni, E., & Esteva, L. (2003a). Optimal maintenance strategies for structures in seismic zones. *Earthquake Engineering and Structural Dynamics*, *32*(2), 245–264. https://doi.org/10.1002/eqe.222

Montes-Iturrizaga, R., Heredia-Zavoni, E., & Esteva, L. (2003b). Optimal maintenance strategies for structures in seismic zones. *Earthquake Engineering & Structural Dynamics*, *32*, 245–264.

Moon, T. K. (1996). The expectation-maximization algorithm. *IEEE Signal Processing Magazine*, *13*(6), 47–60.

Moschonas, I. F., Kappos, A. J., Panetsos, P., Papadopoulos, V., Makarios, T., & Thanopoulos, P. (2009). Seismic fragility curves for greek bridges: Methodology and case studies. *Bulletin of Earthquake Engineering*, *7*(2), 439–468. https://doi.org/10.1007/s10518-008-9077-2

Murià-Vila, D., & Toro Jaramillo, A. M. (1998). Effects of several events recorded at a building founded on soft soil. *11th European Conference on Earthquake Engineering*.

Nikellis, A., Sett, K., & Whittaker, A. S. (2019). Multihazard Design and Cost-Benefit Analysis of Buildings with Special Moment–Resisting Steel Frames. *Journal of Structural Engineering*, *145*(5). https://doi.org/10.1061/(asce)st.1943-541x.0002298

Ogata, Y. (1998). Space-Time Point-Process Models for Earthquake Occurrences. *Annals of the Institute of Statistical Mathematics* , *50*, 379–402.

OpenSees, the open system for earthquake engineering simulation. (2011). Pacific Earthquake Engineering Research Centre.

O'Reilly, G. J., Yasumoto, H., Suzuki, Y., Calvi, G. M., & Nakashima, M. (2022). Risk-based seismic design of base-isolated structures with single surface friction sliders. *Earthquake Engineering and Structural Dynamics*, *51*(10), 2378–2398. https://doi.org/10.1002/eqe.3668

Ozer, E., Feng, D., & Feng, M. Q. (2017). Hybrid motion sensing and experimental modal analysis using collocated smartphone camera and accelerometers. *Measurement Science and Technology*, *28*(10). https://doi.org/10.1088/1361-6501/aa82ac

Pacific Earthquake Engineering Research Center (PEER). (2017). Guidelines for Performance-based Seismic Design of Tall Buildings. In *Version 2.03 (Report 2017/06)*.

Pacifico, A., Chioccarelli, E., & Iervolino, I. (2022). Residential code-conforming structural seismic risk maps for Italy. *Soil Dynamics and Earthquake Engineering*, *153*. https://doi.org/10.1016/j.soildyn.2021.107104

Papadopoulos, A. N., Kohrangi, M., & Bazzurro, P. (2020). Mainshock-consistent ground motion record selection for aftershock sequences. *Earthquake Engineering and Structural Dynamics*, *49*(8), 754–771. https://doi.org/10.1002/eqe.3263

Park, J. , Bazzurro, P., & Baker, J. W. (2007). Modeling spatial correlation of ground motion intensity measures for regional seismic hazard and portfolio loss estimation. *Proc. of the 10th International Conf. on Applied Statistics and Probability*.

Park, Y.-J., & Ang, A. H.-S. (1985). Mechanistic seismic damage model for reinforced concrete. *Journal of Structural Engineering*, *111*, 722–739.

Park, Y.-J., Ang, A. H.-S., & Wen, Y. K. (1985). Seismic damage analysis of reinforced concrete buildings. *Journal of Structural Engineering*, *111*, 740–757.

Perrone, D., Calvi, P. M., Nascimbene, R., Fischer, E. C., & Magliulo, G. (2019). Seismic performance of non-structural elements during the 2016 Central Italy earthquake. *Bulletin of Earthquake Engineering*, *17*(10), 5655–5677. https://doi.org/10.1007/s10518-018-0361-5

Petrini, F., Gkoumas, K., Rossi, C., & Bontempi, F. (2020). Multi-Hazard Assessment of Bridges in Case of Hazard Chain: State of Play and Application to Vehicle-Pier Collision Followed by Fire. *Frontiers in Built Environment*, *6*. https://doi.org/10.3389/fbuil.2020.580854

Polhemus, N. W., & Cakmak, A. S. (1981). Simulation of earthquake ground motions using autoregressive moving average (ARMA) models. *Earthquake Engineering & Structural Dynamics*, *9*(4), 343–354. https://doi.org/10.1002/eqe.4290090404

Porter, K. A. (2003). An Overview of PEER's Performance-Based Earthquake Engineering Methodology. *Ninth International Conference on Applications of Statistics and Probability in Civil Engineering (ICASP9)*.

Porter, K. A. (2004). *A survey of bridge practitioners to relate damage to closure*.

Priestley M.J.N, Calvi, M. C., & Kowalsky, M. J. (2008). Displacement-Based Seismic Design of Structures. *Earthquake Spectra*, *24*(2), 555–557. https://doi.org/10.1193/1.2932170

Proposed AASHTO Guidelines for Performance-Based Seismic Bridge Design, The National Academies Press (2020).

Pugh, J. S. (2012). *Numerical Simulation of Walls and Seismic Design Recommendations for Walled Buildings* [PhD thesis]. University of Washington.

Radomir, F. (2015). Performance based seismic design of concrete buildings structures - bases. *Contemporary Achievements in Civil Engineering* .

Ramamoorthy, S. K., Gardoni, P., & Bracci, J. M. (2006). Probabilistic Demand Models and Fragility Curves for Reinforced Concrete Frames. *J. Struct. Eng*, *132*(10), 1563–1572. https://doi.org/10.1061/ASCE0733-94452006132:101563

Reasenberg, P. A., & Jones, L. M. (1989). Earthquake Hazard after a Mainshock in California. In *New Series* (Vol. 243, Issue 4895).

Rezaeian, S., & Der Kiureghian, A. (2010). *Stochastic Modeling and Simulation of Ground Motions for Performance-Based Earthquake Engineering*.

Rodrigues, H., Arêde, A., Varum, H., & Costa, A. (2013). Evaluation of damage in reinforced concrete columns under biaxial loading. *ECCOMAS Thematic Conference - COMPDYN 2013: 4th International Conference on Computational Methods in Structural Dynamics and Earthquake Engineering, Proceedings - An IACM Special Interest Conference*, 2466–2479. https://doi.org/10.7712/120113.4679.c1365

Rojas, H. A., Foley, C., & Pezeshk, S. (2011). Risk-based seismic design for optimal structural and nonstructural system performance. *Earthquake Spectra*, *27*(3), 857–880. https://doi.org/10.1193/1.3609877

Romão, X., Delgado, R., & Costa, A. (2013). Alternative closed-form solutions for the mean rate of exceedance of structural limit states. *Earthquake Engineering and Structural Dynamics*, *42*(12), 1827–1845. https://doi.org/10.1002/eqe.2300

Rossetto, T., & Elnashai, A. (2003). Derivation of vulnerability functions for European-type RC structures based on observational data. *Engineering Structures*, *25*(10), 1241–1263. https://doi.org/10.1016/S0141-0296(03)00060-9

Sakovych, B., Zharikova, M., & Sherstjuk, V. (2022). *The Probabilistic Graphical Model for Multi-Hazard Risk Evaluation of Critical Infrastructure Impairment*.

Sarabandi, P., Pachakis, D., King, S., & Kiremidjian, A. (2004). EMPIRICAL FRAGILITY FUNCTIONS FROM RECENT EARTHQUAKES. *3th World Conference on Earthquake Engineering* .

Saragoni, G. R., & Hart, G. C. (1973). Simulation of artificial earthquakes. *Earthquake Engineering & Structural Dynamics*, *2*(3), 249–267. https://doi.org/10.1002/eqe.4290020305

Scott, M. H., & Fenves, G. L. (2006). Plastic Hinge Integration Methods for Force-Based Beam–Column Elements. *Journal of Structural Engineering*, *132*(2), 244–252. https://doi.org/10.1061/(asce)0733-9445(2006)132:2(244)

Scozzese, F., Tubaldi, E., & Dall'Asta, A. (2020). Assessment of the effectiveness of Multiple-Stripe Analysis by using a stochastic earthquake input model. *Bulletin of Earthquake Engineering*, *18*(7), 3167–3203. https://doi.org/10.1007/s10518-020-00815-1

SEAOC Vision 2000 Committee. (1995). *Performance-Based Seismic Engineering*.

Sebastiani, G., Govoni, A., & Pizzino, L. (2019). Aftershock Patterns in Recent Central Apennines Sequences. *Journal of Geophysical Research: Solid Earth*, *124*(4), 3881–3897. https://doi.org/10.1029/2018JB017144

Serfozo, R. (2009). *Basics of Applied Stochastic Processes, Probability and its Applications*. Springer Berlin Heidelberg.

Shahnazaryan, D., & O'Reilly, G. J. (2021). Integrating expected loss and collapse risk in performance-based seismic design of structures. *Bulletin of Earthquake Engineering*, *19*(2), 987–1025. https://doi.org/10.1007/s10518-020-01003-x

Shcherbakov, R., Turcotte, D. L., & Rundle, J. B. (2005). Aftershock statistics. In *Pure and Applied Geophysics* (Vol. 162, Issues 6–7, pp. 1051–1076). https://doi.org/10.1007/s00024-004-2661-8

Shekhar, S., & Ghosh, J. (2020). A metamodeling based seismic life-cycle cost assessment framework for highway bridge structures. *Reliability Engineering and System Safety*, *195*. https://doi.org/10.1016/j.ress.2019.106724

Shi, W., Lu, X., & Ye, L. (2012). Uniform-risk-targeted seismic design for collapse safety of building structures. *Science China Technological Sciences*, *55*(6), 1481–1488. https://doi.org/10.1007/s11431-012-4808-7

Shinozuka, M., ASCE, A. M., & Sato, Y. (1967). SIMULATION OF NONSTATIONARY RANDOM PROCESS. *Engineering Mechanics Division*.

Shinozuka, M., Feng, M. Q., Kim, H.-K., & Kim, S.-H. (2000). NONLINEAR STATIC PROCEDURE FOR FRAGILITY CURVE DEVELOPMENT. *JOURNAL OF ENGINEERING MECHANICS*, *126*, 1287–1295.

Shokrabadi, M. (2018). *Stochastic Characterization of Aftershock Building Seismic Performance* [Dissertation].

Shome, N., & Cornell, C. A. (1999). *Probabilistic Seismic Demand Analysis of Nonlinear Structures*. Department of Civil and Environmental Engineering, Stanford University.

Shome, N., Cornell, C. A., Bazzurro, P., & Carballo, J. E. (1998). Earthquakes, records, and nonlinear responses. *Earthquake Spectra*, *14*(3), 469–500. https://doi.org/10.1193/1.1586011

Silva, V., Crowley, H., & Bazzurro, P. (2016a). Exploring risk-targeted hazard maps for Europe. *Earthquake Spectra*, *32*(2), 1165–1186. https://doi.org/10.1193/112514EQS198M

Silva, V., Crowley, H., & Bazzurro, P. (2016b). Exploring risk-targeted hazard maps for Europe. *Earthquake Spectra*, *32*(2), 1165–1186. https://doi.org/10.1193/112514EQS198M

Sinković, N. L., Brozovič, M., & Dolšek, M. (2016). Risk-based seismic design for collapse safety. *Earthquake Engineering and Structural Dynamics*, *45*(9), 1451–1471. https://doi.org/10.1002/eqe.2717

Soyoz, S., & Feng, M. Q. (2008a). Instantaneous damage detection of bridge structures and experimental verification. *Structural Control and Health Monitoring*, *15*(7), 958–973. https://doi.org/10.1002/stc.229

Soyoz, S., & Feng, M. Q. (2008b). Instantaneous damage detection of bridge structures and experimental verification. *Structural Control and Health Monitoring*, *15*(7), 958–973. https://doi.org/10.1002/stc.229

Spacone, E., Filippou, F. C., & Taucer, F. F. (1996a). Fibre beam–column model for non-linear analysis of R/C frames: part I: formulation. In *EARTHQUAKE ENGINEERING AND STRUCTURAL DYNAMICS* (Vol. 25).

Spacone, E., Filippou, F. C., & Taucer, F. F. (1996b). Fibre beam-column model for non-linear analysis of R/C frames: Part II. Applications. *Earthquake Engineering and Structural Dynamics*, *25*(7), 727–742. https://doi.org/10.1002/(SICI)1096-9845(199607)25:7<727::AID-EQE577>3.0.CO;2-O

Spencer, B. F., Ruiz-Sandoval, M. E., & Kurata, N. (2004). Smart sensing technology: Opportunities and challenges. *Structural Control and Health Monitoring*, *11*(4), 349–368. https://doi.org/10.1002/stc.48

Sperotto, A., Molina, J. L., Torresan, S., Critto, A., & Marcomini, A. (2017). Reviewing Bayesian Networks potentials for climate change impacts assessment and management: A multi-risk perspective. In *Journal of Environmental Management* (Vol. 202, pp. 320–331). Academic Press. https://doi.org/10.1016/j.jenvman.2017.07.044

ST Microelectronics. (n.d.). LIS331DL. *Avaialble Online at: Https://Www.St.Com/En/Mems-and-Sensors/Lis331dlh.Html.*

Stefanidou, S. P., & Kappos, A. J. (2017). Methodology for the development of bridge-specific fragility curves. *Earthquake Engineering and Structural Dynamics*, *46*(1), 73–93. https://doi.org/10.1002/eqe.2774

Stefanidou, S. P., Sextos, A. G., Kotsoglou, A. N., Lesgidis, N., & Kappos, A. J. (2017). Soil-structure interaction effects in analysis of seismic fragility of bridges using an intensity-based ground motion selection procedure. *Engineering Structures*, *151*, 366–380. https://doi.org/10.1016/j.engstruct.2017.08.033

Stewart, M. G., Wang, X., & Nguyen, M. N. (2011). Climate change impact and risks of concrete infrastructure deterioration. *Engineering Structures*, *33*(4), 1326–1337. https://doi.org/10.1016/j.engstruct.2011.01.010

Talebi, M., Zare, M., Noroozinejad Farsangi, E., Soghrat, M. R., Maleki, V., & Esmaeili, S. (2021). Development of risk-targeted seismic hazard maps for the

Iranian plateau. *Soil Dynamics and Earthquake Engineering*, *141*. https://doi.org/10.1016/j.soildyn.2020.106506

Thywissen, K. (2006). Core terminology of disaster risk reduction: A comparative glossary. In J. Birkmann (Ed.), *Measuring Vulnerability to Natural Hazards* (pp. 448–496). UNU Press.

Tolentino, D., Márquez-Domínguez, S., & Gaxiola-Camacho, J. R. (2020). Fragility Assessment of Bridges Considering Cumulative Damage Caused by Seismic Loading. *KSCE Journal of Civil Engineering*, *24*(2), 551–560. https://doi.org/10.1007/s12205-020-0659-0

Towashiraporn, P. (2004). *Building Seismic Fragilities Using Response Surface Metamodels* [PhD dissertation]. Georgia Institute of Technology.

Trapani, D., Maroni, A., Debiasi, E., & Zonta, D. (2015). Uncertainty evaluation of after-earthquake damage detection strategy. *Proceedings of the 2015 IEEE Workshop on Environmental, Energy, and Structural Monitoring Systems (EESMS)*.

Tubaldi, E., Barbato, M., & Dall'Asta, A. (2010). Transverse seismic response of continuous steel-concrete composite bridges exhibiting dual load path. *Earthquake Struct*, *1*(1), 21–41.

Tubaldi, E., Barbato, M., & Dall'Asta, A. (2012). Influence of Model Parameter Uncertainty on Seismic Transverse Response and Vulnerability of Steel–Concrete Composite Bridges with Dual Load Path. *Journal of Structural Engineering*, *138*(3), 363–374. https://doi.org/10.1061/(asce)st.1943-541x.0000456

Tubaldi, E., Barbato, M., & Ghazizadeh, S. (2012). A probabilistic performance-based risk assessment approach for seismic pounding with efficient application to linear systems. *Structural Safety*, *36–37*, 14–22. https://doi.org/10.1016/j.strusafe.2012.01.002

Tubaldi, E., Dall'Asta, A., & Dezi, L. (2013). Reduced formulation for post-elastic seismic response of dual load path bridges. *Engineering Structures*, *51*, 178–187. https://doi.org/10.1016/j.engstruct.2013.01.014

Tubaldi, E., Freddi, F., & Barbato, M. (2016). Probabilistic seismic demand model for pounding risk assessment. *Earthquake Engng Struct. Dyn*, *45*, 1743–1758.

Tubaldi, E., Ozer, E., Douglas, J., & Gehl, P. (2022). Examining the contribution of near real-time data for rapid seismic loss assessment of structures. *Structural Health Monitoring*, *21*(1), 118–137. https://doi.org/10.1177/1475921721996218

Tubaldi, E., Turchetti, F., Ozer, E., Fayaz, J., Gehl, P., & Galasso, C. (2022). A Bayesian network-based probabilistic framework for updating aftershock risk of bridges. *Earthquake Engineering and Structural Dynamics*, *51*(10), 2496–2519. https://doi.org/10.1002/eqe.3698

Turchetti, F., Tubaldi, E., Patelli, E., Castaldo, P., & Málaga-Chuquitaype, C. (2023). Damage modelling of a bridge pier subjected to multiple earthquakes: a comparative study. *Bulletin of Earthquake Engineering*, *21*(9), 4541–4564. https://doi.org/10.1007/s10518-023-01678-y

Turcotte, D. L., Holliday, J. R., & Rundle, J. B. (2007). BASS, an alternative to ETAS. *Geophysical Research Letters*, *34*(12). https://doi.org/10.1029/2007GL029696

UNDHA. (1992). *Internationally agreed glossary of basic terms relating to disaster management.*

UNDRO. (1980). *Natural Disasters and Vulnerability Analysis. Report of Experts Group Meeting of 9-12 July 1979.*

UNISDR. (2004). *Living With Risk.*

Vamvatsikos, D., & Allin Cornell, C. (2002). Incremental dynamic analysis. *Earthquake Engineering and Structural Dynamics*, *31*(3), 491–514. https://doi.org/10.1002/eqe.141

Vamvatsikos, D., & Aschheim, M. A. (2016). Performance-based seismic design via yield frequency spectra‡. *Earthquake Engineering and Structural Dynamics*, *45*(11), 1759–1778. https://doi.org/10.1002/eqe.2727

Vamvatsikos, D., Bakalis, K., Kohrangi, M., Pyrza, S., Castiglioni, C. A., Kanyilmaz, A., Morelli, F., Stratan, A., D'Aniello, M., Calado, L., Proença, J. M., Degee, H., Hoffmeister, B., Pinkawa, M., Thanopoulos, P., & Vayas, I. (2020). A risk-consistent approach to determine EN1998 behaviour factors for lateral load resisting systems. *Soil Dynamics and Earthquake Engineering*, *131*. https://doi.org/10.1016/j.soildyn.2019.106008

Vamvatsikos, D., & Cornell, A. C. (2002). Incremental dynamic analysis. *Earthquake Engineering and Structural Dynamics*, *31*(3), 491–514. https://doi.org/10.1002/eqe.141

Vamvatsikos, D., & Dolšek, M. (2011). Equivalent constant rates for performance-based seismic assessment of ageing structures. *Structural Safety*, *33*(1), 8–18. https://doi.org/10.1016/j.strusafe.2010.04.005

Vanzi, I., Marano, G. C., Monti, G., & Nuti, C. (2015). A synthetic formulation for the Italian seismic hazard and code implications for the seismic risk. *Soil Dynamics and Earthquake Engineering*, *77*, 111–122. https://doi.org/10.1016/j.soildyn.2015.05.001

Vosooghi, A., & Saiid Saiidi, M. (2012). Experimental Fragility Curves for Seismic Response of Reinforced Concrete Bridge Columns. *ACI Struct*, *109*(6), 825–834.

Wald, D., Lin, K. W., Porter, K., & Turner, L. (2008). ShakeCast: Automating and improving the use of shakemap for post-earthquake deeision-making and response. *Earthquake Spectra*, *24*(2), 533–553. https://doi.org/10.1193/1.2923924

Wang, Z., Padgett, J. E., & Dueñas-Osorio, L. (2014). Toward a uniform seismic risk design of reinforced concrete bridges: A displacement-based approach. *Structural Safety*, *50*, 103–112. https://doi.org/10.1016/j.strusafe.2014.03.009

White, G. F. (1973). Natural hazards research. In R. J. Chorley (Ed.), *Directions in Geography* (pp. 193–216). Methuen and Co.

Yamaguchi, N., & Yamazaki, F. (2000). *Fragility curves for buildings in Japan based on damage surveys after the 1995 Kobe earthquake.* https://www.researchgate.net/publication/228946661

Yamamoto, Y., & Baker, J. W. (2013). Stochastic model for earthquake ground motion using wavelet packets. *Bulletin of the Seismological Society of America*, *103*(6), 3044–3056. https://doi.org/10.1785/0120120312

Zaghi, A. E., Padgett, J. E., Bruneau, M., Barbato, M., Li, Y., Mitrani-Reiser, J., & McBride, A. (2016). Establishing Common Nomenclature, Characterizing the Problem, and Identifying Future Opportunities in Multihazard Design. *Journal of Structural Engineering*, *142*(12). https://doi.org/10.1061/(asce)st.1943-541x.0001586

Zakeri, B., & Zareian, F. (2017). Bridge Design Framework for Target Seismic Loss. *Journal of Bridge Engineering*, *22*(10). https://doi.org/10.1061/(asce)be.1943-5592.0001075

Zanini, M. A., & Hofer, L. (2019). Center and Characteristic Seismic Reliability as new indexes for accounting uncertainties in seismic reliability analysis. *Soil Dynamics and Earthquake Engineering*, *123*, 110–123. https://doi.org/10.1016/j.soildyn.2019.04.028

Zanini, M. A., Toska, K., Feltrin, G., Hofer, L., & Pellegrino, C. (2022). Seismic Reliability Assessment of an Open-Spandrel Reinforced Concrete Arch Bridge. *In: Pellegrino, C., Faleschini, F., Zanini, M.A., Matos, J.C., Casas, J.R., Strauss, A. (Eds) Proceedings of the 1st Conference of the European Association on Quality Control of Bridges and Structures. EUROSTRUCT 2021. Lecture Notes in Civil Engineering*.

Zhang, L., Goda, K., De Luca, F., & De Risi, R. (2020). Mainshock-aftershock state-dependent fragility curves: A case of wood-frame houses in British Columbia, Canada. *Earthquake Engng Struct Dyn*, *49*, 884–903.

Žižmond, J., & Dolšek, M. (2019). Formulation of risk-targeted seismic action for the force-based seismic design of structures. *Earthquake Engineering and Structural Dynamics*, *48*(12), 1406–1428. https://doi.org/10.1002/eqe.3206

Appendix A

The 703 mainshocks (MS) – aftershock (AS) ground-motion (GM) sequences selected from the database provided by Goda & Taylor (2012) and. Goda et al. (2015) are used to compute their RotD50Sa spectra (Boore, 2010) for 2% damped oscillator at 40 periods. The 703 mainshocks and aftershock spectra are presented in **Figure A-1**. To select the ground motions appropriately while considering higher mode effects and period elongation effects, average RotD50Sa (denoted as RotD50Sa,avg) is utilised as the selected ground-motion intensity measure. RotD50Sa,avg is computed as the mean of RotD50Sa between $0.5T_1$ to $2T_1$ (Fayaz et al., 2021) where $T_1 = 0.432$ secs. The histograms of the RotD50Sa,avg computed for the database, are presented in **Figure A-2** .
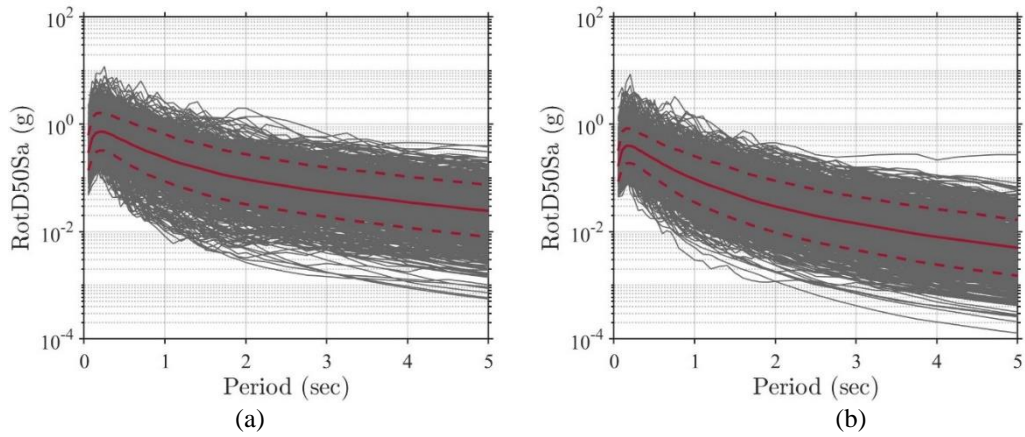
Figure A-1 RotD50Sa spectra (2% damped) of: (a) Mainshocks and (b) Aftershocks of the selection database (703 GMs)
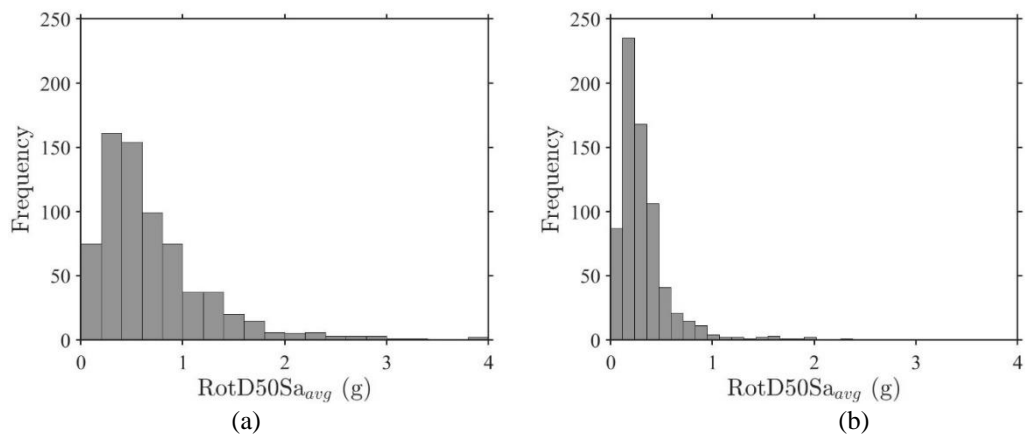

Figure A-2 Average RotD50Sa (RotD50Sa,avg) of: (a) Mainshocks and (b) Aftershocks of the selection database (703 GMs)

Firstly, MS GMs are chosen such that 10 GMs are selected for 20 levels of RotD50Sa,avg ranging from 0.1g to 2.0g at an interval of 0.1g with the requirement of no scaling. This leads to a total of 200 MS unscaled GMs. **Figure A-3a** shows the histogram of RotD50Sa,avg of the selected MS unscaled GMs. It can be observed from the histogram, ~10 GMs are selected for each level of the 20 RotD50Sa,avg with slightly lesser number of GMs available for higher RotD50Sa,avg (i.e., RotD50Sa,avg >1.6 g). This due to the lack of recorded GM options for higher intensity levels. Finally, the 200 unscaled GMs are scaled such that 10 GMs exactly match each level of the RotD50Sa,avg to have precisely 10 GMs for each of the 20 RotD50Sa,avg levels. The histogram of the scaling factors is shown in **Figure A-3b**, and it can be observed that they range very close to 1, thereby signifying lower scaling levels.
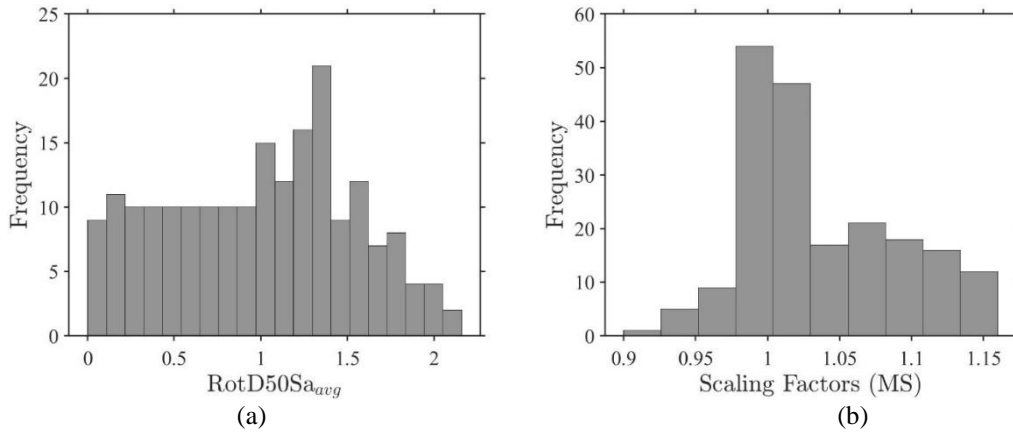
Figure A-3 Selected MS GMs: (a) Unscaled RotD50Sa,avg (b) Scaling Factors

The natural unscaled AS GMs corresponding to the 200 unscaled MS GMs selected above are selected for the AS sequence to maintain mainshock-aftershock *IM* correlations. This leads to 200 unscaled AS GMs whose RotD50Sa,avg is presented in **Figure A-4a**. **Figure A-5a** further shows the RotD50Sa,avg of the 200 unscaled MS GMs, vs. the RotD50Sa,avg of the corresponding natural 200 unscaled AS GMs. It can be observed that for lower levels of MS RotD50Sa,avg levels, the RotD50Sa,avg levels of AS GMs tend to be very small, and the scatter plot tends to be very sparse for high AS RotD50Sa,avg levels. To remedy this, the selected unscaled AS GMs are scaled (with minimal scaling) such that for each MS RotD50Sa,avg level (i.e., 20 levels ranging from 0.1g to 2.0g at an interval of 0.1g), the corresponding ten unscaled AS GMs lead to ten levels of RotD50Sa,avg ranging from 0.1g to 1.9g at an interval of 0.2g. The histogram of the utilised scaling factors is shown in **Figure A-4b**, and the RotD50Sa,avg of the selected scaled MS and AS GMs is shown in **Figure A-5b**. To ensure that minimal scaling is used for the AS GMs, for each level of MS RotD50Sa,avg, the corresponding ten unscaled AS GMs are scaled such that each one requires minimal scaling to achieve RotD50Sa,avg between 0.1g and 1.9g. This process leads to mainshock-aftershock sequences with RotD50Sa,avg shown in **Figure A-5b**.
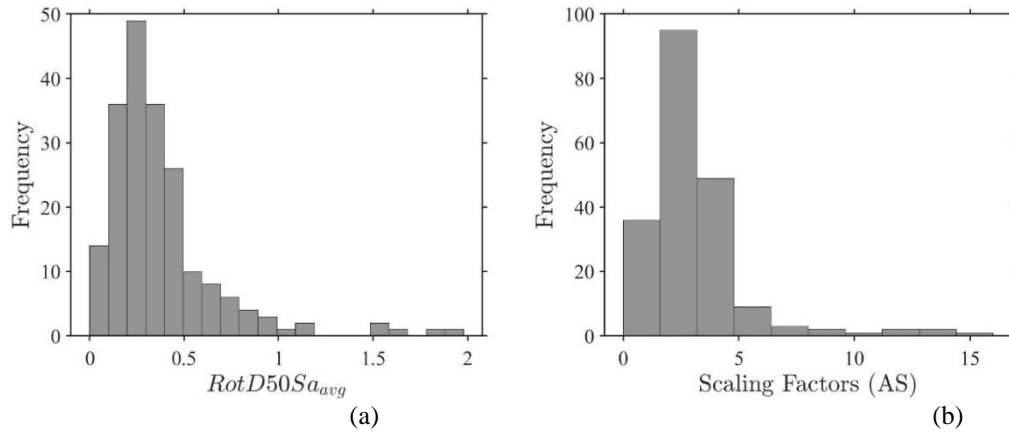
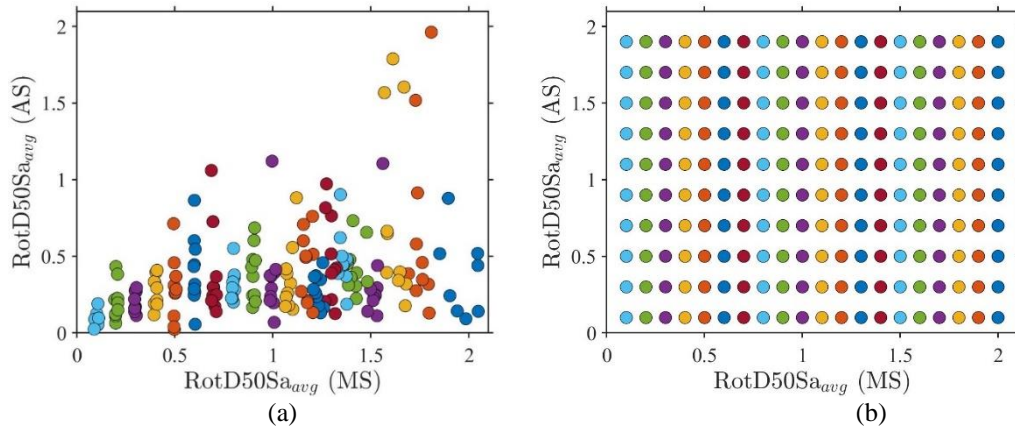**Figure A-4** Selected AS GMs': (a) Unscaled RotD50Sa,avg (b) Scaling Factors

Figure A-5 RotD50Sa,avg of the selected MS vs. AS GMs: (a) Unscaled mainshock-aftershock GMs and (b) Scaled mainshock-aftershock GMs

Furthermore, the magnitudes of the mainshock and aftershock remained consistent with the statistical knowledge obtained from the history of recordings where the selected mainshock-aftershock led to mean MS magnitude = 8.15 and mean AS magnitude = 6.80. This is consistent with the literature available that mentions that the magnitude of AS is on average 1 to 1.2 points lower than the magnitude of MS event (Shokrabadi, 2018). The magnitudes of the MS and AS events of selected ground motions are shown in **Figure A-6a** and **Figure A-6b**, respectively. To further introduce randomness in the ground motions, the "as recorded" components of the 200 MS and AS ground motions were rotated at random angles. However, it was made sure that both MS and AS GMs of the sequence were rotated to the same random angle in order to maintain the internal correlations.
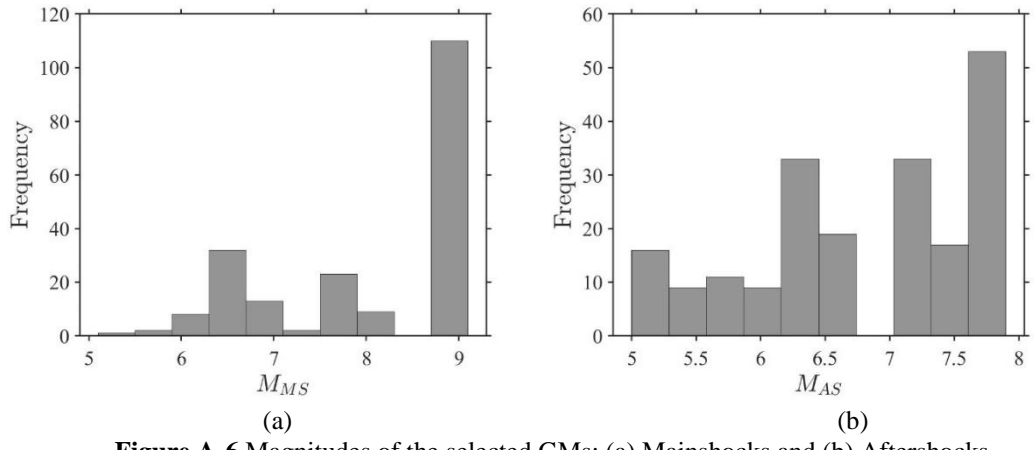
Figure A-6 Magnitudes of the selected GMs: (a) Mainshocks and (b) Aftershocks

Appendix B

The regression coefficients for the average model of Equation (4-7) are listed in **Table B-1**.

Table B-1 Coefficients of the bilinear regression model of Equation (4-7) for the various *EDPs* of interest

Coefficient	*RD*	*TD*	*PA*	ε_{cc}	ε_{ct}	D_{MS}
a_1	-13. 220	-4.850	-0.208	-9.142	-9.192	-3.442
b_1	2.445	1.11	0.720	1.532	1.974	1.306
b_2	1.480	0.260	0.369	0.499	0.653	0.427

The covariance matrices Σ^I and Σ^{II}, collecting the information on the variance of the error variables (in the lognormal space) and their correlation, for the two branches of the PSDM for the mainshock damage assessment (corresponding respectively to $IM_{MS} \leq IM*$ and $IM_{MS} > IM*$), are:

$$\Sigma^I = \begin{bmatrix} 2.264 & 0.518 & 0.021 & 0.879 & 1.180 & 0.625 \\ 0.518 & 0.221 & 0.016 & 0.315 & 0.409 & 0.277 \\ 0.021 & 0.016 & 0.183 & 0.033 & 0.060 & 0.041 \\ 0.879 & 0.315 & 0.033 & 0.537 & 0.707 & 0.436 \\ 1.180 & 0.409 & 0.060 & 0.707 & 0.961 & 0.564 \\ 0.563 & 0.277 & 0.040 & 0.436 & 0.564 & 0.440 \end{bmatrix} \tag{B-1}$$

$$\sum\nolimits^{II} = \begin{bmatrix} 2.56 & 0.599 & 0.193 & 1.040 & 1.366 & 0.980 \\ 0.599 & 0.267 & 0.090 & 0.414 & 0.525 & 0.447 \\ 0.193 & 0.090 & 0.146 & 0.129 & 0.165 & 0.123 \\ 1.040 & 0.414 & 0.129 & 0.713 & 0.895 & 0.730 \\ 1.366 & 0.525 & 0.165 & 0.895 & 1.172 & 0.925 \\ 0.980 & 0.447 & 0.123 & 0.730 & 0.925 & 0.823 \end{bmatrix}$$

and the corresponding correlation matrices are:

$$\mathbf{C}^I = \begin{bmatrix} 1 & 0.733 & 0.032 & 0.798 & 0.800 & 0.627 \\ 0.733 & 1 & 0.081 & 0.914 & 0.887 & 0.890 \\ 0.032 & 0.081 & 1 & 0.105 & 0.144 & 0.143 \\ 0.798 & 0.914 & 0.105 & 1 & 0.984 & 0.899 \\ 0.799 & 0.887 & 0.144 & 0.984 & 1 & 0.869 \\ 0.627 & 0.890 & 0.143 & 0.899 & 0.869 & 1 \end{bmatrix}$$

$$\mathbf{C}^{II} = \begin{bmatrix} 1 & 0.772 & 0.338 & 0.828 & 0.841 & 0.719 \\ 0.772 & 1 & 0.455 & 0.949 & 0.940 & 0.952 \\ 0.338 & 0.455 & 1 & 0.401 & 0.398 & 0.354 \\ 0.828 & 0.950 & 0.401 & 1 & 0.978 & 0.953 \\ 0.841 & 0.938 & 0.398 & 0.978 & 1 & 0.942 \\ 0.719 & 0.952 & 0.354 & 0.953 & 0.942 & 1 \end{bmatrix}$$

(B-2)

Table B-2 presents the regression coefficients for the average model of Equation (4-11). The estimate of the standard deviation of ε_n is 0.603.

Table B-2 Coefficients of the multilinear regression model of Equation (4-11)

Coefficient	Value
c_n	0.233
d_n	0.935
e_n	0.166
f_n	-0.173

Appendix C

Source-to-site distances can differ for typology (hypo-central distance, epicentral distance, seismogenic depth, etc.) and for the geometry of the source zone (**Figure C-1**) (Baker et al., 2021) .
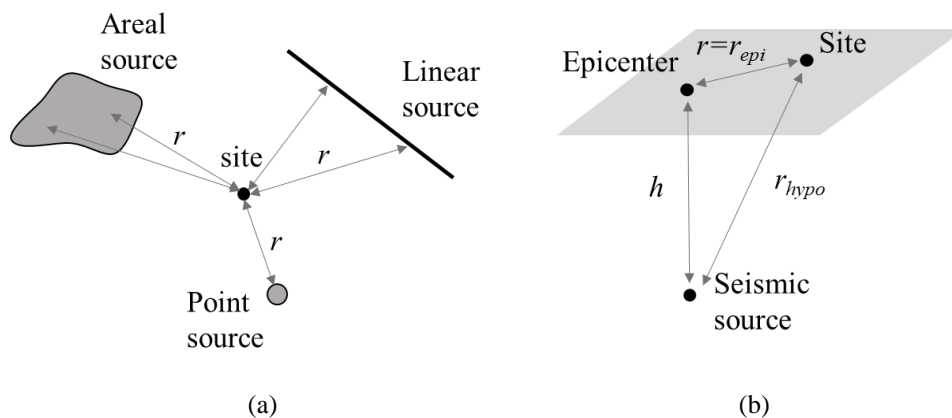

Figure C-1 (a) Different geometries of a source zone; (b) Types of distances

The simplest model is the point source model. This model is usually adopted for representing particularly small seismic faults or volcanic phenomenon. The point source model is probabilistically described by the following PDF:

$$f_R(r) = \begin{cases} 1, & if \ r = r_p \\ 0, & otherwise \end{cases} \tag{C-1}$$

The linear source model is detailed in **Figure C-2**, where L_f is the maximum length of the seismic fault, r_{min} is the orthogonal distance from the site to the midpoint of the line fault, r is the distance of the site from the epicenter and d is $\sqrt{r^2 - r_{min}^2}$ and it is mainly used to represent shallow faults. In this model, it is assumed that earthquakes are equally likely to occur at any point of the fault line and the only parameters to set are L_f and r_{min}.
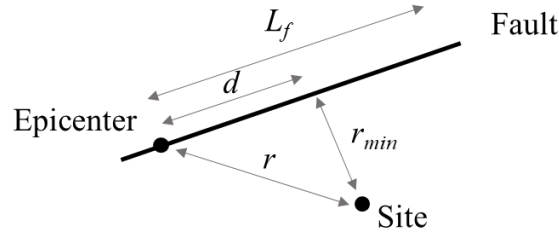

Figure C-2 Illustrative example of a linear source

Having assumed these two quantities, the CDF $F_R(r)$ and the PDF $f_R(r)$ can be obtained applying the Pythagorean theorem on the triangle formed by d, r and r_{min}:

$$F_R(r) = \begin{cases} 0, & if \ r < r_{min} \\ \dfrac{2d}{L_f} = \dfrac{2\sqrt{r^2 - r_{min}^2}}{L_f}, & if \ r_{min} \le r < \left(\dfrac{L_f}{2} + 1\right) \\ 1, & otherwise \end{cases} \tag{C-2}$$

$$f_R(r) = \begin{cases} \dfrac{2r}{L_f\sqrt{r^2 - r_{min}^2}}, & if \ r_{min} \le r < \left(\dfrac{L_f}{2} + 1\right) \\ 0, & otherwise \end{cases} \tag{C-3}$$

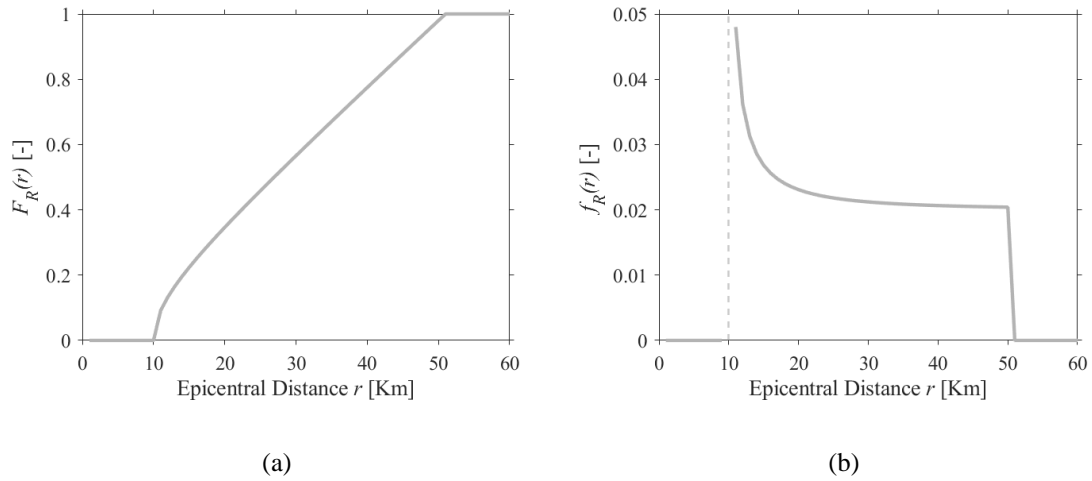The plots of the CDF and PDF are shown in **Figure C-3**.

Figure C-3 (a) CDF and (b) PDF plots of the source-to-site distance of a linear source

Figure C-4 depicts a circular areal fault model. In an areal fault model, it is assumed that the seismic source is producing random earthquakes with equal likelihood anywhere within a given fixed distance (r_{max}) from the site, beyond which the seismic effects become negligible. This type of model is adopted when a specific fault structure is not identified.
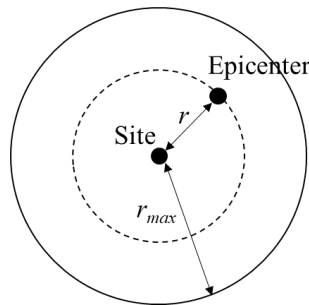

Figure C-4 Illustrative example of an areal source

The CDF and the PDF can be obtained based on the geometry of the fault model. The CDF depends on the square value of the epicentral distance r while the PDF is linear because it is the first derivative of the CDF. The plots of the CDF and the PDF respectively are presented in Figure C-5. The equations of the CDF and the PDF are respectively:

$$F_R(r) = \begin{cases} 0, & if\ r < 0 \\ \dfrac{\pi(r)^2}{\pi(r_{max})^2} = \dfrac{r^2}{r_{max}^2}, & if\ 0 \le r < r_{max} \\ 1, & otherwise \end{cases} \tag{C-4}$$

$$f_R(r) = \begin{cases} \dfrac{2r}{r_{max}^2}, & if\ 0 \le r < r_{max} \\ 0, & otherwise \end{cases} \tag{C-5}$$
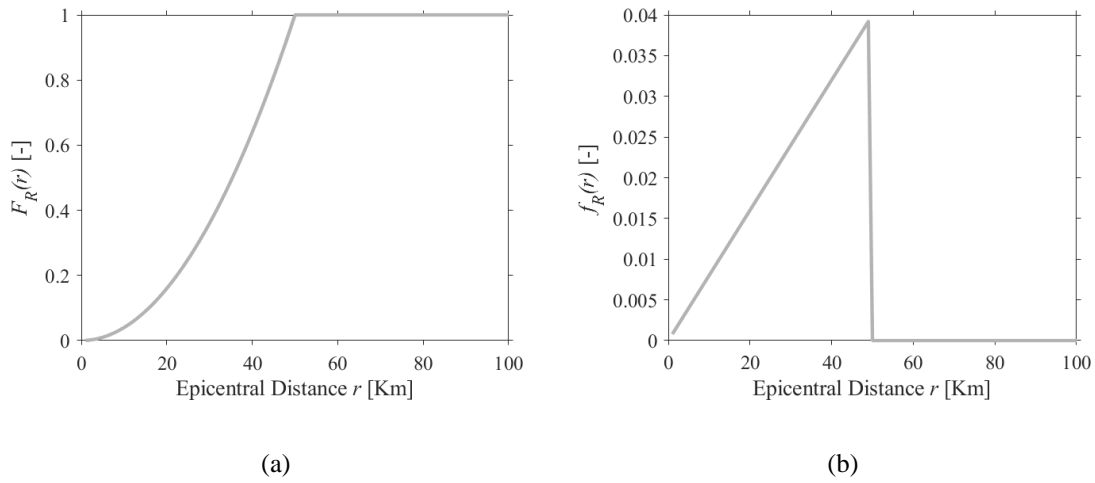

Figure C-5 (a) CDF and (b) PDF plots of the source-to-site distance of an areal source

The other random variable involved in the hazard analysis is the earthquake magnitude. In 1944 Gutenberg and Richter found a linear relation between the magnitude and the logarithmic of mean annual frequency of exceedance (Equation (C-6)) (Gutenberg & Richter, 1942). This so-called Gutenberg-Richter law can be also expressed in the exponential form as reported in Equation (C-7). It provides an estimate of the mean number of events with magnitude M that exceed a magnitude value m within a given time frame. Typically, the time frame is assumed to be one year.

$$v_M(m) = 10^{a-bm} = e^{\alpha - \beta m} \tag{C-6}$$

$$\log[v_M(m)] = a - bm \tag{C-7}$$

The relation depends on two parameters, *a* and *b*. The parameter *a* accounts for the mean annual number of events expected in a given seismic source above a given magnitude threshold; this quantity reflects the seismicity of the region of interest. The parameter *b* describes the ratio of small to large magnitude events. These two parameters are source-dependent and the value of the constant *b* is commonly assumed to be 1.0. The Gutenberg-Richter law is employed in seismic assessment to generate sets of magnitude values.

In the applications, the Gutenberg-Richter law is bounded within a given interval of magnitudes (McGuire & Arabasz, 1990). The lower bound of the interval m_0 represents the minimum magnitude below which no effects are observed on structures. The upper bound value m_{Max} is the highest magnitude considered, beyond this value there are no earthquakes expected, or they wouldn't have a physical meaning. Using this upper and lower bound, the CDF and the PDF are expressed as:

Lower bound magnitude $m < m_0$

$$v_M(m) = v_M(m_0)e^{-\beta(m-m_0)} = (e^{\alpha-\beta m_0})e^{-\beta(m-m_0)} \qquad m > m_0 \qquad \text{(C-8)}$$

$$F_M(m) = P(M < m | M \geq m_0) = \frac{v_M(m_0) - v_M(m)}{v_M(m_0)} = 1 - e^{-\beta(m-m_0)} \qquad \text{(C-9)}$$

$$f_M(m) = \beta e^{-\beta(m-m_0)} \qquad \text{(C-10)}$$

Upper bound magnitude $m > m_{max}$

$$v_M(m) = v_M(m_0)\frac{e^{-\beta(m-m_0)} - e^{-\beta(m_{Max}-m_0)}}{1 - e^{-\beta(m_{Max}-m_0)}} \qquad m_0 \leq m \leq m_{Max} \qquad \text{(C-11)}$$

$$F_M(m) = P(M < m | m_0 \leq m \leq m_{Max}) = \frac{1 - e^{-\beta(m-m_0)}}{1 - e^{-\beta(m_{Max}-m_0)}} \qquad \text{(C-12)}$$

$$f_M(m) = \beta \frac{e^{-\beta(m-m_0)}}{1 - e^{-\beta(m_{Max}-m_0)}} \qquad \text{(C-13)}$$

$v_M(m)$ denotes the mean annual number of events with magnitude M that exceed a magnitude value m and $F_M(m)$ and $f_M(m)$ are the CDF and the PDF respectively.

Appendix D

The mathematical expression of $S(f)$ is:

$$S(f) = \varepsilon_{mod} S_0(f) \cdot S_n(f) \cdot S_f(f) \cdot V(f) \tag{D-1}$$

The two corner frequencies point-source spectrum is represented by $S_0(f)$

$$S_0(f) = C \cdot M_0 \cdot (2\pi f)^2 \cdot \left((1-\varepsilon) \cdot \frac{1}{1 + \left(\frac{f}{f_a}\right)^2} + \varepsilon \cdot \frac{1}{1 + \left(\frac{f}{f_b}\right)^2} \right) \tag{D-2}$$

M_0 is the seismic moment expressed as:

$$M_0 = 10^{\frac{2}{3}(M_m + 10.70)} \tag{D-3}$$

C is a constant:

$$C = 10^{-20} \frac{\hat{R} \cdot V \cdot F_s}{4\pi\rho\beta^3} \tag{D-4}$$

where $\hat{R}$ is the radiation pattern ($\hat{R} = 0.55$), V is a factor partitioning the total shear-wave energy into 2 horizontal components ($V = 0.71$), F_s is the free-surface amplification factor ($F_s = 2.0$), ρ is the soil density ($\rho = 2.8$ t/m^3) and β is the wave velocity ($\beta = 3.5$ km/s) near the source. The two corner frequencies f_a and f_b, and the ε parameter are related to the magnitude by

$$\log(f_a) = 2.181 - 0.496 \cdot M_m \tag{D-5}$$

$$\log(f_b) = 1.380 - 0.227 \cdot M_m \tag{D-6}$$

$$\log(f_\varepsilon) = 3.223 - 0.670 \cdot M_m \tag{D-7}$$

The $S_n(f)$ function characterizes the path effects of seismic waves and is expressed as:

$$S_n(f) = \frac{1}{R} e^{\frac{-\pi f R}{Q(f)\beta}} \tag{D-8}$$

$Q(f) = Q_0 f^n$ is called the quality factor and accounts for the effect of waves-transmission, with $Q_0 = 180$ and $n = 0.45$ regional parameters.

The $S_f(f)$ is given by:

$$S_f(f) = e^{(-\pi k f)} \left[1 + \left(\frac{f}{f_{max}} \right)^8 \right]^{-0.5} \tag{D-9}$$

where $k = 0.03$ and $f_{max} = 100$ Hz.

$V(f)$ is the soil amplification factor (Boore and Joyner 1997) ($V_{S,30} = 310$ m/s for a generic soil) and ε_{mod} is the model-error parameter used for increasing the record-to-record variability. The latter is a lognormal random variable with $\mu_{\ln \varepsilon} = 0$, $\sigma_{\ln \varepsilon} = 0.5$.

The envelope function $e(t)$ is defined by

$$e(t) = a \cdot \left(\frac{t}{T_n} \right)^b \exp\left(-c \left(\frac{t}{T_n} \right) \right) \tag{D-10}$$

$$b = -\varepsilon \cdot \frac{\ln(\eta)}{[1+\varepsilon(\ln \varepsilon - 1)]}; c = \frac{b}{\varepsilon}; a = \left(\frac{\exp(1)}{\varepsilon} \right)^b; \eta = 0.05; \varepsilon = 0.2 \tag{D-11}$$

The total duration of a ground motion is

$$T_n = 2T_w = 2 \cdot \left(0.05 \cdot R + \frac{1}{2 f_a(M_m)} \right) \qquad \text{(D-12)}$$

The hypo-central distance R, i.e. the distance from the earthquake source to the site, is defined as:

$$R = \sqrt{r_e^2 + h^2} \qquad \text{(D-13)}$$

where r_e is the epicentral distance and h is the moment dependent nominal pseudo-depth.